

METASOMATISM AND MAGMATIC ASSIMILATION AT A GABBRO-LIMESTONE CONTACT,  
CHRISTMAS MOUNTAINS, BIG BEND REGION, TEXAS

Thesis by  
Raymond Leonard Joesten

In Partial Fulfillment of the Requirements  
for the degree of  
Doctor of Philosophy

California Institute of Technology  
Pasadena, California

1974  
(Submitted May 30, 1973)

## ACKNOWLEDGEMENTS

The author wishes to express his sincere thanks to Professor Arden Albee, sponsor of the thesis, for providing all necessary support for the project while allowing the author complete freedom in the choice of topic and the approaches used in carrying out the investigation. Professor Stephen Clabaugh of the University of Texas at Austin provided the author with unpublished manuscripts of previous geologic investigations in the Christmas Mountains without which a study of this nature could not have been made. I would like to thank Harold Wynne of the Terlingua Ranch Company and Robert Marks of the Great Western Corporation for granting access to land under their management. The Howard Gibsons, Bill Gibsons and Joseph Fandriches of Study Butte, Texas were gracious hosts to the author in the field. Art Chodos was a patient teacher of the techniques of electron microprobe analysis and Lily Ray gave unselfishly of her time to help the author with programming problems.

Field and laboratory expenses of this project were supported by N.S.F. Grant 12867 to Professor Albee, G.S.A. Penrose Grant 1319-69 to the author and by Caltech General Funds. The electron microprobe laboratory was developed with the support of N.S.F., the Jet Propulsion Laboratory and the Union Pacific Foundation. The author gratefully acknowledges support of a Graduate Teaching Assistantship, 1968-69, California State Scholarship, 1969-70 and N.S.F. Graduate Fellowship, 1969-71.

Preparation of the manuscript was supported by the University of Connecticut. The author wishes to thank Lori Grant,

Marie Millette and Selma Woolman for typing the manuscript,  
Raymond Blanchette and Patrice Stanton for drafting the figures and  
Richard Gaskill for printing the photographs.

This thesis is dedicated to the memory of Professor C. E. Tilley  
whose pioneering studies of contact metamorphism and magmatic  
assimilation of limestone at Scawt Hill and Camas Mor provided the  
inspiration for this study.

## ABSTRACT

A composite stock of alkaline gabbro and syenite is intrusive into limestone of the Del Carmen, Sue Peaks and Santa Elena Formations at the northwest end of the Christmas Mountains. There is abundant evidence of solution of wallrock by magma but nowhere are gabbro and limestone in direct contact. The sequence of lithologies developed across the intrusive contact and across xenoliths is gabbro, pyroxenite, calc-silicate skarn, marble. Pyroxenite is made up of euhedral crystals of titanite and sphene in a leucocratic matrix of nepheline, wollastonite and alkali feldspar. The uneven modal distribution of phases in pyroxenite and the occurrence of nepheline syenite dikes, intrusive into pyroxenite and skarn, suggest that pyroxenite represents an accumulation of clinopyroxene "cemented" together by late-solidifying residual magma of nepheline syenite composition. Assimilation of limestone by gabbroic magma involves reactions between calcite and magma and/or crystals in equilibrium with magma and crystallization of phases in which the magma is saturated, to supply energy for the solution reaction. Gabbroic magma was saturated with plagioclase and clinopyroxene at the time of emplacement. The textural and mineralogic features of pyroxenite can be produced by the reaction



Plagioclase in pyroxenite has corroded margins and is rimmed by nepheline, suggestive of resorption by magma. Anorthite and wollastonite enter solid solution in titanite. For each mole of

calcite dissolved, approximately one mole of clinopyroxene was crystallized. Thus the amount of limestone that may be assimilated is limited by the concentration of potential clinopyroxene in the magma. Wollastonite appears as a phase when magma has been depleted in iron and magnesium by crystallization of titanite. The predominance of mafic and ultramafic compositions among contaminated rocks and their restriction to a narrow zone along the intrusive contact provides little evidence for the generation of a significant volume of desilicated magma as a result of limestone assimilation.

Within 60 m of the intrusive contact with the gabbro, nodular chert in the Santa Elena Limestone reacted with the enveloping marble to form spherical nodules of high-temperature calc-silicate minerals. The phases wollastonite, rankinite, spurrite, tilleyite and calcite, form a series of sharply-bounded, concentric monomineralic and two-phase shells which record a step-wise decrease in silica content from the core of a nodule to its rim. Mineral zones in the nodules vary with distance from the gabbro as follows:

- 0-5 m CALCITE + SPURRITE + RANKINITE + WOLLASTONITE
- 5-16 m CALCITE + TILLEYITE ± SPURRITE + RANKINITE + WOLLASTONITE
- 16-31 m CALCITE + TILLEYITE + WOLLASTONITE
- 31-60 m CALCITE + WOLLASTONITE
- 60-plus CALCITE + QUARTZ

The mineral of a one-phase zone is compatible with the phases bounding it on either side but these phases are incompatible in the same volume of P-T-X<sub>CO<sub>2</sub></sub> space.

Growth of a monomineralic zone is initiated by reaction between minerals of adjacent one-phase zones which become unstable with rising temperature to form a thin layer of a new single phase that separates the reactants and is compatible with both of them. Because the mineral of the new zone is in equilibrium with the phases at both of its contacts, gradients in the chemical potentials of the exchangeable components are established across it. Although zone boundaries mark discontinuities in the gradients of bulk composition, two-phase equilibria at the contacts demonstrate that the chemical potentials are continuous. Hence, Ca, Si and CO<sub>2</sub> were redistributed in the growing nodule by diffusion. A monomineralic zone grows at the expense of an adjacent zone by reaction between diffusing components and the mineral of the adjacent zone. Equilibria between two phases at zone boundaries buffers the chemical potentials of the diffusing species. Thus, within a monomineralic zone, the chemical potentials of the diffusing components are controlled external to the local assemblage by the two-phase equilibria at the zone boundaries.

Mineralogically zoned calc-silicate skarn occurs as a narrow band that separates pyroxenite and marble along the intrusive contact and forms a rim on marble xenoliths in gabbro. Skarn consists of melilite or idocrase pseudomorphs of melilite, one or two stoichiometric calc-silicate phases and accessory Ti-Zr garnet, perovskite and magnetite. The sequence of mineral zones from pyroxenite to marble, defined by a characteristic calc-silicate, is wollastonite, rankinite, spurrite, calcite. Mineral assemblages of adjacent skarn zones are compatible

and the set of zones in a skarn band defines a facies type, indicating that the different mineral assemblages represent different bulk compositions recrystallized under identical conditions. The number of phases in each zone is less than the number that might be expected to result from metamorphism of a general bulk composition under conditions of equilibrium, trivariant in P, T and  $\bar{u}_{CO_2}$ . The "special" bulk composition of each zone is controlled by reaction between phases of the zones bounding it on either side. The continuity of the gradients of composition of melilite and garnet solid solutions across the skarn is consistent with the local equilibrium hypothesis and verifies that diffusion was the mechanism of mass transport. The formula proportions of Ti and Zr in garnet from skarn vary antithetically with that of Si which systematically decreases from pyroxenite to marble. The chemical potential of Si in each skarn zone was controlled by the coexisting stoichiometric calc-silicate phases in the assemblage. Thus the formula proportion of Si in garnet is a direct measure of the chemical potential of Si from point to point in skarn. Reaction between gabbroic magma saturated with plagioclase and clinopyroxene produced nepheline pyroxenite and melilite-wollastonite skarn. The calc-silicate zones result from reaction between calcite and wollastonite to form spurrite and rankinite.

## TABLE OF CONTENTS

	Page
ACKNOWLEDGEMENT.....	ii
ABSTRACT.....	iv
LIST OF FIGURES.....	xii
LIST OF PLATES.....	xvi
LIST OF TABLES.....	xvii
INTRODUCTION.....	1
1. GEOLOGY OF THE WESTERN PART OF THE CHRISTMAS MOUNTAINS..	5
GEOLOGIC SETTING.....	5
STRATIGRAPHY AND LITHOLOGY OF THE SEDIMENTARY ROCKS.....	9
Del Carmen Limestone.....	9
Sue Peaks Formation.....	9
Santa Elena Limestone.....	12
Boquillas Formation.....	12
THE GABBRO COMPLEX.....	13
Intrusive Relationships.....	14
Pyroxenite.....	17
Skarn.....	20
POST-GABBRO IGNEOUS ROCKS.....	22
2. PETROLOGY OF THE GABBRO COMPLEX.....	24
INTRODUCTION.....	24
COARSE-GRAINED OLIVINE-BIOTITE-TITANAUGITE GABBRO.....	25
FINE-GRAINED BIOTITE-TITANAUGITE GABBRO.....	55
PORPHYRITIC OLIVINE-BIOTITE-TITANAUGITE GABBRO.....	57

## TABLE OF CONTENTS (Continued)

	Page
PYROXENE SYENITE.....	63
SUMMARY.....	65
3. THE GENESIS OF MAFIC ALKALINE ROCKS BY ASSIMILATION OF LIMESTONE BY GABBROIC MAGMA.....	67
INTRODUCTION.....	67
CONTAMINATED ROCKS.....	68
Pyroxenite.....	68
Nepheline Syenite.....	68
Nepheline Gabbro.....	73
Bulk Composition of Contaminated Rocks.....	76
TITANAUGITE.....	77
LIMESTONE ASSIMILATION.....	93
The Plagioclase Reaction.....	94
Clinopyroxene Accumulation.....	98
The Olivine Reaction.....	99
SUMMARY.....	102
4. METASOMATIC GROWTH OF ZONED CALC-SILICATE NODULES FROM THE CONTACT AUREOLE.....	105
INTRODUCTION.....	105
GEOLOGIC SETTING.....	107
MORPHOLOGY OF NODULES.....	108
MINERALOGY.....	112
PETROGENETIC GRID.....	123
CONDITIONS OF METAMORPHISM.....	134
THERMAL HISTORY.....	142

## TABLE OF CONTENTS (Continued)

	Page
GROWTH MODEL.....	145
THE PHASE RULE.....	153
SUMMARY AND CONCLUSIONS.....	158
5. METASOMATIC GROWTH OF THE ZONED CALC-SILICATE SKARN AT THE INTRUSIVE CONTACT.....	161
INTRODUCTION.....	161
MINERALOGY.....	169
Melilite.....	169
Idocrase.....	170
Calc-silicate Phases.....	192
Calcium-Magnesium Orthosilicates.....	194
Titanian-Zirconian Garnet.....	195
Perovskite and Magnetite.....	209
MINERAL ASSEMBLAGES.....	212
COMPOSITIONAL GRADIENTS.....	223
Melilite.....	224
Garnet.....	229
Bulk Composition.....	247
PHYSICAL CONDITIONS OF METAMORPHISM AND SKARN GENESIS...	256
BULK COMPOSITION OF LIMESTONE AND SKARN.....	267
Integrated Bulk Composition of Skarn.....	267
Bulk Composition of Limestone.....	271
GROWTH MODEL.....	272
The Reaction-Diffusion Model.....	272

## TABLE OF CONTENTS (Continued)

	Page
Mass Balance Calculations.....	282
SUMMARY.....	296
REFERENCES.....	301
APPENDIX A.....	308
ELECTRON MICROPROBE ANALYSIS OF MINERALS.....	309
ELECTRON MICROPROBE ANALYSIS OF ROCKS.....	310
APPENDIX B.....	321
APPENDIX C.....	377

## LIST OF FIGURES

	Page
CHAPTER 1	
1. Geologic map of the western part of the Christmas Mountains.....	7
CHAPTER 2	
1. Electron microprobe analyses of clinopyroxene plotted on the pyroxene quadrilateral.....	30
2. Electron microprobe analyses of clinopyroxene, atomic fraction Al plotted against atomic fraction Ti.....	35
3. Electron microprobe analyses of clinopyroxene, formula proportion Al plotted against 2.O-Formula proportion Si.....	40
4. Electron microprobe analyses of Feldspar plotted in terms of molecular AN, AB and OR.....	45
CHAPTER 3	
1. Electron microprobe analyses of clinopyroxene plotted on the pyroxene quadrilateral.....	81
2. Electron microprobe analyses of clinopyroxene, atomic fraction Al plotted against atomic fraction Ti.....	84
3. Electron microprobe analyses of clinopyroxene, formula proportion Al plotted against 2.O-formula proportion Si.....	87
4. Concentration profiles across zoned titanite from pyroxenite.....	90
CHAPTER 4	
1. Mineral phases in the system CaO-SiO <sub>2</sub> -CO <sub>2</sub> .....	113
2. Schematic P-T diagram for the system CaO-SiO <sub>2</sub> -CO <sub>2</sub> .....	130
3. Calibrated P-T diagram for the system Ca-SiO <sub>2</sub> -CO <sub>2</sub> .....	132

LIST OF FIGURES (CONT.)	Page
4. Gradient of maximum temperatures attained in the contact aureole.....	137
5. Isobaric T-X <sub>CO<sub>2</sub></sub> diagram for the system CaO-SiO <sub>2</sub> -CO <sub>2</sub> at pressure of 300 bars.....	140
6. Schematic composition-distance profiles across chert and calc-silicate nodules.....	146
7. Schematic isothermal-isobaric chemical potential diagram ( $u_{\text{SiO}_2} - u_{\text{CO}_2}$ ) for system CaO-SiO <sub>2</sub> -CO <sub>2</sub> .....	156
 CHAPTER 5	
1. Schematic cross-section of pyroxenite and skarn developed at contact between porphyritic gabbro and Sue Peaks Limestone.....	165
2. Sketch map of two xenoliths of Santa Elena (?) Limestone in fine-grained gabbro.....	167
3. Atomic fraction of Ca in coexisting melilite and idocrase from skarn.....	179
4. Atomic fraction of Si in coexisting melilite and idocrase from skarn.....	181
5. Atomic fraction of Al in coexisting melilite and idocrase from skarn.....	183
6. Atomic fraction of Fe in coexisting melilite and idocrase from skarn.....	185
7. Atomic fraction of Mg in coexisting melilite and idocrase from skarn.....	187
8. Atomic fraction of Na in coexisting melilite and idocrase from skarn.....	189
9. Formula proportion of Ti plotted against 3.0-formula proportion Si in garnet from skarn.....	200
10. Formula proportion of Zr plotted against 3.0-formula proportion Si in garnet from skarn.....	202
11. Formula proportion of Ti + Zr plotted against 3.0 - formula proportion Si in garnet from skarn.....	204

LIST OF FIGURES (CONT.)	Page
12. Mineral assemblages in skarn plotted on the simplified skarn tetrahedron.....	215
13. Bulk composition of skarn samples from main contact traverse plotted on the Ca-(Fe+Mg)-Si face of the simplified skarn tetrahedron.....	219
14. Bulk composition of skarn samples from xenolith traverse plotted on Ca-(Fe+Mg)-Si face of the simplified skarn tetrahedron.....	221
15. Composition-distance plot of major cations in melilite in skarn of main contact traverse.....	225
16. Composition-distance plot of major cations in melilite in skarn of xenolith traverse.....	227
17. Molecular proportions of Al, Mg and Fe in melilite from skarn.....	230
18. Composition-distance plot of major cations in garnet from skarn of main contact traverse.....	233
19. Composition-distance plot of major cations in garnet from skarn of xenolith traverse.....	235
20. Composition-distance plot of weight % ZrO <sub>2</sub> in garnet and ppm Zr in skarn of main contact traverse.....	238
21. Molecular proportions of Ca, Si and Ti+Zr in garnet from skarn of main contact traverse.....	242
22. Molecular proportions of Ca, Si and Ti+Zr in garnet from skarn of xenolith traverse.....	244
23. Composition-distance plot of major oxides in skarn of main contact traverse.....	248
24. Composition-distance plot of major oxides in skarn of xenolith traverse.....	250
25. Mineral assemblages in sample CM-108 plotted on the simplified skarn tetrahedron.....	262

## LIST OF FIGURES (CONT.)

Page

26. Mineral assemblages in sample CM-273-5 plotted on the simplified skarn tetrahedron.....	278
27. Molecular proportion of Ca, (Fe+Mg) and Si of porphyritic gabbro, Sue Peaks Limestone and integrated bulk composition of skarn of main contact traverse.....	288
28. Molecular proportion of Ca, Al and Si of porphyritic gabbro, Sue Peaks Limestone and integrated bulk composition of skarn of the main contact traverse.....	290
29. Molecular proportion of Ca, (Fe+Mg) and Si of fine-grained gabbro, Del Carmen and Santa Elena Limestone and integrated bulk composition of skarn of xenolith traverse.....	292
30. Molecular proportions of Ca, Al and Si of fine-grained gabbro, Del Carmen and Santa Elena Limestone and integrated bulk composition of skarn of xenolith traverse.....	294

## APPENDIX B

B-1. Electron microprobe analyses of igneous rocks plotted on Harker variation diagrams.....	327
B-2. Electron microprobe analyses of igneous rocks plotted as molecular proportions of Na+K, Fe and Mg.....	336
B-3. Electron microprobe analyses of igneous rocks plotted as molecular proportions of Ca, Na and K.....	338
B-4. Electron microprobe analyses of contaminated igneous rocks plotted on Harker variation diagrams.....	347
B-5. Electron microprobe analyses of contaminated igneous rocks plotted as molecular proportions of Na+K, Fe and Mg.....	356
B-6. Electron microprobe analyses of contaminated igneous rocks plotted as molecular proportions of Ca, Na and K.....	360

## LIST OF PLATES

	Page
CHAPTER 2	
1. Photomicrograph of composite feldspar phenocryst in porphyritic gabbro.....	60
CHAPTER 3	
1. Pyroxenite developed at contact between fine-grained gabbro and limestone xenolith.....	69
2. Photomicrographs of products of the reaction CALCITE + PLAGIOCLASE = NEPHELINE + WOLLASTONITE + ANORTHITE + CO <sub>2</sub> .....	71
3. Photomicrographs of products of the reaction OLIVINE + MAGMA = CLINOPYROXENE + MAGNETITE.....	100
CHAPTER 4	
1. Chert and calc-silicate nodules in limestone and marble...	109
2. Zoned calc-silicate nodule collected 15m from intrusive contact.....	116
CHAPTER 5	
1. Idocrase replacement of melilite along fractures in skarn.	171
2. Photomicrographs of partial and complete pseudomorphs of fibrous idocrase after euhedral crystals of melilite.....	174
3. Photomicrograph of replacement of melilite by idocrase along edge of idocrase veinlet in skarn.....	176
4. Photomicrographs of Ti-Zr garnet from skarn.....	196
5. Planar contact between brown melilite skarn and white spurrite skarn.....	253
6. Products of the reaction MONTICELLITE + SPURRITE = MERWINITE + CALCITE.....	264

## LIST OF TABLES

	Page
CHAPTER 1	
1. Sedimentary rocks of Cretaceous age in the Christmas Mountains.....	10
CHAPTER 2	
1. Mode and mineral composition of coarse-grained gabbro.....	28
2. Electron microprobe analyses of clinopyroxene.....	29
3. Mode and mineral composition of fine-grained gabbro.....	56
4. Mode and mineral composition of porphyritic gabbro.....	58
5. Mode and mineral composition of syenite.....	64
CHAPTER 3	
1. Mineral assemblages in syenite.....	74
2. Composition of coexisting nepheline, plagioclase, alkali feldspar and wollastonite in contaminated igneous rocks...	75
3. Electron microprobe analyses of clinopyroxene from pyroxenite.....	79
4. Electron microprobe analyses of clinopyroxene from nepheline syenite.....	80
CHAPTER 4	
1. Mineral assemblages in chert and calc-silicate nodules....	115
2. Mineral reactions in the system $\text{CaO-SiO}_2\text{-CO}_2$ .....	128
3. Physical parameters for heat conduction calculations.....	144
CHAPTER 5	
1. Mineral assemblages in skarn.....	162
2. Electron microprobe analyses of garnet from skarn.....	210
3. Mineral assemblages in skarn of main contact traverse.....	213

## LIST OF TABLES (Continued)

	Page
4. Mineral assemblages in skarn of xenolith traverse.....	214
5. Integrated bulk composition of skarn.....	270
6. Mass balance calculation for growth of skarn - constant volume model.....	284
7. Mass balance calculation for growth of skarn - fixed mass of CaO model.....	286
APPENDIX A	
A-1. Electron microprobe analyses of U.S.G.S. standard granite G-2 (ARL).....	313
A-2. Electron microprobe analyses of U.S.G.S. standard granodiorite GSP-1 (ARL).....	314
A-3. Electron microprobe analyses of U.S.G.S. standard andesite AGV-1 (ARL).....	315
A-4. Electron microprobe analyses of U.S.G.S. standard basalt BCR-1 (ARL).....	316
A-5. Electron microprobe analyses of U.S.G.S. standard granite G-2 (MAC).....	317
A-6. Electron microprobe analyses of U.S.G.S. standard granodiorite GSP-1 (MAC).....	318
A-7. Electron microprobe analyses of U.S.G.S. standard andesite AGV-1 (MAC).....	319
A-8. Electron microprobe analyses of U.S.G.S. standard basalt BCR-1 (MAC).....	320
APPENDIX B	
B-1. Analyzed igneous rocks.....	322
B-2. Electron microprobe analyses of coarse-grained gabbro...	323
B-3. Electron microprobe analyses of fine-grained gabbro.....	324
B-4. Electron microprobe analyses of porphyritic gabbro.....	325
B-5. Electron microprobe analyses of syenite.....	326

## LIST OF TABLES (Continued)

	Page
B-6. Analyzed igneous rocks.....	340
B-7. Electron microprobe analyses of contaminated rocks derived from coarse-grained gabbro.....	344
B-8. Electron microprobe analyses of contaminated rocks derived from fine-grained gabbro.....	345
B-9. Electron microprobe analyses of contaminated rocks derived from porphyritic gabbro.....	346
B-10. Electron microprobe analyses of olivine from igneous rocks.....	360
B-11. Electron microprobe analyses of clinopyroxene from igneous rocks.....	362
B-12. Electron microprobe analyses of amphibole from igneous rocks.....	366
B-13. Electron microprobe analyses of wollastonite from igneous rocks.....	367
B-14. Electron microprobe analyses of biotite from igneous rocks.....	368
B-15. Electron microprobe analyses of ilmenite from igneous rocks.....	370
B-16. Electron microprobe analyses of lamellar ilmenite from igneous rocks.....	372
B-17. Electron microprobe analyses of magnetite from igneous rocks.....	374
 APPENDIX C	
C-1. Analyzed samples from skarn.....	378
C-2. Electron microprobe analyses of melilite and idocrase from skarn.....	380
C-3. Electron microprobe analyses of calc-silicate minerals..	385
C-4. Electron microprobe analyses of orthosilicates from skarn.....	386

## LIST OF TABLES (Continued)

	Page
C-5. Electron microprobe analyses of garnet from skarn.....	387
C-6. Electron microprobe analyses of perovskite and magnetite from skarn.....	391
C-7. Electron microprobe analyses of skarn.....	392
C-8. Spectrographic determination of zirconium in limestone, skarn, pyroxenite, gabbro and syenite.....	396
C-9. Electron microprobe and spectrographic analyses of limestone.....	397

## INTRODUCTION

Rock units made up of a series of sharply bounded mineral zones, each consisting of a relatively small number of phases developed at the contact between chemically dissimilar rocks, commonly are interpreted as being metasomatic in origin. Working models to aid in the interpretation of the origin of metasomatic rocks have taken two forms, one based on the application of Gibbs phase rule to the mineral assemblage of each zone in an effort to determine the number of components whose chemical potentials were controlled by their initial concentration and the number whose potentials were controlled external to the local system (Korzhinskii, 1949; 1950, p. 50-52; 1959, p. 17-18; Thompson, 1959), the other based on an analysis of the compatibility relationships between mineral assemblages of adjacent zones in an effort to distinguish between the transport mechanisms of diffusion and infiltration (Korzhinskii, 1970). Although the phase rule with the boundary conditions proposed by Korzhinskii provides a powerful test of specific models for metasomatic growth, its application to petrologic systems has been criticized by Weill and Fyfe (1964, 1967; see also replies by Korzhinskii, 1966, 1967 and by Thompson, 1970) because the simple counting of phases cannot be used to uniquely determine the variance of a system whose composition has changed through time, without independent information about the path leading from the initial to the final state of the system.

The purpose of this thesis is to examine a suite of rocks which on the basis of field relationships are of unquestioned metasomatic origin in order to determine the nature and scale of chemical exchange and equilibration. Calc-silicate rocks were chosen for study because mineral assemblages in them are very sensitive to small differences both in bulk composition and in the environmental variables of pressure, temperature and fluid phase composition, while the composition of individual mineral phases are quite simple. By study of calc-silicate skarn developed at an intrusive contact, it is possible to examine both the products of metasomatism and the initial reactants, unaffected by reaction. Thus, one can construct a growth model, based on knowledge of the initial and final states of the system, against which to critically test the criteria proposed by Korzhinskii for the identification and interpretation of metasomatic rocks.

The locality chosen for this study, in the Christmas Mountains in the Big Bend Region of Texas, consists of a composite stock of alkaline gabbro and syenite that intruded the core of a small anticlinal mountain range. The zoned calc-silicate skarn developed in limestone at the intrusive contact and in xenoliths within the gabbro is similar in many respects to the skarn at Crestmore, California described by Burnham (1959) but it is simpler both in its mineralogy and structural setting. Alkaline pyroxenite, of magmatic origin, separates gabbro from skarn along the entire length of the intrusive contact and forms rims on skarn xenoliths. The

pyroxenite and its alkali-rich differentiates are mineralogically similar to those at Scawt Hill and Camas Mor that resulted from the assimilation of limestone by basaltic magma (Tilley, 1952; Tilley and Harwood, 1931). The consistent spatial association of contaminated igneous rocks and zoned calc-silicate skarn both in the Christmas Mountains and at the localities described by Burnham and by Tilley, suggests that the processes of limestone assimilation and metasomatic growth of skarn are both part of a single reaction process involving magma and limestone.

The thesis consists of five parts:

- (1) Geologic description of the western part of the Christmas Mountains to provide stratigraphic and structural control on the carbonate rocks involved in metasomatism and assimilation and to determine the sequence and mechanism of emplacement of the igneous rocks.
- (2) Brief petrographic and chemical description of gabbroic and syenitic rocks to provide a basis for comparison of normal evolutionary trends of rock and mineral compositions in uncontaminated igneous rocks with those resulting from the solution of limestone by gabbroic magma.
- (3) Petrographic and chemical study of contaminated igneous rocks to determine the steps in the derivation of pyroxenite and nepheline syenite from gabbro magma by assimilation of limestone. It will be shown that the mineral assemblages of pyroxenite and skarn may be derived by reaction between limestone and magma saturated with plagioclase and clinopyroxene.

- (4) Graphical analysis of mineral assemblages in zoned calc-silicate nodules from the contact aureole that were derived by reaction between nodular chert and enveloping limestone to determine conditions of P, T and  $X_{\text{CO}_2}$  during metamorphism and to derive a general model for the growth of zoned calc-silicate skarn by reaction between incompatible phases and consequent diffusion.
- (5) Petrographic and chemical study of mineral assemblages in zoned calc-silicate skarn developed both at the intrusive contact and in a large marble xenolith gabbro to determine compatibility relationships between mineral assemblages of adjacent zones, compare gradients in composition of solid solutions and bulk rock across a skarn band and to test the local equilibrium hypothesis and reaction-diffusion model for the metasomatic growth of the skarn.

## 1. GEOLOGY OF THE WESTERN PART OF THE CHRISTMAS MOUNTAINS

## GEOLOGIC SETTING

The Christmas Mountains include an elliptical dome of Cretaceous sedimentary rocks which dip radially away from a core of intrusive gabbro centered near the northwest end of the range. The sedimentary section exposed on the flanks of the dome consists of massively bedded limestones of the Early Cretaceous Comanchean Series, which are disconformably overlain by a sequence of thin-bedded limestone, shale, fluvio-marine sandstone and bentonitic clay of the Late Cretaceous Gulfian Series. In basins flanking the range, the Cretaceous rocks are overlain by terrigenous conglomerate, sandstone and clay of Tertiary age which are interbedded with pyroclastic units and lava flows.

The Christmas Mountains lie at the center of the "Sunken Block", a graben 50 to 65 km in width, with 1200 to 1800 meters of structural relief, bounded on the east by the Sierra del Carmen and on the west by the Terlingula Fault and Solitario Uplift. Faults and fold axes within the Sunken Block trend north-northwest, parallel to the boundary faults. The anticlinal axis and normal fault system in the Christmas Mountains parallel this trend.

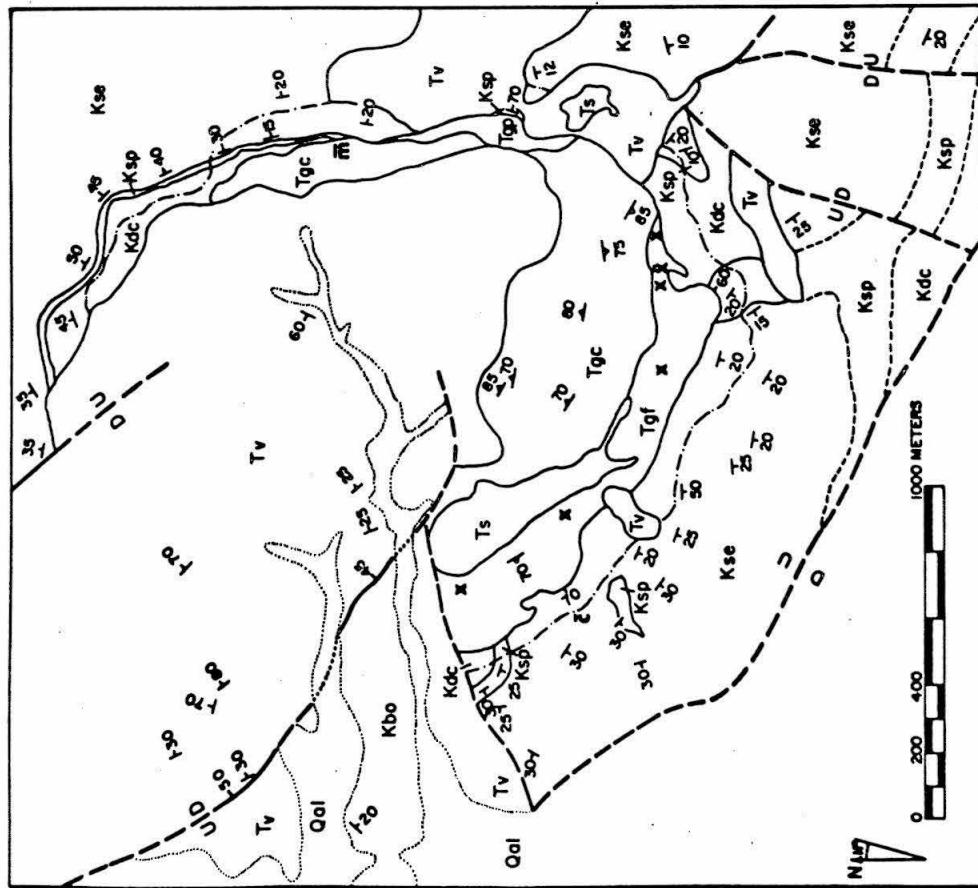
Hundreds of shallow intrusions and extrusions of alkaline igneous rocks pierce the graben floor. The igneous rocks, part of the Late Cretaceous and Early Tertiary alkaline igneous province of West Texas, can be subdivided into a critically undersaturated gabbro-syenite suite, members of which occur primarily as concordant sills and laccoliths, and a suite of peralkaline trachyandesites, trachytes and rhyolites, which occur mainly in discordant plugs and

stocks and as pyroclastic units. The gabbro and syenite intrusives in the Christmas Mountains belong to the first suite.

R. R. Bloomer (1949) mapped the geology of the northwestern part of the Christmas Mountains, including the gabbro complex, at a scale of 1:62500 and R. A. Maxwell (Maxwell, Lonsdale, Hazzard and Wilson, 1967) mapped the southeastern flank at the same scale. S. E. Clabaugh (1953) described the contaminated igneous rocks and the calc-silicate skarn developed at the contact between gabbro and limestone. W C Swadley (1958) and E. C. Jenkins (1959) made a detailed plane table map of the contact of the gabbro with the limestone along the eastern margin of the intrusion at a scale of 1:1200. However, because Bloomer's mapping was not sufficiently detailed and Swadley and Jenkins's map included only half of the exposed length of the gabbro-limestone contact, the gabbro complex and surrounding rocks were remapped in the present study. An enlargement of a single aerial photograph (U. S. Army Map Service photograph 26777) was used as a base for mapping at a scale of about 1:18000 (Figure 1).

Figure 1. Geologic map of the western part of the Christmas Mountains, Big Bend Region, Texas.

GEOLOGY OF THE WESTERN CHRISTMAS MOUNTAINS, BIG BEND REGION, TEXAS



- |   |   |
|---|---|
| <span style="border: 1px solid black; padding: 2px;">Qal</span> | ALLUVIUM  |
| <span style="border: 1px solid black; padding: 2px;">Tv</span>  | INTRUSIVE, EXTRUSIVE AND VOLCANOCLASTIC ROCKS     |
| <span style="border: 1px solid black; padding: 2px;">Ts</span>  | AUGITE SYENITE                                    |
| <span style="border: 1px solid black; padding: 2px;">Tgf</span> | FINE-GRAINED BIOTITE-TITANAUGITE GABBRO           |
| <span style="border: 1px solid black; padding: 2px;">Tgp</span> | PORPHYRITIC BIOTITE-OLIVINE-TITANAUGITE GABBRO    |
| <span style="border: 1px solid black; padding: 2px;">Tgc</span> | COARSE-GRAINED OLIVINE-BIOTITE-TITANAUGITE GABBRO |
| <span style="border: 1px solid black; padding: 2px;">Kbo</span> | BOQUILLAS FORMATION                               |
| <span style="border: 1px solid black; padding: 2px;">Kse</span> | SANTA ELENA LIMESTONE                             |
| <span style="border: 1px solid black; padding: 2px;">Ksp</span> | SUE PEAKS FORMATION                               |
| <span style="border: 1px solid black; padding: 2px;">Kdc</span> | DEL CARMEN LIMESTONE                              |
| $\phi$  | ATTITUDE OF BEDDING                               |
| $\rho$  | ATTITUDE OF FOLIATION IN GABBRO                   |
| $\overline{D}$  | STRATIGRAPHIC OR INTRUSIVE CONTACT                |
| $\frac{45}{70}$   | FAULT   |
| $\frac{45}{70}$   | OUTER LIMIT OF MARBLE ZONE                        |
| x   | SKARN XENOLITH                                    |

GEOLOGY BY RAYMOND JOESTEN

## STRATIGRAPHY AND LITHOLOGY OF THE SEDIMENTARY ROCKS

Stratigraphic units that crop out in the Christmas Mountains are listed, with their approximate thickness, in Table 1 (Bloomer, 1949 and Maxwell et. al., 1967). A comprehensive discussion of the Cretaceous stratigraphy of the Big Bend Region is given by Maxwell and Hazzard (Maxwell et. al., 1967, p. 28-96). Only the Del Carmen, Sue Peaks and Santa Elena Formations occur in intrusive contact with rocks of the gabbro complex, so the discussion of stratigraphy and lithology will be limited to rocks of these formations.

## Del Carmen Limestone

The Del Carmen Limestone is a thick-bedded to massive, microcrystalline limestone that is dark-gray to black on a fresh surface and medium-gray where weathered. The black color is probably due to the presence of finely divided carbonaceous matter, uniformly distributed through the rock. On recrystallization to marble, it is redistributed in streaky bands, giving the rock a gray and white striped appearance. Black chert occurs locally in discontinuous, tabular, masses a few centimeters in thickness but as much as two meters in length, that lie parallel to bedding.

## Sue Peaks Formation

Maxwell and Hazzard (Maxwell et. al., 1967, p. 40) have defined the Sue Peaks Formation as "the soft lithostratigraphic unit that forms a slope separating the sheer escarpments formed by the Del Carmen Limestone below from the Santa Elena Limestone above." The type section of the Sue Peaks Formation has been divided into a lower calcareous shale (marl) member, 25 meters in thickness, and an upper

TABLE 1

SEDIMENTARY ROCKS OF CRETACEOUS AGE  
CHRISTMAS MOUNTAINS, TEXAS

Series	Name of Formation	Thickness
GULFIAN	Javelina Formation	260 meters
	Aguja Formation	275 meters
	Pen Formation	215 meters
	Boquillas Formation	245 meters
COMANCHEAN	Buda Limestone	15 meters
	Del Rio Clay	25 meters
	Santa Elena Limestone	930 meters
	Sue Peaks Formation	25 meters
	Del Carmen Limestone	Base not Exposed

thin-bedded limestone and shale member, about 80 meters thick (Maxwell et. al., 1967, p. 41-42). Extensive thermal metamorphism of the Sue Peaks rocks by the gabbro has rendered the slope-forming characteristic of the Sue Peaks Formation of little practical value as a mapping criterion in the Christmas Mountains. However, a 25 meter thick section marked by alternating beds of tan and rusty-brown weathering, argillaceous limestone can be easily distinguished from the massive beds of Del Carmen and Santa Elena limestones and has been mapped as the Sue Peaks Formation. It is probably correlative with the lower shale member at the type Sue Peaks locality.

Rocks of the Sue Peaks Formation, so defined, consist of two lithologic components, a dark-gray, argillaceous microcrystalline limestone that weathers light-gray to tan and a light-gray, argillaceous microcrystalline limestone that weathers rusty-brown and stands out in bold relief from surrounding tan limestone on a weathered surface. The rusty-brown limestone occurs as bands, 2mm to 20 cm in width in the upper 8 meters of the formation. The wide bands are made up of individual, paper-thin lamellae interbedded with tan limestone. In the lower 17 meters of the Sue Peaks section, the rusty-brown limestone occurs as irregular, anastomosing layers enclosing "eyes" of tan limestone giving the rock a "chain-link" texture on weathered surfaces. The ratio of rusty-brown limestone to tan limestone increases upward in the section from about 1:10 in the lower third to 2:1 near the top.

### Santa Elena Limestone

The Santa Elena Limestone is virtually identical to that of the Del Carmen in both stratification and lithology. It differs significantly from it, however, in the character of its nodular chert. Very irregular, branching nodules of black, calcareous chert with a rusty-weathered rind are sparsely distributed throughout the Santa Elena Limestone. Nodules range in size from less than one centimeter to about 20 cm. Although nodular chert is a minor constituent of the formation, in some beds it makes up as much as 20 per cent of the rock. With the exception of nodular chert, the Santa Elena, like the Del Carmen, is made up of relatively pure calcite limestone.

### Boquillas Formation

A fault-bounded slice of Boquillas limestone, extensively intruded by dikes of rhyolite, trachyte and basalt occurs north of Mud Springs Draw. Although baking by the dikes has altered the lithologic character of the rock, it has been correlated with the lower member (Ernst Member) of the Boquillas Formation by the presence of Inoceramus labiatus (Schlotheim) (Maxwell, et. al., 1967, p. 64; Adkins, 1928, p. 94 and Böse 1913, p. 25-28.)

## THE GABBRO COMPLEX

The Christmas Mountains alkaline gabbro complex consists of a series of olivine- and nepheline-normative gabbros and syenites that are discordantly intrusive into limestones of the Del Carmen, Sue Peaks and Santa Elena Formations at the northwestern end of the range. Figure 1 is a geologic map of the gabbro complex and surrounding limestone. Gabbroic rocks crop out in a crescent-shaped body, astride the anticlinal axis of the Christmas Mountains dome. The slender eastern limb of the gabbro outcrop is occupied by a coarse-grained, olivine-biotite-titanaugite gabbro and a porphyritic olivine-biotite-titanaugite gabbro. The coarse-grained gabbro also crops out on the bulbous southwestern limb, where it is separated from limestone by an arcuate body of fine-grained, biotite-titanaugite gabbro, 150 to 250 meters in width. A large, irregular mass of fine-grained to pegmatitic pyroxene syenite has been intruded along the contact between the coarse- and fine-grained gabbros, along much of its length.

Intrusion and crystallization of the gabbroic rocks recrystallized the limestone to marble in a zone 60 to 180 meters in width, parallel to the contact. Gabbro and marble are never in direct contact, however. They are always separated by a zone of alkaline pyroxenite, 0.2 to 6 meters in width, which in turn is separated from marble by a 0.2 to 1 meter wide band of mineralogically-zoned, calc-silicate skarn.

### Intrusive Relationships

Because coarse-grained gabbro is intruded by both fine-grained and porphyritic gabbro and by syenite, it is, by inference, the oldest member of the gabbro complex. Within 50 meters of their contact, the coarse-grained gabbro is cut by a network of small dikes of fine-grained gabbro, proving that the latter is the younger of the two. Although coarse-grained gabbro is massive within 100 m of its contact with fine-grained gabbro, planar alignment of plagioclase laths in the interior of the intrusion imparts a moderately well-developed foliation to the rock that is parallel to the contact with the younger, fine-grained gabbro. The foliation of the interior of the coarse-grained gabbro body probably results from viscous drag on the partially solidified coarse-grained gabbro due to emplacement of the fine-grained gabbro.

The arcuate body of fine-grained gabbro probably was intruded along the contact between coarse-grained gabbro and marble. Several large, marble-cored skarn xenoliths occur in fine-grained gabbro within 75 m of its contact with marble. Mafic schlieren in fine-grained gabbro, found within a few meters of its contact with coarse-grained gabbro may represent relicts of the pyroxenite formed at the original contact between coarse-grained gabbro and marble.

Porphyritic gabbro is exposed in an arcuate mass, 60 to 150 meters in width, intruded into coarse-grained gabbro and marble. Most of the original contact has been removed by intrusions of trachyte and rhyolite which postdate the gabbro complex. However, a dike-like extension of the porphyritic gabbro body, 0.3 to 3 meters wide,

dipping steeply beneath the marble, is exposed along the east limb of the coarse-grained gabbro outcrop. Because there are neither dikes nor xenoliths of one gabbro in the other, the age relationships are based on the observation that porphyritic gabbro is intrusive into pyroxenite and skarn formed as a result of interaction of coarse-grained gabbro with limestone. Intrusion of porphyritic gabbro into pyroxenite and along the contact between skarn and marble is clear evidence that it is younger than the coarse-grained gabbro. The porphyritic and fine-grained gabbros are nowhere in mutual contact, so that relative ages cannot be determined.

Thin dikes of fine-grained titanaugite syenite are intrusive into gabbro of all three types. Syenite dikes of two generations are intrusive into fine-grained gabbro in an embayment into marble at the southeastern end of the complex. The earlier of the two is a coarse-grained olivine-biotite-kaersutite-augite-nepheline syenite. Irregular dikes of fine-grained augite syenite of the second generation enclose numerous angular blocks of fine-grained gabbro and coarse-grained nepheline syenite up to 30 cm across.

A large, arcuate body of kaersutite-titanaugite syenite was intruded along the contact between coarse- and fine-grained gabbro. The syenite ranges in texture from fine-grained to pegmatitic. Where cross-cutting relations are seen, the pegmatitic phase is the younger. Within 5 to 15 meters of the contact, fine-grained gabbro is extensively fractured and intruded by fine-grained syenite. Syenite dikes in the coarse-grained gabbro are rare.

On the basis of cross-cutting relations, the sequence of intrusion in the gabbro complex is: (1) coarse-grained olivine-biotite-titanaugite gabbro, (2a) porphyritic olivine-biotite-titanaugite gabbro, (2b) fine-grained biotite-titanaugite gabbro, (3) coarse-grained olivine-biotite-kaersutite-titanaugite-nepheline syenite and (4) kaersutite-titanaugite syenite.

The present outcrop pattern and the distribution of gabbro xenoliths in trachyandesite breccia suggest that the coarse-grained gabbro was probably intruded into limestone as a cylindrical body about 1400 meters in diameter. Shrinkage of the gabbro mass on solidification would have created a tensional field concentric with the contact, thus providing zones of access along which the arcuate bodies of porphyritic and fine-grained gabbro and of syenite were emplaced.

Although the folding that produced the Christmas Mountains dome probably predated intrusion of the gabbro, gabbro emplacement modified the structure near its contacts. The intrusive contact between gabbro and limestone everywhere dips beneath the latter at a dip of  $60^{\circ}$  or more, making an angle of about  $50^{\circ}$  with the bedding. However, the strike of bedding in the limestone is roughly parallel to the gabbro contact, indicating a doming of the strata during intrusion of the gabbro. The parallelism of the Sue Peaks outcrop pattern to the marble zone north of the gabbro body lends further support to the hypothesis that the original form of the coarse-grained gabbro intrusion was that of a cylinder.

## Pyroxenite

Pyroxenite, developed at the contact between gabbro and limestone which was subsequently transformed to skarn, consists of titanaugite and nepheline with accessory sphene and, in some cases, wollastonite. Characterized by 60 to 90 percent modal titanaugite, pyroxenite is readily distinguished from gabbro, in which clinopyroxene usually amounts to no more than 30 volume percent. The contact between gabbro and pyroxenite is generally sharp, but it is never cross cutting. There are neither dikes nor xenoliths of one rock in the other. Mineralogically similar pyroxenites are developed between each of the three gabbros at contacts with each of the three limestones.

The contact between pyroxenite and skarn, which closely represents the original contact between gabbroic magma and limestone, is everywhere discordant. It dips beneath the marble with a dip of at least  $60^{\circ}$ , truncating bedding in marble that dips away from the intrusion with dips of  $10^{\circ}$  to  $30^{\circ}$ .

Although the contact between nepheline pyroxenite and idocrase-wollastonite skarn is sharp, it has an irregular, undulating form, characterized by sinusoidal to lobate embayments of pyroxenite into skarn. Because mineralogical and textural zonation in the skarn are parallel to the irregularities in the pyroxenite-skarn contact, its present shape must have been established at or shortly after the time of gabbro emplacement. In many cases, embayments in skarn are filled by pyroxenite, the result being a relatively planar gabbro-pyroxenite contact in contrast to the scalloped pyroxenite-skarn contact.

The irregular, but smoothly curved shape of the pyroxenite-skarn contact is suggestive of extensive solution of wallrock by magma, but because their contact is sharp, reaction must have involved limestone rather than skarn. There is, however, a narrow zone at the pyroxenite-skarn contact, 1 to 5 cm in width, in which skarn preserves relict texture of pyroxenite, indicating that exchange and reaction across the contact continued after solidification of the pyroxenite.

Although everywhere mineralogically similar, the thickness of the pyroxenite zone varies both with the local shape of the contact and with the gabbro type from which it was derived. Pyroxenite related to coarse-grained gabbro occurs in a zone averaging 1.5 to 3 meters in thickness, whereas that derived from fine-grained or porphyritic gabbro is seldom more than 20 to 40 cm thick.

Small xenoliths of green idocrase-grossular-wollastonite skarn, 2 to 15 cm across, are quite abundant in the thick pyroxenite zone associated with coarse-grained gabbro, but none have been found in the gabbro itself. The xenoliths range in shape from ellipsoidal to very irregular, branching forms. Within 0.5 meters of the contact, crudely-tabular skarn xenoliths, 5 to 10 cm thick, are aligned parallel to the contact. The presence of skarn xenoliths enclosed in pyroxenite indicates that fragmentation of the wallrock was effective on a local scale during gabbro emplacement. However, their lobate form and smooth, rounded edges offer further evidence of the effectiveness of solution and reaction between carbonate and magma.

Small skarn xenoliths, similar in size, shape and mineralogy to those found in pyroxenite are locally common in the fine-grained

gabbro near the contact with marble. These xenoliths which occur in gabbro are separated from gabbro by a concentric shell of pyroxenite, 1 to 2 cm thick.

There are eight large skarn xenoliths, most 1 to 3 meters in size, but as large as 3 x 13 meters, in the fine-grained gabbro within 75 meters of its contact with marble along the southern margin of the complex. Like the smaller xenoliths in the fine-grained gabbro, skarn is separated from gabbro by a proportionately thick shell of pyroxenite, 0.2 to 1 meter thick. In contrast to the smaller xenoliths, which are made up entirely of idocrase-wollastonite skarn, many of the larger xenoliths are compositionally zoned, with a core of calcite marble, surrounded by concentric shells characterized by the minerals, spurrite, melilite and in contact with pyroxenite, idocrase.

In further contrast to the small xenoliths, which are restricted in occurrence to a zone quite close to the marble, the large xenoliths are not only found as much as 75 meters from the nearest contact, but in one case, show evidence for vertical transport of similar magnitude. A skarn xenolith, exposed on the southeastern flank of the peak with an elevation of 1590 meters (4881 feet), has a core of marble which preserves the distinctive thin-bedded tan and rusty-brown weathering, argillaceous limestone characteristic of the upper part of the Sue Peaks Formation. Projection of the Santa Elena-Sue Peaks contact into the gabbro at this point demonstrates that this xenolith has been carried upward about 100 meters by the gabbro magma.

Gabbro and skarn are never in direct contact, but are always separated by a zone of pyroxenite. That the pyroxenite is magmatic in origin rather than representing the innermost zone of skarn developed in limestone, is clearly demonstrated by pyroxenite dikes that are intruded into skarn in the large xenoliths. Because pyroxenite probably represents an accumulation of titanite precipitated from gabbroic magma in response to reaction with limestone, the pyroxenite dikes were probably emplaced as a crystal mush. However, fine-grained dike borders against skarn look like chilled margins and suggest the possibility that a significant proportion of the titanite in the dikes crystallized directly from a pyroxenite magma.

Dikes of calcic nepheline syenite with accessory sphene, wollastonite and rarely, andradite and perovskite, are intrusive into both pyroxenite and skarn in xenoliths and at the main contact. Such calcic nepheline syenite dikes may represent either a differentiate of pyroxenite magma or the alkali-rich residue squeezed out of a titanite crystal mush.

#### Skarn

Calc-silicate skarn occurs in a band, 0.1 to 1 meter in width, that everywhere separates pyroxenite developed from the interaction of gabbroic magma with marble, from the marble itself. It is found all along the contact between rocks of the gabbro complex with the enclosing marble and as rims on large, marble-cored xenoliths in the fine-grained, biotite-titanite gabbro. Skarn also occurs in small, ellipsoidal to lobate xenoliths found both in pyroxenite derived from

coarse-grained, olivine-titanaugite gabbro and in fine-grained gabbro where the xenoliths are enveloped by a thin shell of pyroxenite.

The most widely developed skarn mineral assemblages consist of either melilite or idocrase and one or two of the phases wollastonite, rankinite, spurrite and calcite. Titanian-zirconian garnet, perovskite and magnetite are ubiquitous accessory phases. Zonation of mineral assemblages across a band of skarn results from the presence of wollastonite in the zone in contact with pyroxenite, rankinite with either wollastonite or spurrite in the middle of the skarn band and of spurrite in the zone in contact with marble. Although this mineralogic zonation is inconspicuous in the field, two and locally three distinct mineralogic zones can be recognized in most skarn outcrops. In sequence from pyroxenite to marble, these zones consist of green idocrase skarn, brown melilite skarn and, in contact with marble, white spurrite skarn. The boundaries between these zones do not, in general, coincide with those of the calc-silicate zones. The contact between the green skarn and brown skarn marks the outer limit of hydration of melilite to form idocrase. It usually occurs within the wollastonite zone. However, idocrase, pseudomorphous after melilite, occurs locally throughout the skarn, usually developed along fractures. The contact between the brown skarn and the white skarn, which records a sharp decrease in the modal abundance of melilite, invariably occurs within either the spurrite or spurrite-calcite zones. In most exposures along the main intrusive contact and in

smaller xenoliths, replacement of melilite by idocrase is complete, and the zone of brown skarn does not occur.

Within 20 meters of the gabbro contact, mineral assemblages identical to those of the melilite and spurrite-calcite skarn zones are developed across silica- and alumina-rich beds of the Sue Peaks Formation. The symmetry of the mineral zonation in these beds as well as the fact that they are separated from one another and from the main skarn by beds of relatively pure calcite marble, shows that skarn mineral assemblages may result from metamorphism of impure limestone. However, proof that the mineralogic zonation in skarn is the result of metasomatic introduction of material from gabbro, rather than the isochemical metamorphism of a bedded sediment, is demonstrated by the observations that (1) the sequence of mineral zones is the same in skarns formed from the relatively pure limestones of the Del Carmen and Santa Elena Formations and from rocks of the impure, compositionally variable Sue Peaks Formation, (2) the zoning is parallel to the pyroxenite contact which is discordant to bedding in marble and (3) mineralogy and sequences of zones are the same on all sides of marble-skarn xenoliths enclosed by gabbro.

#### POST-GABBRO IGNEOUS ROCKS

The western part of the Christmas Mountains remained as a center of igneous activity after emplacement of the rocks of the gabbro complex. Post-gabbro igneous rocks consist of a suite of extrusive and near-surface intrusive rocks that range in composition from basalt through trachyandesite and peralkaline trachyte to rhyolite. Within the eastern part of the map area shown in Figure 1,

Swadley (1958) and Jenkins (1959) identified 9 intrusive rock units and worked out relative age relations between them. The sequence of intrusion, from oldest to youngest is:

- I. Sill-like intrusions parallel to gabbro-marble contact, along eastern margin of gabbro complex.
  1. Rhyolite
  2. Peralkaline trachyandesite
- II. Stocks, centered at southeastern margin of gabbro complex.
  3. Porphyritic trachyandesite
  4. Syenite
  5. Rhyolite
- III. Stocks with radial dike swarms, intruded along northern and western margins of present gabbro outcrop.
  6. Porphyritic basalt
  7. Trachyandesite breccia
  8. Peralkaline trachyte
  9. Porphyritic olivine basalt

No attempt has been made in this study to extend detailed mapping of the post-gabbro igneous rocks beyond the area mapped by Swadley (1958) and Jenkins (1959).

Although several of the post-gabbro igneous rocks are intrusive into limestone, there is no evidence for reaction between any of the magmas with limestone and no skarn has been found at any of their contacts with limestone.

## 2. PETROLOGY OF THE GABBRO COMPLEX

### INTRODUCTION

Igneous rocks of the Christmas Mountains alkaline gabbro complex consist of olivine- and nepheline- normative gabbro and syenite. Nepheline seldom appears in the mode, however. Its presence in the norms reflects the high aluminum content of the clinopyroxene and magnetite. Ferromagnesian and oxide phases of the igneous rocks are characterized by high titanium contents. Three types of gabbro were distinguished in the field on the basis of textural differences and cross-cutting intrusive relationships. The volumetrically important rock types are, in order of emplacement:

- (1) coarse-grained olivine-biotite-titanaugite gabbro
- (2) porphyritic olivine-biotite-titanaugite gabbro
- (3) fine-grained biotite-titanaugite gabbro
- (4) pyroxene syenite

Although the three gabbro types are composed of essentially the same minerals, with similar compositions, rocks of each group have distinctly different bulk compositions. A petrographic and chemical study was made of the gabbroic and syenitic rocks in order to compare normal evolutionary trends of rock and mineral composition with those resulting from the interaction of gabbroic magma with limestone.

In order to understand the sequence of reactions between gabbroic magma and limestone that lead to the formation of pyroxenite and calcic nepheline syenite, it is necessary to know the mineral assemblages characteristic of gabbro and syenite, the compositions of

solid solutions involved in the reactions and the phases in which each magma was saturated or supersaturated on emplacement.

Bulk chemical compositions of individual samples of igneous rocks were determined by electron microprobe analysis of glass discs made by fusing equal parts by weight of pulverized rock and lithium tetraborate at 1000°C in carbon crucibles in an electric muffle furnace. Sample preparation and analytical methods as well as tests for precision and accuracy are described in Appendix A. A list of igneous rocks analyzed, with mineral assemblages and approximate modes, is given in Table B-1 (Appendix B). Bulk compositions and norms of rocks from the gabbro complex are listed in Tables B-2 through B-5 and are portrayed graphically on a set of Harker diagrams in Figure B-1 and on triangular AFM and Ca-Na-K diagrams in Figures B-2 and B-3.

Mineral compositions were determined by electron microprobe analysis of the phases, in situ, in polished thin sections. Mean values for mineral compositions in igneous and contaminated igneous rocks are listed in Tables B-10 through B-17.

#### COARSE-GRAINED OLIVINE-BIOTITE-TITANAUGITE GABBRO

Coarse-grained olivine-biotite-titanaugite gabbro is characterized by a sub-ophitic intergrowth of plagioclase and titanaugite, with alkali feldspar and analcite, when present, occupying angular interstices between plagioclase laths. The average grain-size is 2 to 8 mm. Mafic silicate and oxide phases tend to occur together in polyphase aggregates. Although olivine commonly is in contact with titanaugite, it is never completely enclosed by it. The most common textural habit of biotite is as rims on iron-titanium oxide grains.

The probable sequence of the beginning of crystallization of the phases is olivine, plagioclase, Fe-Ti oxide, titanaugite, alkali feldspar, biotite. An averaged mode and mineral compositions for coarse-grained gabbro are listed in Table 1.

Clinopyroxene from coarse-grained gabbro is characterized by moderately strong optical absorption and pleochroism. The pleochroic scheme is X=Z=rose, Y=yellow. Pyroxene commonly is zoned, with the absorption of the rim greater than that of the core. Zone boundaries are sharp and planar.

Compositional characteristics of titanaugite are summarized in Table 2, and on Figures 1a, 2a and 3a. The proportions of the pyroxene molecules listed in Table 2 and plotted on Figure 1 were computed by the normative procedure outlined by Kushiro (1962). The main compositional variation in titanaugite from coarse-grained gabbro is in the relative proportions of aluminum, titanium and silicon. Although the concentrations of Al and Ti vary, the ratio Al/Ti is approximately a constant (Figure 2a). The concentration of aluminum and, by analogy, that of titanium, vary inversely with the formula proportion of silicon in clinopyroxene (Figure 3a). There is a consistent excess of aluminum over that needed to balance the tetrahedral silicon deficiency. The strongly absorbing zone of titanaugite has a ratio of  $(Al+Ti)/Si$  that is greater than that in the weakly absorbing zone. The range of variation in the ratio  $(Fe+Mn)/(Fe+Mn+Mg)$  is small and the median values of this ratio are identical for clinopyroxene from each of the three gabbro types (Table 2).

Iron-titanium oxide phases occur as composite grains of titanian magnetite and ilmenite. Ilmenite occurs both as irregularly bounded, optically homogeneous regions within the composite oxide grains and as lamellae, generally 1 to 4 but as much as 20 microns in width, oriented along (111) of the host magnetite. The concentrations of magnesium and manganese are essentially identical in homogeneous and lamellar ilmenite (Tables B-15 and B-16) but the lamellar phase is very slightly enriched in the hematite component, computed by the scheme of Buddington and Lindsley (1964). Magnesium and manganese are concentrated in ilmenite relative to magnetite, while aluminum is strongly fractionated to magnetite. Although the composition of coexisting magnetite and lamellar ilmenite varies from sample to sample, the conditions of subsolidus oxidation, determined with the curves of Buddington and Lindsley (1964) are consistently in the range 680 to 750°C and  $10^{-17}$  to  $10^{-19}$  bars oxygen fugacity.

Biotite is strongly pleochroic, with X=yellow-brown and Y=Z=deep red to deep red-brown. Biotite has a uniform titanium content of 0.9 atoms per formula unit of 16 cations. The main compositional variable in biotite is the ratio  $Fe/(Fe+Mg)$  which ranges between 0.29 and 0.54. Although biotite forms rims on Fe-Ti oxide grains, there is no consistent pattern of zonation in Fe or Ti.

Plagioclase shows both normal and oscillatory zoning. The range of compositional variation of feldspar from two samples of coarse-grained gabbro are shown on Figures 4a and 4b.

TABLE 1

AVERAGE MODE AND MINERAL COMPOSITION OF  
COARSE-GRAINED OLIVINE-BIOTITE-TITANAUGITE GABBRO

2%	Olivine	$FO_{57}FA_{43}-FO_{50}FA_{50}$
25%	Titanaugite	$Ca_{0.88}Na_{0.04}Mg_{0.73}Fe_{0.28}Mn_{0.01}Ti_{0.06}Al_{0.16}Si_{1.85}O_6$
2%	Biotite	$K_{1.78}Na_{0.17}Ca_{0.01}(Mg,Fe)_{5.0}Mn_{0.02}Ti_{0.89}Al_{2.54}Si_{5.57}(O,OH)_{24}$
7%	Opaque	Magnetite USP- $USP_{45}$ Exsolved Ilmenite $HEM_2-HEM_3$ Homogeneous Ilmenite $HEM_2-HEM_3$
60%	Plagioclase	$AN_{68}AB_{31}OR_1 - AN_{37}AB_{60}OR_3$
3%	Alkali Feldspar	$AN_3AB_{44}OR_{53}$
1%	Apatite	

TABLE 2

ELECTRON MICROPROBE ANALYSES OF CLINOPYROXENE CHRISTMAS MOUNTAINS, BIG BEND REGION, TEXAS									
FORMULA PROPORTION OF CATIONS (MEDIAN VALUES)									
	Ca	Na	Mg	Fe	Mn	Al	Ti	Si	O
Cg	0.88	0.04	0.73	0.28	0.01	0.16	0.06	1.85	6
Fg	0.90	0.04	0.73	0.30	0.01	0.08	0.03	1.90	6
Pg	0.88	0.05	0.73	0.29	0.01	0.12	0.04	1.89	6
Sy	0.89	0.08	0.46	0.56	0.02	0.06	0.01	1.92	6
PROPORTION PYROXENE MOLECULES									
Cg	WO <sub>45</sub> EN <sub>41</sub> FS <sub>14</sub>						AC <sub>9</sub> DI <sub>68</sub> HED <sub>23</sub>		
Fg	WO <sub>46</sub> EN <sub>40</sub> FS <sub>14</sub>						AC <sub>9</sub> DI <sub>67</sub> HED <sub>24</sub>		
Pg	WO <sub>46</sub> EN <sub>40</sub> FS <sub>14</sub>						AC <sub>11</sub> DI <sub>66</sub> HED <sub>23</sub>		
Sy	WO <sub>47</sub> EN <sub>25</sub> FS <sub>28</sub>						AC <sub>15</sub> DI <sub>40</sub> HED <sub>45</sub>		
RANGE OF VARIATION IN CATION PROPORTIONS									
	$\frac{(Fe+Mn)}{(Fe+Mn+Mg)}$	Median	Al	Ti	Al/Ti				
Cg	0.24-0.34	0.29	0.06-0.27	0.02-0.09	2.7				
Fg	0.25-0.37	0.29	0.04-0.18	0.02-0.03	3.2				
Pg	0.19-0.39	0.29	0.04-0.39	0.01-0.11	3				
Sy	0.48-0.67	0.56	0.05-0.04	0.05-0.04	4				

- Cg Median or range of 90 point analyses of clinopyroxene from coarse-grained gabbro
- Fg Median or range of 43 point analyses of clinopyroxene from fine-grained gabbro
- Pg Median or range of 68 point analyses of clinopyroxene from porphyritic gabbro
- Sy Median or range of 23 point analyses of clinopyroxene from syenite

- Figure 1. Electron microprobe analyses of clinopyroxene from igneous rocks plotted on pyroxene quadrilateral. Proportion of end-member molecules computed by the normative scheme of Kushiro (1962).
- a. 90 point analyses from coarse-grained gabbro
  - b. 43 point analyses from fine-grained gabbro
  - c. 68 point analyses from porphyritic gabbro
  - d. 23 point analyses from syenite

1a

MOLLASTONITE

CHRISTMAS MOUNTAINS IGNEOUS ROCKS--CARRRO-CG

1.000E 02 ♦

8.000E 01 ♦

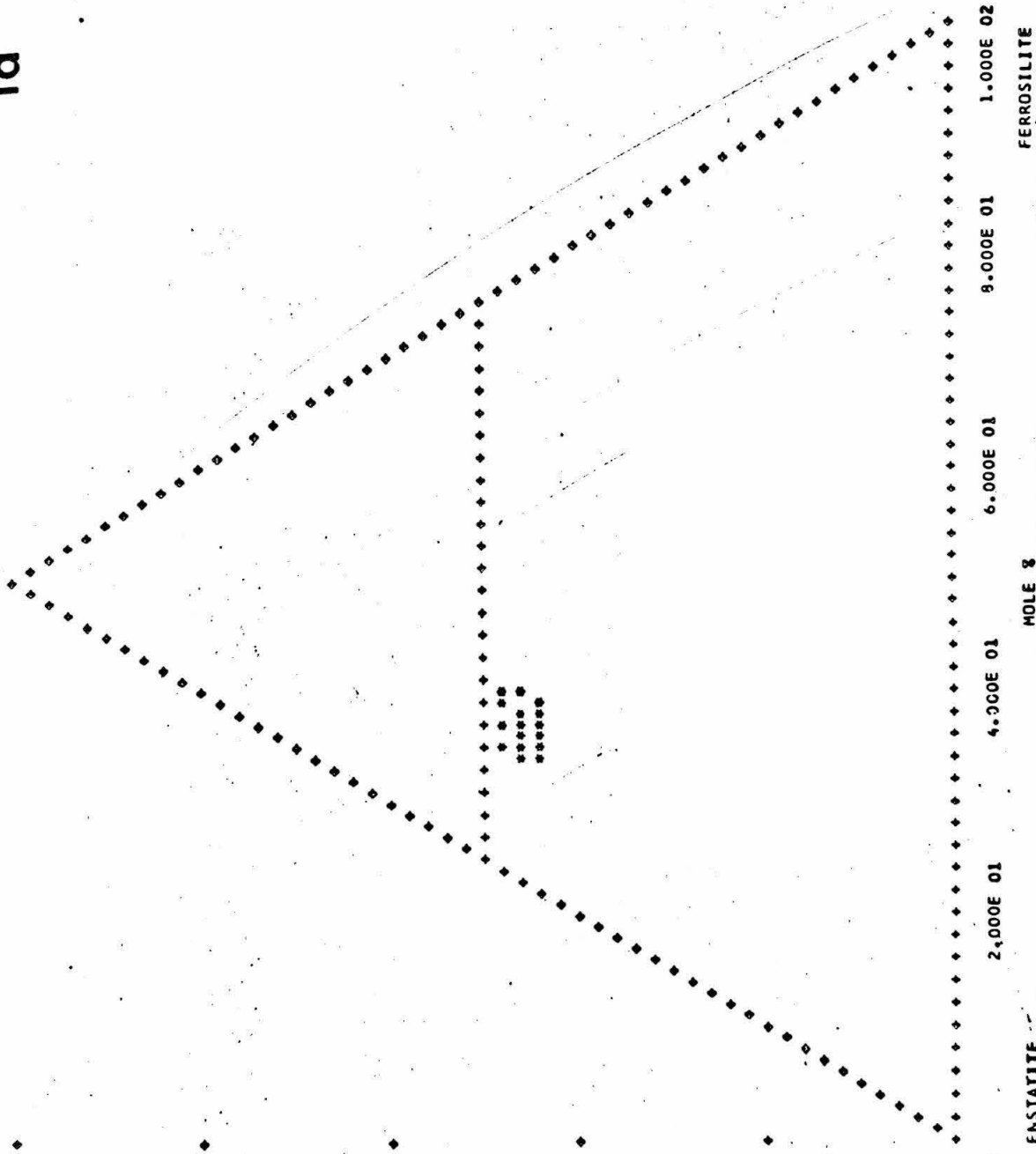
6.000E 01 ♦

4.000E 01 ♦

2.000E 01 ♦

0.0

W/P= 0 0.0

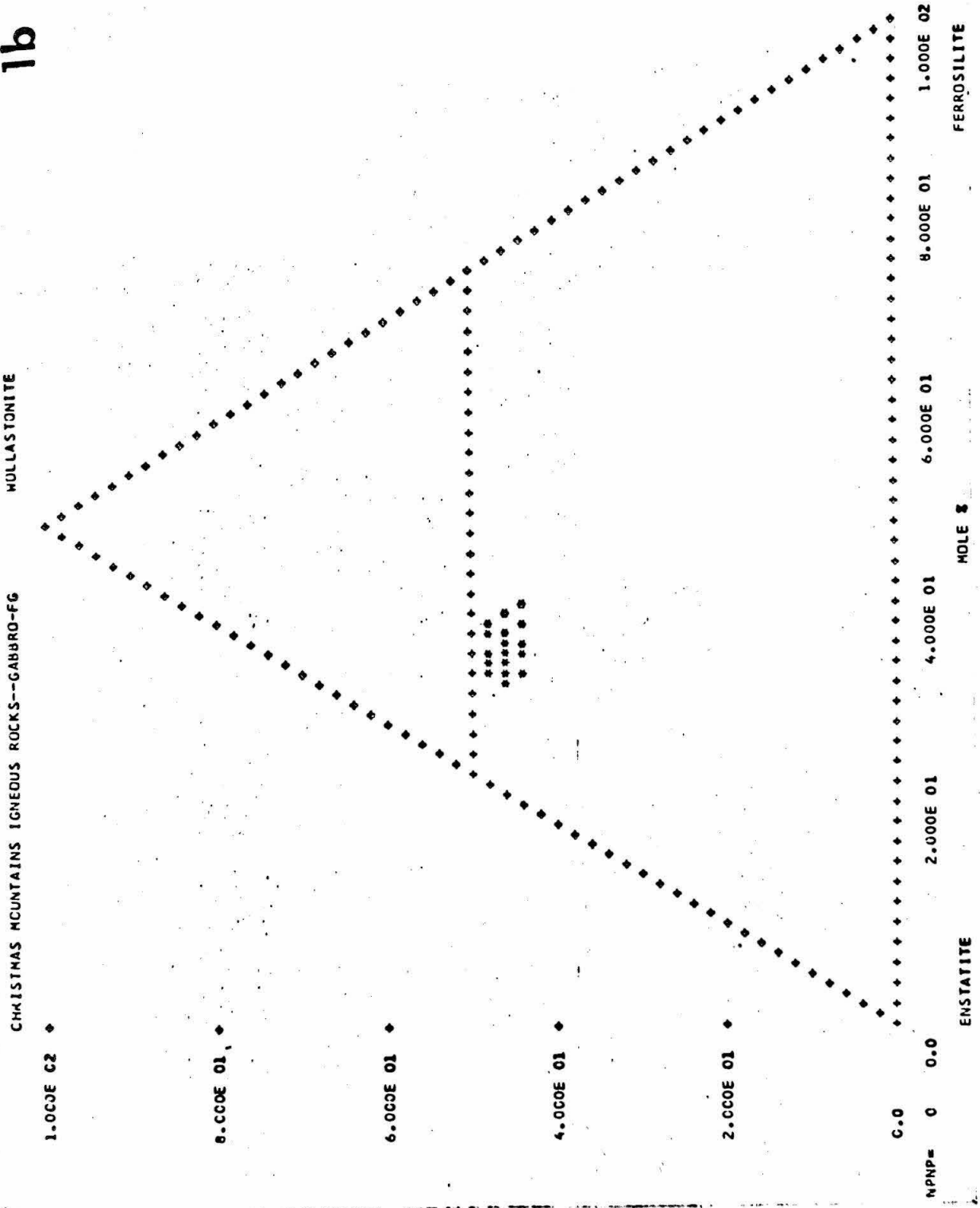


ENSTATITE

MOLE %

FERROSILITE

1b



1c

MOLLASTONITE

CHRISTMAS MOUNTAINS IGNEOUS ROCKS--PLAG PORPHYRY

1.000E 02 ◆

8.000E 01 ◆

6.000E 01 ◆

4.000E 01 ◆

2.000E 01 ◆

0.0

MNP# 0 0.0

ENSTATITE

2.000E 01

4.000E 01

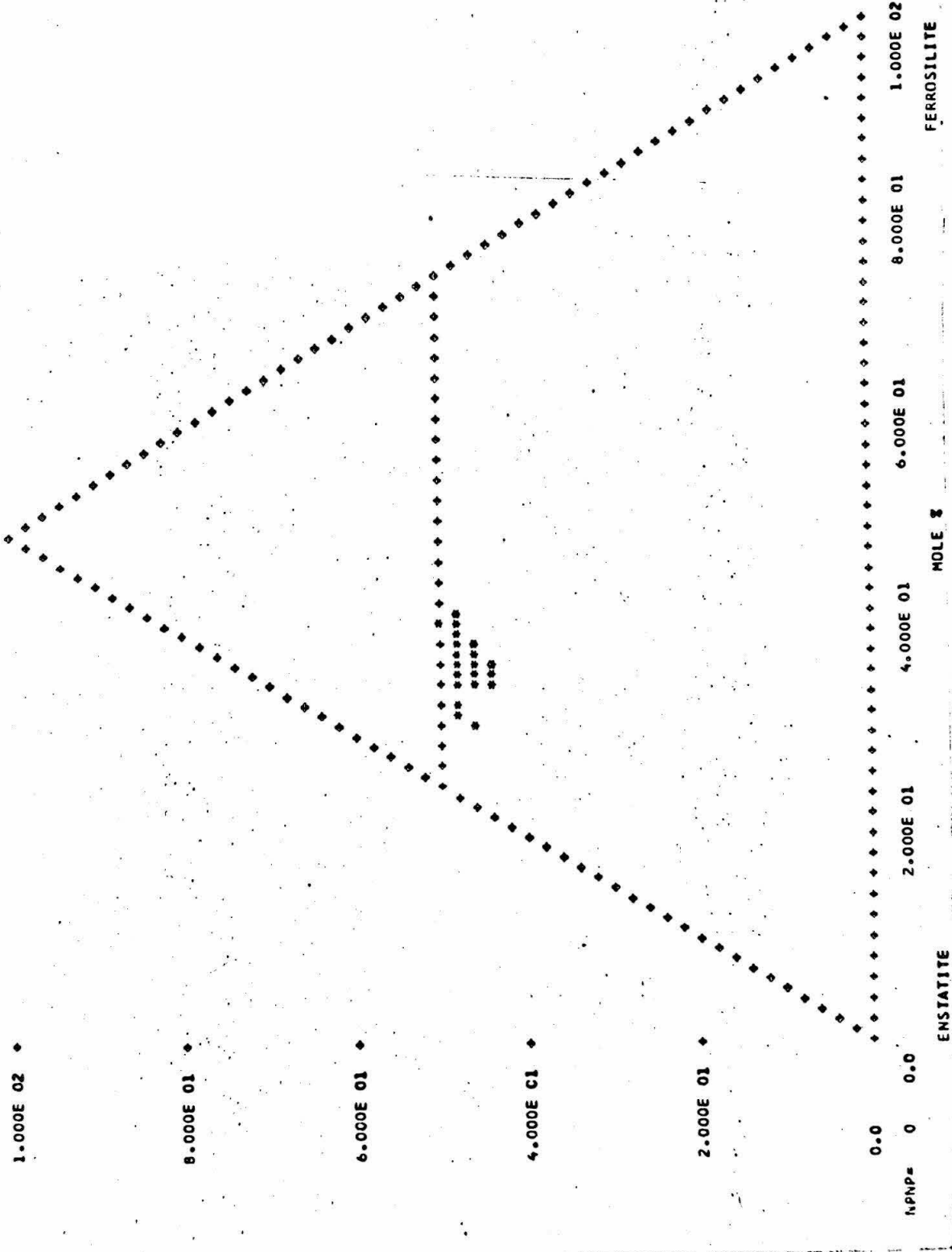
6.000E 01

8.000E 01

1.000E 02

MOLE %

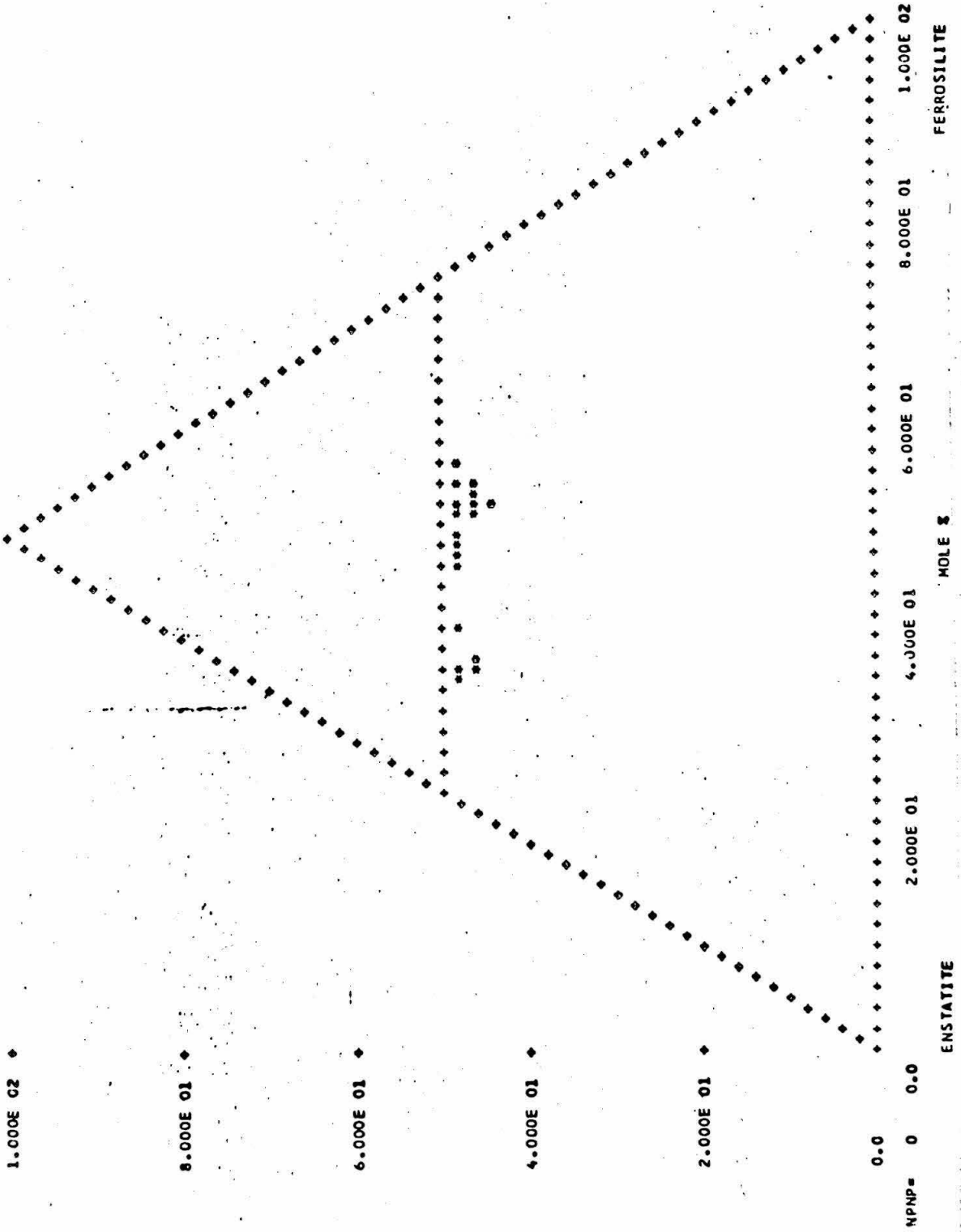
FERROSILITE



1d

CHRISTMAS MOUNTAINS IGNEOUS ROCKS--SYENITE

MOLLASTONITE



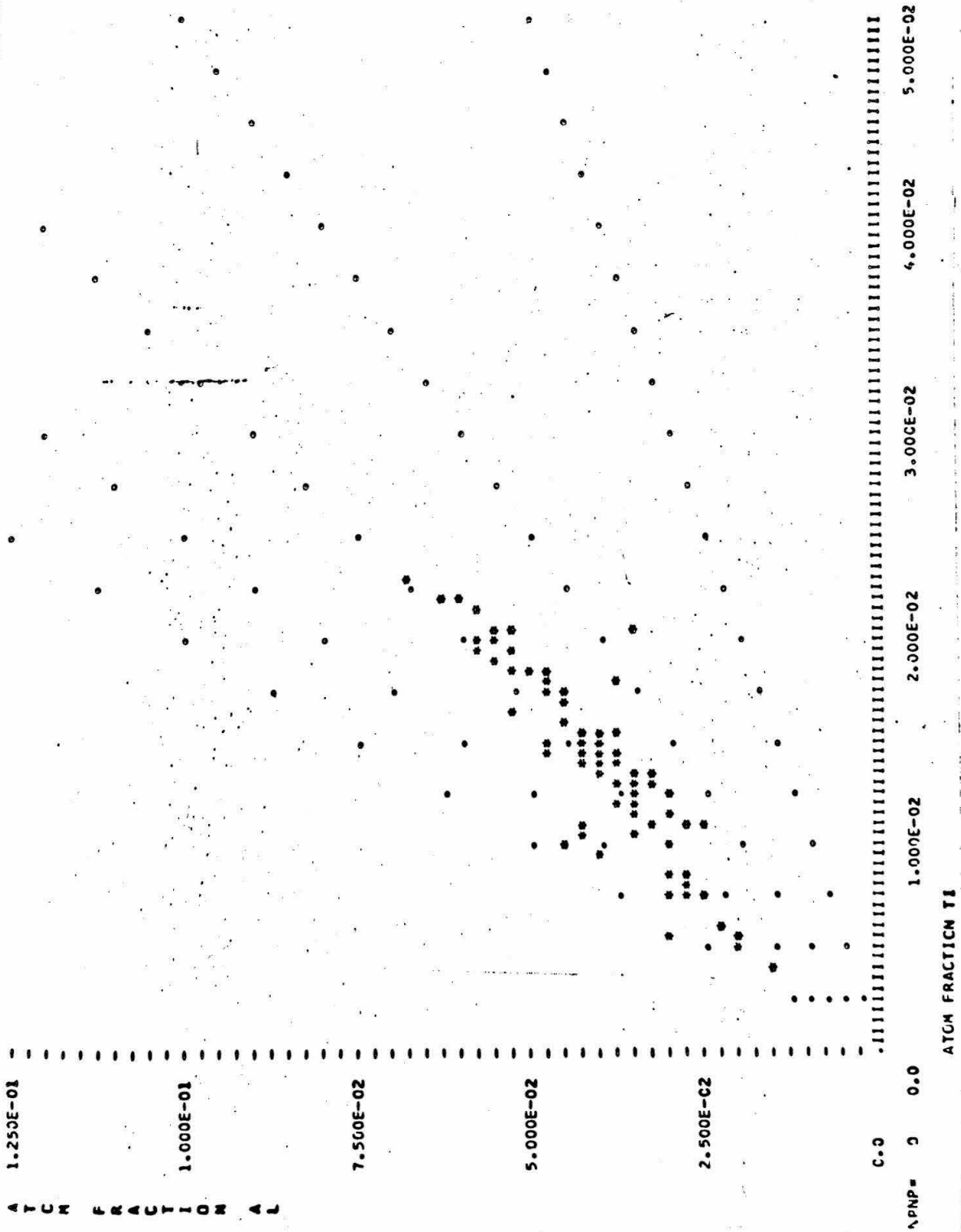
MPNP= 0 0.0

Figure 2. Electron microprobe analyses of clinopyroxene from igneous rocks. Atomic fraction aluminum plotted against atomic fraction titanium. Points which plot along a straight line that passes through the origin have the same ratio of Al/Ti. Dotted lines represent Al/Ti of 1, 2, 3, 4, and 5.

- a. 90 point analyses from coarse-grained gabbro
- b. 43 point analyses from fine-grained gabbro
- c. 68 point analyses from porphyritic gabbro
- d. 23 point analyses from syenite

2a

CHRISTMAS MOUNTAINS IGNEOUS ROCKS--GABBRO-CG



1.250E-01

1.000E-01

7.500E-02

5.000E-02

2.500E-02

C-0

ATCM FRACTION T

1.000E-02

2.000E-02

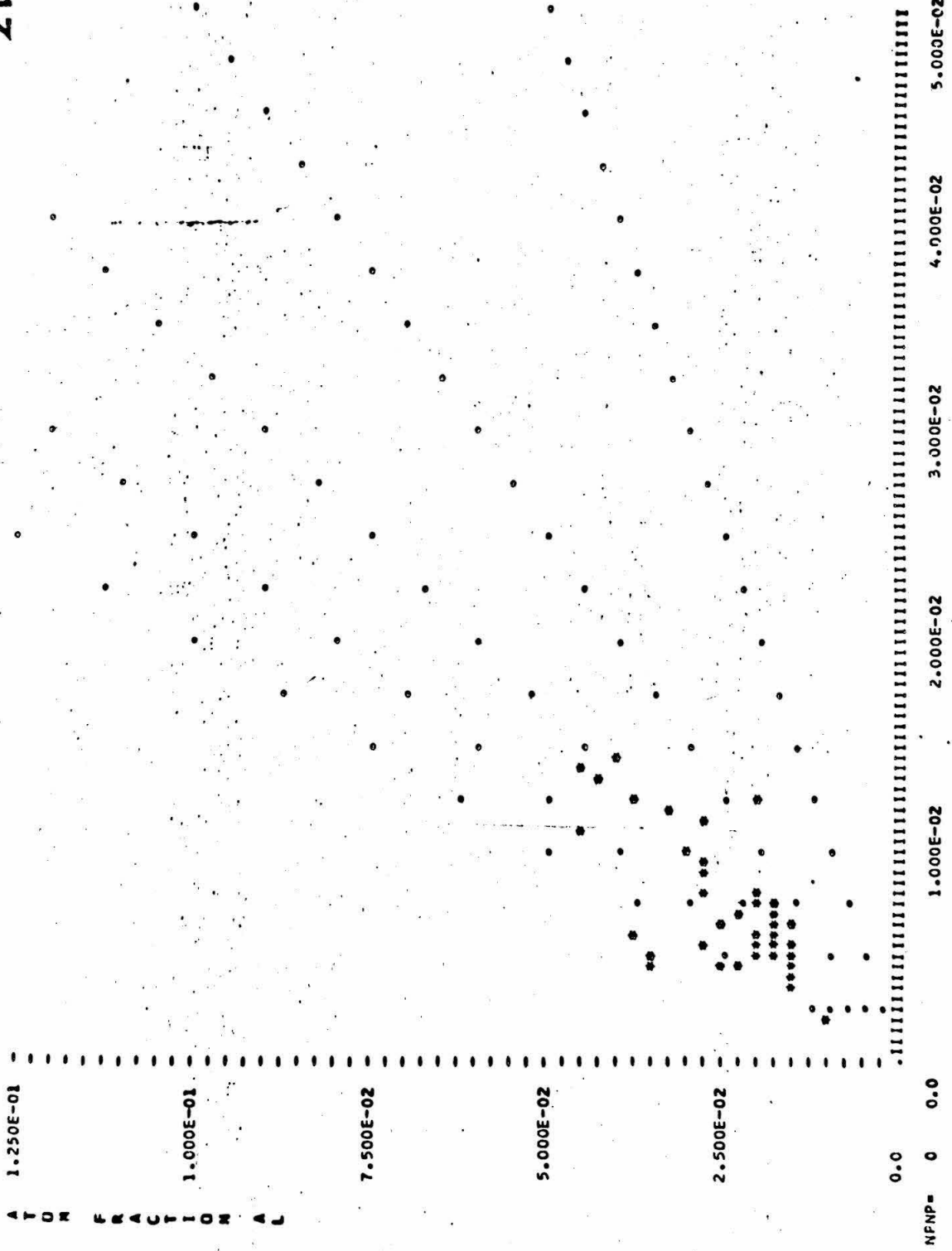
3.000E-02

4.000E-02

5.000E-02

2b

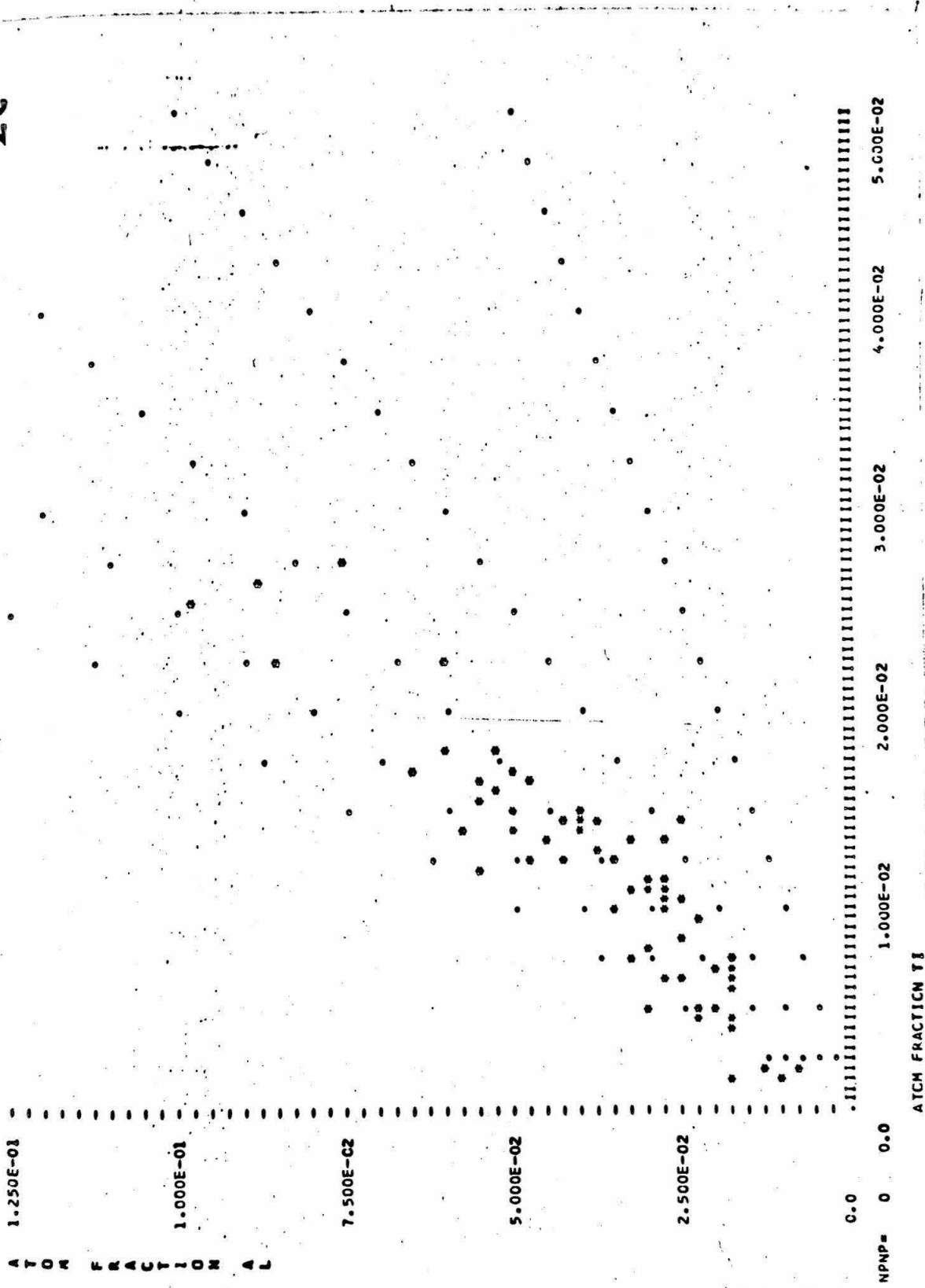
CHRISTMAS MOUNTAINS IGNEOUS RIXKS--CABBRU-FG



NFP= 0 0.0

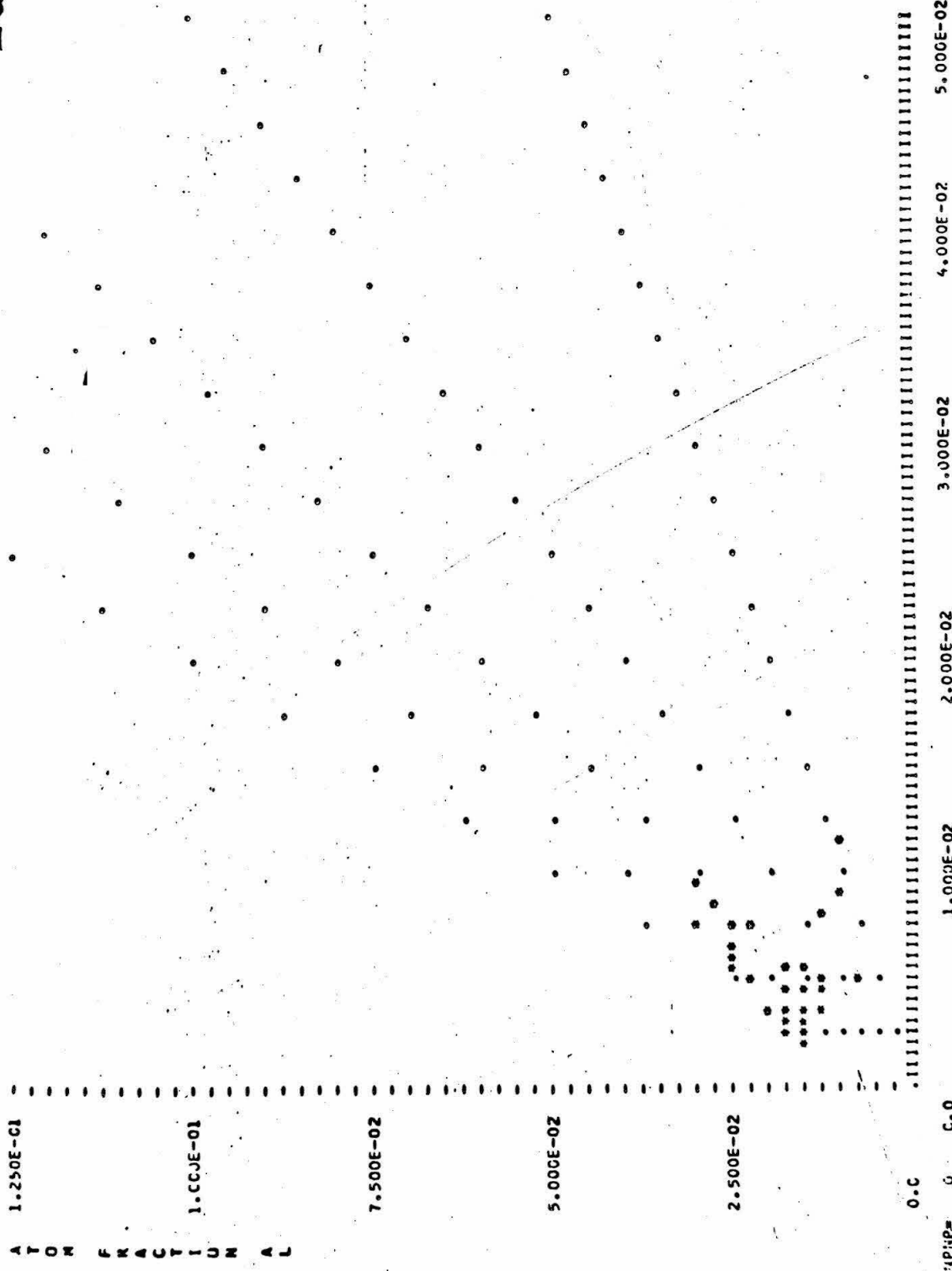
2c

CHRISTMAS MOUNTAINS IGNEOUS ROCKS---PLAGIOCLASE PORPHYRY



2d

CHRISTMAS MOUNTAINS IGNEOUS ROCKS



1.250E-01

1.000E-01

7.500E-02

5.000E-02

2.500E-02

0.0

1.000E-02

2.000E-02

3.000E-02

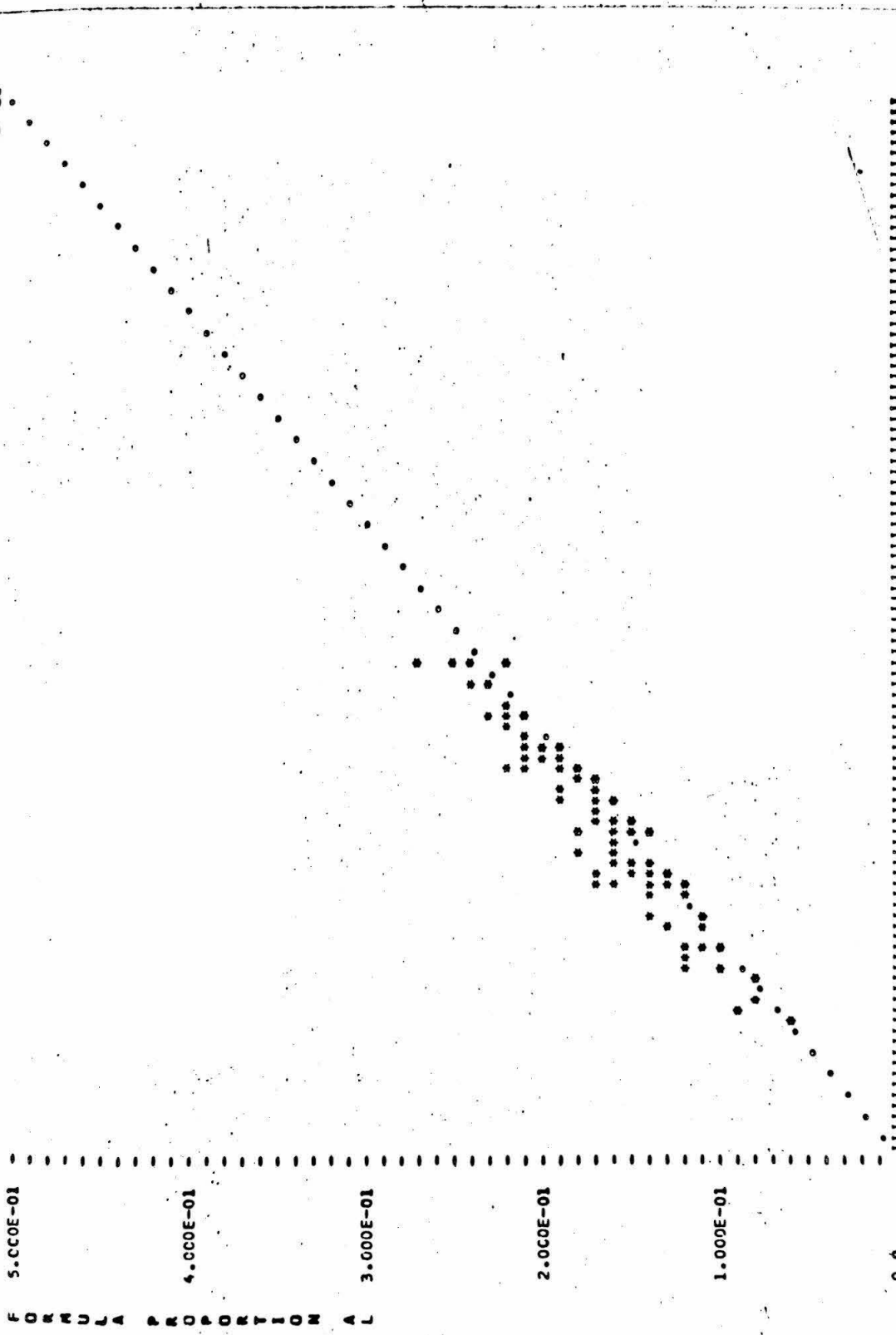
4.000E-02

5.000E-02

- Figure 3. Electron microprobe analyses of clinopyroxene from igneous rocks, formula proportion aluminum plotted against tetrahedral silicon deficiency, defined as 2.0 minus the formula proportion of silicon, for a mineral formula based on 4.0 cations.
- a. 90 point analyses from coarse-grained gabbro
  - b. 43 point analyses from fine-grained gabbro
  - c. 68 point analyses from porphyritic gabbro
  - d. 23 point analyses from syenite

3a

CHRISTMAS MOUNTAINS IGNEOUS ROCKS--GABBRO-CG



FORMULA PROPORTION

5.000E-01

4.000E-01

3.000E-01

2.000E-01

1.000E-01

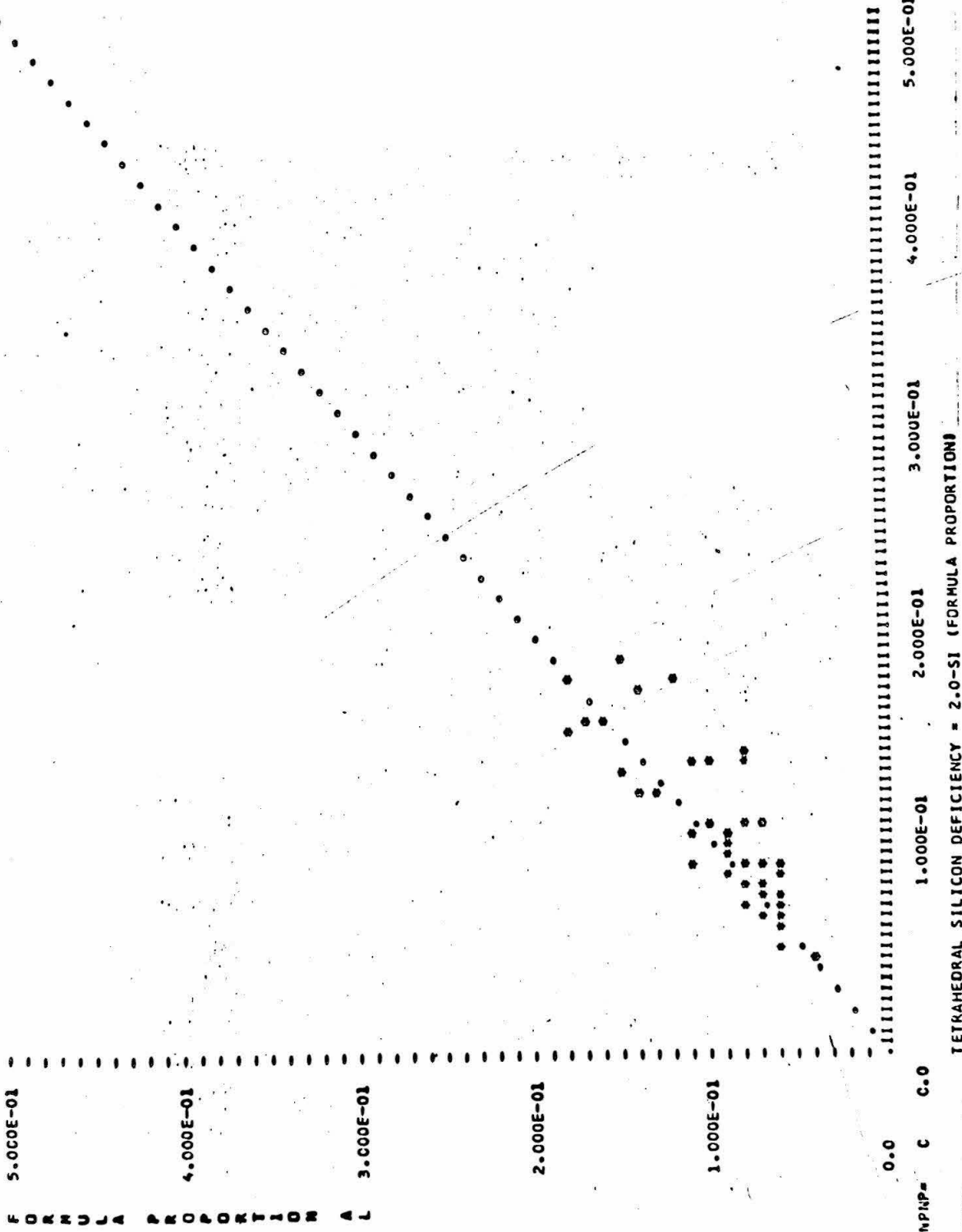
0.0

TETRAHEDRAL SILICON DEFICIENCY = 2.0-SI (FORMULA PROPORTION)

0.0 1.000E-01 2.000E-01 3.000E-01 4.000E-01 5.000E-01

3b

CHRISTMAS MOUNTAINS IGNEOUS ROCKS--GABBR0-f6

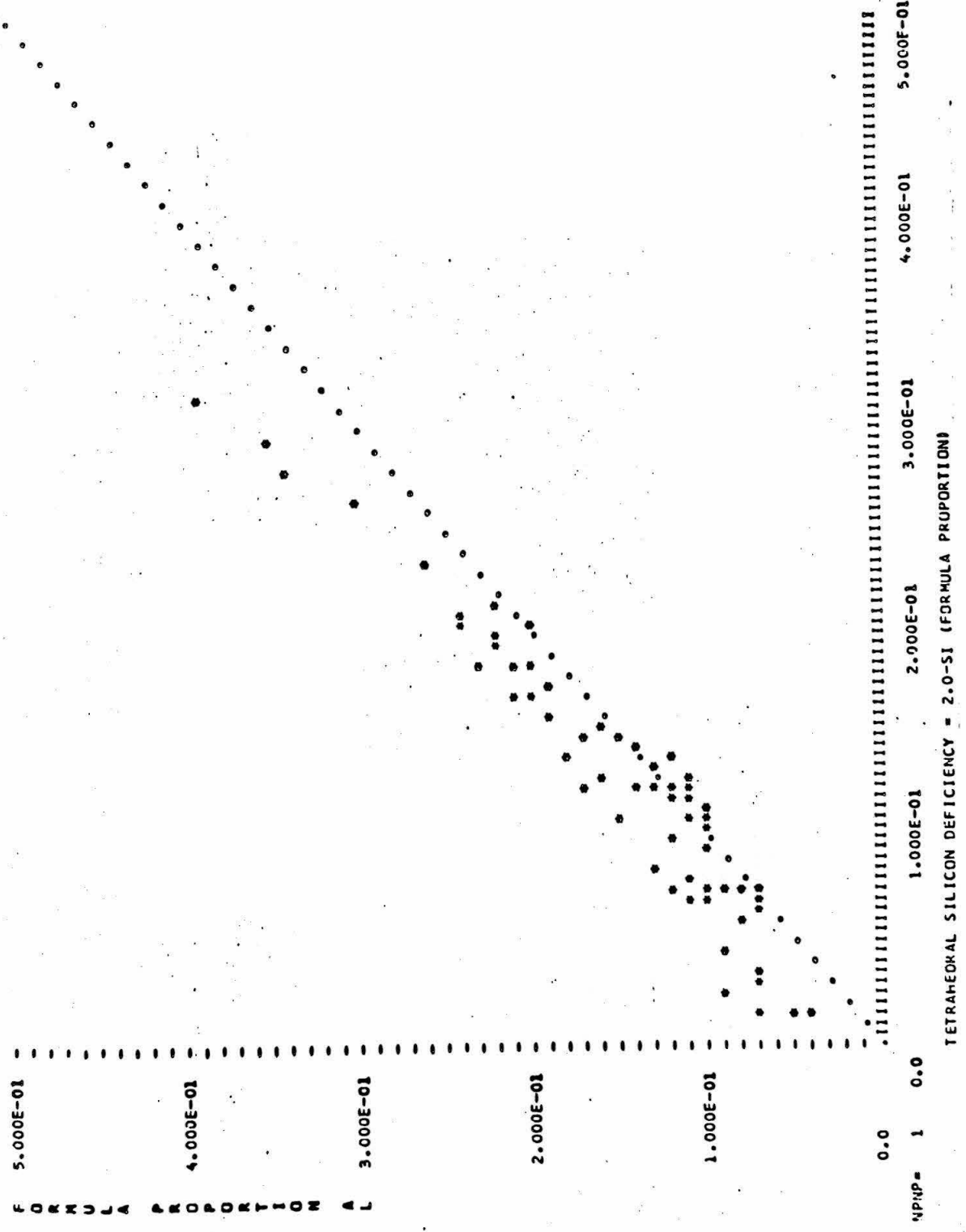


F 5.000E-01  
 O  
 R  
 M  
 U  
 J  
 A  
 P 4.000E-01  
 R  
 O  
 P  
 O  
 R  
 T  
 I  
 O  
 N  
 A 3.000E-01  
 L

NPMP= C C.O  
 0.0 1.000E-01 2.000E-01 3.000E-01 4.000E-01 5.000E-01

3c

CHRISTMAS MOUNTAINS IGNEOUS ROCKS---PLAGIOCLASE PORPHYRY



5.000E-01

4.000E-01

3.000E-01

2.000E-01

1.000E-01

0.0

MPNP= 1 0.0

1.000E-01

2.000E-01

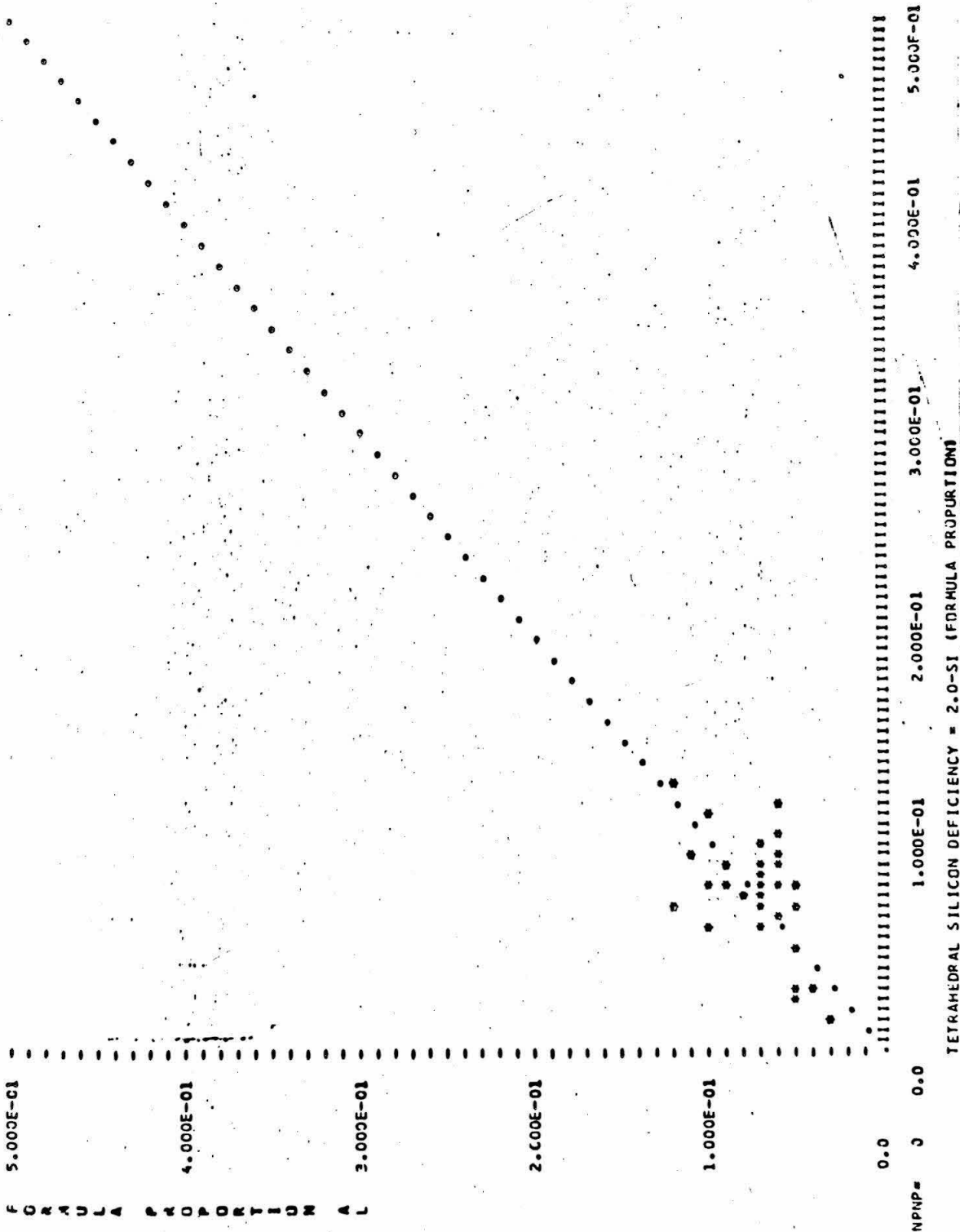
3.000E-01

4.000E-01

5.000E-01

3d

CHRISTMAS MOUNTAINS IGNEOUS ROCKS--SYENITE



5.000E-01

4.000E-01

3.000E-01

2.000E-01

1.000E-01

0.0

NPMP# 0 0.0

1.000E-01

2.000E-01

3.000E-01

4.000E-01

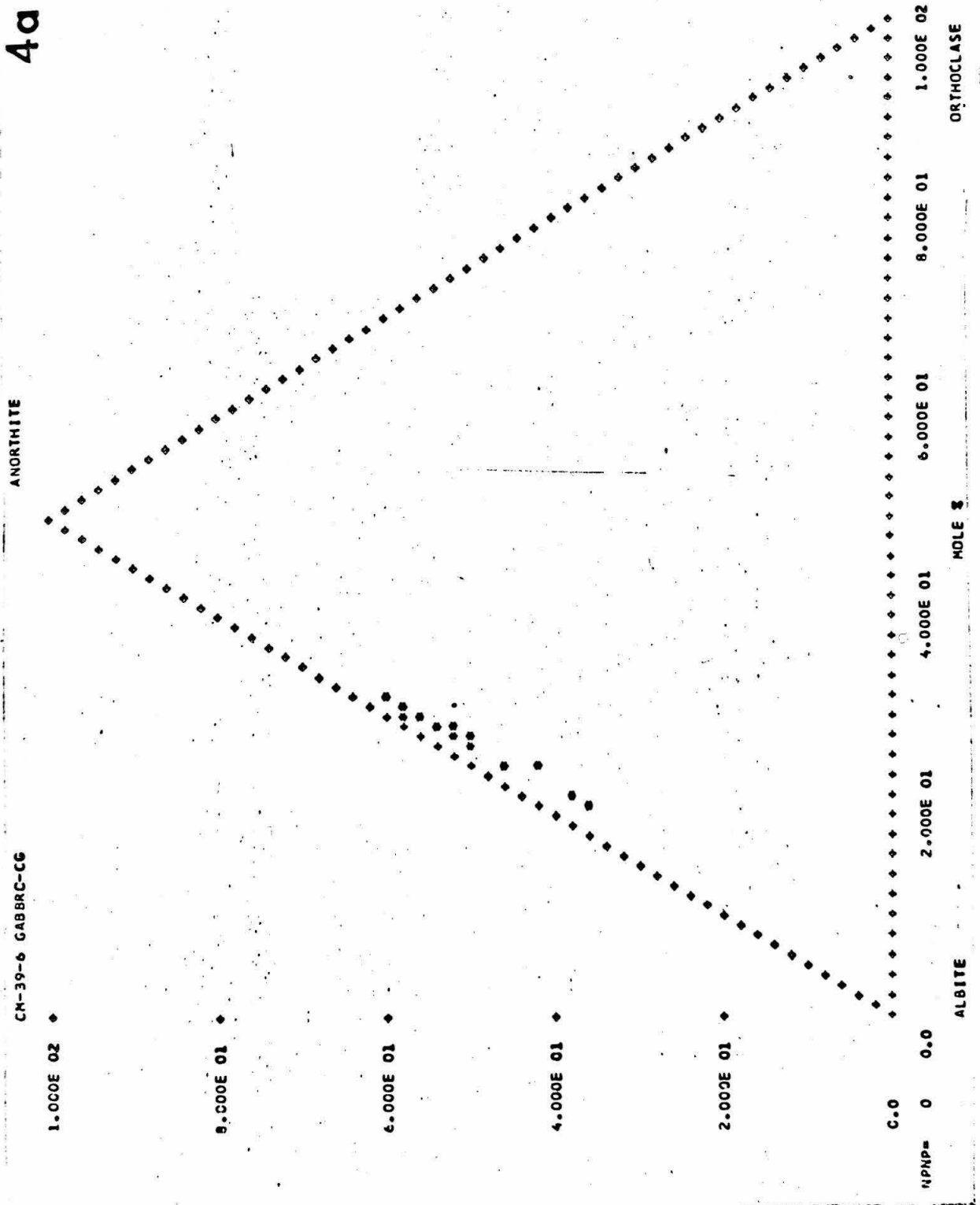
5.000E-01

F O R M U L A P R O P O R T I O N A L

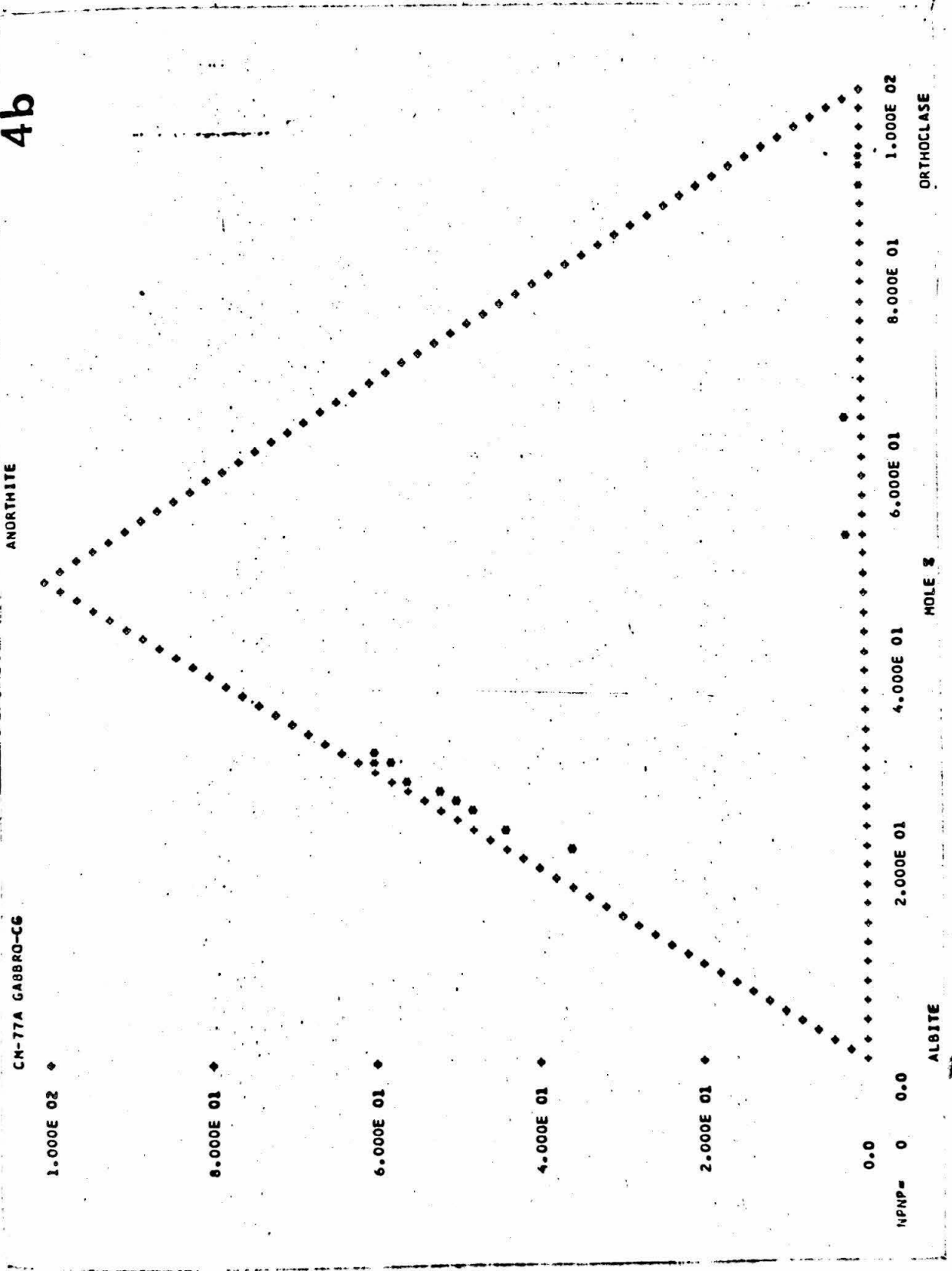
TETRAHEDRAL SILICON DEFICIENCY = 2.0-SI (FORMULA PROPORTION)

- Figure 4. Electron microprobe analyses of feldspar from igneous rocks.
- a. 23 point analyses from coarse-grained gabbro, CM-39-6
  - b. 29 point analyses from coarse-grained gabbro, CM-77A
  - c. 9 point analyses from fine-grained gabbro CM-109-5
  - d. 19 point analyses from fine-grained gabbro CM-136
  - e. 22 point analyses from fine-grained gabbro CM-276
  - f. 58 point analyses from porphyritic gabbro CM-39-1
  - g. 63 point analyses from porphyritic gabbro CM-69
  - h. 19 point analyses from syenite CM-81
  - i. 27 points analyses from syenite CM-294A

4a



4b



4c

ANORTHITE

CM-109-5 GABBRD-FG

1.000E C2 ♦

8.000E 01 ♦

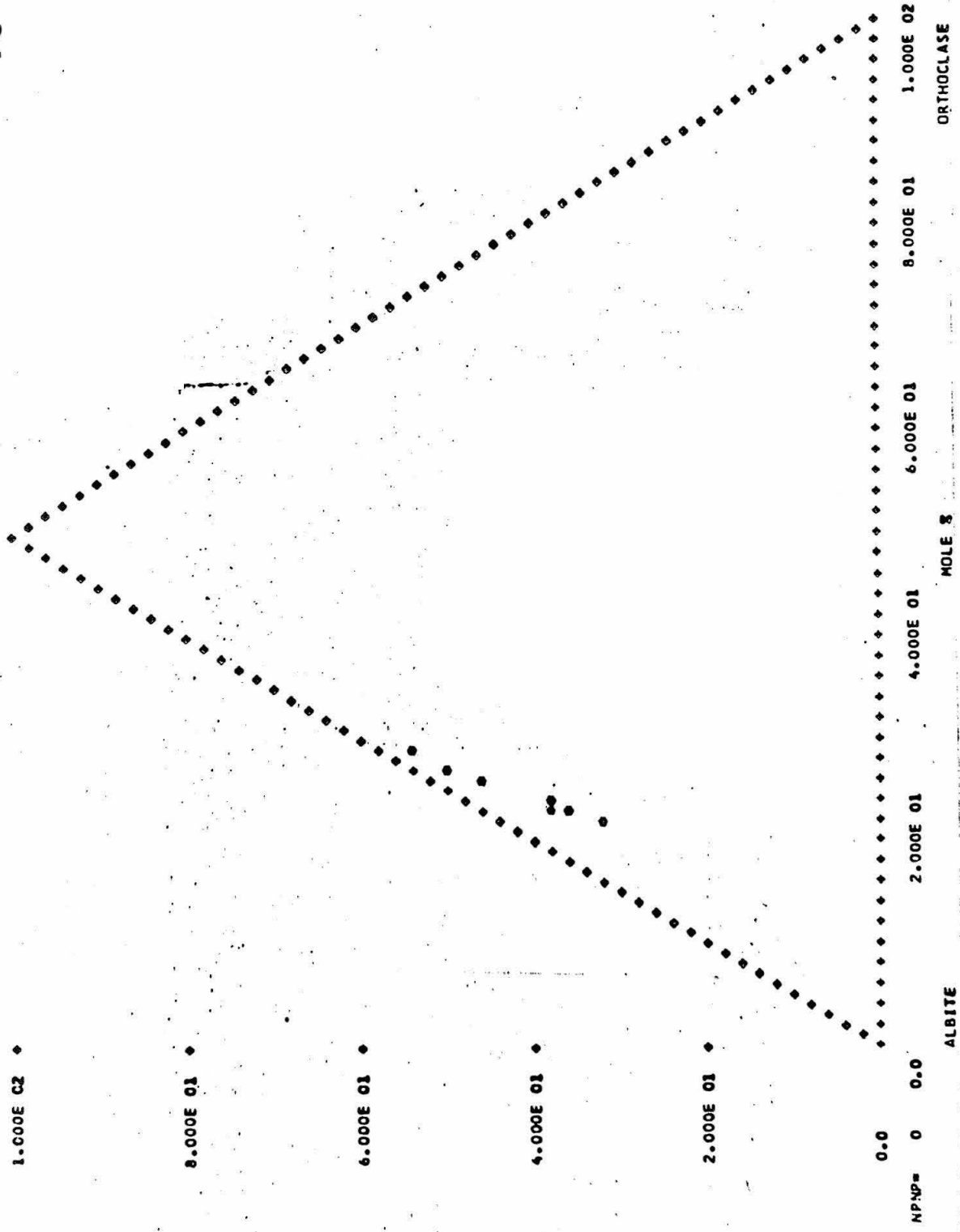
6.000E 01 ♦

4.000E 01 ♦

2.000E 01 ♦

0.0

MP:MP= 0 0.0

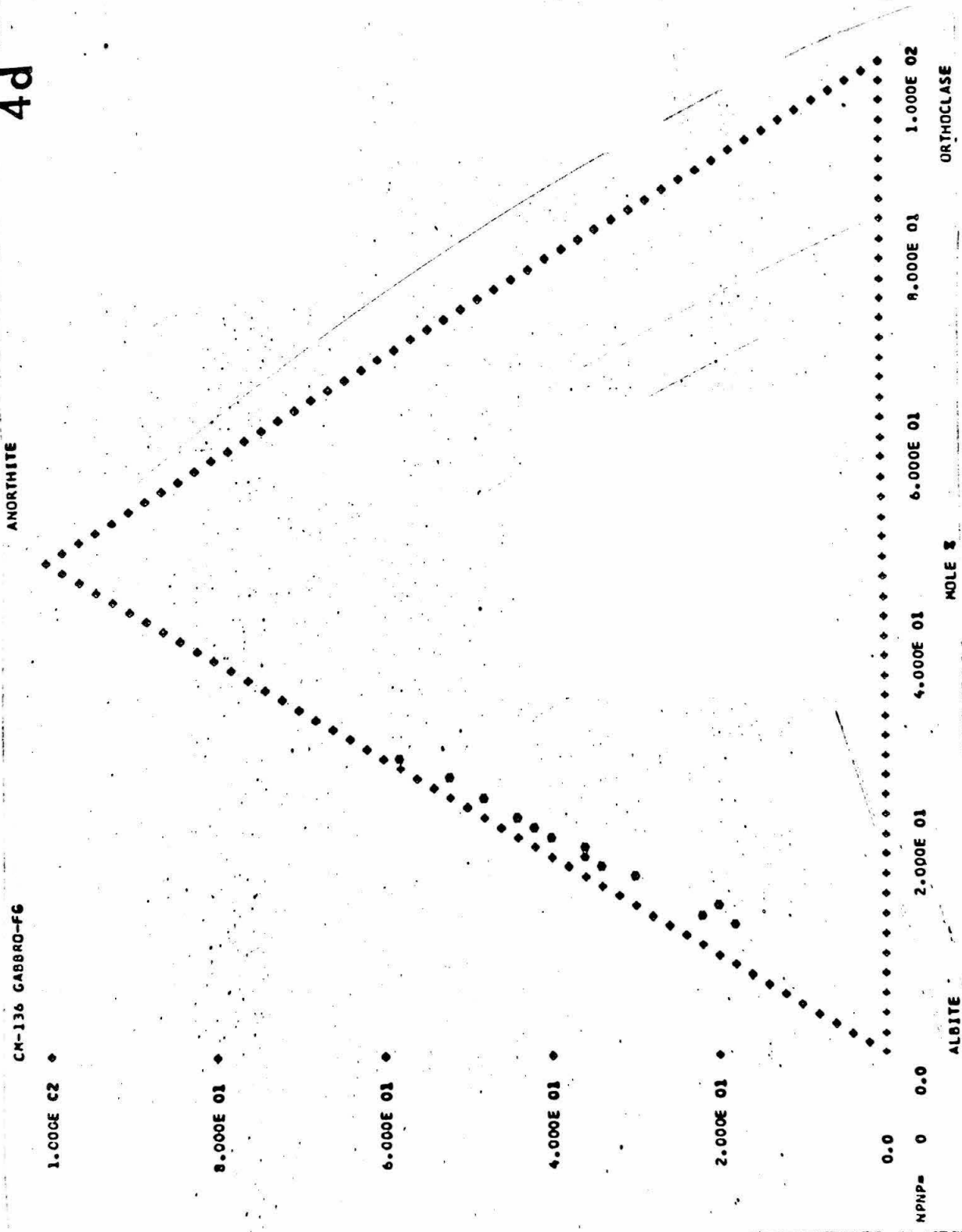


ALBITE

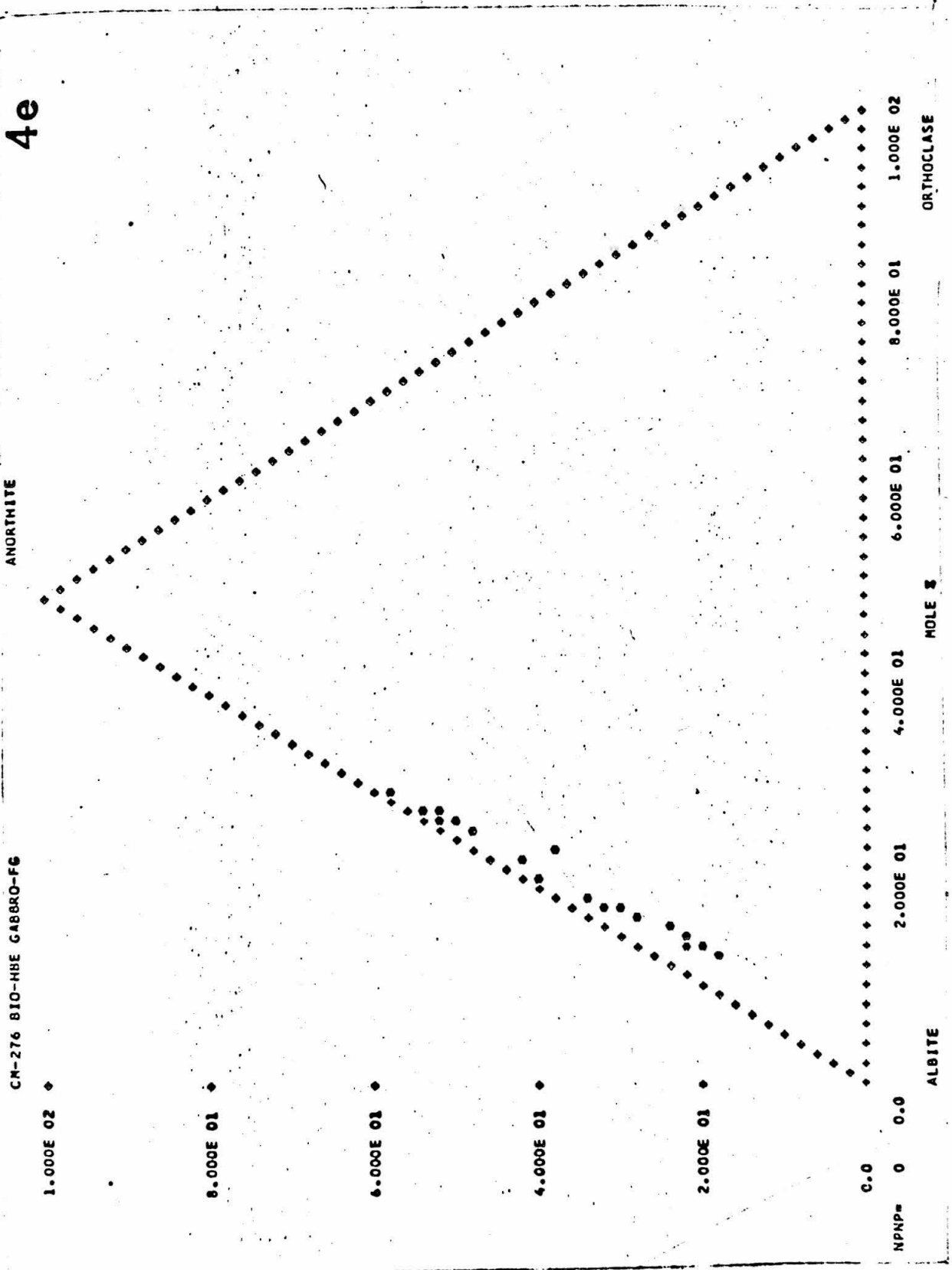
MOLE %

ORTHOCASE

4d



4e



ANORTHITE

CM-276 B10-HBE GABRO-F6

1.000E 02

8.000E 01

6.000E 01

4.000E 01

2.000E 01

0.0

NPP# 0 0.0

2.000E 01

4.000E 01

6.000E 01

8.000E 01

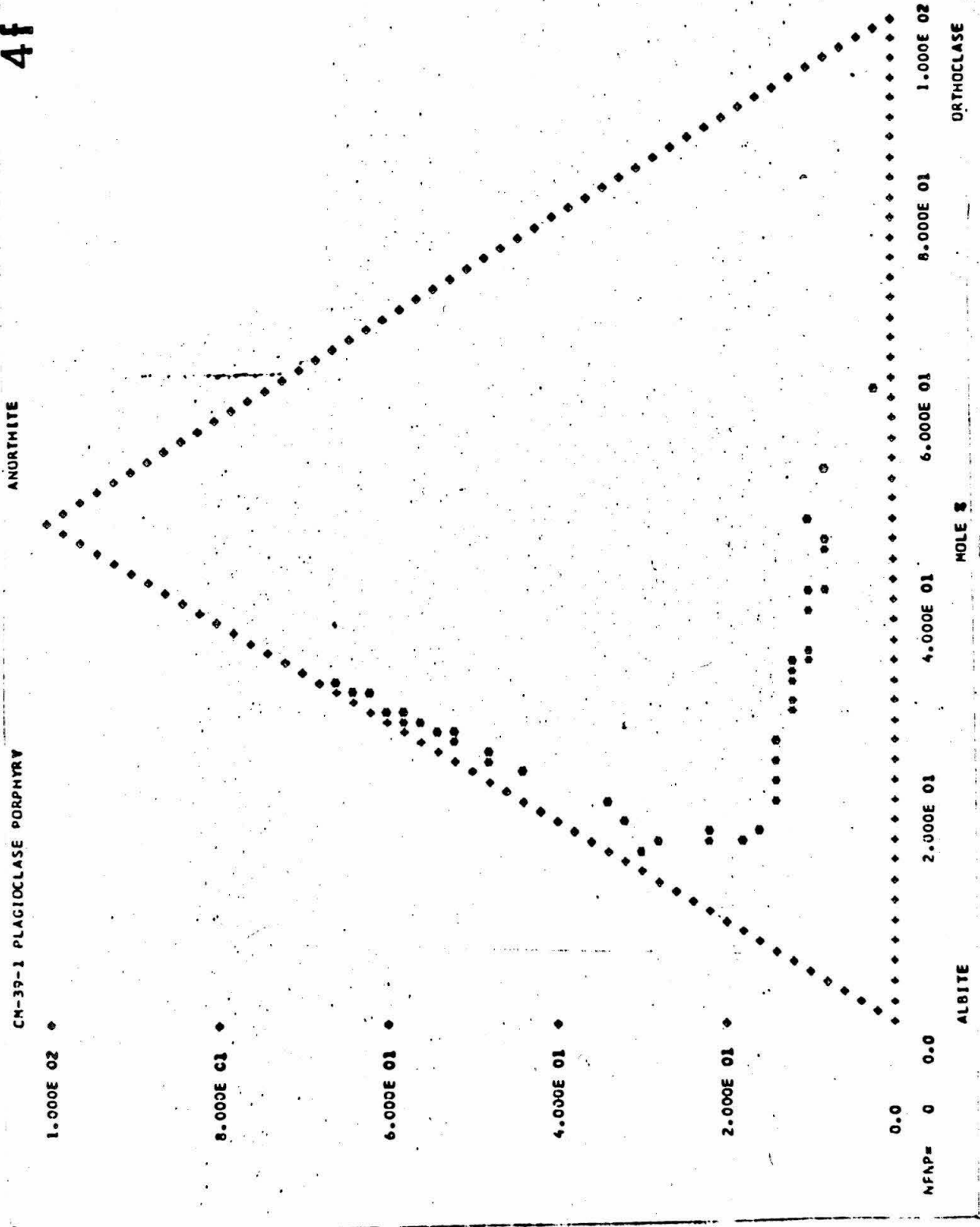
1.000E 02

ALBITE

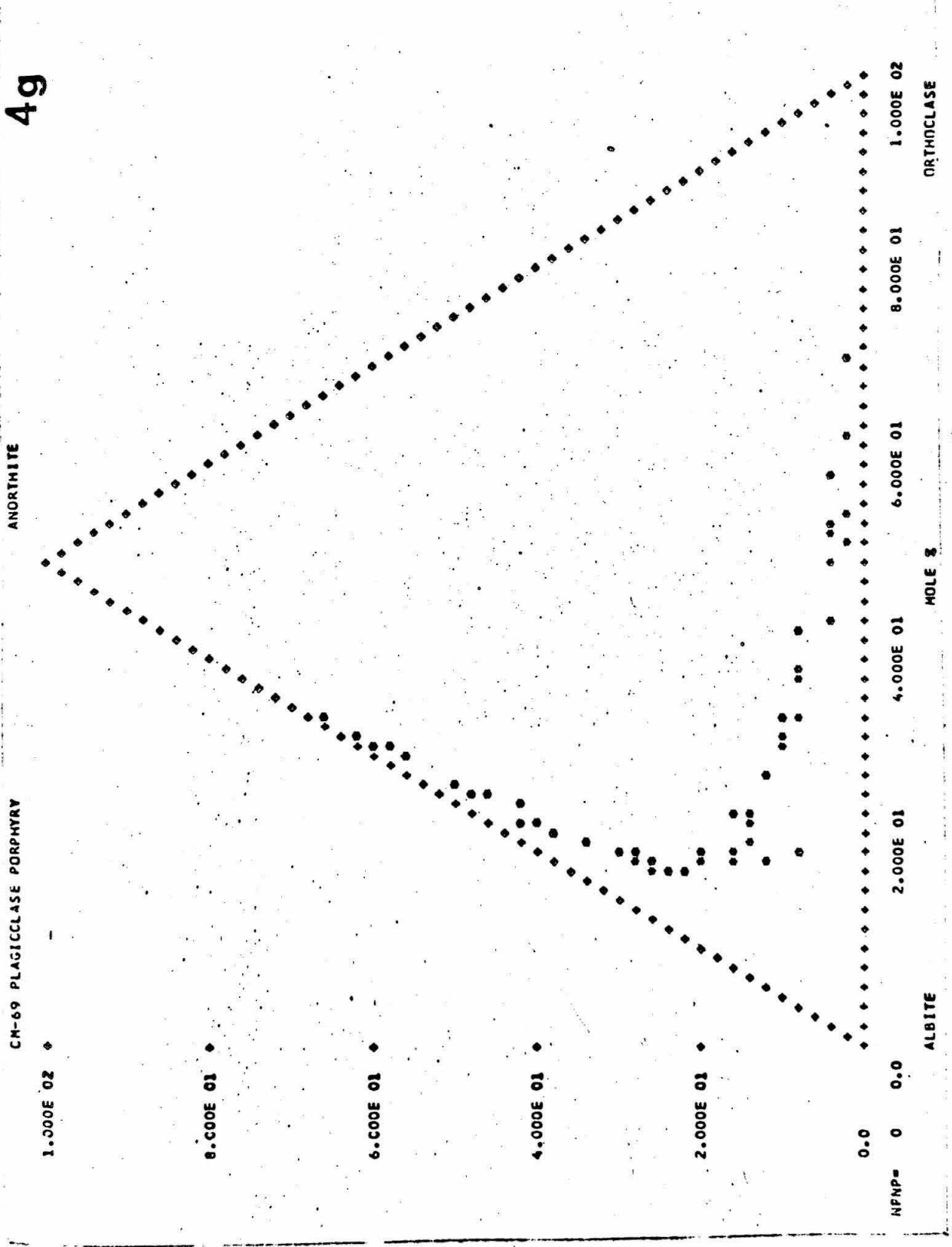
MOLE %

ORTHOCLASE

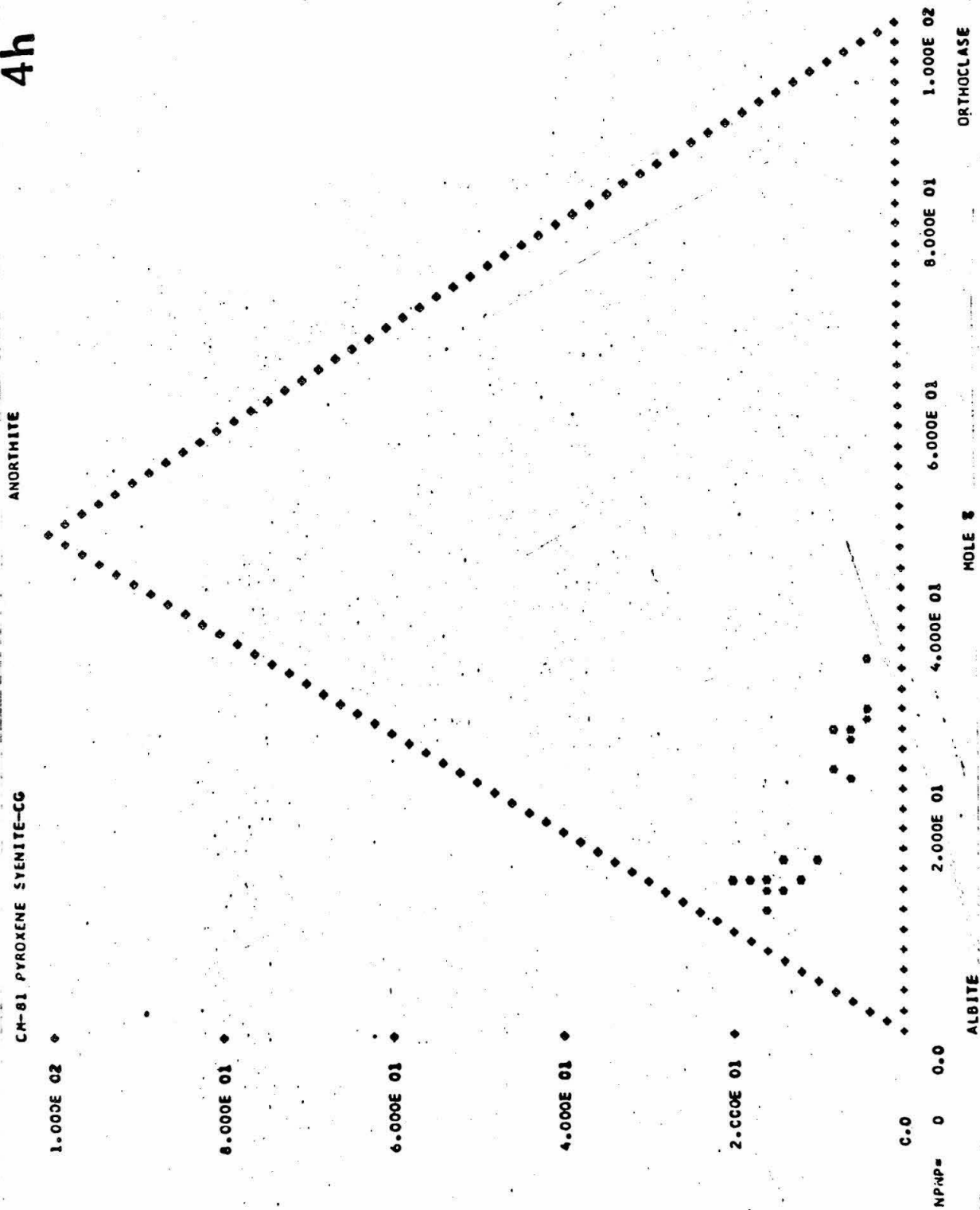
4f



49



4h



4i

ANORTHITE

CM-294A HBE-CPX SYENITE-FG

1.000E 02 ◆

8.000E 01 ◆

6.000E 01 ◆

4.000E 01 ◆

2.000E 01 ◆

0.0

NPMP= 0 0.0

ALBITE

2.000E 01

4.000E 01

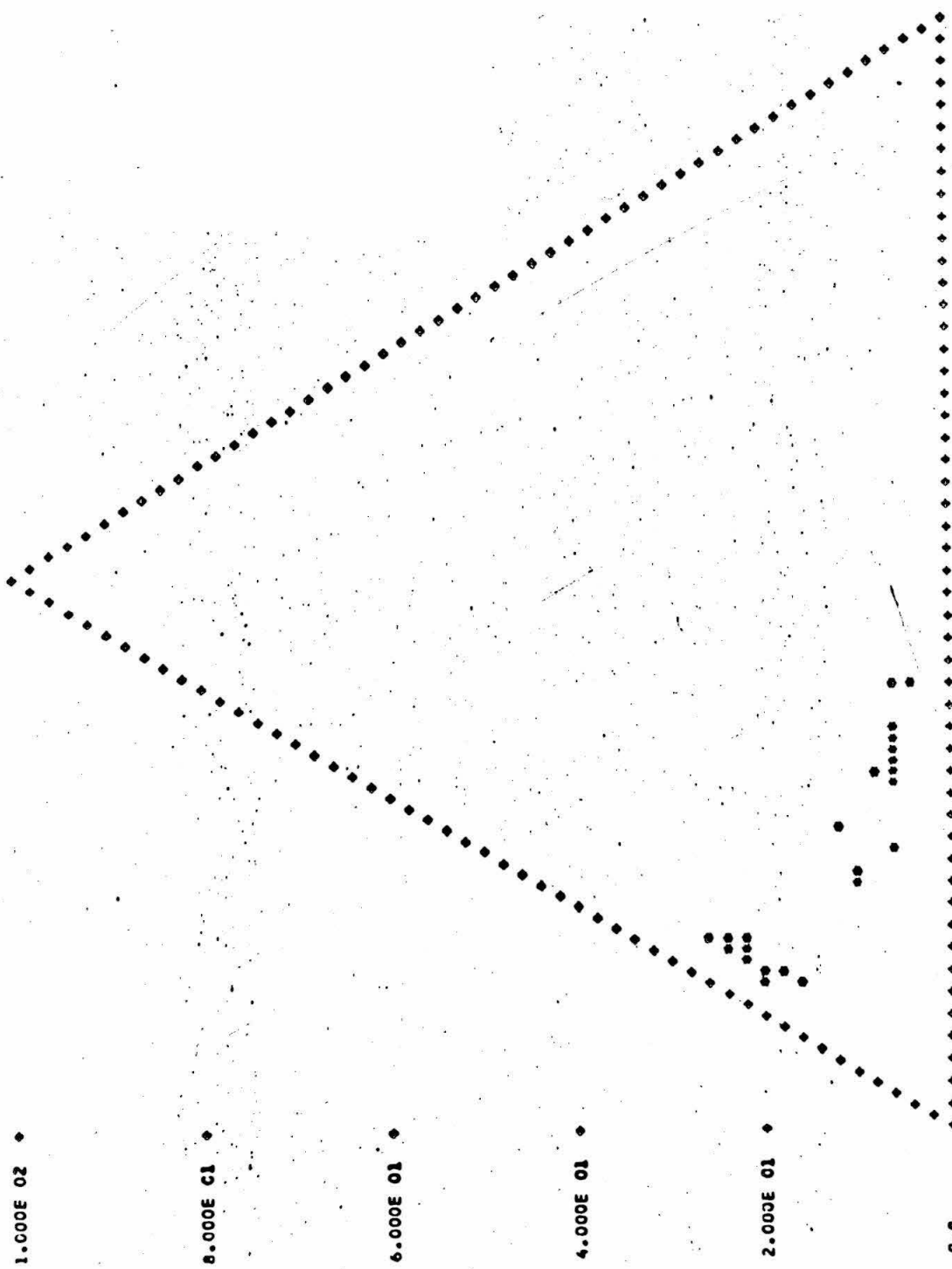
6.000E 01

8.000E 01

1.000E 02

ORTHOCLASE

MOLE %



## FINE-GRAINED BIOTITE-TITANAUGITE GABBRO

Fine-grained biotite-titanaugite gabbro is an equigranular rock with an average grain size of 2 to 4 mm. An averaged mode and mineral compositions are listed in Table 3. Mafic silicate and Fe-Ti oxide phases tend to occur in clots within a matrix of plagioclase laths. Titanaugite occurs in equidimensional, subhedral to anhedral grains, with no included plagioclase. Ophitic biotite grains commonly have inclusions of Fe-Ti oxide. Large (1 to 5 cm), optically continuous, sieve-textured grains of biotite impart a crude foliation to some samples. The ratio of included plagioclase, titanaugite, Fe-Ti oxide and apatite to host biotite is approximately 7:3. The inferred sequence of beginning of crystallization of phases is plagioclase, titanaugite, Fe-Ti oxide, amphibole, biotite.

In contrast to the deeply-colored titanaugite of the coarse-grained gabbro, titanaugite from the fine-grained gabbro is nearly colorless and only weakly pleochroic. The pleochroic scheme is X=Z= very pale green, Y=very pale yellow. Large grains commonly are zoned, the rim having the pleochroism just described and the core having a scheme like that of the clinopyroxene from the coarse-grained gabbro, but with very pale tints.

Compositional characteristics of clinopyroxene from fine-grained gabbro are summarized in Table 2 and on Figures 1b, 2b and 3b. The range and median values of the ratio  $(Fe+Mn)/(Fe+Mn+Mg)$  in clinopyroxene from fine-grained gabbro are identical to those of clinopyroxene from coarse-grained gabbro. Although the ranges of aluminum and titanium concentration overlap for clinopyroxenes from the two rock

TABLE 3

AVERAGE MODE AND MINERAL COMPOSITION OF  
FINE-GRAINED BIOTITE-TITANAUGITE GABBRO

18%	Titanaugite	Ca <sub>0.90</sub>	Na <sub>0.04</sub>	Mg <sub>0.73</sub>	Fe <sub>0.30</sub>	Mn <sub>0.01</sub>	Ti <sub>0.03</sub>	Al <sub>0.08</sub>	Si <sub>1.90</sub>	O <sub>6</sub>
10%	Biotite	K <sub>1.79</sub>	Na <sub>0.16</sub>	Ca <sub>0.01</sub>	Mg <sub>2.41</sub>	Fe <sub>2.57</sub>	Mn <sub>0.02</sub>	Ti <sub>0.89</sub>	Al <sub>2.54</sub>	Si <sub>5.55</sub> (O,OH) <sub>24</sub>
10%	Opaque	Magnetite	Exsolved Ilmenite	Homogeneous Ilmenite	USP <sub>18</sub> -USP <sub>23</sub>	HEM <sub>2</sub> -HEM <sub>3</sub>	HEM <sub>3</sub>			
60%	Plagioclase	AN <sub>59</sub>	AB <sub>40</sub>	OR <sub>1</sub>	- AN <sub>18</sub>	AB <sub>78</sub>	OR <sub>4</sub>			
2%	Apatite									
±	Kaersutite	Ca <sub>1.84</sub>	Na <sub>0.92</sub>	K <sub>0.22</sub>	Mg <sub>2.32</sub>	Fe <sub>1.96</sub>	Mn <sub>0.03</sub>	Ti <sub>0.63</sub>	Al <sub>1.91</sub>	Si <sub>6.17</sub> (O,OH) <sub>24</sub>

types, median concentrations of Al and Ti are significantly lower in clinopyroxene from the fine-grained gabbro.

Although the modal proportion of biotite in fine-grained gabbro is greater than that in either coarse-grained or porphyritic gabbro, its composition is essentially the same in each of the rock types. The ratio  $Fe/(Fe+Mg)$  varies between 0.48 and 0.53 in biotite from fine-grained gabbro.

Opaque phases consist of individual grains of optically homogeneous ilmenite and of titanian magnetite with lamellae of ilmenite, 1 to 8 microns in width, exsolved along (111). The distribution of magnesium, manganese and aluminum between homogeneous and lamellar ilmenite and between lamellar ilmenite and magnetite is similar to that determined for Fe-Ti oxide phases in coarse-grained gabbro. Conditions of subsolidus oxidation recorded by lamellar ilmenite and titanian magnetite are 600 to 620°C at  $10^{-20}$  to  $10^{-21}$  bars oxygen fugacity.

Plagioclase shows normal and diffuse patchy zoning. The range of compositional variation in plagioclase from three samples of fine-grained gabbro are shown in Figures 4c, 4d and 4e.

#### PORPHYRITIC OLIVINE-BIOTITE-TITANAUGITE GABBRO

Porphyritic olivine-biotite-titanaugite gabbro is characterized by 5 to 10 mm phenocrysts of plagioclase, rimmed by alkali feldspar and set in a matrix of 0.05 to 2 mm grains of titanaugite, Fe-Ti oxides and alkali feldspar. An averaged mode and mineral compositions are listed in Table 4. The dominant textural features of the porphyritic gabbro are the composite phenocrysts which consist of two

TABLE 4

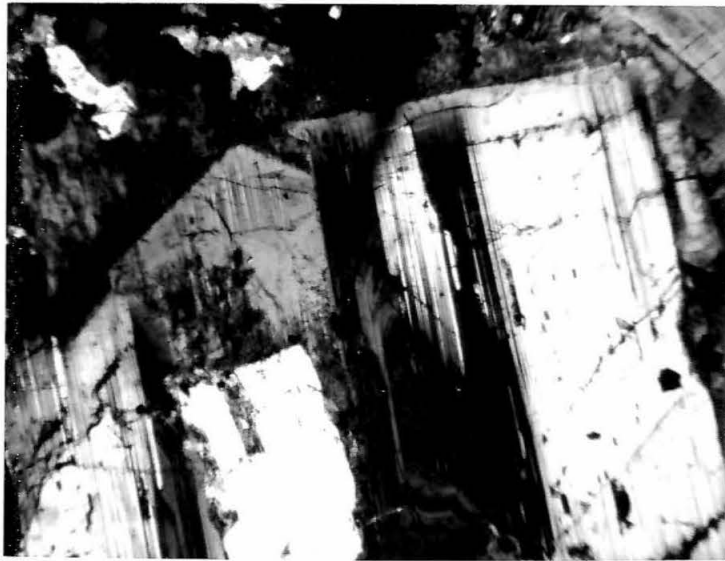
AVERAGE MODE AND MINERAL COMPOSITION OF PORPHYRITIC OLIVINE-BIOTITE-TITANAUGITE GABBRO	
2%	Olivine FO <sub>67</sub> FA <sub>33</sub> -FO <sub>53</sub> FA <sub>47</sub>
10%	Titanaugite Ca <sub>0.88</sub> Na <sub>0.05</sub> Mg <sub>0.73</sub> Fe <sub>0.29</sub> Mn <sub>0.01</sub> Ti <sub>0.04</sub> Al <sub>0.12</sub> Si <sub>1.89</sub> O <sub>6</sub>
4%	Biotite K <sub>1.80</sub> Na <sub>0.17</sub> Ca <sub>0.00</sub> Mg <sub>3.05</sub> Fe <sub>1.95</sub> Mn <sub>0.02</sub> Ti <sub>0.86</sub> Al <sub>2.48</sub> Si <sub>5.62</sub> (O,OH) <sub>24</sub>
8%	Opaque Magnetite USP <sub>31</sub> -USP <sub>55</sub> Exsolved Ilmenite HEM <sub>4</sub> -HEM <sub>7</sub> Homogeneous Ilmenite HEM <sub>4</sub> -HEM <sub>7</sub>
58%	Plagioclase AN <sub>66</sub> AB <sub>33</sub> OR <sub>1</sub> -AN <sub>21</sub> AB <sub>70</sub> OR <sub>9</sub>
12%	Alkali Feldspar AN <sub>20</sub> AB <sub>71</sub> OR <sub>9</sub> - AN <sub>2</sub> AB <sub>28</sub> OR <sub>70</sub>
3%	Nepheline AN <sub>5</sub> NE <sub>80</sub> KA <sub>15</sub>
2%	Analcite
1%	Apatite

or more euhedral, oscillatory-zoned crystals of plagioclase, joined in a synneusis relation (Vance, 1969), and enveloped by an euhedral, post-synneusis plagioclase overgrowth which in turn may be enveloped by a rim of alkali feldspar (Plate 1). The same rimming relationships are developed on phenocrysts with a single plagioclase crystal in the core. The matrix of the rock consists of a xenomorphic aggregate of alkali feldspar and nepheline with irregular, anhedral to euhedral grains of titanite, Fe-Ti oxides included within ragged flakes of biotite and olivine, partially to wholly enveloped by a thin reaction-rim of granular clinopyroxene and magnetite. There is no plagioclase in the groundmass. Inclusions of titanite magnetite and olivine in plagioclase, the presence of euhedral titanite in the matrix and the mantling of plagioclase phenocrysts by alkali feldspar suggest that the sequence of beginning of crystallization was olivine and magnetite, plagioclase, titanite, alkali feldspar, nepheline, biotite.

Titanite in porphyritic gabbro is indistinguishable optically from that in fine-grained gabbro. Compositional characteristics are summarized in Table 2 and on Figures 1c, 2c and 3c. Despite wide variation in bulk rock composition, clinopyroxene from each of the three gabbros are very similar in composition. Median values of the ratio  $(\text{Fe}+\text{Mn})/(\text{Fe}+\text{Mn}+\text{Mg})$  are identical. The main difference between clinopyroxene from the three rock types is in the relative proportion of aluminum, titanium and silicon.

Fe-Ti oxide phases consist of individual grains of optically homogeneous ilmenite and of titanite magnetite with lamellae of

Plate 1. Photomicrograph of composite feldspar phenocryst in porphyritic gabbro. Composition of individual plagioclase grains in core range from  $AN_{66}AB_{33}OR_1$  to  $AN_{39}AB_{58}OR_3$ . Composition of the plagioclase overgrowth ranges from  $AN_{34}AB_{63}OR_3$  to  $AN_{20}AB_{70}OR_{10}$ . Alkali feldspar rim varies in composition from  $AN_9AB_{61}OR_{30}$  to  $AN_2AB_{28}OR_{70}$ .



ilmenite exsolved along (111). There are two distinct populations of ilmenite lamellae within single crystals of titanian magnetite, a coarse set, 15 to 35 microns in width, and a fine set, 1 to 4 microns in width. Compositional differences between the sets are small and although differences in conditions of subsolidus oxidation are probably not significant, the fine set may have exsolved at a slightly lower temperature and oxygen fugacity than did the coarse set. Conditions of subsolidus oxidation are 700 to 800°C at  $10^{-15}$  to  $10^{-16}$  bars oxygen fugacity.

Electron microprobe point analyses of feldspars from porphyritic gabbro show continuous variation in composition between limits of  $AN_{66}AB_{33}OR_1$  and  $AN_2AB_{28}OR_{70}$  and outline the ternary feldspar solvus on a triangular plot of molecular anorthite, albite and orthoclase (Figures 4f and 4g). Individual feldspar phenocrysts consist of two or three optically distinct feldspar phases which exist in a mantling relationship. There is no evidence for simultaneous crystallization of two feldspars. Analyses taken across individual mantled phenocrysts indicate that although compositional continuity between the plagioclase core and the alkali feldspar rim exists in some grains, others exhibit distinct compositional gaps. Alkali feldspar with composition  $AN_9AB_{61}OR_{30}$  mantles plagioclase with a rim composition of  $AN_{20}AB_{70}OR_{10}$  in sample CM-69 (Plate 1). Where compositional gaps do not occur, compositional gradients are steep.

The extreme compositional zoning of the feldspars and the lack of evidence for simultaneous crystallization of two feldspars indicate that the feldspar did not continuously equilibrate with the

melt and that the liquid completely solidified before its composition reached the two feldspar-liquid cotectic. The continuous zoning records the fanning of the tie-lines joining solid and melt necessary to maintain tangency between each tie-line and the path of liquid descent on the ternary phase diagram. Because the path of liquid descent roughly parallels the trace of the ternary solvus along the anorthite-albite and albite-orthoclase side-lines, large changes in liquid composition result in relatively small changes in the composition of coexisting feldspar, for feldspar compositions over the ranges  $AN_{70}AB_{30}$  to  $AN_{35}AB_{65}$  and  $AB_{70}OR_{30}$  to  $AB_{30}OR_{70}$ . However, for feldspar compositions that outline the trace of the solvus, in the region where the solvus is strongly curved, a small change in the composition of the liquid produces a large change in the composition of the coexisting feldspar. Rapid cooling through this interval results in a compositional gap in the zoning of solid feldspar.

#### PYROXENE SYENITE

Syenite from the arcuate body intruded along the contact between coarse-grained and fine-grained gabbro is made up of a xenomorphic aggregate of alkali feldspar, some grains of which have plagioclase cores, and stubby to prismatic crystals of green clinopyroxene. Grain size is highly variable on the scale of an outcrop. It ranges from very fine-grained (1 mm) to pegmatitic. An averaged mode and mineral compositions are listed in Table 5.

Clinopyroxene in syenite is characterized by moderate to strong optical absorption and pleochroism. The pleochroic scheme is X=Z=green, Y=yellow. Electron microprobe analyses, summarized in Table 2 and on

TABLE 5

AVERAGE MODE AND MINERAL COMPOSITION OF  
PYROXENE SYENITE

6%	Clinopyroxene	Ca <sub>0.89</sub> Na <sub>0.08</sub> Mg <sub>0.46</sub> Fe <sub>0.56</sub> Mn <sub>0.02</sub> Ti <sub>0.01</sub> Al <sub>0.06</sub> Si <sub>1.92</sub> O <sub>6</sub>
3%	Opaque	Magnetite USP <sub>29</sub> -USP <sub>41</sub> Ilmenite HEM <sub>4</sub>
15%	Plagioclase	AN <sub>24</sub> AB <sub>71</sub> OR <sub>5</sub> -AN <sub>16</sub> AB <sub>74</sub> OR <sub>5</sub>
75%	Alkali Feldspar	AN <sub>9</sub> AB <sub>73</sub> OR <sub>18</sub> -AN <sub>5</sub> AB <sub>58</sub> OR <sub>37</sub>
1%	Apatite	
±	Kaersutite	Ca <sub>1.79</sub> Na <sub>0.87</sub> K <sub>0.31</sub> Mg <sub>1.75</sub> Fe <sub>2.84</sub> Mn <sub>0.08</sub> Ti <sub>0.28</sub> Al <sub>1.89</sub> Si <sub>6.20</sub> (O,OH) <sub>24</sub>
±	Biotite	

Figures 1d, 2d and 3d, show that clinopyroxene from syenite differs from those from the gabbros in having greater ratio of  $(Fe+Mn)/(Fe+Mn+Mg)$  and significantly lower concentrations of Al and Ti.

Large xenomorphic grains of alkali feldspar commonly have a core of plagioclase. Electron microprobe analyses of alkali feldspar and plagioclase (Figures 4h and 4i) show a gap between the composition of the most sodic plagioclase and the most sodic alkali feldspar. The composition of the normative feldspar in each of the two analyzed samples coincides with the composition of the most potassic alkali feldspar analyzed in that sample. The compositional gap occurs in the region of maximum curvature of the trace of the ternary feldspar solvus. Using the model developed for the crystallization of the porphyritic gabbro, the compositional gap results from the inability of sodic feldspar to equilibrate with the melt on cooling due to the relatively large changes in solid composition produced by very small changes in liquid composition.

#### SUMMARY

Petrologic observations pertinent to an understanding of the genesis of alkaline pyroxenite and calcic nepheline syenite by reaction between gabbroic magma and limestone are:

1. Gabbroic and syenitic rocks are critically undersaturated. Both olivine and nepheline appear in their norms.
2. Clinopyroxene, biotite, ilmenite, magnetite and plagioclase are common to each of the three gabbros. Olivine, amphibole, alkali feldspar and nepheline occur in one or more rock types.

3. The composition of each mineral is essentially the same in each of the three gabbros in which it occurs. In particular, the median value of the ratio  $(\text{Fe}+\text{Mn})/(\text{Fe}+\text{Mn}+\text{Mg})$  is identical in clinopyroxene from each of the three gabbros.
4. Clinopyroxene, biotite, magnetite and where present, amphibole, have high concentrations of titanium and aluminum.
5. Gabbroic magmas probably were saturated or nearly saturated with plagioclase and clinopyroxene at the time of emplacement.

### 3. GENESIS OF MAFIC ALKALINE ROCKS BY ASSIMILATION OF LIMESTONE BY GABBROIC MAGMA

Nowhere in the Christmas Mountains do gabbro and marble occur in direct contact. The sequence of lithologies developed across the intrusive contact and across marble xenoliths in gabbro is invariably gabbro, pyroxenite, calc-silicate skarn, marble. The consistent spatial relationship between the four rock types indicates that pyroxenite and calc-silicate skarn were formed by reaction between gabbro and limestone. The contact between pyroxenite and skarn is characterized by sinusoidal to lobate embayments of pyroxenite into skarn, that are suggestive of extensive solution of wallrock by magma. Because mineral assemblages in pyroxenite and skarn are compatible, solution involved limestone rather than skarn. Proof that the pyroxenite is a magmatic rock rather than the innermost zone of calc-silicate skarn developed in solid limestone is demonstrated by the presence of pyroxenite dikes that are intrusive into skarn.

Similar alkaline ultramafic rocks developed at contacts between tholeiitic basalt and limestone at Scawt Hill and Camas Mor in the British Isles have been described by Tilley (Tilley and Harwood, 1931; Tilley, 1952). Tilley concluded that although alkaline rocks were produced by assimilation of limestone by subalkaline basaltic magma, the predominance of mafic and ultramafic compositions among the contaminated rocks and their restriction to a narrow zone along the intrusive contact provided little support for limestone assimilation hypothesis of Daly (1910) for the genesis of alkaline magma. There is no evidence in the

Christmas Mountains for development of contaminated igneous rocks on more than a local scale, however, reactions between gabbroic magma and limestone play an essential role in the growth of the calc-silicate skarn both at the intrusive contact and in xenoliths.

#### CONTAMINATED ROCKS

##### Pyroxenite

Typical pyroxenite consists of 50 to 80 volume percent titanite with nepheline and alkali feldspar accounting for most of the remainder of the mode (Table B-6, appendix). Sphene and apatite, as euhedral crystals, are ubiquitous accessory minerals. The fabric of pyroxenite consists of individual, euhedral crystals of titanite and sphene, enclosed within large single crystals of nepheline and/or alkali feldspar. Local concentrations of titanite and leucocratic patches of nepheline and alkali feldspar produce the uneven modal distribution of phases that is characteristic of pyroxenite (Plate 1). Within leucocratic patches, wollastonite occurs as elongate bladed crystals which have a skeletal habit with rounded margins, suggestive of reaction with magma or with the enveloping nepheline (Plate 2, Figure 1). The highly irregular modal distribution of titanite in pyroxenite suggests that pyroxenite represents a crystal mesh of euhedral titanite "cemented" together by a late-solidifying alkali-rich residual magma of nepheline syenite composition.

##### Nepheline Syenite

Nepheline syenite, which occurs in dikes that intrude both pyroxenite and skarn, has the same mineral assemblage as pyroxenite, with a mode like that of the leucocratic patches in pyroxenite

Plate 1. Pyroxenite developed at contact between fine-grained gabbro and xenolith of Santa Elena(?) limestone. Sample CM-111 collected from the north margin of the more southerly of two xenoliths shown on map in Figure 2, Chapter 5. Re-entrant of skarn at left of photograph is surrounded by successive zones of fine-grained nepheline-plagioclase pyroxenite and coarse-grained nepheline-alkali feldspar leuco-pyroxenite. Field of view is 50 x 65 mm.

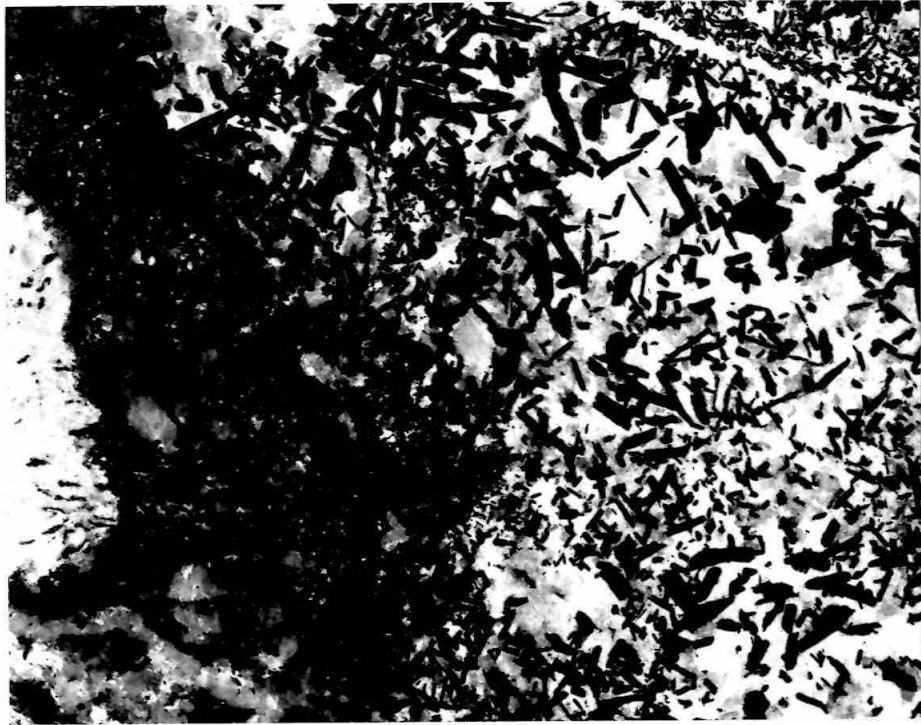


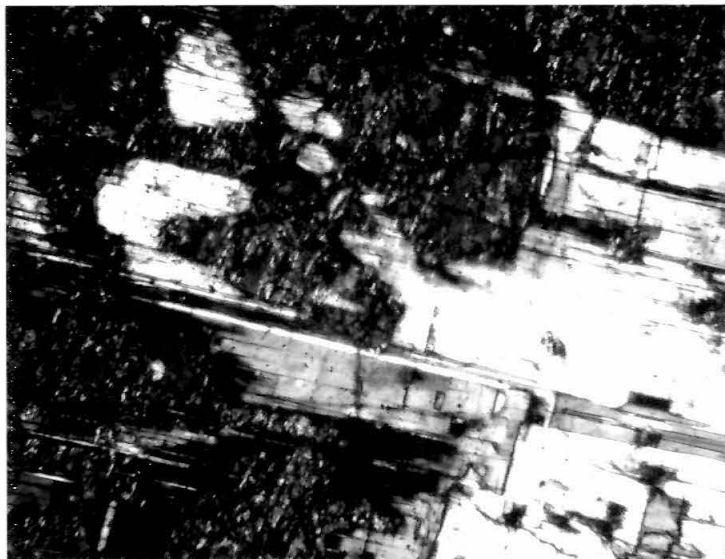
Plate 2. Products of reaction: CALCITE + PLAGIOCLASE =  
NEPHELINE + WOLLASTONITE + ANORTHITE + CO<sub>2</sub>.

Figure 1. Skeletal crystal of wollastonite within single crystal of nepheline, sample CM-6-3B. Field of view is 0.58 x 0.85 mm, plane light. Compositions of coexisting phases are:

WO WO<sub>96</sub>EN<sub>1</sub>FS<sub>3</sub>  
NE AN<sub>04</sub>NE<sub>78</sub>KA<sub>18</sub>

Figure 2. Partially resorbed plagioclase phenocryst in nepheline gabbro, CM-33-12. Field of view is 0.58 x 0.85 mm, crossed nicols. Compositions of coexisting phases are:

PLAG AN<sub>53</sub>AB<sub>45</sub>OR<sub>02</sub>  
NE AN<sub>06</sub>NE<sub>78</sub>KA<sub>16</sub>



(Tables 1 and B-6). The compositional similarity of nepheline syenite to the leucocratic fraction of pyroxenite and the restricted occurrence of nepheline syenite dikes to pyroxenite and skarn suggest that contaminated syenite represents a portion of the alkali-rich residual magma squeezed out of solidifying pyroxenite.

Titanian andradite and perovskite occur in a dike of nepheline syenite intrusive into skarn (CM-340, Table 1, Assemblage 4). Garnet is black in hand specimen and nearly opaque in thin-section. The formula of the garnet,

$(\text{Ca}_{2.84}\text{Mg}_{0.10}\text{Mn}_{0.02}\text{Na}_{0.03})(\text{Ti}_{1.23}\text{Zr}_{0.02}\text{Fe}_{0.76})(\text{Al}_{0.18}\text{Fe}_{0.54}\text{Si}_{2.28})\text{O}_{12}$ , differs from that of titanian-zirconian garnet which coexists with wollastonite and perovskite in calc-silicate skarn in that there is a large excess of titanium over that needed to balance the tetrahedral silicon deficiency. Therefore the garnet in syenite cannot be a xenocryst from skarn, but is magmatic in origin.

#### Nepheline Gabbro

The assemblage titanite + nepheline + sphene  $\pm$  alkali feldspar  $\pm$  wollastonite, which characterizes pyroxenite and nepheline syenite, appears to represent the end product of reaction between alkali gabbro magma and limestone. The phases olivine, plagioclase, biotite and magnetite-ilmenite, which are characteristic of the gabbro, seldom occur in the pyroxenite. Their absence may be the result of precipitation and subsequent reaction with either limestone or contaminated magma or their components may have been held in solution in contaminated magma and precipitated directly as other phases due to the change in bulk composition of the magma or to

TABLE 1

MINERAL ASSEMBLAGES IN SYENITE  
CHRISTMAS MOUNTAINS, BIG BEND REGION, TEXAS

	1	2	3	4
CLINOPYROXENE	X	X	X	X
AMPHIBOLE	±	..	..	..
BIOTITE	±	..	..	..
ILMENITE	±	..	..	..
MAGNETITE	X	..	..	..
SPHENE	..	X	X	X
PEROVSKITE	..	..	..	X
GARNET	..	..	..	X
WOLLASTONITE	..	..	X	X
PLAGIOCLASE	X	..	..	..
ALKALI FELDSPAR	X	X	X	X
NEPHELINE	..	X	X	X

1. Uncontaminated syenite
2. Contaminated syenite
3. Contaminated syenite
4. Contaminated syenite

TABLE 2

COEXISTING NEPHELINE, PLAGIOCLASE, ALKALI FELDSPAR AND WOLLASTONITE IN CONTAMINATED IGNEOUS ROCKS  
CHRISTMAS MOUNTAINS, BIG BEND REGION, TEXAS

	NEPHELINE	PLAGIOCLASE	ALKALI FELDSPAR	WOLLASTONITE
6-3B	AN <sub>04</sub> NE <sub>78</sub> KA <sub>18</sub>	---	---	WO <sub>96</sub> EN <sub>1</sub> FS <sub>3</sub>
33-6	AN <sub>05</sub> NE <sub>75</sub> KA <sub>20</sub> -AN <sub>2</sub> NE <sub>74</sub> KA <sub>24</sub>	---	---	WO <sub>96</sub> EN <sub>1</sub> FS <sub>3</sub>
29B	AN <sub>10</sub> NE <sub>74</sub> KA <sub>16</sub>	AN <sub>95</sub> AB <sub>05</sub> OR <sub>0</sub> -AN <sub>79</sub> AB <sub>20</sub> OR <sub>1</sub>	---	---
29B	AN <sub>05</sub> NE <sub>77</sub> KA <sub>17</sub>	AN <sub>35</sub> AB <sub>59</sub> OR <sub>6</sub> -AN <sub>31</sub> AB <sub>62</sub> OR <sub>7</sub>	---	WO <sub>96</sub> EN <sub>1</sub> FS <sub>3</sub>
33-12	AN <sub>12</sub> NE <sub>68</sub> KA <sub>20</sub> -AN <sub>6</sub> NE <sub>80</sub> KA <sub>14</sub>	AN <sub>81</sub> AB <sub>18</sub> OR <sub>1</sub> -AN <sub>31</sub> AB <sub>62</sub> OR <sub>7</sub>	AN <sub>4</sub> AB <sub>42</sub> OR <sub>54</sub> -AN <sub>1</sub> AB <sub>16</sub> OR <sub>83</sub>	---
41-8	AN <sub>06</sub> NE <sub>78</sub> KA <sub>16</sub>	AN <sub>63</sub> AB <sub>35</sub> OR <sub>2</sub> -AN <sub>36</sub> AB <sub>59</sub> OR <sub>5</sub>	AN <sub>3</sub> AB <sub>29</sub> OR <sub>68</sub> -AN <sub>2</sub> AB <sub>26</sub> OR <sub>72</sub>	---
29-70	AN <sub>00</sub> NE <sub>80</sub> KA <sub>20</sub>	---	AN <sub>1</sub> AB <sub>21</sub> OR <sub>78</sub> -AN <sub>0</sub> AB <sub>12</sub> OR <sub>88</sub>	---
111 CG	AN <sub>04</sub> NE <sub>80</sub> KA <sub>16</sub>	---	AN <sub>4</sub> AB <sub>31</sub> OR <sub>65</sub> -AN <sub>2</sub> AB <sub>19</sub> OR <sub>79</sub>	---
141-8	AN <sub>05</sub> NE <sub>76</sub> KA <sub>19</sub>	---	AN <sub>4</sub> AB <sub>55</sub> OR <sub>41</sub> -AN <sub>3</sub> AB <sub>29</sub> OR <sub>68</sub>	---
141-4	AN <sub>02</sub> NE <sub>81</sub> KA <sub>17</sub>	---	AN <sub>1</sub> AB <sub>36</sub> OR <sub>63</sub> -AN <sub>1</sub> AB <sub>30</sub> OR <sub>69</sub>	WO <sub>95</sub> EN <sub>1</sub> FS <sub>4</sub>

different conditions of water or oxygen fugacity brought about by solution of limestone. Olivine and plagioclase, minerals that begin to crystallize early in the crystallization sequence of uncontaminated gabbro magma, show textural evidence for reaction to form clinopyroxene and nepheline, respectively, in pyroxenite and in gabbro in contact with pyroxenite. Biotite and magnetite-ilmenite do not occur in plagioclase-free pyroxenite or in nepheline syenite. Because there is no textural evidence for reactions involving biotite or magnetite-ilmenite in contaminated rocks, it must be concluded that potassium and titanium combined with other components of the magma to precipitate directly as alkali feldspar and as titanite and sphene.

#### Bulk Composition of Contaminated Rocks

Bulk chemical compositions of contaminated igneous rocks are listed in Tables B-7 through B-9. Compositional trends overlap those of uncontaminated rocks on Harker diagrams and continue trends to lower concentrations of  $\text{SiO}_2$  (Figures B-1 and B-4). Analyses of pyroxenite and nepheline syenite do not show the trend toward iron enrichment with increasing alkali content that is characteristic of suites of contaminated rocks derived from the interaction of tholeiitic magma with limestone (Tilley and Harwood, 1931; Tilley, 1952, Figure B-5). Analyses of contaminated igneous rocks, plotted on variation diagrams, show more scatter around compositional trends than do analyses of uncontaminated rocks on similar diagrams. The scatter of the former about the compositional trends reflects the extreme local variability in the modal proportions of titanite

and nepheline in pyroxenite which is a result of the nearly complete crystallization of titanite before the onset of crystallization of nepheline. Compared with gabbros from which they were derived, pyroxenites are enriched in calcium and depleted in silicon and aluminum. There is no consistent pattern of enrichment or depletion of other elements in pyroxenite relative to gabbro. Metasomatic growth of the calc-silicate skarn by reaction between gabbroic magma and limestone requires the introduction of silicon, aluminum, titanium and iron to the country rock. Because elemental abundances in pyroxenite do not differ greatly from those in corresponding gabbro, the volume of pyroxenite developed at the intrusive contact probably represents the product of reaction of a similar volume of gabbroic magma with limestone. Pyroxenite is not the accumulated product of limited reaction of a large volume of magma with wallrock.

#### TITANAUGITE

Clinopyroxene in pyroxenite and nepheline syenite is characterized by strong optical absorption and pleochroism. The pleochroic scheme of titanite from pyroxenite derived from coarse-grained gabbro is X=deep rose, Y=yellow, Z=deep rose or gray-green. Zoning is common and the intensity of absorption increases from core to rim. The pleochroic scheme of clinopyroxene from pyroxenite derived from fine-grained or porphyritic gabbro is X=Z=green and Y=yellow. Although most grains of clinopyroxene in pyroxenite derived from fine-grained or porphyritic gabbro are optically homogeneous, some of the larger crystals are zoned with a pale- to deep-rose core and a green rim. Clinopyroxene from

nepheline syenite and nepheline gabbro derived from each of the three gabbro types invariably show strong color zoning like that just described. Sector zoning is not common but is well developed in clinopyroxene from wollastonite-nepheline syenite (CM-141-4, Table 4).

Mineral formulae of clinopyroxene from pyroxenite and nepheline syenite are listed in Tables 3 and 4. The range of compositional variation are shown graphically on Figures 1, 2 and 3. Although the range of concentration of iron, titanium and aluminum in titanaugite from pyroxenite and nepheline syenite overlap those of titanaugite from uncontaminated gabbro, the median concentrations of these elements are significantly higher in clinopyroxene from contaminated rocks. Core compositions of zoned titanaugite from pyroxenite and nepheline syenite are similar to the composition of titanaugite in the corresponding uncontaminated gabbro, suggesting that clinopyroxene in contaminated rocks began crystallization in uncontaminated magma. Electron microprobe profiles across a zoned titanaugite from pyroxenite derived from coarse-grained gabbro are shown in Figure 4. The concentrations of iron and manganese increase sympathetically at the expense of magnesium, from the core of the crystal to its rim. The concentrations of aluminum and titanium rise from minima in the core to maxima near the rim, then decrease to intermediate values at the rim. This zoning pattern is common to titanaugite in pyroxenite and nepheline syenite derived from each of the three gabbro types.

TABLE 3

ELECTRON MICROPROBE ANALYSES OF CLINOPYROXENE FROM PYROXENITE  
CHRISTMAS MOUNTAINS, BIG BEND REGION, TEXAS

FORMULA PROPORTION OF CATIONS (MEDIAN VALUES)

	Ca	Na	Mg	Fe	Mn	Al	Ti	Si	O
Cg	0.94	0.05	0.41	0.47	0.01	0.32	0.09	1.71	6
Fg	0.90	0.08	0.47	0.48	0.01	0.24	0.06	1.76	6
Pg	0.92	0.06	0.44	0.50	0.01	0.19	0.05	1.82	6

RANGE OF VARIATION IN CATION PROPORTIONS

	$\frac{\text{Fe}+\text{Mn}}{\text{Fe}+\text{Mn}+\text{Mg}}$	Median	Al	Ti	Al/Ti
Cg	0.31-0.65	0.54	0.12-0.48	0.04-0.14	3.6
Fg	0.48-0.60	0.51	0.11-0.33	0.03-0.09	4.0
Pg	0.26-0.65	0.54	0.07-0.34	0.03-0.10	4.0

---

Cg Median or range of 59 point analyses of clinopyroxene from pyroxenite derived from coarse-grained gabbro. Samples CM-6-3B, CM-33-6, CM-29B

Fg Median or range of 11 point analyses of clinopyroxene from pyroxenite derived from fine-grained gabbro. Sample CM-111B

Pg Median or range of 57 point analyses of clinopyroxene from pyroxenite derived from porphyritic gabbro. Samples CM-8-1B, CM-41-2

TABLE 4

ELECTRON MICROPROBE ANALYSES OF CLINOPYROXENE  
FROM NEPHELINE SYENITE  
CHRISTMAS MOUNTAINS, BIG BEND REGION, TEXAS

FORMULA PROPORTION OF CATIONS (MEDIAN VALUES)

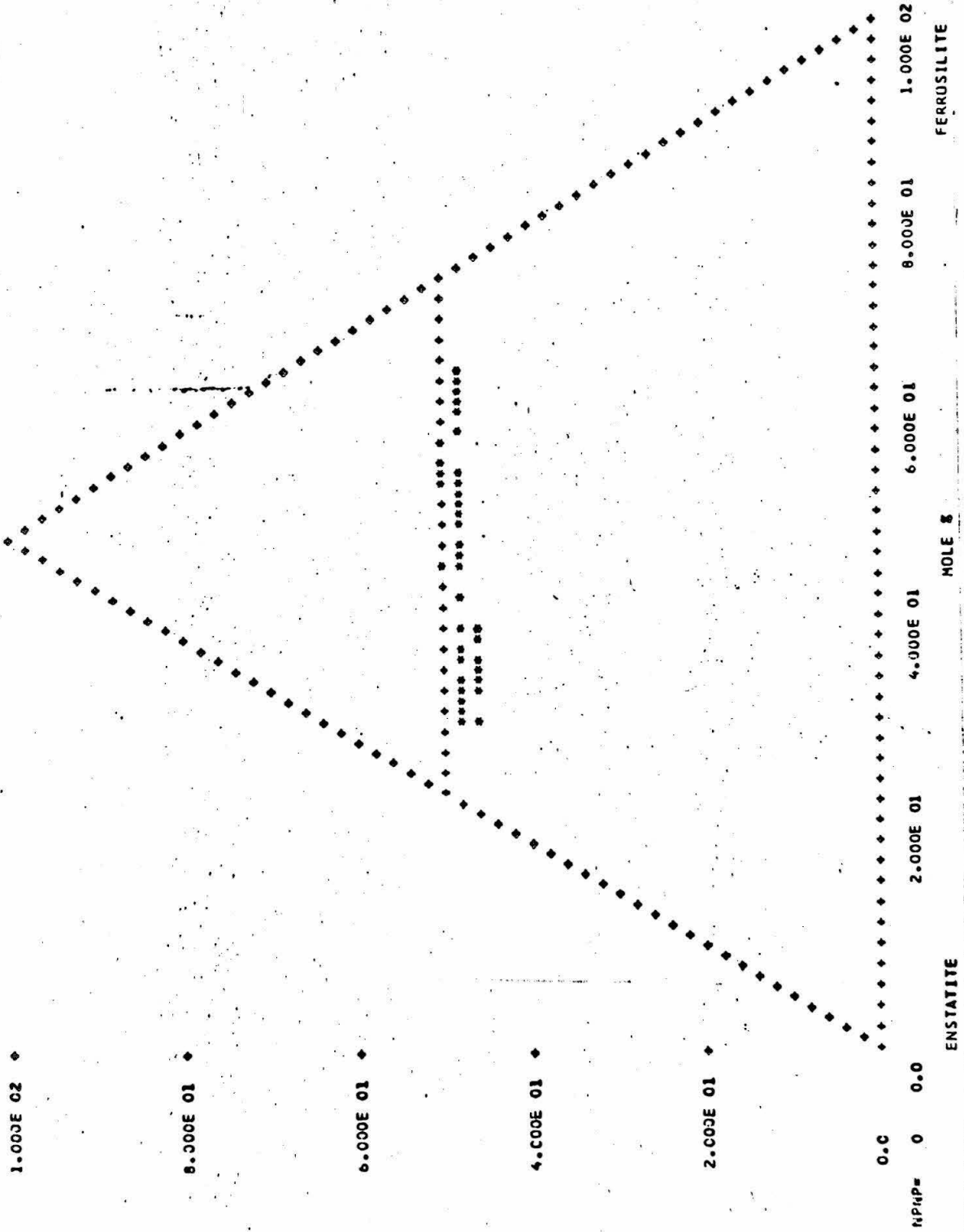
	Ca	Na	Mg	Fe	Mn	Al	Ti	Si	O
29-70									
Core	0.89	0.05	0.71	0.28	0.01	0.10	0.03	1.92	6
Rim	0.88	0.11	0.39	0.58	0.02	0.08	0.02	1.91	6
141-8									
Core	0.90	0.04	0.69	0.31	0.01	0.14	0.06	1.85	6
Rim 1	0.90	0.07	0.54	0.39	0.01	0.20	0.07	1.81	6
Rim 2	0.86	0.11	0.21	0.78	0.02	0.10	0.03	1.89	6
141-4 Sector Zoned									
(100)	0.94	0.04	0.42	0.42	0.01	0.44	0.13	1.61	6
(001)	0.94	0.04	0.47	0.42	0.01	0.31	0.08	1.72	6
Rim	0.87	0.11	0.17	0.81	0.02	0.09	0.02	1.91	6
340									
Core	0.94	0.06	0.48	0.48	0.01	0.06	0.03	1.93	6
Rim	0.73	0.27	0.07	0.90	0.02	0.03	0.02	1.96	6
8-1A									
Aegirine	0.14	0.87	0.01	0.92	0.00	0.03	0.02	1.98	6

Figure 1. Electron microprobe analyses of clinopyroxene from contaminated igneous rocks plotted on the pyroxene quadrilateral. Proportion of end-member molecules computed by the normative scheme of Kushiro (1962)

- a. 50 point analyses from nepheline syenite
- b. 187 point analyses from nepheline gabbro and pyroxenite.

1a

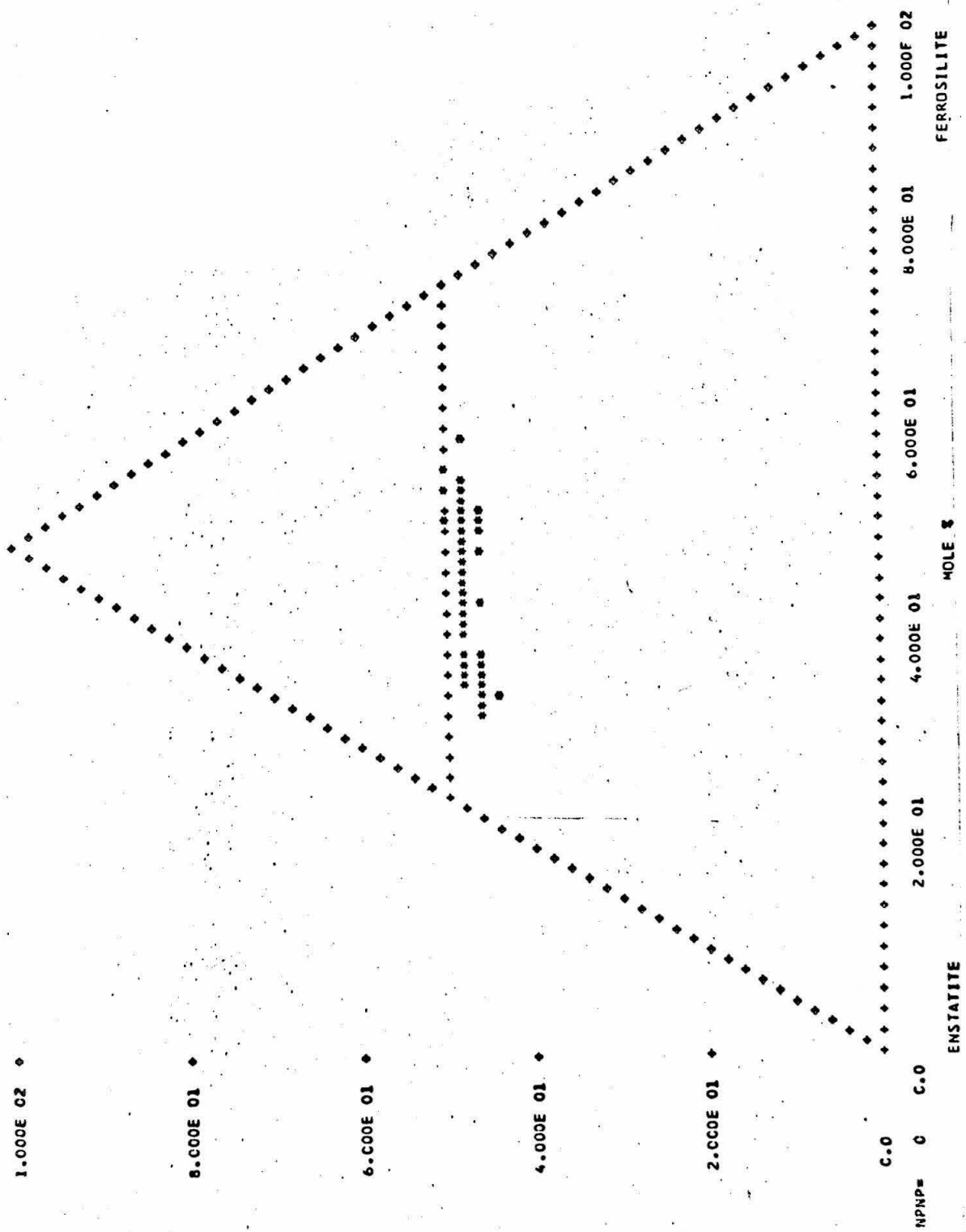
CHRISTMAS MOUNTAINS IGNEOUS ROCKS--NEPH SVENITE MULLASTUNITE



1b

CHRISTMAS MOUNTAINS IGNEOUS ROCKS--PYROXENITE

MOLLASTONITE



1.000E 02

8.000E 01

6.000E 01

4.000E 01

2.000E 01

0

ENSTATITE

0

2.000E 01

4.000E 01

6.000E 01

8.000E 01

1.000E 02

ENSTATITE

MOLE %

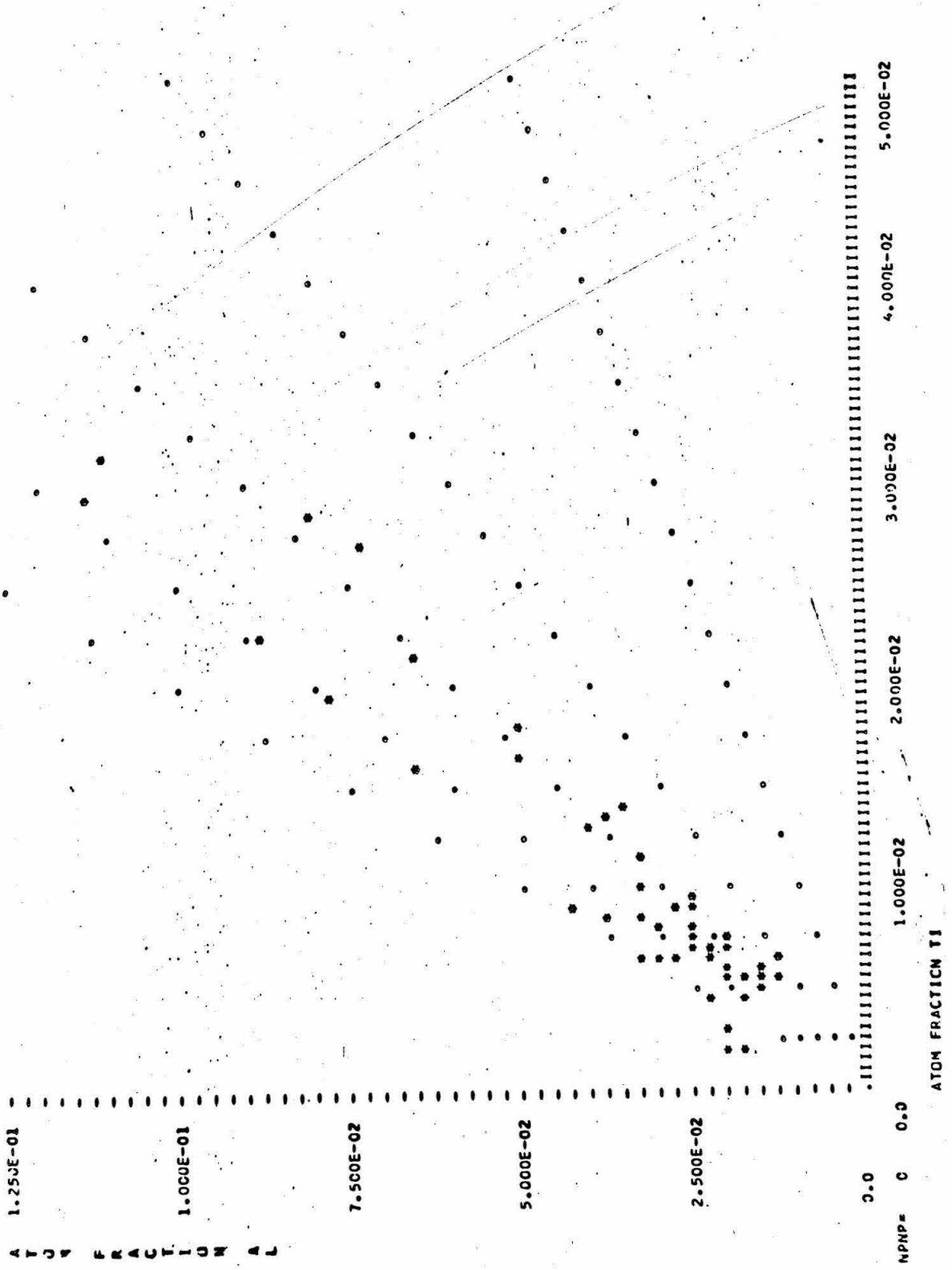
FERROSILITE

Figure 2. Electron microprobe analyses of clinopyroxene from contaminated igneous rocks. Atomic fraction aluminum plotted against atomic fraction titanium. Points which plot along a straight line that passes through the origin have the same ratio of Al/Ti. Dotted lines represent Al/Ti of 1, 2, 3, 4 and 5.

- a. 50 point analyses from nepheline syenite
- b. 187 point analyses from nepheline gabbro and pyroxenite.

2a

CHRISTMAS MOUNTAINS IGNEOUS ROCKS--NEPHELINE SYENITE

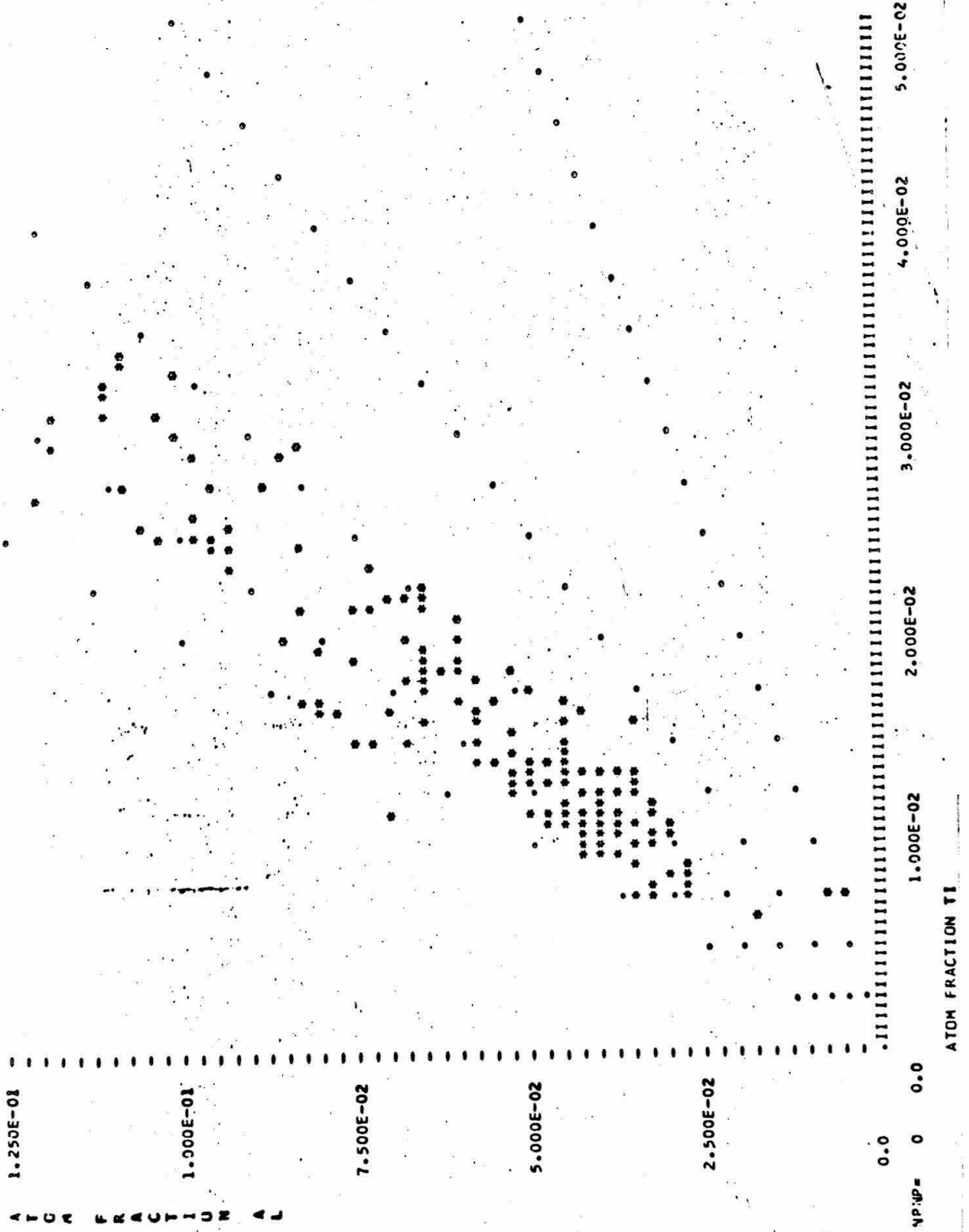


NPNP= C 0.0

ATOM FRACTION TI

2b

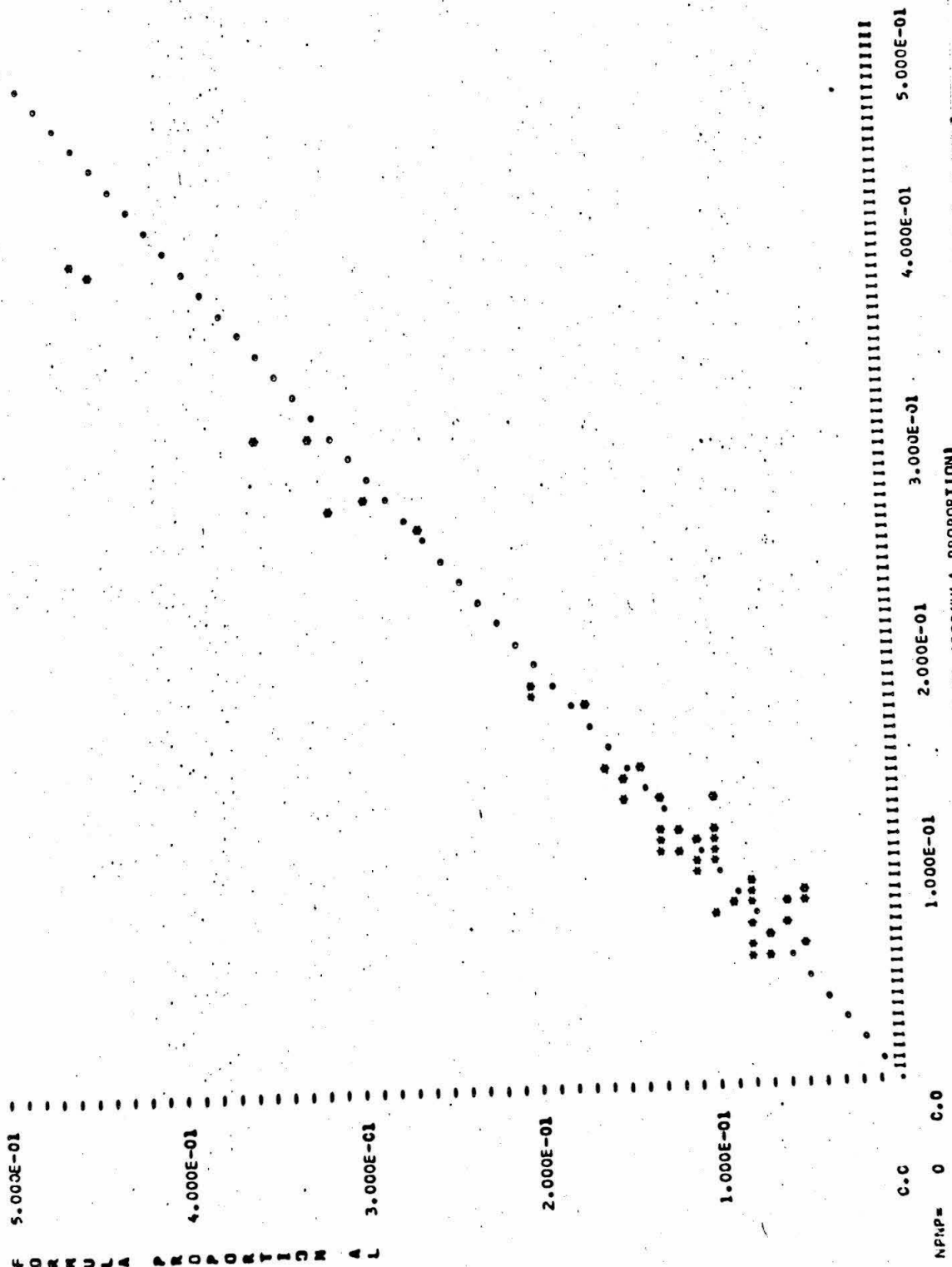
CHRISTMAS MOUNTAINS IGNEOUS ROCKS--PYROXENITE



- Figure 3. Electron microprobe analyses of clinopyroxene from contaminated igneous rocks. Formula proportion of aluminum plotted against tetrahedral silicon deficiency, defined as 2.0 minus the formula proportion of silicon, for a mineral formula based on 4.0 cations.
- a. 50 point analyses from nepheline syenite
  - b. 187 point analyses from nepheline gabbro and pyroxenite

3a

CHRISTMAS MOUNTAINS IGNEOUS ROCKS--NEPHELINE SYENITE



5.000E-01

4.000E-01

3.000E-01

2.000E-01

1.000E-01

C.C

NPMP= 0 C.0

5.000E-01

4.000E-01

3.000E-01

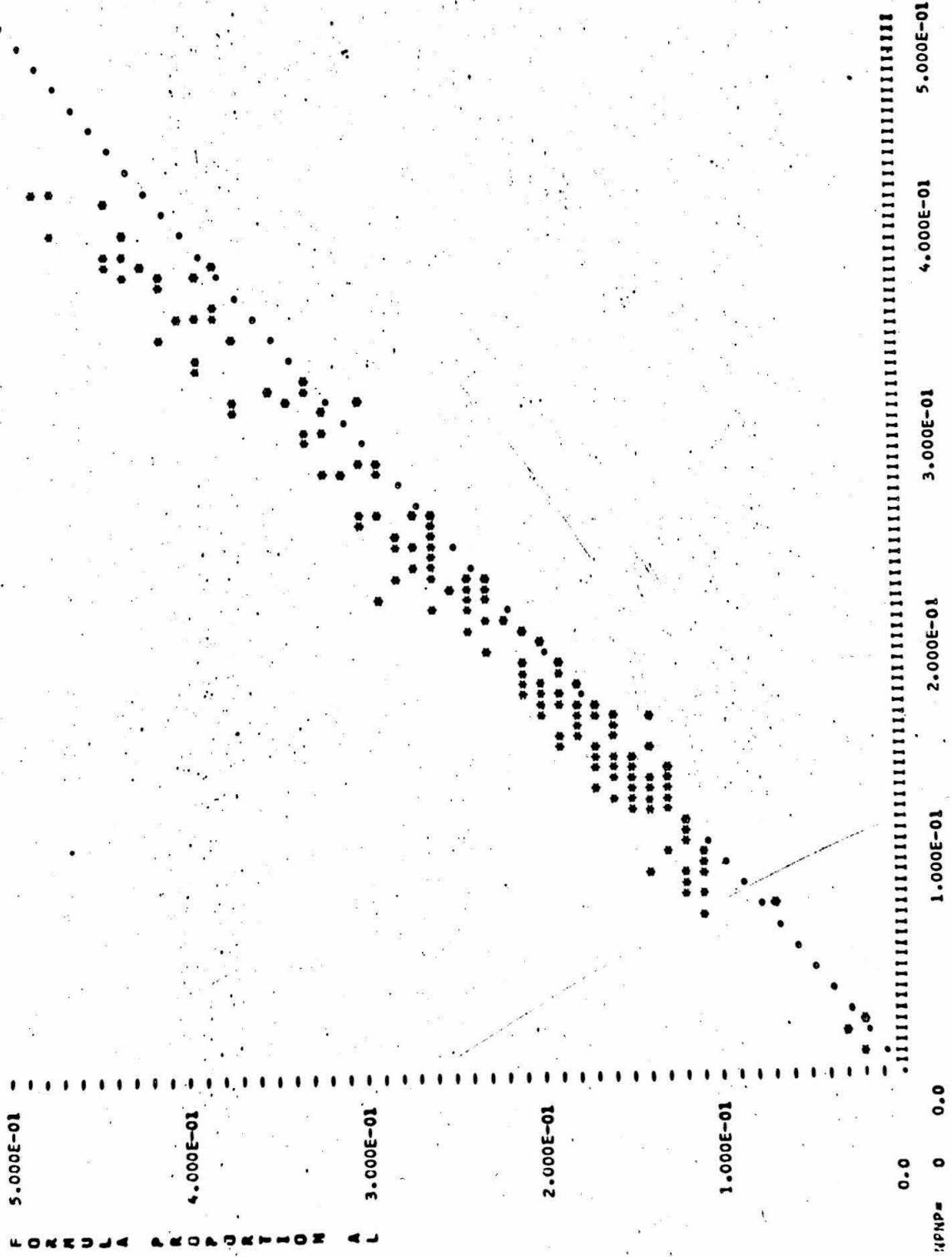
2.000E-01

1.000E-01

TETRAHEDRAL SILICON DEFICIENCY = 2.0-SI (FORMULA PROPORTION)

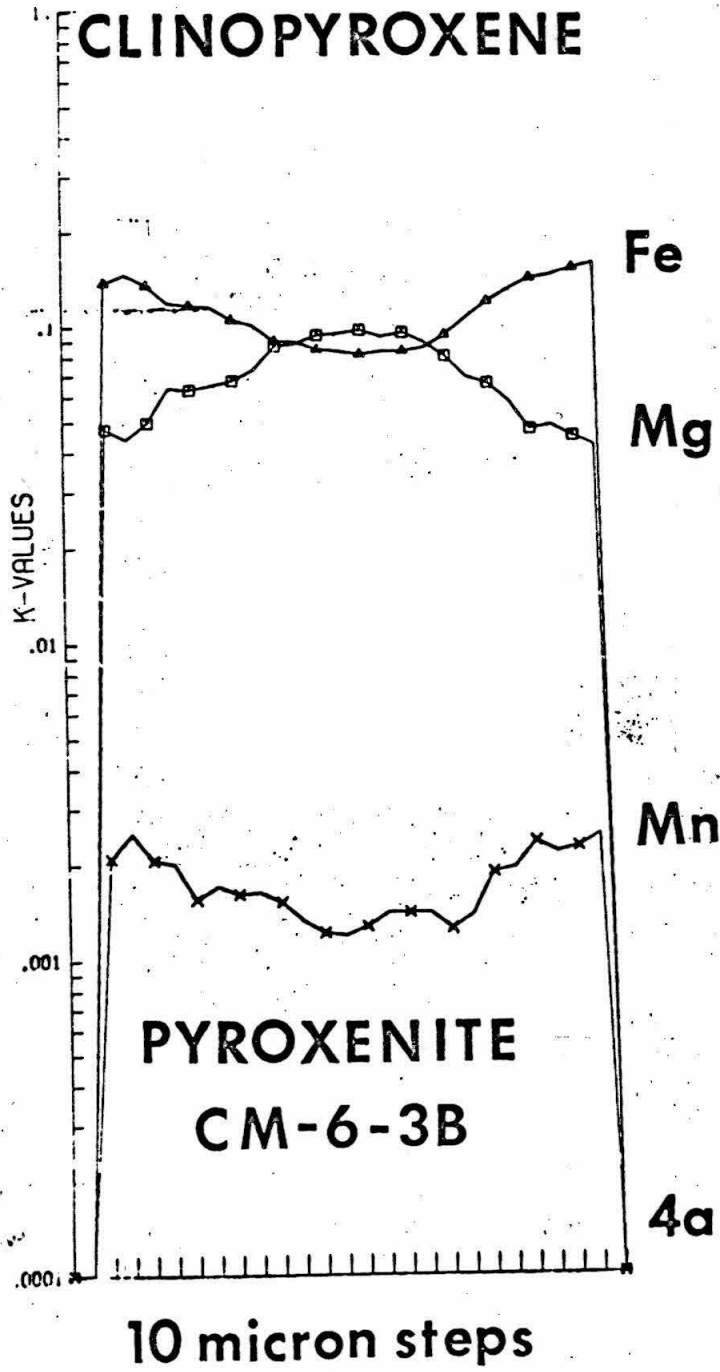
3b

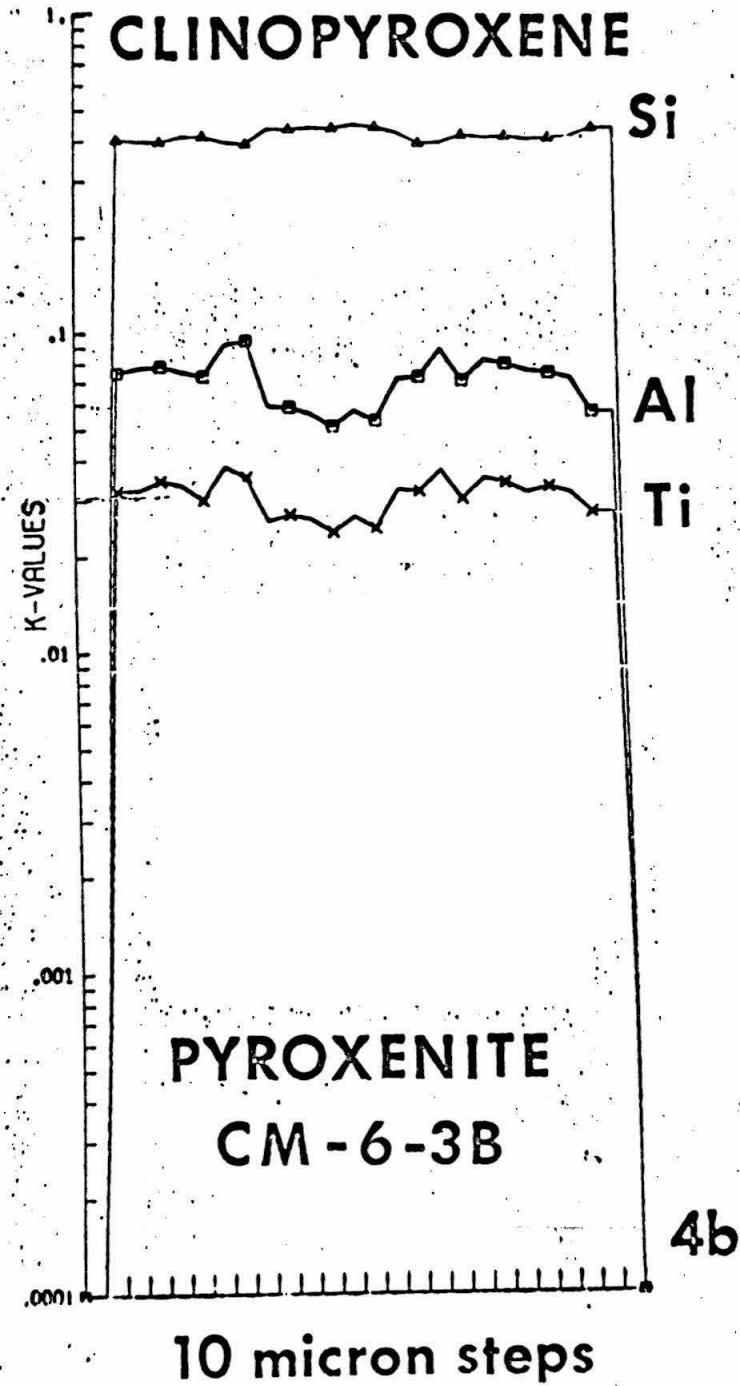
CHRISTMAS MOUNTAINS IGNEOUS ROCKS--PYROXENITE



TETRAHEDRAL SILICON DEFICIENCY = 2.0-SI (FORMULA PROPORTION)

- Figure 4. Concentration profiles across zoned titanite from pyroxenite derived from coarse-grained gabbro. K-value is ratio of X-ray intensity of element in sample to that of pure oxide standard (Bence and Albee, 1968).
- a. Simultaneous analyses of Fe, Mn and Mg.
  - b. Simultaneous analyses of Al, Ti and Si.





As shown on Figure 3, the formula proportion of aluminum in clinopyroxene just balances the tetrahedral silicon deficiency, with a small excess. The antithetic relationship between aluminum and silicon, common in clinopyroxene from alkaline igneous rocks, has lead to the suggestion that the primary control of the concentration of aluminum in clinopyroxene is the activity of  $\text{SiO}_2$  of the magma (Kushiro, 1960; Le Bas, 1962; Verhoogen, 1962 and Carmichael, Nicholls and Smith, 1970). As discussed below, selective magmatic resorption of the albite component of plagioclase to produce a melt saturated in anorthite and nepheline produces a steady lowering of the activity of  $\text{SiO}_2$  in the contaminated magma. Thus, although the progressive increase of the ratio  $(\text{Fe}+\text{Mn})/(\text{Fe}+\text{Mn}+\text{Mg})$  from the core to the rim of individual grains of clinopyroxene records the progressive depletion of magnesium in contaminated magma due to copious crystallization of titanite, variation in the ratio  $\text{Al}/(\text{Al}+\text{Si})$  reflects control of the activity of  $\text{SiO}_2$  in the melt by feldspar-liquid equilibria.

#### LIMESTONE ASSIMILATION

A model for the evolution of pyroxenite by reaction between gabbroic magma and limestone has been developed as a part of the growth model for the skarn described in Chapter 5. Aspects of the model necessary for an understanding of the genesis of pyroxenite and nepheline syenite will be developed here. Reaction between gabbroic magma and limestone involves two processes, (1) Decarbonation reactions between calcite and magma and/or crystals in equilibrium with magma, and (2) Crystallization of phases with which the magma

is saturated, to supply energy for the endothermic decarbonation reactions. Because the chemical potential of a component is equal in all phases in mutual equilibrium, its value is a characteristic of the system, not of the individual phases or their physical states. Thus, to describe reaction between gabbroic magma and limestone, reactions may be written between calcite and minerals that may crystallize from the magma, but the actual phases participating in the reaction may be either the magma or the solids in equilibrium with it.

#### The Plagioclase Reaction

The crystallization sequences of each of the three gabbros indicate that gabbroic magma was saturated with and probably was crystallizing plagioclase and clinopyroxene at the time of emplacement. Although clinopyroxene shows little textural evidence for reaction with magma, plagioclase in nepheline gabbro has corroded margins and is rimmed by nepheline (Plate 2, Figure 2). To a first approximation the initiation of reaction between gabbroic magma and limestone may be described by a reaction between calcite and plagioclase



Solid plagioclase need not be directly involved in the decarbonation reaction. Conversion of the albite component of the magma to nepheline by reaction between magma and calcite requires resorption of any crystalline plagioclase available, to maintain equilibrium. Although exceedingly rare in pyroxenite, plagioclase has two modes of occurrence with distinctive textures and compositions. The more

widespread occurrence of plagioclase is as isolated single crystals, with corroded margins, enveloped by large, euhedral crystals of nepheline (Plate 2, Figure 2). This textural relationship clearly shows that plagioclase was involved in a resorption reaction with magma. The range of composition of plagioclase in this paragenesis overlaps that of plagioclase from uncontaminated gabbro (Table 2). Because the corroded grains of plagioclase are not enriched in the anorthite component, resorption of plagioclase by the magma involves solution of both the albite and the anorthite components and the "plagioclase effect" (Bowen, 1945; Watkinson and Wyllie, 1969, p. 1570-71) does not appear to be important.

The products of the decarbonation reaction, anorthite, wollastonite and nepheline, go into solution in the melt and in clinopyroxene. Anorthite-rich plagioclase occurs locally in a thin, discontinuous zone at the contact with skarn (Table 2). Individual grains of anorthite do not show any evidence for reaction and probably crystallized directly from contaminated magma. The rare occurrence of anorthite in pyroxenite and the progressive enrichment in the calcium tschermak component from the core outward in titanaugite suggest that calcium and aluminum from resorbed plagioclase enter into the pyroxene solid solution (Tilley and Harwood, 1931, p. 462). Entry of  $\text{CaAl}_2\text{SiO}_6$  into clinopyroxene is favored so long as the activity of  $\text{SiO}_2$  is buffered by the coexistence of albite and nepheline (Carmichael, Nicholls and Smith, 1970, p. 255). It will be shown in the growth model for the skarn (Chapter 5) that anorthite and the calcium tschermak component of titanaugite may react with

calcite to form the gehlenite component of melilite in skarn.

Because wollastonite does not occur in nepheline gabbro in which plagioclase is partially resorbed, it is concluded that wollastonite derived from reaction between plagioclase and calcite enters into solid solution in titanaugite. Wollastonite appears as a phase in pyroxenite and nepheline syenite where the concentration of CaO exceeds that needed to combine with available iron and magnesium to form clinopyroxene. Wollastonite in pyroxenite occurs as skeletal crystals, with rounded margins, suggestive of resorption by magma. In contrast to wollastonite from skarn which is essentially pure  $\text{CaSiO}_3$ , wollastonite from pyroxenite and nepheline syenite contains about 2.5 mole percent FeO plus MnO (Table C-3). Thus the wollastonite in contaminated rocks cannot represent partially digested xenocrysts from skarn. Wollastonite that coexists with nepheline and alkali feldspar in syenite shows no evidence of resorption.

Nepheline appears to have been the last phase to crystallize in pyroxenite. Large crystals of nepheline may enclose several euhedral crystals of titanaugite and sphene and nepheline is euhedral against partially resorbed crystals of wollastonite. The uneven modal distribution of nepheline and titanaugite in pyroxenite suggests that pyroxenite represents a crystal mesh of titanaugite and sphene, "cemented" together by a late-solidifying, alkali-rich magma of nepheline syenite composition. Dikes of nepheline syenite that are intrusive into pyroxenite and skarn represent

residual contaminated magma, that was pressed out of the pyroxene mesh.

On the basis of experimentally determined melting relationships on the join albite-calcite-H<sub>2</sub>O, Watkinson and Wyllie (1969) proposed a model for the progressive assimilation of limestone by a water-saturated albite melt. According to the model, progressive solution of limestone at constant temperature causes

1. Precipitation of plagioclase
2. Precipitation of wollastonite
3. Resorption of plagioclase
4. Precipitation of nepheline
5. Complete solidification
6. Subsolvus reaction between wollastonite and calcite to yield stoichiometric calc-silicate phases

The sequence of precipitation and resorption of phases in pyroxenite due to reaction between gabbroic magma, saturated with plagioclase, and limestone is broadly consistent with the model for the simple system. Enrichment of plagioclase in anorthite in the incipient stage of reaction was not well documented. In general, the composition of partially resorbed plagioclase in nepheline gabbro and pyroxenite lies within the range of composition of plagioclase from uncontaminated gabbro. The anorthite component of resorbed plagioclase enters into solid solution in clinopyroxene.

Wollastonite produced by reaction between plagioclase and calcite enters into solid solution in titanite. When sufficient

clinopyroxene solidified to deplete the contaminated magma of iron and magnesium, wollastonite crystallized from the alkali-rich residue. Further reaction with calcite caused resorption of wollastonite from pyroxenite and growth of stoichiometric calc-silicate minerals in skarn.

Nepheline was the last phase to crystallize in pyroxenite. In the experimentally investigated system, nepheline crystallized only in runs with greater than about 20 weight percent calcite (Watkinson and Wyllie, 1969, p. 1574). However, nepheline, replacing plagioclase, appears in the incipient stages of reaction between gabbroic magma and limestone. This probably is due to the high initial anorthite content of plagioclase in uncontaminated gabbro.

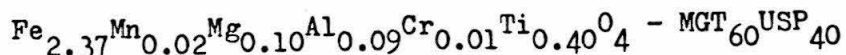
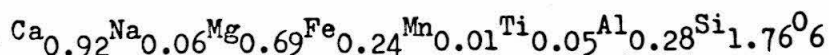
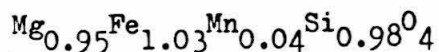
#### Clinopyroxene Accumulation

Textural and paragenetic relationships between plagioclase, nepheline and wollastonite in pyroxenite can be explained in terms of a model based on the decarbonation reaction between plagioclase and calcite. The accumulation of titanaugite at the original contact between gabbroic magma and limestone to form pyroxenite is a consequence of the model. The decarbonation reaction between calcite and plagioclase is endothermic with an enthalpy of 19.9 kilocalories per mole of calcite at 1300<sup>o</sup>K (Robie and Waldbaum, 1968). The energy required for the reaction between magma and calcite can be supplied by crystallization of the phases with which the magma is saturated, thus liberating the enthalpy of fusion (Bowen, 1928, p. 175-91). Titanaugite concentrated in the

pyroxenite was probably crystallized in response to reaction between magma and carbonate. The enthalpy of fusion of diopside, 24.3 Kcal/mole (Bowen, 1928, p. 178), is comparable in magnitude to the enthalpy of the decarbonation reaction, but opposite in sign when diopside crystallizes from a melt. Thus for each mole of calcite taken into solution by the magma, approximately one mole of clinopyroxene was crystallized to supply the energy necessary for the endothermic decarbonation reaction. The amount of limestone that may be assimilated by a given volume of gabbroic magma is limited by the concentration of potential clinopyroxene in uncontaminated magma.

#### The Olivine Reaction

Olivine in pyroxenite and nepheline gabbro derived from porphyritic gabbro is restricted in occurrence to the cores of large grains of titanite where it is rimmed by vermicular magnetite (Plate 3, Figure 1). The former presence of olivine in these rocks is marked by vermicular magnetite in the core of zoned grains of titanite (Plate 3, Figure 2). Compositions of coexisting olivine, titanite and magnetite from the assemblage of Plate 3, Figure 1 (CM-8-1A) are



The composition of titanite in contact with olivine is the most magnesian in the rock. Although composition of olivine in this and

Plate 3. Products of reaction: OLIVINE + MAGMA = CLINOPYROXENE  
+ MAGNETITE

Figure 1. Vermicular magnetite in clinopyroxene developed along grain boundary of relict olivine, sample CM-8-1B. Field of view is 1.2 x 1.6 mm, plane light. Compositions of coexisting phases are:

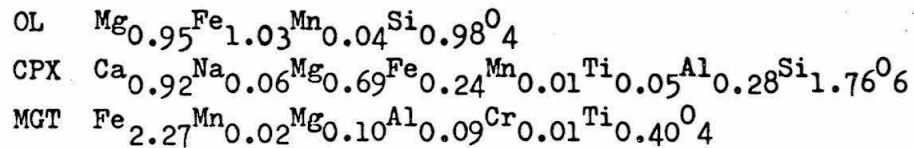
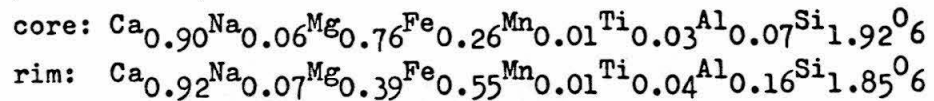
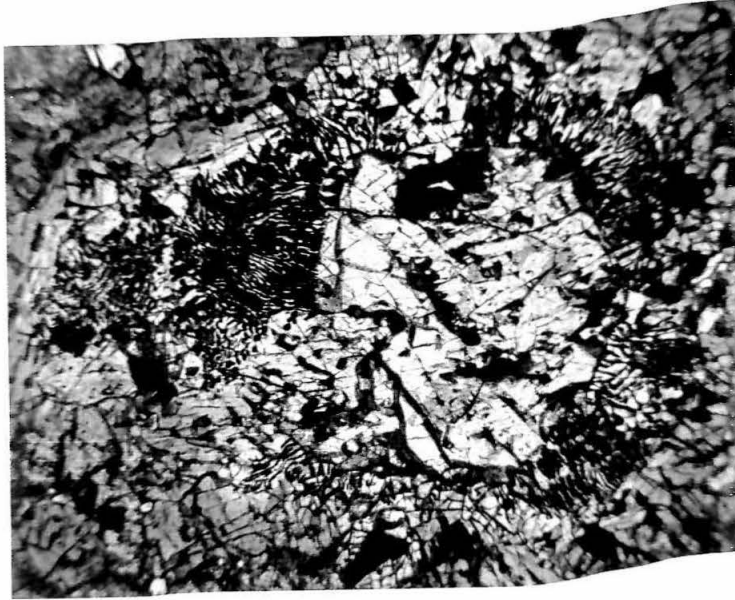


Figure 2. Vermicular magnetite in core of zoned clinopyroxene, sample CM-8-1B. Field of view is 1.2 x 1.6 mm, plane light. Clinopyroxene is zoned from





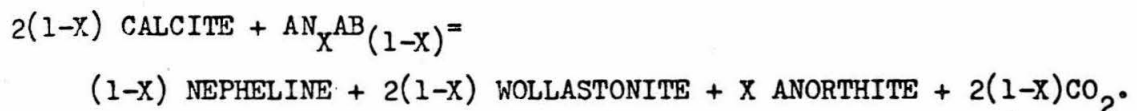
other analyzed samples (CM-8-9, CM-41-2) ranges from  $FO_{64}FA_{36}$  to  $FO_{47}FA_{53}$ , the ratio  $(Fe+Mn)/(Fe+Mn+Mg)$  of coexisting titanaugite and the composition of coexisting magnetite are essentially identical to those listed above. The reaction of olivine to clinopyroxene + magnetite requires an external source of titanium. The reaction probably involves contaminated magma and is analogous to the olivine reaction relationship in alkali basalts experimentally demonstrated by Schairer and Yoder (1960).

#### SUMMARY

Pyroxenite and calc-silicate skarn developed at the contact between gabbro and limestone are the result of reaction between gabbroic magma and limestone. The assemblage titanaugite + nepheline + sphene  $\pm$  alkali feldspar  $\pm$  wollastonite is the end product of assimilation of limestone by alkaline gabbro magma. The uneven modal distribution of titanaugite and nepheline in pyroxenite suggests that pyroxenite represents a crystal mesh of euhedral titanaugite "cemented" together by a late-solidifying, residual magma of nepheline syenite composition. The phases olivine, plagioclase, biotite and magnetite-ilmenite which are characteristic of the gabbro seldom occur in pyroxenite. Olivine and plagioclase in pyroxenite show textural evidence for reaction to form titanaugite + magnetite and nepheline, respectively. Potassium from biotite and titanium from biotite and ilmenite combined with other components of the magma to precipitate directly as alkali feldspar and as titanaugite and sphene. Compared with uncontaminated gabbro, pyroxenite is enriched in calcium and depleted in silicon and

aluminum. There is no systematic pattern of enrichment or depletion of other elements.

Assimilation of limestone by gabbroic magma involves two processes, (1) decarbonation reactions between calcite and magma and/or crystals in equilibrium with magma, and (2) crystallization of phases with which the magma is saturated, to supply energy for the endothermic decarbonation reactions. The essential mineralogic and textural features of pyroxenite can be produced by reaction between plagioclase and calcite,



Plagioclase in pyroxenite has corroded margins and is rimmed by nepheline, indicating resorption by the melt. Reaction between calcite and the plagioclase component of the magma caused resorption of crystalline plagioclase. Products of the decarbonation reaction went into solution in the contaminated magma. On crystallization, wollastonite entered clinopyroxene solid solution or combined with titanium to form sphene. Wollastonite occurs as a phase only in those rocks with an excess of CaO over that needed to combine with FeO and MgO as clinopyroxene. The anorthite component of the melt entered the clinopyroxene as  $\text{CaAl}_2\text{SiO}_6$ . Nepheline, the last phase to crystallize from contaminated magma, "cemented" together the aggregate of accumulated titanite.

The energy required for the endothermic decarbonation reactions was supplied by the crystallization of titanite from contaminated magma, liberating the enthalpy of fusion. For each mole of calcite

dissolved by the magma, approximately one mole of clinopyroxene was crystallized. Because the energy needed for the decarbonation reaction is provided by crystallization of the "heat equivalent" of clinopyroxene, the amount of limestone that may be assimilated is limited by the concentration of potential clinopyroxene in uncontaminated magma. Compositional zoning of titanite records the progressive depletion of magnesium and iron in the contaminated magma and preserves a record of the silica activity. Nepheline, the last phase to crystallize, "cemented" the clinopyroxene aggregate together.

On the basis of the spatial association of alkaline igneous rocks and limestone, R. A. Daly (1910) proposed the hypothesis that alkaline magma is produced by the desilication of subalkaline magma by the assimilation of limestone. Alkaline pyroxenite and nepheline syenite, developed at the intrusive contact in the Christmas Mountains are the result of assimilation of limestone by critically undersaturated gabbroic magma. However, the restricted occurrence of contaminated rocks in a narrow zone along the intrusive contact and the predominance of contaminated rocks of mafic and ultramafic composition provides little evidence for the generation of a significant volume of desilicated magma as a result of limestone assimilation.

#### 4. METASOMATIC GROWTH OF ZONED CALC-SILICATE NODULES FROM THE CONTACT AUREOLE INTRODUCTION

Within 60 meters of the intrusive contact with the Christmas Mountains gabbro, nodular chert in the Del Carmen and Santa Elena Limestones reacted with the enveloping marble to form spheroidal nodules of high-temperature calc-silicate minerals. Stoichiometric phases in the system  $\text{CaO-SiO}_2\text{-CO}_2$  form a series of concentric monomineralic and two-phase shells which record a step-wise decrease in the concentration of  $\text{SiO}_2$  from the core of a nodule to its rim. Wollastonite forms the core of each calc-silicate nodule and calcite marble forms the rim. In nodules collected within 30 meters of the gabbro, the calcite and wollastonite zones are separated by a monomineralic zone of tilleyite. Within 16 meters of the contact, the tilleyite zone is separated from wollastonite by a zone consisting of tilleyite plus spurrite and/or rankinite.

The sequence of monomineralic zones and consequent discontinuous gradient in bulk composition across each of the calc-silicate nodules are analogous to those developed by reaction between incompatible phases in the hypothetical example described by J. B. Thompson in his discussion of local equilibrium in metasomatism (Thompson, 1959, p. 430-34). Zoned calc-silicate nodules formed by reaction of chert with enclosing carbonate during thermal metamorphism have been described from several localities in the British Isles (Tilley and Alderman, 1934; Tilley, 1951b; W. Q. Kennedy, 1959). However, none of these nodule suites record the wide range of metamorphic temperatures while retaining the simplicity of mineralogy shown by the nodules from the Christmas Mountains.

Chemographic and experimental studies of mineral equilibria in the system  $\text{CaO-SiO}_2\text{-CO}_2$  suggest that, except for special compositions that correspond to those of the phases themselves, thermal metamorphism of siliceous limestone should result in mineral assemblages consisting of two solid phases (Bowen, 1940; Zharikov and Shmulovich, 1969). The fundamental problem posed by the calc-silicate nodules is that of why the initial compositional discontinuity between calcite and chert propagated as a series of monomineralic zones rather than as sequence of two-phase assemblages with continuous variation in modal composition.

Rocks made up of a series of mineral zones, each consisting of a relatively small number of phases, are commonly interpreted as being metasomatic in origin. D. S. Korzhinskii (1949, 1959) has developed theories to explain equilibrium among a small number of phases consisting of a large number of chemical species and to explain growth of mineral zones in an open system (Korzhinskii, 1970). However, Korzhinskii's methods have met with some criticism (Weill and Fyfe, 1964, 1967; Korzhinskii, 1966, 1967). The simplicity of the chemical system involved coupled with the knowledge of the initial and present configurations of mineral zones in the calc-silicate nodules suggested that a growth model might be constructed by comparison of local one- and two-phase assemblages from the nodules with those developed under conditions of equilibrium in a closed system, for a sequence of states leading from coexisting calcite + chert at low temperature to the monomineralic zones developed under conditions of intense thermal metamorphism. The simple example of the zoned calc-silicate nodules will perhaps provide fresh

insight into the role of the local mineral assemblage in the control of the chemical potentials of transported components and into the mechanisms of growth of monomineralic zones as the result of reaction between incompatible phases and consequent diffusion.

#### GEOLOGIC SETTING

Nodules of rusty-weathering, calcareous chert are sparsely distributed throughout the Lower Cretaceous Del Carmen and Santa Elena Limestones in the Christmas Mountains. Although nodular chert generally is a trace constituent in the stratigraphic section, at some horizons it makes up as much as 20 per cent of the rock. Nodules from one such horizon, exposed at an elevation of 1370 meters along the crest of the flat-topped ridge that forms the south wall at the mouth of Mud Springs Draw, were sampled at closely spaced intervals along a 120 meter traverse, normal to the contact with the Christmas Mountain gabbro, which dips 70° beneath the limestone at this locality.

Cross-cutting relations indicate that the rocks of the gabbro complex are the oldest of a series of intrusive and extrusive igneous rocks in the western part of the Christmas Mountains (Bloomer, 1949; Swadley, 1958; Jenkins, 1959). According to Maxwell (Maxwell, Lonsdale, Hazzard and Wilson, 1967, p. 300), during the early Tertiary, sedimentary and volcanic rocks accumulated in a basin bounded on the west by the then uplifted Christmas Mountains. It is thus likely that the maximum stratigraphic thickness in the Christmas Mountains at the time of gabbro emplacement was that of the complete Cretaceous section.

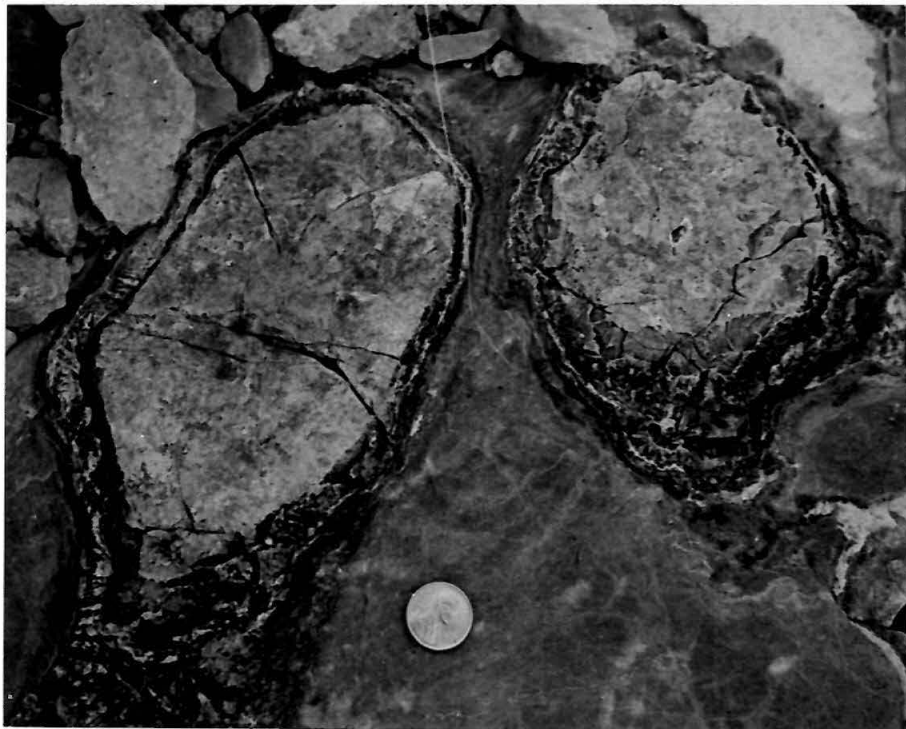
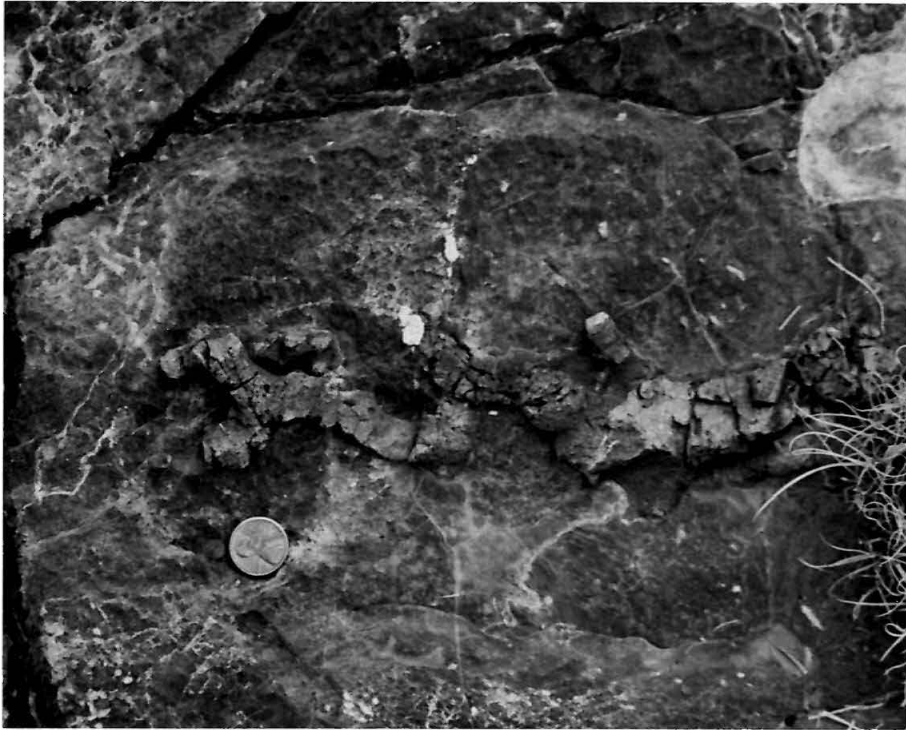
The sampled chert nodule bed is in the Santa Elena Limestone, about 115 meters stratigraphically above the base of the underlying Sue Peaks formation. The total thickness of strata, from the base of the Sue Peaks formation to the top of the Cretaceous section is 1345 meters (Bloomer, 1949; Maxwell et al., 1967), thus the sampled horizon was overlain by, at most, 1230 meters of rock at the time of gabbro emplacement. The lithostatic pressure at this depth was 325 bars, if an average rock density of  $2.7 \text{ gm/cm}^3$  is assumed.

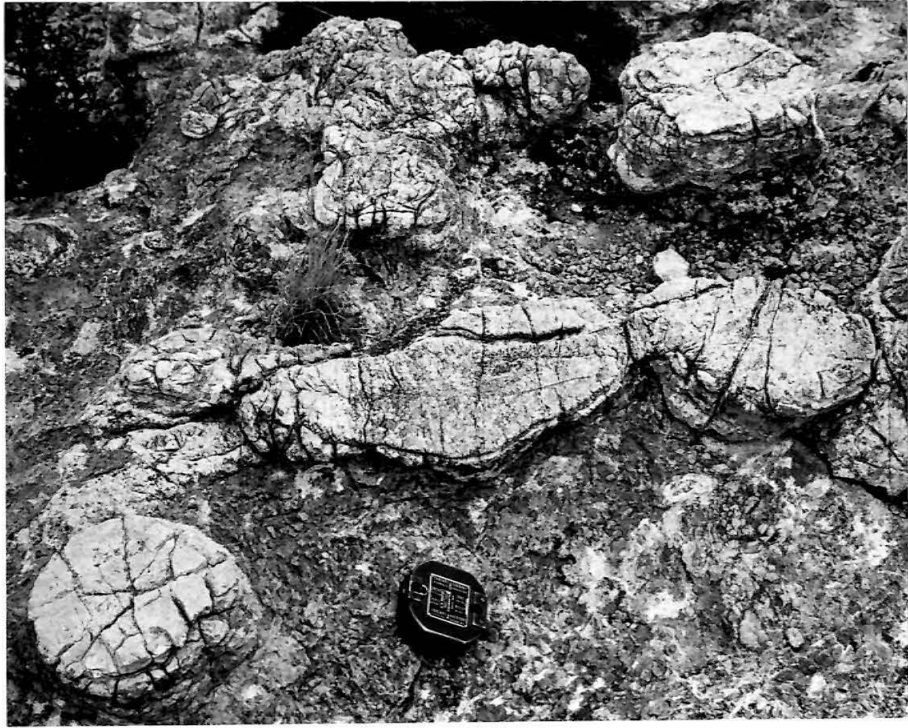
#### MORPHOLOGY OF NODULES

As the gabbro contact is approached along the traverse, a series of progressive changes take place in both the shape and the mineralogy of the chert nodules as a result of reaction between chert and limestone. In the unmetamorphosed limestone, chert nodules range in shape from equidimensional to very irregular, branching forms (Plate 1, figure 1). When the chert recrystallized to quartz or reacted with the enclosing limestone to form concentric shells of calc-silicate minerals, morphological irregularities were smoothed out. The resulting nodules are spherical or ellipsoidal in shape (Plate 1, figures 2-4). Although contacts between mineral zones within the calc-silicate nodules are generally parallel to the outer surface of the nodule, in some cases an internal contact may preserve an irregular feature which is smoothed on the outer surface (Plate 1, figure 3). Where nodules are closely spaced, two or more ellipsoidal nodules may be enclosed by a common rim (Plate 1, figure 4).

Plate 1. Chert and calc-silicate nodules in limestone and marble.

- Figure 1. Irregularly shaped nodules of rusty-weathering, black, aphanitic chert in dark-gray limestone, 122 meters from intrusive contact with gabbro. Penny, diameter 18 mm, gives scale.
- Figure 2. Spherical and ellipsoidal nodules of granular quartz in very fine-grained marble, 100 meters from intrusive contact with gabbro. Rim is idocrase + magnetite + quartz.
- Figure 3. Ellipsoidal nodules of coarse-grained wollastonite, rimmed by tilleyite in coarse-grained marble, 15 meters from intrusive contact with gabbro. Brunton compass, 70 mm square, gives scale.
- Figure 4. Zoned calc-silicate nodule in marble, 15 meters from intrusive contact with gabbro. Core of wollastonite is surrounded by zone of tilleyite + rankinite, 4 mm in width which in turn is surrounded by rim of tilleyite, 11-14 mm in width. Irregular shape of the wollastonite core is probably the result of coalescence, during growth, of two adjacent nodules.





## MINERALOGY

Perhaps the most striking feature of the nodules as seen in the field, is the change from homogeneous, aphanitic chert to concentrically zoned nodules of coarse-grained calc-silicate minerals. In addition to wollastonite, which forms the core of the nodules, and calcite, which forms the rim, individual calc-silicate nodules may contain rankinite, spurrite and tilleyite. The phases present in a given nodule are a function of the distance from the intrusive contact and reflect, in a general way, the thermal history of that point in the aureole. The calc-silicate minerals are distributed in concentric one- and two-phase shells, separated from one another by sharp contacts. Hence, the sequence of mineral assemblages across a nodule results in a radial compositional gradient along which the ratio of  $\text{CaO}$  to  $\text{SiO}_2$  increases in steps from the core of the nodule to the rim.

Mineral assemblages in the chert and calc-silicate nodules are listed in Table 1. The assemblages, as listed from left to right, correspond to the sequence of zones from the rim of the nodule to the core. As considered here, a mineral assemblage consists of those phases that are observed to be in mutual contact. In this context, the phases on either side of the boundary between monomineralic zones might be considered as a two-phase assemblage, but they have been listed as such in the table only in those cases in which the two phases are intergrown. Zone boundaries commonly are quite sharp and smoothly curving in three dimensions (Plate 2, figures 1-3). There is a marked tendency for one-phase assemblages to occur, but two- and rarely, three-phase assemblages are found in nodules collected within 18 meters of the gabbro.

Figure 1. Mineral phases in the system  $\text{CaO-SiO}_2\text{-CO}_2$ .  
Compositions of calcite, tilleyite and spurrite have been projected from  $\text{CO}_2$  onto the join  $\text{CaO-SiO}_2$ .

MINERAL PHASES IN THE SYSTEM  $CaO - SiO_2 - CO_2$

- C CALCITE
- T TILLEYITE
- S SPURRITE
- L LARNITE
- R RANKINITE
- W WOLLASTONITE
- Q QUARTZ

- $CaCO_3$
- $Ca_5Si_2O_7(CO_3)_2$
- $Ca_5Si_2O_8CO_3$
- $Ca_2SiO_4$
- $Ca_3Si_2O_7$
- $CaSiO_3$
- $SiO_2$

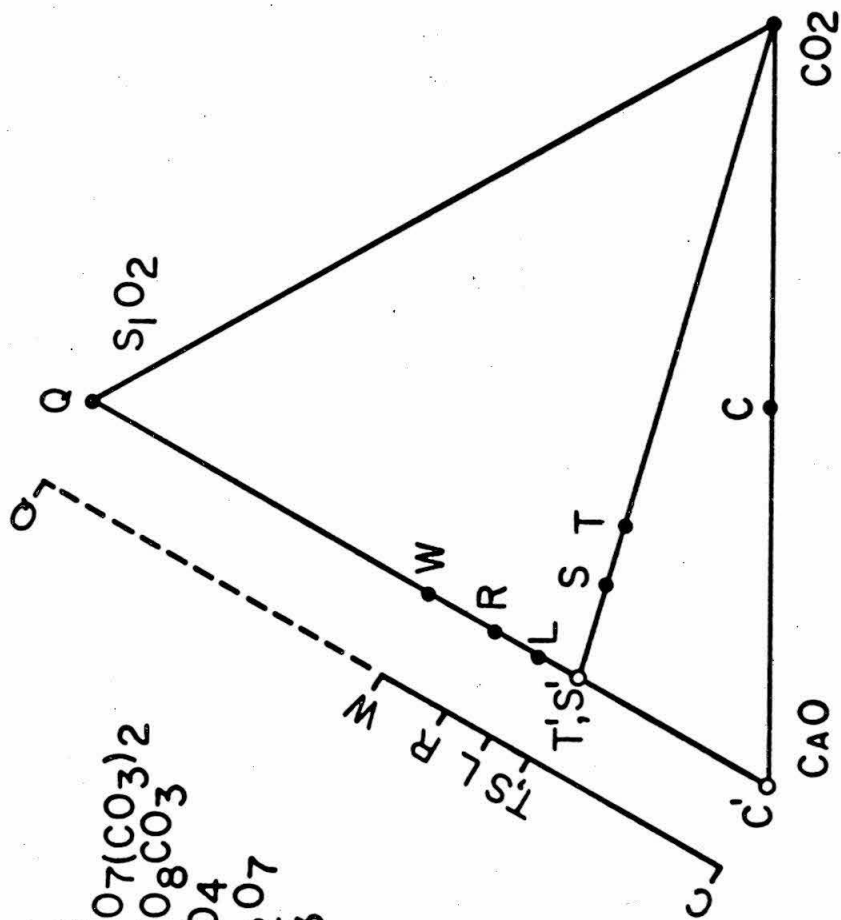


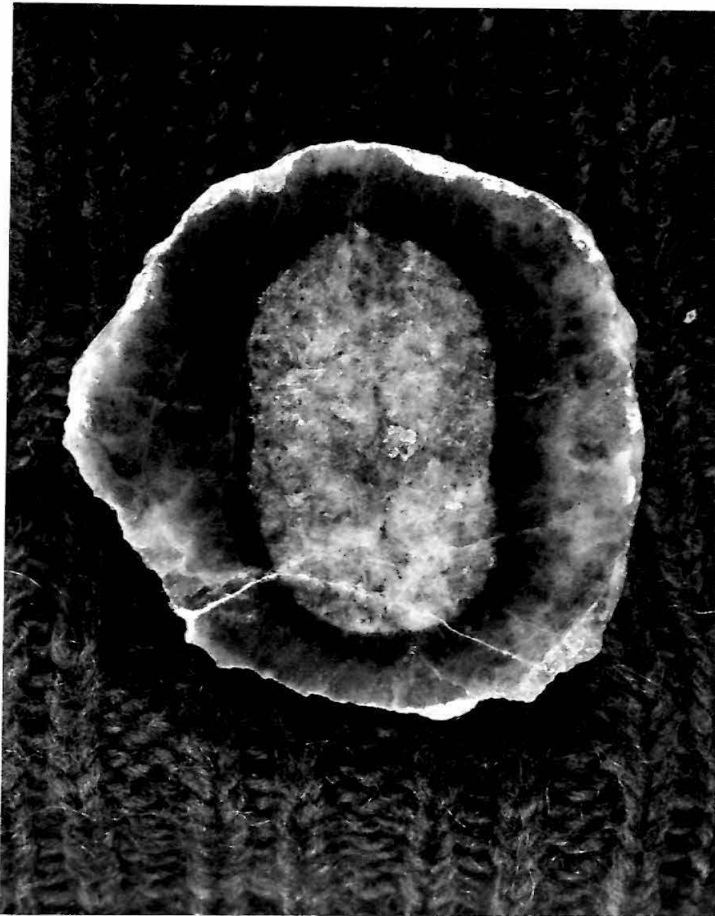


Plate 2. Zoned calc-silicate nodule, CM-124, collected 15 meters from intrusive contact with gabbro.

Figure 1. Slab cut through center of nodule, 50 mm in diameter. Core is wollastonite. Light gray outer rim is granoblastic tilleyite. Black zone between wollastonite and granoblastic tilleyite is made up of tilleyite, each grain of which is oriented with its C-axis perpendicular to the contact with wollastonite.

Figure 2. Thin section cut from slab facing that photographed in Figure 1, crossed nicols, negative print. Core of wollastonite is enclosed by rim of "radial" tilleyite. Granoblastic tilleyite is visible at upper left and upper right corners. Thin section is 20 x 37 mm.

Figure 3. Contact between zone of "radial" tilleyite and single crystal of wollastonite. Crossed nicols, field is 2.3 x 3.0 mm.





Chert nodules from unmetamorphosed limestone consist of microcrystalline silica and calcite. Calcite occurs in irregular patches of granular grains and as microfossils. Although it is not uniformly distributed within a nodule, calcite generally makes up about ten per cent of its volume. Contacts between chert and enclosing limestone are sharp. In the interval 70 to 100 meters from the gabbro, microcrystalline silica has been recrystallized to a xenoblastic aggregate of quartz.

Although minor amounts of magnesium, aluminum, titanium and iron occur in the chert, more than 99 per cent of the volume of an individual calc-silicate nodule consists of stoichiometric phases of the system  $\text{CaO-SiO}_2\text{-CO}_2$ . Unmetamorphosed nodules of black, aphanitic chert have a rusty, weathered rind of iron oxide. Magnetite, and rarely, perovskite and yellow titanian andradite are accessory phases in the tilleyite zone of calc-silicate nodules. Pseudomorphs of idocrase after euhedral melilite commonly form a discontinuous rim separating calcite marble from the wollastonite or tilleyite zone of calc-silicate nodules.

Nodules collected between 30 and 60 meters from the gabbro-marble contact consist entirely of fine- to very coarse-grained, prismatic wollastonite. The contact between the wollastonite nodule and enclosing calcite marble is sharp. The assemblage wollastonite-quartz has not been found.

Nodules collected between 18 and 30 meters from the contact have a core of coarse, prismatic wollastonite which is separated from marble by a rim of granoblastic tilleyite, 0.5 to 1 centimeter in width. In most of the nodules from this interval, tilleyite is nearly completely

replaced by fibrous scawtite(?), but irregular relicts of fresh tilleyite confirm its presence in this zone. Apart from this fibrous alteration of tilleyite, calcite, tilleyite and wollastonite occur in well-defined, monomineralic zones. There are no incompatible phases in contact across zone boundaries. That is, calcite and wollastonite are never found in mutual contact.

Calc-silicate nodules collected within 16 meters of the gabbro contain calcite, tilleyite, rankinite, wollastonite and, in some cases, spurrite. However, the pattern of simple monomineralic zonation established for calc-silicate nodules from the interval 16 to 70 meters from the contact is modified by the presence of two- and three-phase assemblages. Calcite, tilleyite and wollastonite form monomineralic zones as before, but spurrite and rankinite occur exclusively in two- and three-phase assemblages with tilleyite or wollastonite. One- and two-phase assemblages form distinct zones in the calc-silicate nodules but three-phase assemblages usually consist of isolated grains of the third phase within a two-phase zone. For example, the observed three-phase assemblages, tilleyite-spurrite-rankinite and tilleyite-rankinite-wollastonite consist of single grains of spurrite or wollastonite in zones consisting mainly of tilleyite and rankinite.

The most commonly occurring two-phase assemblages consist of tilleyite and either calcite, spurrite, rankinite or wollastonite. The assemblage tilleyite-wollastonite occurs in nearly every nodule sampled within 16 meters of the gabbro. If it is assumed that each of the solid phases coexists with  $\text{CO}_2$ , then tilleyite and wollastonite should be

incompatible in a zoned nodule containing rankinite and/or spurrite. Tilleyite occurs in three distinct textural habits, two of which are present in every nodule that has a zone with the assemblage tilleyite-wollastonite. Where it occurs in a monomineralic zone or in a two-phase assemblage with either calcite or spurrite, tilleyite forms a granoblastic aggregate of equidimensional grains. Tilleyite is free of inclusions and the second phase, where present, is interstitial to it. In the interval 11 to 16 meters from the gabbro, nodule cores of monomineralic wollastonite are separated from granoblastic tilleyite by a zone of prismatic crystals of tilleyite, the long axes (C-axes) of which are oriented perpendicular to the surface of contact between the concentric shells (Plate 2, figures 2 and 3). The inner part of the zone of "radial" tilleyite consists of two- and rarely, three-phase assemblages involving rankinite and/or wollastonite. The outer part of the zone is monomineralic. Within 11 meters of the gabbro, tilleyite in the cores of nodules forms irregular, spongy crystals with numerous poikiloblastic inclusions of either rankinite or wollastonite. The ratio of inclusion to host is more or less constant across the two phase zone, the bulk composition of which approximates that of rankinite + carbon dioxide. The occurrence of tilleyite in two distinct textural habits within a single nodule suggests that it may have grown under different environmental conditions by different mineral reactions. Granoblastic tilleyite probably represents growth under prograde conditions whereas the "radial" and "spongy" habits result from reaction of spurrite and/or rankinite with varying amounts of  $\text{CO}_2$  on cooling.

Nodules collected within 16 meters of the intrusive contact differ from the other calc-silicate nodules in two important respects. The first is the abrupt appearance, in a single nodule, of two new phases, spurrite and rankinite, as contrasted with the appearance of a single new phase in each of the other calc-silicate zones. Second, the restriction of spurrite and rankinite to two- and three-phase assemblages is a significant departure from the pattern of monomineralic assemblages characteristic of calc-silicate nodules from the outer part of the aureole.

No calc-silicate nodules were sampled nearer the intrusive contact than 4.6 meters. However, the sequence of carbonate and calc-silicate minerals which coexist with melilite, titanian andradite, perovskite and magnetite across the one meter wide skarn formed at the contact between marble and gabbro is calcite, spurrite, rankinite and wollastonite. Although the bulk chemistry of the skarn is quite removed from the system  $\text{CaO-SiO}_2\text{-CO}_2$ , the presence of a single phase from the simple system in each of the skarn mineral zones is suggestive of the pattern of monomineralic zonation that might be found in a calc-silicate nodule formed at that location in the aureole.

Neglecting, for the moment, the two- and three-phase assemblages, the sequence of sets of phases in nodules and skarn, listed in the order encountered as the intrusive contact is approached is:

CALCITE-QUARTZ

CALCITE-WOLLASTONITE

CALCITE-TILLEYITE-WOLLASTONITE

CALCITE-TILLEYITE+SPURRITE-RANKINITE-WOLLASTONITE

CALCITE-SPURRITE-RANKINITE-WOLLASTONITE

Each set of phases differs from its neighbor by the appearance or disappearance of a single phase. The exception to this is the sequence of assemblages found in nodules collected within 18 meters of the gabbro, in which spurrite and rankinite make their first appearance together. The question naturally arises as to whether spurrite and rankinite resulted from a single reaction or from two separate reactions. If the latter were the case, the order in which they formed with increasing temperature may yield information which would place limits on the pressure and fluid phase composition during metamorphism.

The first step in the development of a growth model for the zoned calc-silicate nodules is the determination of whether the two-phase assemblages at the boundaries between monomineralic zones are compatible with equilibrium. It is thus necessary to examine the chemographic relationships among phases in the system  $\text{CaO-SiO}_2\text{-CO}_2$  and to construct a petrogenetic grid relating the sequence of possible mineral reactions to variations in the intensive environmental variables of temperature, pressure and fluid phase composition.

#### PETROGENETIC GRID

From consideration of natural parageneses and chemographic relationships in the system  $\text{CaO-MgO-SiO}_2\text{-CO}_2$ , N. L. Bowen deduced a sequence of reactions or steps which take place between the minerals of siliceous limestone or dolomite with increasing temperature (Bowen, 1940). The network on a pressure-temperature diagram resulting from the intersection of these decarbonation and solid-solid reactions forms a "petrogenetic grid" which, when experimentally calibrated, allows the estimation of

the pressure and temperature conditions of metamorphism from mineral assemblages of metamorphosed siliceous carbonate rocks. A calibrated petrogenetic grid has been constructed for the system  $\text{CaO-SiO}_2\text{-CO}_2$  based on the experimental data of Harker and Tuttle (1956) and Zharikov and Shmulovich (1969).

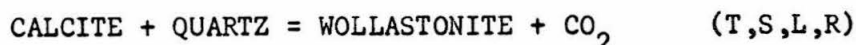
The chemical compositions of the six phases, calcite, tilleyite, spurrite, larnite, rankinite and wollastonite can be completely described in terms of their component oxides,  $\text{CaO}$ ,  $\text{SiO}_2$  and  $\text{CO}_2$ . Graphical representation of the compositions of minerals in the system  $\text{CaO-SiO}_2\text{-CO}_2$  is shown in Figure 1. However, by restricting consideration to only those assemblages that equilibrated with a fluid phase containing carbon dioxide, the chemical potential or mole fraction of  $\text{CO}_2$  in the fluid may be treated as an independent environmental variable and the number of components reduced to two (Thompson, 1957, p. 844-45). Using the combinatorial rules of Korzhinskii (1959, p. 128), a pressure-temperature diagram for a two component system with six phases will consist of 15 invariant points joined together by 20 univariant lines. Construction of such a diagram requires knowledge of 14 geometrically independent parameters such as the P-T coordinates of invariant points and the slopes of univariant lines.

The 20 univariant reactions are specified by the stoichiometry of the phases and may be determined by listing all possible combinations of the six phases, taken three at a time. In treating the system in terms of two components, tilleyite and spurrite become compositionally indistinguishable or degenerate (Zen, 1966, p. 30), so that the four reactions

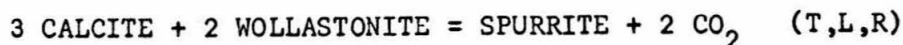
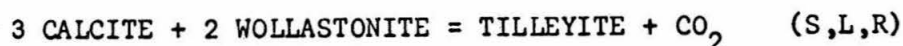
involving only these two phases coincide stable to metastable. The result is that there are only 17 distinct, but not independent, mineral reactions. These reactions, labeled by placing the abbreviations for the phases which do not participate in the reaction in parentheses, are listed in Table 2.

Zharikov and Shmulovich (1969) experimentally determined the P-T coordinates of four algebraically independent univariant reactions in this system. Knowledge of the slopes of these reactions as well as their position on the P-T plane is sufficient to allow computation of the slopes of the 13 remaining univariant reactions and location of the 15 invariant points.

R. I. Harker and O. F. Tuttle experimentally determined the pressure-temperature coordinates of the reaction:



(Harker and Tuttle, 1956) and of the three univariant reactions involving the phases, calcite, tilleyite, spurrite, wollastonite and carbon dioxide:

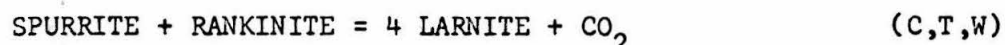
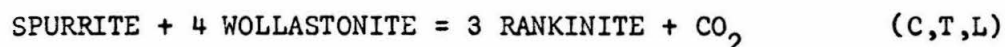


(Tuttle and Harker, 1957, Harker, 1959). Although Harker was able to reverse both reactions involving tilleyite, he was unable to do so without the introduction of  $\text{Al}_2\text{O}_3$  and  $\text{CaF}_2$  into the system.

Zharikov and Shmulovich (1969) redetermined the pressure-temperature curves for reactions (S,L,R) and (C,L,R,W) without recourse to the use

of flux. Their results, which at a given pressure, lie 10° to 40°C above those of Harker, have been used in the computations that follow in order that an internally consistent set of data may be used in construction of the petrogenetic grid.

Zharikov and Shmulovich (1969) also determined the pressure-temperature coordinates for the following reactions for the breakdown of rankinite and larnite in the presence of carbon dioxide:



A petrogenetic grid for the system  $\text{CaO-SiO}_2\text{-CO}_2$  was constructed by plotting the univariant curves determined by Zharikov and Shmulovich (1969) on a pressure-temperature diagram and applying Schreinemaker's rules (Zen, 1966) to generate additional reactions to complete the bundles at points of intersection. Because the location of invariant points is very sensitive to the slopes of the reactions involved, the pressure-temperature coordinates of the univariant curves used in construction of the petrogenetic grid were determined by fitting a line to each set of experimentally bracketed reversals on a plot of the natural log of the equilibrium constant (K), corrected to constant pressure, as a function of the reciprocal of absolute temperature (1/T) (Orville and Greenwood, 1965; Anderson, 1970). As pointed out by Anderson (1970), the treatment of experimental data by this method has two distinct advantages over the fitting of a curve to the bracketed reversals on a pressure-temperature plot. First, the curve can be accurately extrapolated beyond the range of conditions of the experiment because a univariant curve is linear on

a plot of  $\ln K$  versus  $(1/T)$ . Second, such a curve is capable of yielding a self-consistent set of thermochemical data needed for computation of slopes of those reactions which complete the petrogenetic grid.

The slope of a univariant curve on the  $\ln K - (1/T)$  diagram is equal to the negative of the standard enthalpy of reaction ( $\Delta H_R^\circ$ ), divided by the gas constant. The numerical value of the equilibrium constant,  $K$ , and hence, the value of  $\Delta H_R^\circ$ , depends on the choice of standard states for the species involved in the reaction. Anticipating the need for the enthalpy of reaction ( $\Delta H_R$ ) for computation of isobaric temperature-fluid composition sections through the pressure-temperature diagram, standard states were chosen which approximate the conditions of the equilibrium states. The standard states which satisfy this criterion consist of pure crystalline solids and pure fluid carbon dioxide at the temperature of equilibrium and a uniform pressure, taken in this case to be 500 bars. For this choice of standard states, the activities of all components of the solids are unity, so that the equilibrium constant reduces to the fugacity of  $\text{CO}_2$  which would maintain the equilibrium at the temperature of the experiment and a pressure of 500 bars. The standard reaction enthalpies, corrected to a pressure of 1 atmosphere, computed from the experimental data of Harker and Tuttle (1956) and Zharikov and Shmulovich (1969) are listed in Table 2.

Pressure-temperature coordinates of reactions (S,L,R), (C,L,R,W), (C,T,L), and (C,T,W) as well as that involving calcite, quartz and wolastonite, were derived from  $\ln K - (1/T)$  plots by expressing the equilibrium constant in terms of the fugacity of carbon dioxide which was

TABLE 2  
MINERAL REACTIONS IN THE SYSTEM CaO-SiO<sub>2</sub>-CO<sub>2</sub>

LABEL	REACTION	$\Delta H_1^\circ$ atm KCAL/MOL
(C,T,S)	RANKINITE = LARNITE + WOLLASTONITE	4.3
(C,T,L)	SPURRITE + 4 WOLLASTONITE = 3 RANKINITE + CO <sub>2</sub>	31.7
(C,T,R)*	SPURRITE + WOLLASTONITE = 3 LARNITE + CO <sub>2</sub>	44.4
(C,T,W)	SPURRITE + RANKINITE = 4 LARNITE + CO <sub>2</sub>	48.7
(C,S,L)	TILLEYITE + 4 WOLLASTONITE = 3 RANKINITE + 2CO <sub>2</sub>	56.3
(C,S,R)	TILLEYITE + WOLLASTONITE = 3 LARNITE + 2 CO <sub>2</sub>	69.0
(C,S,W)	TILLEYITE + RANKINITE = 4 LARNITE + 2 CO <sub>2</sub>	73.3
(C,L,R,W)	TILLEYITE = SPURRITE + CO <sub>2</sub>	24.6
(T,S,L)*	CALCITE + 2 WOLLASTONITE = RANKINITE + CO <sub>2</sub>	27.3
(T,S,R)	CALCITE + WOLLASTONITE = LARNITE + CO <sub>2</sub>	31.5
(T,S,W)*	CALCITE + RANKINITE = 2 LARNITE + CO <sub>2</sub>	35.8
(T,L,R)	3 CALCITE + 2 WOLLASTONITE = SPURRITE + 2 CO <sub>2</sub>	50.2
(T,L,W)*	2 CALCITE + RANKINITE = SPURRITE + CO <sub>2</sub>	22.9
(T,R,W)	SPURRITE = CALCITE + 2 LARNITE	12.9
(S,L,R)	3 CALCITE + 2 WOLLASTONITE = TILLEYITE + CO <sub>2</sub>	25.6
(S,L,W)*	TILLEYITE = 2 CALCITE + RANKINITE	1.7
(S,R,W)	TILLEYITE = CALCITE + 2 LARNITE + CO <sub>2</sub>	37.7
(T,S,L,R)	CALCITE + QUARTZ = WOLLASTONITE + CO <sub>2</sub>	24.5

\* Reaction is metastable at all pressures and temperatures. Enthalpies of reactions (T,S,L,R), (S,L,R), (C,L,R,W), (C,T,L) and (C,T,W) were derived from slope on  $\ln K - (1/T)$  plot of experimentally bracketed reversals using standard states consisting of pure crystalline solids and pure fluid CO<sub>2</sub> at the temperature of the experiment and a pressure of 500 atm. Enthalpies of all other reactions result from linear combinations of the enthalpies of the experimentally determined reactions. All enthalpies have been corrected to a pressure of 1 atmosphere.

then converted to pressure using the fugacity data of Majumdar and Roy (1956). Thirteen additional reactions are required to complete the bundles at the invariant points formed by the intersection of the experimentally determined curves. The  $\ln K - (1/T)$  coordinates of these reactions were computed from their standard reaction enthalpies as derived from linear combinations of the standard enthalpies of the experimentally determined reactions, with the constraint that they originate at an invariant point and lie between the appropriate stable and metastable extensions of adjacent reactions. The latter condition posed a real test of the self-consistency of the thermochemical data which was passed in all cases. The standard reaction enthalpies, corrected to a pressure of one atmosphere, are listed in Table 2.

The pressure-temperature grid consists of 15 invariant points, of which 6 are stable, joined by 20 univariant curves, only 12 of which represent both stable and distinct reactions. The topological relationships between stable invariant points, univariant curves and chemographically compatible mineral assemblages or facies types (Albee, 1965, p. 514) are shown schematically on Figure 2 and are plotted to scale with respect to pressure and temperature on Figure 3.

The intersecting univariant reactions partition off the pressure-temperature plane on a fine scale so that the P-T gradients in contact metamorphism may be closely defined on the basis of the sequence of facies types encountered on traversing a contact aureole. Due to the existence of several stable invariant points within a geologically reasonable range of P and T, the sequence of decarbonation reactions

Figure 2. Schematic pressure-temperature diagram for system  $\text{CaO-SiO}_2\text{-CO}_2$ . Univariant reactions are labeled by a list of phases which do not take part in the reaction, enclosed in parentheses ( ). Invariant points are labeled by a list of the phases which are not involved, enclosed in square brackets [ ]. Abbreviations for minerals are as listed in Figure 1.



Figure 3. Calibrated pressure-temperature diagram for system  $\text{CaO-SiO}_2\text{-CO}_2$  for  $X_{\text{CO}_2}$  in fluid phase equal to one. Pressure-temperature<sup>2</sup> coordinates for univariant curves and invariant points computed from experimentally bracketed reversals for reactions (S,L,R), (C,T,L), (C,T,W) and (C,L,R,W) determined by Zharikov and Shmulovich (1969) and for reaction (T,S,L,R) determined by Harker and Tuttle (1956). Abbreviations as on Figure 1.



in the progressive metamorphism of a siliceous limestone proposed by Bowen (1940) and modified by Tilley (1951), represents but one of several possible P-T gradients or facies series.

#### CONDITIONS OF METAMORPHISM

The calc-silicate nodules are ideally suited for the definition of the thermal gradient resulting from the emplacement of the Christmas Mountains gabbro complex because they occur within a limited stratigraphic interval, exposed across the full width of the contact aureole and because the range of bulk compositions represented by the set of mineral zones in each nodule completely defines a facies type in the simple system, at least in the ideal case. The very narrow temperature range over which some of the critical facies types are stable poses the practical problem of demonstrating their formation in that they may be readily overstepped and easily retrograded.

The P-T gradient across the aureole may be estimated to within narrow limits on the basis of the observed sequence of facies types. In addition, an independent estimate of the lithostatic pressure allows an estimate of the maximum temperature represented by each facies type, and hence, reconstruction of the thermal gradient across the aureole. A stratigraphic reconstruction based on the argument that the maximum thickness of strata overlying the calc-silicate nodule horizon at the time of gabbro emplacement was that of the Cretaceous units, 1230 meters, results in a maximum lithostatic pressure of about 325 bars.

The P-T gradient based on the sequence of facies types in the aureole is consistent with this estimate, but the evidence is not entirely

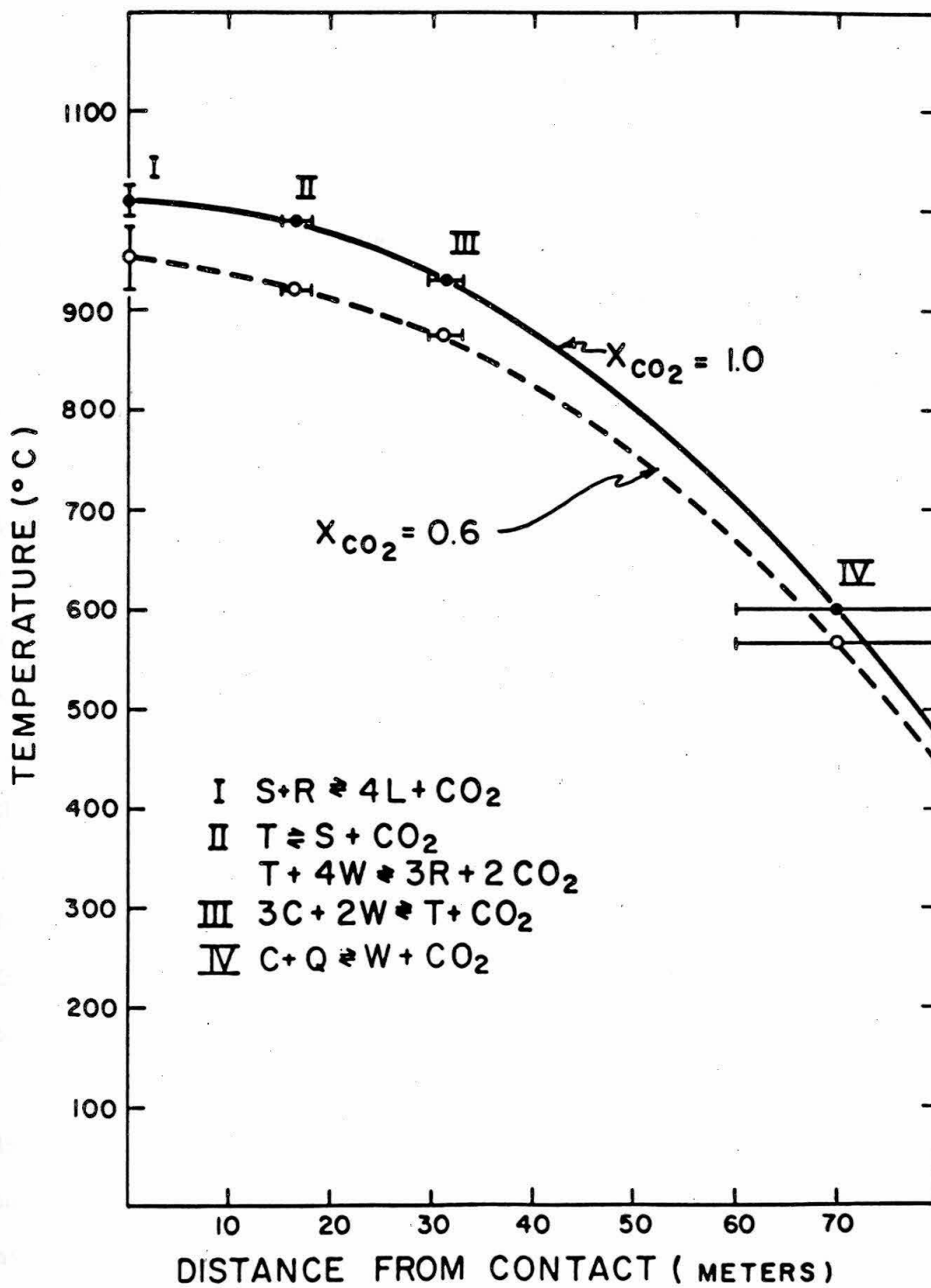
unequivocal. The coexistence of calcite with spurrite, spurrite with rankinite and rankinite with wollastonite in the skarn at the gabbro contact limits the maximum lithostatic pressure to that of the [C,W] invariant point, 500 bars. The difficulty in assigning a lower limit to pressure lies in the interpretation of the two- and three-phase assemblages of the nodules collected within 16 meters of the gabbro contact. The problem involves the identification of the facies type that is transitional between the contact skarn in which spurrite and rankinite coexist and calc-silicate nodules with coexisting tilleyite and wollastonite. The transition may be made via either of two facies types, depending on whether the lithostatic pressure was greater than or less than that of the [C,L] invariant point. If the pressure was less than about 150 bars, the assemblage spurrite + wollastonite should occur and spurrite should make its first appearance in a nodule farther from the gabbro contact than that in which rankinite first occurs. Conversely, if the pressure exceeded 150 bars, the assemblage tilleyite + rankinite should be found to the exclusion of spurrite + wollastonite, and rankinite should appear before spurrite on a traverse across the aureole, toward the gabbro. However, rather than appearing sequentially, both spurrite and rankinite make their first appearance in a single nodule, 15 meters from the gabbro contact. This complication might have been anticipated in that the temperature intervals over which the facies types defined by the assemblages spurrite + wollastonite and by tilleyite + rankinite are at most 10°C in width. Although relationships are partially obscured by tilleyite of probable retrograde origin, the

common occurrence of the assemblages tilleyite + rankinite and tilleyite + spurrite and the fact that the assemblage spurrite + wollastonite was not found, suggest that metamorphism took place at pressure greater than that of the [C,L] invariant point. Thus, metamorphism took place at a lithostatic pressure of 150 to 500 bars, a range consistent with the stratigraphic estimate of 325 bars.

The absence of the assemblages spurrite + larnite and larnite + rankinite in the skarn indicates that the temperature of reaction (C,T,W) was not exceeded. At a lithostatic pressure of 325 bars, the maximum temperature at the contact was between 995 and 1025°C, if pure CO<sub>2</sub> was present. A thermal gradient, recording maximum temperature attained from point to point across the aureole may be constructed by plotting the temperature at 325 bars, for each univariant reaction bracketed by the sequences of facies types as a function of its location in the contact aureole (Figure 4). The temperatures on which the gradient is based are those at which the reactions would take place in the presence of a fluid phase consisting of pure CO<sub>2</sub>. If the fluid phase was not pure, or if none was present, the temperatures would be lower.

However, the assumption that metamorphism of the chert nodules involved a relatively pure CO<sub>2</sub> fluid is not unreasonable. Carbon dioxide was generated in each of the prograde mineral reactions at the zone boundaries. Diffusing radially outward under an internally generated pressure gradient, CO<sub>2</sub> would readily mix with or displace any water in the neighborhood of a reacting nodule. The extent of a decarbonation reaction necessary to produce sufficient CO<sub>2</sub> to saturate the local

Figure 4. Gradient of maximum temperatures attained in the contact aureole as determined by position of reactions divariant in  $P-T-X_{CO_2}$ . Horizontal bar is uncertainty in location of reaction due to spacing of samples. Temperature at contact was greater than that of reaction II but less than that of I.



environment of a nodule is small. For example, reaction of 1 mole of calcite with 1 mole of quartz to form 1 mole of wollastonite plus 1 mole of  $\text{CO}_2$  yields  $225 \text{ cm}^3$  of  $\text{CO}_2$  at  $600^\circ\text{C}$  and 325 bars. For a spherical chert nodule with an initial radius of 3 cm, 1 mole of wollastonite would form a concentric shell, separating calcite from quartz, 0.4 cm thick. The answer to the question of whether or not the fluid phase in the local environment of a reacting nodule was pure carbon dioxide depends on the relative rates at which  $\text{CO}_2$  is generated by mineral reactions and either transported away from the reaction site or diluted by  $\text{H}_2\text{O}$ .

However, because the lithostatic pressure may be estimated independently of the mineralogy of the calc-silicate nodules, the sequence of facies types developed across the aureole provides a test of the fluid phase composition. Figure 5 is an isobaric temperature-fluid phase composition section through the petrogenetic grid in the vicinity of the [C,L] invariant point. Univariant curves on the  $T\text{-}X_{\text{CO}_2}$  diagram represent the projection of divariant reaction surfaces from  $P\text{-}T\text{-}X_{\text{CO}_2}$  space onto the  $T\text{-}X_{\text{CO}_2}$  plane. The  $T\text{-}X_{\text{CO}_2}$  coordinates of the reactions were computed from the reaction enthalpies derived from the phase equilibrium data of Zharikov and Shmulovich (1969) using the integrated form of equation 9 of Greenwood (1967, p. 546).

If coexisting tilleyite and rankinite in nodules collected within 15 meters of the gabbro represent stable equilibration within the field bounded by reactions (C,S,L) and (C,L,R,W), then the projected position of the [C,L] invariant point limits possible fluid phase compositions to those in which the mole fraction of  $\text{CO}_2$  is greater than 0.6. A lower

Figure 5. Isobaric temperature-fluid composition diagram for system  $\text{CaO-SiO}_2\text{-CO}_2$  at pressure of 300 bars. Abbreviations as in Figure 1.



limit to the thermal gradient across the aureole, constructed using the temperatures of the reactions for  $X_{\text{CO}_2} = 0.6$ , is shown as a dashed line on Figure 4. In the case of the maximum possible dilution of carbon dioxide-rich fluid phase, reaction temperatures are depressed 40 to 60°C below those involving pure  $\text{CO}_2$ .

#### THERMAL HISTORY

The present gabbro outcrop is shaped like a letter "J", but doming of the limestone along the contact suggests that the older olivine-titanaugite gabbro was emplaced as a cylindrical body, about 1400 meters across. Biotite-titanaugite gabbro, in contact with nodule-bearing limestone on one side and olivine-titanaugite gabbro on the other, was intruded as an arcuate mass, 150 to 250 meters in width, along the original gabbro-limestone contact. Although matching of the inferred thermal gradient across the aureole by a mathematical model is made very difficult by the two-stage emplacement history of the gabbroic rocks, the general features of the gradient can be understood by means of a simple model based on a plane-sheet geometry. The restriction of fluid phase compositions to those rich in  $\text{CO}_2$  rules out the possibility that heat was convectively transferred by a water-rich magmatic fluid, expanding outward into the aureole. Thus, it is realistic to treat the heat flow problem as one in which conduction is the dominant transport mechanism.

The model used in the thermal calculations is based on Neumann's solution to the Fourier conduction equation for the case involving dissimilar physical properties of solidified magma and country rock. The details of the solution and some representative applications are given by Carslaw

and Jaeger (1959, p. 288-289) and by Jaeger (1959, p. 45-46; 1964, p. 452-453). Numerical values of the physical parameters and the notation used in the calculations are listed in Table 3, along with the pertinent equations.

As a first approximation, the composite intrusion may be treated as an infinite plane sheet, 1625 meters thick. At the time of complete solidification, about 20,000 years after intrusion, the gradient across the aureole is approximately linear, ranging from 750°C at the contact to 690°C, 80 meters out in the marble. Comparison of the calculated gradient with that inferred from the mineralogy of the calc-silicate nodules shows that the computed gradient is not as steep as that observed, particularly in the outer part of the aureole, and that the temperatures near the contact are about 200°C lower than required by the mineralogy while those in the outer part of the aureole are about 100°C too high.

A model which takes into account the geologic history of the gabbro complex, while retaining the simple plane sheet geometry, can be constructed by considering a sheet of magma, 1400 meters thick, intruded into limestone, followed by the emplacement of a 225 meter thick magma sheet along the original limestone contact on one side of the first sheet, after the first sheet has partially solidified. Partial solidification of the first sheet prior to intrusion of the second, would impose a steep thermal gradient across the aureole. If solidification proceeded 300 meters inward from the contact by the time the second sheet was intruded, the initial temperature at the plane of contact between the second sheet and the limestone would be about 325°C. Intrusion of the second sheet

TABLE 3  
PHYSICAL PARAMETERS AND EQUATIONS FOR HEAT  
CONDUCTION CALCULATIONS

	GABBRO(i)	LIMESTONE(c)
Density ( $\rho$ ) gm/cm <sup>3</sup>	2.94	2.66
Heat Capacity (c) cal/gm-°C	0.29	0.30
Thermal Conductivity (K) cal/cm-sec-°C	0.0049	0.0042
Diffusivity ( $\kappa$ ) cm <sup>2</sup> /sec	0.0057	0.0053
Enthalpy of Fusion (L) cal/gm	93	
Melting Temperature (Tm) °C	1200	

Temperature at time, t at distance, x from contact of intrusion of width, 2a:

$$T = T_0 \left( 1 + \operatorname{erf} \frac{a - x}{2\sqrt{\kappa_c t}} \right)$$

Where the contact temperature  $T_0$  is:

$$T_0 = \frac{\sigma(T_m - T_i)}{(\sigma + \operatorname{erf} \lambda)}$$

$T_i$  is the initial temperature,

$$\sigma = \frac{K_i \sqrt{\kappa_c}}{K_c \sqrt{\kappa_i}}$$

and  $\lambda$  is the root of:

$$\lambda e^{\lambda^2} (\sigma + \operatorname{erf} \lambda) = \frac{c_i (T_m - T_i)}{L\sqrt{\pi}}$$

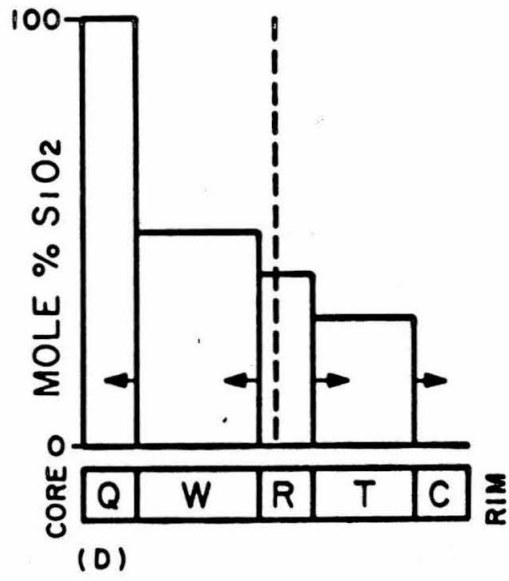
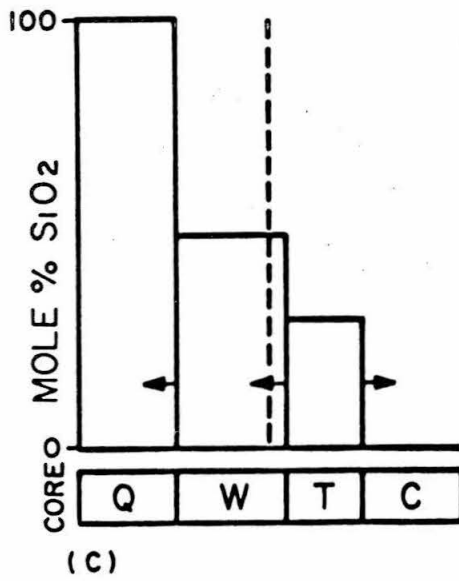
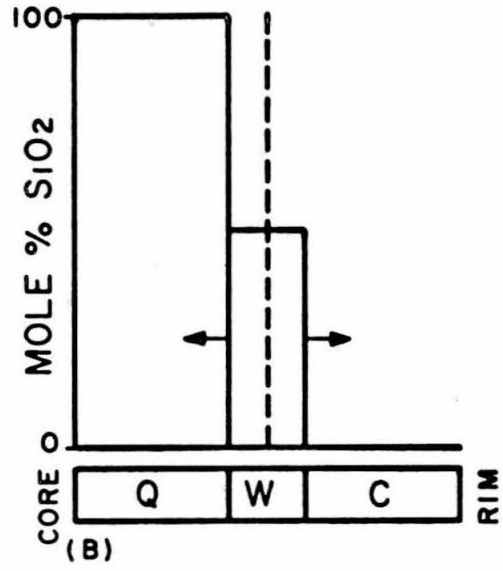
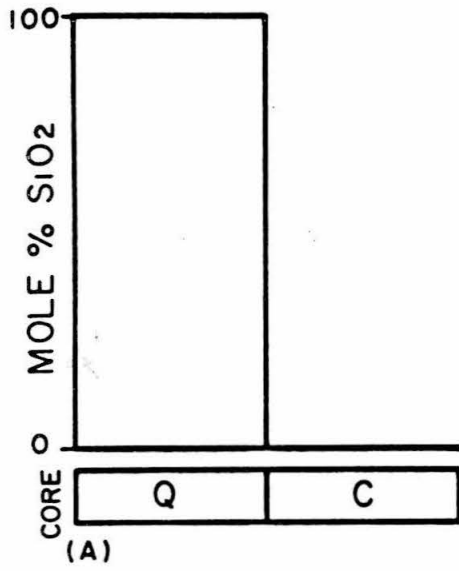
would immediately raise the temperature at the limestone contact to 870°C. The temperature gradient across the aureole is the result of the superposition of the thermal contributions from (1) the intrusion and partial solidification of the first magma sheet, prior to emplacement of the second sheet, (2) emplacement, solidification and cooling of the second sheet and (3) solidification and cooling of the remaining mass of the first sheet, after emplacement of the second.

Although an analytical solution to this problem is difficult to obtain, the model qualitatively explains the observed thermal gradient. The contact temperature is raised to a value near that required by the mineralogy of the skarn due to the high initial temperature at the contact. The gradient across the aureole is steepened due to the superposition of the thermal contribution of the second gabbro onto the steep gradient produced by partial solidification of the first gabbro.

#### GROWTH MODEL

The monomineralic zones in the calc-silicate nodules form a set of concentric shells, separated by sharp contacts, which preserve a discontinuous, step-function gradient in bulk composition from that of wollastonite in the core, to that of calcite in the rim. The resulting sequence of mineral zones is exactly like that developed between quartz and periclase in the hypothetical example described by J. B. Thompson (1959, p. 430-35) in his discussion of the principle of local equilibrium. The sequence of mineral zones, from the core of a nodule to its rim, along with the resulting gradient in composition are shown schematically in Figure 6 for each facies type represented by the calc-silicate

Figure 6. Composition distance profiles across monomineralic zones for nodules of each facies type developed in contact aureole. Arrows point in direction of movement of boundary of each growing zone within the range of P, T and  $X_{CO_2}$  in which that facies type is stable. Dashed line marks initial position of calcite-quartz interface.



nodules. Although the end result of the hypothetical and natural examples are analogous, their initial configurations were distinctly different. Thompson demonstrated that monomineralic zones, separated by sharp contacts, develop by reaction between incompatible phases, infinitesimally separated along a continuous gradient in composition produced by mechanical mixing of stoichiometric phases from a binary join. The initial compositional gradient in the calc-silicate nodules was discontinuous, resulting from the juxtaposition of chert against calcite. However, the sequence of mineral zones and their growth history can be understood in the context of a local equilibrium model.

Although the boundaries between monomineralic zones represent discontinuities in the gradient of bulk composition, comparison of nodule parageneses of Table 1 with the P-T diagram of Figure 3 and the T- $X_{CO_2}$  diagram of Figure 5 shows that the minerals in contact across zone boundaries are mutually compatible within a particular volume of P-T- $X_{CO_2}$  space. The minerals on either side of a monomineralic zone are incompatible within this same volume. Herein lie the answers to the questions of why the zones are monomineralic and why each zone has a bulk composition that corresponds to that of a stoichiometric phase in the system  $CaO-SiO_2-CO_2$ .

As shown on Figure 3, the mineral pairs, calcite + quartz, calcite + wollastonite and tilleyite + wollastonite, each become incompatible at successively higher temperature, and react to form the solid phases wollastonite, tilleyite and rankinite, respectively, by reactions (T,S,L,R), (S,L,R) and (C,S,L). Each reaction involves the combination of two solid

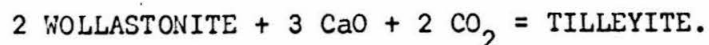
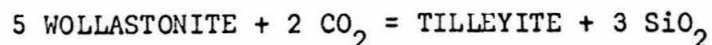
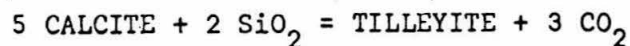
phases to form a single solid phase plus fluid  $\text{CO}_2$ . Hence, the growth of a monomineralic zone is initiated by reaction between two incompatible phases to produce a single phase, compatible with both. However, once the incompatible phases are separated by an infinitesimally thin layer of the stable product, reaction should cease and growth of the layer stop because equilibrium has been established at the boundaries on either side of the new monomineralic zone. At the contact between two monomineralic zones, the chemical potential ( $\mu_i^\phi$ ) of each of the exchangeable chemical species must be equal in both of the phases if the two phase assemblage is to represent equilibrium at a fixed pressure and temperature (Reiss, 1965, p. 108-113; Denbigh, 1966, p. 86). Within a monomineralic zone, however, there must be gradients in the chemical potentials of the exchangeable species from the values fixed or buffered by the two-phase assemblage at one contact to those buffered by the two-phase assemblage at the other. Were the chemical potentials to remain constant across a one-phase zone, the necessary conditions for equilibrium would be met by the two incompatible phases on either side of the zone, and the three solid phases would coexist in equilibrium. This clearly is not the case.

Although zone boundaries mark discontinuities in the gradients of bulk composition, the equality of the chemical potentials across the contacts show that the gradients of the chemical potentials are continuous. This continuity is a necessary condition both for the treatment of the two-phase assemblages as local systems in equilibrium (Thompson,

1959, p. 430) and for identification of diffusion as the mechanism of mass transport (Korzhinskii, 1970, p. 114; Hoffman, 1972, p. 82).

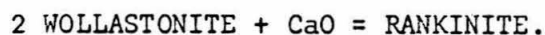
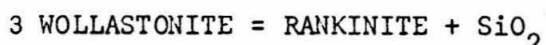
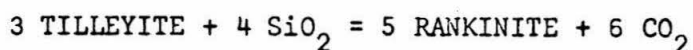
Knowledge of the initial and present distribution of mineral zones in the chert and calc-silicate nodules makes it clear that calcium, silicon and  $\text{CO}_2$  have been redistributed during metamorphism. Radial symmetry of the distribution of mineral assemblages in the nodules, compatibility of minerals in adjacent zones and the aforementioned continuity of the chemical potentials across zone boundaries suggest that the redistribution was accomplished by diffusion rather than by infiltration (Korzhinskii, 1970, p. 114; Hoffman, 1972, p. 82). The gradients in the chemical potentials across monomineralic zones are the driving force for the diffusion and elemental redistribution.

Because incompatible phases are separated by a thin zone of the stable product phase, reactions which result in the growth of a monomineralic zone are not the same as that which caused its formation. Growth of a one-phase zone takes place by reaction between transported species of calcium, silicon and  $\text{CO}_2$  and the mineral of the adjacent zone. Hence, the monomineralic zone may grow by different reactions on each of its boundaries. For example, a zone of tilleyite, enclosed by calcite and wollastonite may grow by the reactions



Note, however, that growth may occur at only one boundary if the phase in an adjacent zone is also growing. For example, in a nodule in which

tilleyite and rankinite are stable, the tilleyite zone will grow at the expense of calcite by the first reaction above, while the rankinite zone will grow at the expense of both tilleyite and wollastonite by the reactions



Because the transported reactants must diffuse through the growing zone to reach the reaction site, the rate limiting step in the growth of a monomineralic zone is the rate of diffusion through the zone itself. Since the values of the chemical potentials are buffered by the two-phase assemblages at the zone boundaries, their gradients are flattened only by the widening of the one-phase zone. Hence, the tendency toward diffusion is diminished with growth of the monomineralic zone.

Figure 6 is a series of idealized composition-distance profiles across chert and calc-silicate nodules for each of the facies-types found in the contact aureole. The steps in the growth of a nodule can be traced by following through the diagrams for each of the facies types developed with rising temperature up to and including that represented by the present nodule assemblage.

Figure 6A shows the initial compositional discontinuity between quartz and calcite. If a chert nodule is heated to a temperature within the range bounded by reactions (T,S,L,R) and (S,L,R), a thin zone of wollastonite will form at the quartz-calcite interface and grow at the

expense of both quartz and calcite (Figure 6B). The nodule will continue to grow until the quartz in the core is used up. On the basis of its smaller ionic radius and smaller coordination polyhedron with oxygen, one might expect the diffusing silicon species to be transported more rapidly than that of calcium, thus causing the wollastonite zone to grow more rapidly at the calcite boundary than at the quartz boundary. However, the identity of the diffusing species is unknown. Except where nodules are closely spaced in limestone, there is an effectively infinite reservoir of calcite available for reaction. Hence, net growth of the nodule should occur regardless of the relative diffusion rates.

Figure 6C shows the compositional gradient across a nodule that has been heated to a temperature within the field bounded by the reactions (S,L,R) and (C,S,L). At temperatures within this range, the tilleyite zone grows at the expense of both calcite and wollastonite, while the wollastonite zone grows only at the contact with quartz. When the supply of quartz in the core of the nodule is depleted, the diameter of the wollastonite zone will begin to decrease as the tilleyite zone encroaches upon it. The tilleyite zone will continue to grow so long as wollastonite remains in the core of the nodule.

Figure 6D shows the compositional gradient across a nodule heated to a temperature within the field bounded by the reactions (C,S,L) and (C,L,R,W). At these temperatures, rankinite grows at the expense of tilleyite and wollastonite. Because the nodule is enclosed by calcite, the tilleyite zone will continue to grow only if the rate of diffusion of silicon in tilleyite exceeds that of silicon in rankinite. Decarbonation

of tilleyite to form spurrite by reaction (C,L,R,W) will not change the shape of the compositional gradient for silica nor will it alter the sense of movement of the zone boundaries.

#### THE PHASE RULE

Growth of the monomineralic zones of the calc-silicate nodules has been explained in terms of an actualistic model based on knowledge of the initial state of the system and possible reactions leading to its present state. The hypothesis that both the monomineralic zones and the two-phase assemblages at their boundaries represent local systems in equilibrium may be tested by application of Gibbs phase rule to each local assemblage. Understanding of the growth history of the nodules allows the determination for each local assemblage, of the number of chemical species whose chemical potentials are determined by the composition of the phases in the local assemblage and the number of those whose chemical potentials are determined by conditions external to the local system. It must be emphasized, however, that this number can be determined only on the basis of knowledge of the history of growth of the nodules. It cannot be determined by enumeration of phases in each local assemblage without an assumption of the path leading from the initial to the present state of the system (Weill and Fyfe, 1964, p. 568-73, 1967, p. 1171-72; Thompson, 1970, p. 542).

Following Thompson (1970, p. 541-43), the number of intensive parameters necessary for the formulation of Gibbs phase rule for a local assemblage can be determined by writing a Gibbs-Duhem equation for each

of the phases present. Consideration of the Gibbs-Duhem equation for a single phase, consisting of  $N$  chemical species,

$$S^{\phi}dT - V^{\phi}dP + \sum_i n_i d\mu_i^{\phi} = 0 ,$$

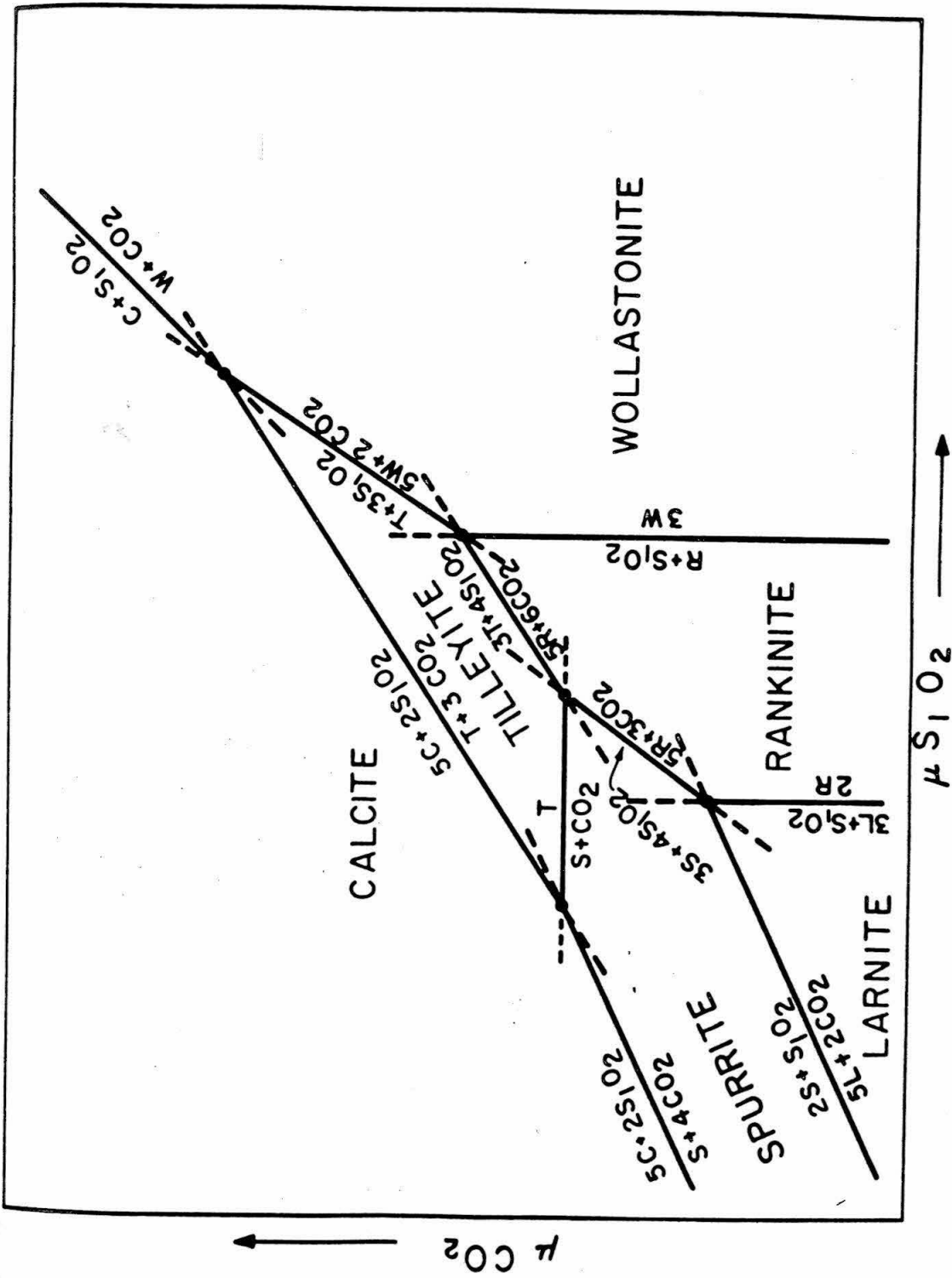
shows that for an arbitrary choice of temperature and pressure, the chemical potentials of at most  $N-1$  chemical species are independently variable (Denbigh, 1966, p. 93). Metamorphism of chert, enveloped by calcite, to form the calc-silicate minerals involved redistribution of  $\text{CaO}$ ,  $\text{SiO}_2$  and  $\text{CO}_2$  by diffusion down gradients of their respective chemical potentials. Within a monomineralic zone, however, the chemical potentials of at most two of the three transported species are independent, for a general choice of  $P$  and  $T$ . Thus, in formulation of Gibbs phase rule for a one-phase zone, two species can be considered to have behaved as "perfectly mobile" or "boundary value" components (Zen, 1963, p. 930) and the resulting variance is four. In this case, the upper and lower limits of the values of the chemical potentials of the boundary value components are controlled external to the local system by the two-phase equilibria at the zone contacts. The slopes of their gradients are controlled by the width of the one-phase zone.

At the zone boundaries, the number of transported chemical species is three, as in the monomineralic zones, but because of the equilibrium between the two phases, the number of independently variable chemical potentials is reduced by one. For a two-phase assemblage, the number of boundary value components is one and the variance is three. The loss of a degree of freedom is the result of the buffering of the chemical potentials by the two-phase assemblage.

The chert nodule example serves to further emphasize the distinction that must be made between the mobility of a component in the sense of Korzhinskii's original definition (1949) and the physical mobility involved in mass transport (Korzhinskii, 1959, p. 16; Zen, 1963, p. 930; Mueller, 1967, p. 580; Thompson, 1970, p. 543). Calcium, silicon and  $\text{CO}_2$  have been redistributed throughout the nodules during metamorphism, hence all three were physically mobile. But, in a monomineralic zone, two species behaved as "boundary value" or "perfectly mobile" components, while at the zone boundaries where two phases coexist, only one of the three behaved as a "perfectly mobile" component.

The relationship between mineral assemblage, possible reactions and their variance can be shown graphically on a chemical potential diagram (Korzhinskii, 1959, p. 117-22). Figure 7 is a schematic isothermal-isobaric section showing relations between mineral assemblages and the chemical potentials of  $\text{SiO}_2$  and  $\text{CO}_2$  for the region of the P-T plane in which both larnite and rankinite are stable. Relationships at lower temperatures may be portrayed by successive elimination of the fields of larnite, spurrite, rankinite and tilleyite. The chemical potentials for  $\text{SiO}_2$  and  $\text{CO}_2$  were chosen as variables because the resulting diagram includes fields for all of the phases observed in the calc-silicate nodules. Note that each one phase field represents a variance of four, while each of the reaction lines is trivariant. The loss of a degree of freedom is the result of the buffering of one of the chemical potentials by the two phase assemblage.

Figure 7. Schematic isothermal-isobaric chemical potential diagram ( $u_{\text{SiO}_2} - u_{\text{CO}_2}$ ) for system  $\text{CaO-SiO}_2\text{-CO}_2$  at pressure and temperature at which larnite + rankinite coexist with either tilleyite or spurrite. Topological relationships at lower temperatures or higher pressures may be shown by successive elimination of fields of larnite, spurrite, rankinite and tilleyite.



Two types of buffering are possible. Equilibria involving larnite + rankinite and rankinite + wollastonite fix the value of the chemical potential of  $\text{SiO}_2$  while the chemical potential of  $\text{CO}_2$  may vary independently. Similarly, the assemblage tilleyite + spurrite fixes the chemical potential of  $\text{CO}_2$  for a range of independent values of the chemical potential of  $\text{SiO}_2$ . All other two-phase assemblages are stable over a range of values of the chemical potentials of  $\text{SiO}_2$  and  $\text{CO}_2$ , the only constraint being that they both lie on the trivariant surface.

As shown on Figure 7, each of the facies types observed in the calc-silicate nodules may be generated isothermally and isobarically along a gradient in the chemical potential of  $\text{SiO}_2$ . This reinforces the argument that the mineral zones in a single nodule are formed in response to the metamorphism of a range in bulk rock composition on the join  $\text{CaO-SiO}_2$  in the presence of relatively pure fluid  $\text{CO}_2$ .

#### SUMMARY AND CONCLUSIONS

The monomineralic zones that make up an individual calc-silicate nodule represent a set of topologically compatible mineral assemblages stable within a limited volume of  $P\text{-}T\text{-}X_{\text{CO}_2}$  space. The mineral making up a one-phase zone is compatible with the monomineralic assemblage at each of its contacts, while the phases bounding it on either side are incompatible. Three solid phases which form a sequence of monomineralic zones are related by a divariant reaction in  $P\text{-}T\text{-}X_{\text{CO}_2}$  space in which the two exterior phases are the reactants and the phase separating them is the product. Thus, although metasomatic in origin, the sequence of monomineralic zones in an individual calc-silicate nodule may be understood as

the mineralogical response to metamorphism in a limited volume of  $P$ - $T$ - $X_{CO_2}$  space of a wide range of bulk compositions within the system  $CaO$ - $SiO_2$ - $CO_2$ .

Due to the existence of several stable invariant points within a geologically reasonable range of pressure and temperature, the sequence of nodule facies types across the aureole closely defines a trajectory through  $P$ - $T$ - $X_{CO_2}$  space. Because a lithostatic pressure of 325 bars can be determined, independent of the mineral assemblages, the sequence of facies types limits the compositions of fluids present during metamorphism to those in which the mole fraction of  $CO_2$  was greater than 0.6, the lower limit being that of the [C,L] invariant point on the  $T$ - $X_{CO_2}$  plane. For this range of fluid phase composition, maximum temperatures in the aureole, as recorded by divariant mineral reactions, are 925 to 1025°C at the gabbro contact, 920 to 990°C at 16 meters, 875 to 930°C at 32 meters and 565 to 600°C at 70 meters.

Growth of a monomineralic zone is initiated by reaction between minerals of adjacent one-phase zones, which become incompatible with rising temperature, to form a thin layer of a single solid phase which separates the reactants and is compatible with both of them. Because the mineral of the new monomineralic zone is in equilibrium with the phases at both of its contacts, a gradient in the chemical potentials of exchangeable species is established across it. Although the zone boundaries mark discontinuities in the gradients of bulk composition across a nodule, the two-phase equilibria at the contacts demonstrate that the chemical potentials are continuous across the zone boundaries. Calcium,

silicon and  $\text{CO}_2$  were redistributed in a nodule by diffusion down the chemical potential gradients across the monomineralic zones.

Once established, a monomineralic zone grows at the expense of an adjacent zone by reaction between the diffusing species and the mineral of the adjacent zone. Thus, a one-phase zone may grow by different reactions at each of its boundaries or it may grow at one boundary while being consumed at the other by an adjacent zone which is also growing.

Equilibria between two solid phases at the zone boundaries buffers the chemical potentials of the diffusing species. Thus, within a monomineralic zone, the upper and lower limits of the values of the chemical potentials of the perfectly mobile components are controlled external to the local system by the two-phase equilibria at the zone boundaries. Calcium, silicon and  $\text{CO}_2$  were redistributed in the nodules during metamorphism, hence all three were mobile in the sense that they were transported. But, in a monomineralic zone, two species behaved as perfectly mobile components while at the zone boundaries, where two phases coexist, only one of the three behaved as a perfectly mobile component.

## 5. METASOMATIC GROWTH OF THE ZONED CALC-SILICATE SKARN AT THE INTRUSIVE CONTACT

## INTRODUCTION

Calc-silicate skarn occurs in a band, 0.1 to 1 meter in width, that everywhere separates pyroxenite developed from the interaction of gabbroic magma with marble, from the marble itself. It is found all along the contact between rocks of the gabbro complex with the enclosing marble and as rims on large, marble-cored xenoliths in the fine-grained, biotite-titanaugite gabbro. Skarn also occurs in small, ellipsoidal to lobate xenoliths occurring both in pyroxenite derived from coarse-grained, olivine-titanaugite gabbro and in fine-grained gabbro where the xenoliths are enveloped by a thin shell of pyroxenite.

Mineral assemblages found in skarn are listed in Table 1. The most widely developed mineral assemblages in the skarn consist of either melilite or idocrase and one or two of the phases wollastonite, rankinite, spurrite and calcite. Titanian-zirconian garnet, perovskite and magnetite are ubiquitous accessory phases. Zonation of mineral assemblages across a band of skarn results from the presence of wollastonite in the zone in contact with pyroxenite, rankinite with either wollastonite or spurrite in the middle of the skarn band and of spurrite in the zone in contact with marble. Although this mineralogic zonation is inconspicuous in the field, two and locally three distinct mineralogic zones can be recognized in most skarn outcrops. In sequence from pyroxenite to marble, these zones consist of green idocrase skarn, brown melilite skarn and, in contact with marble, white spurrite skarn. The boundaries between these zones do not, in general, coincide with those of the calc-silicate zones. The

TABLE I  
MINERAL ASSEMBLAGES IN SKARN  
CHRISTMAS MOUNTAINS, TEXAS

ASSEMBLAGE NO.	1	2	3	4	5	6	7	8	9	10	11	12	13	14	15
CALCITE	x														
TILLEYITE											x			x	
SPURRITE							x	x							
LARNITE						x	x								
RANKINITE					x	x									
WOLLASTONITE		x		x											
PHASE "T"			x			x									
MERWINITE															
MONTICELLITE							x								
MELILITE				x		x		x							
IDOCRASE	x	x													
GROSSULAR	x														
TI-ZR GARNET															
PEROVSKITE															
MAGNETITE	x														

\*idocrase, pseudomorphous after melilite may occur in all melilite-bearing assemblages

contact between the green skarn and brown skarn marks the outer limit of hydration of melilite to form idocrase. It usually occurs within the wollastonite zone. However, idocrase, pseudomorphous after melilite, occurs locally throughout the skarn, usually developed along fractures. The contact between the brown skarn and the white skarn, which records a sharp decrease in the modal abundance of melilite, invariably occurs within either the spurrite or spurrite-calcite zones. In most exposures along the main intrusive contact and in smaller xenoliths, replacement of melilite by idocrase is complete, and the zone of brown skarn does not occur.

Within 20 meters of the gabbro contact, mineral assemblages identical to those of the melilite and spurrite-calcite skarn zones are developed within silica- and alumina-rich beds of the Sue Peaks Formation. The symmetry of the mineral zonation in these beds as well as the fact that they are separated from one another and from the main skarn by beds of relatively pure calcite marble, shows that skarn mineral assemblages may result from metamorphism of impure limestone. However, proof that the mineralogic zonation in skarn at the intrusive contact is the result of metasomatic introduction of material from gabbro, rather than the isochemical metamorphism of a bedded sediment, is demonstrated by the observations that (1) the sequence of mineral zones is the same in skarns formed from the relatively pure limestones of the Del Carmen and Santa Elena Formations and from rocks of the impure, compositionally-variable Sue Peaks Formation, (2) the zoning is parallel to the pyroxenite contact which is discordant to bedding in marble and (3) mineralogy and sequences

of zones are the same on all sides of marble-skarn xenoliths enclosed by gabbro.

The sequence of mineral zones across the skarn defined by the stoichiometric calc-silicate phases indicates the presence of steep concentration gradients in CaO and SiO<sub>2</sub> between pyroxenite and marble. The zonation involving melilite suggests the presence of gradients in iron, magnesium and aluminum as well. In order to determine the relationship between mineral assemblage, mineral composition and bulk rock composition as well as the variation of these parameters with position within a zoned skarn band, samples from two traverses taken across the skarn were studied in detail.

Traverse CM-8-n, designated "main contact", was collected across the skarn developed at the contact between pyroxenite derived from porphyritic olivine-biotite-titanaugite gabbro and argillaceous limestone from the lower part of the Sue Peaks Formation. A schematic cross-section of the main contact at this locality showing the location of analyzed samples is shown in Figure 1. Traverse CM-103-n, designated "xenolith", was taken across the south margin of a large xenolith of Santa Elena(?) Limestone in the fine-grained biotite-titanaugite gabbro, located about 15 meters from the main intrusive contact between gabbro and Santa Elena Limestone. Figure 2 is a sketch map of this xenolith showing the locations of the analyzed samples. Field relationships for all analyzed samples are listed in Table C-1 (appendix).

Figure 1. Schematic cross-section of pyroxenite and skarn developed at contact between porphyritic gabbro and Sue Peaks Limestone (Point "m", Figure 1, Chapter 1). Positions of analyzed samples of main contact traverse are marked with symbol which denotes the assemblage of stoichiometric calc-silicate phases in skarn or marble. Abbreviations for phases are W=wollastonite, R=rankinite, S=spurrite and C=calcite.

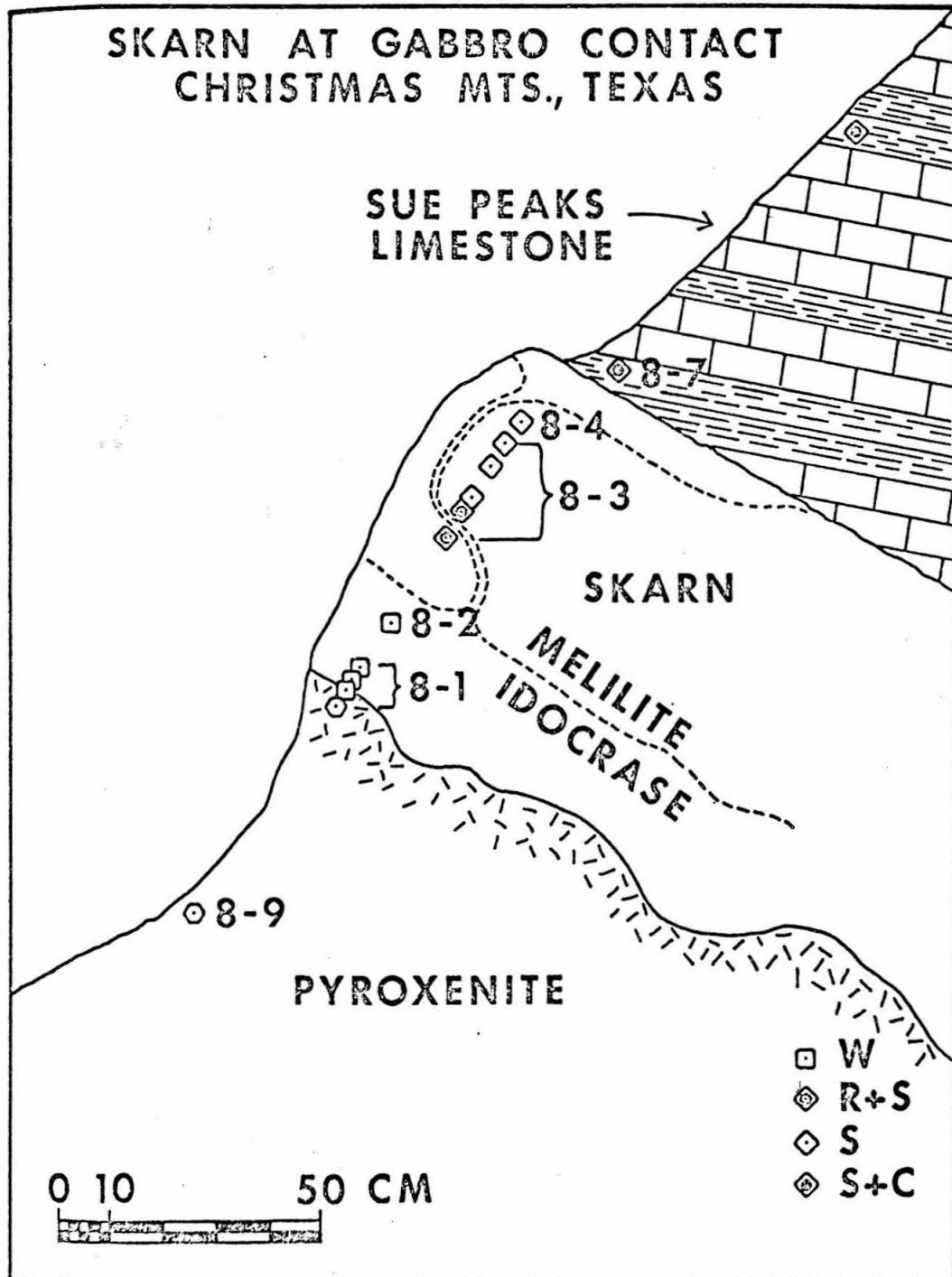
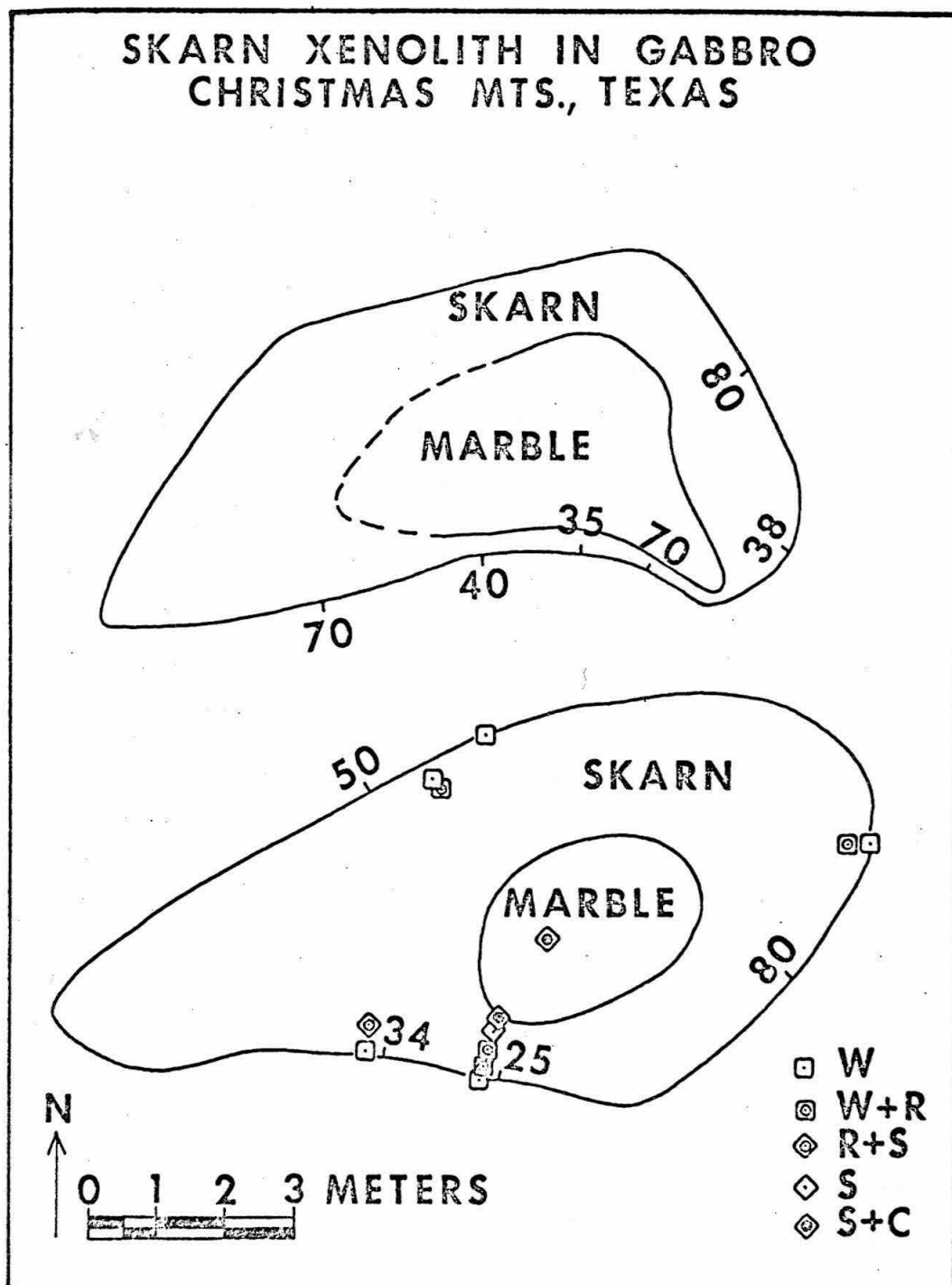


Figure 2. Sketch map of two xenoliths of Santa Elena (?) limestone in fine-grained gabbro (Point "x", Figure 1, Chapter 1). Analyzed samples from xenolith traverse were collected along line from south margin to the core of the more southerly of the two xenoliths. Mineral assemblage symbols as on Figure 1.

SKARN XENOLITH IN GABBRO  
CHRISTMAS MTS., TEXAS



## MINERALOGY

## Melilite

The presence of 50 to 80 volume percent melilite imparts the deep yellow-brown color characteristic of rocks from the brown skarn zone. In these rocks melilite forms aggregates of subhedral crystals that are colorless to very pale yellow in thin section. Mutual contacts between three grains meeting at angles of about  $120^{\circ}$  are common. In calcite-spurrite assemblages within the brown or white skarn zones, melilite occurs in euhedral, rectangular prisms. There is no textural evidence to suggest that melilite bears a reaction relationship to any minerals other than idocrase or merwinite.

Electron microprobe analyses of melilite from skarn are listed in Table C-2. Compositions listed represent the mean of 3 to 8 spot analyses from a single polished thin section. Although concentrations of major elements in melilite from a single thin section may vary between 0.5 and 5 percent of the amount present, there is no consistent pattern of chemical zonation within single grains. Within the total sample, melilite varies in composition between 55 and 70 mole percent gehlenite end-member, while the ratio of  $Mg/(Mg+Fe)$  of the akermanite end-member varies between 0.40 and 0.85. Despite the fact that the alkali gabbro involved in the genesis of the skarn contains 4 to 8 weight percent combined  $Na_2O + K_2O$ , melilite, the only skarn mineral in which significant alkali substitution is possible, generally contains less than 1 weight percent  $Na_2O + K_2O$ .

### Idocrase

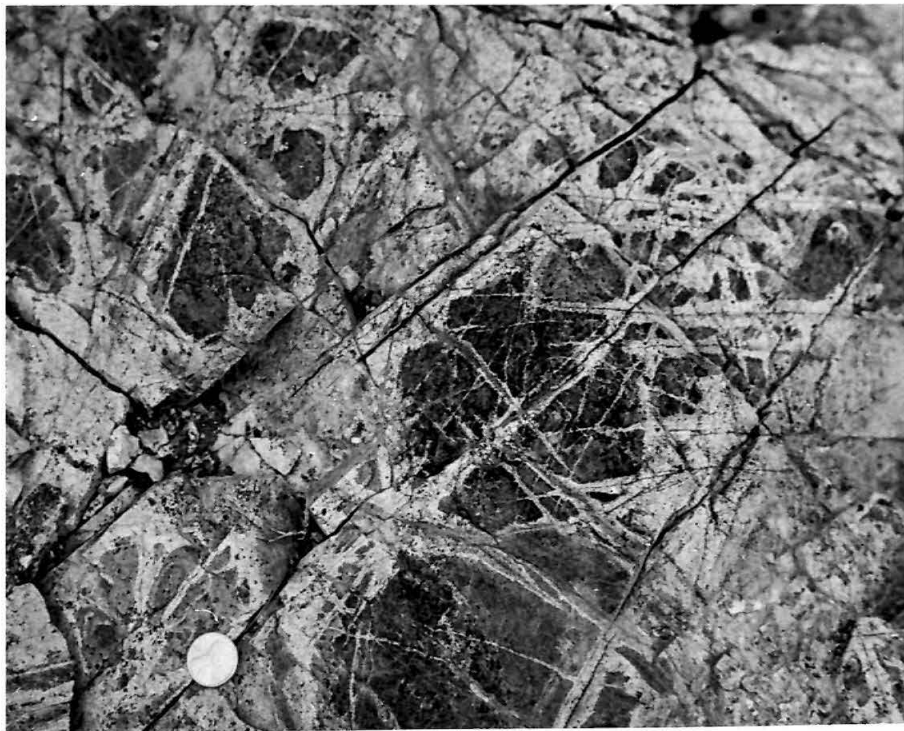
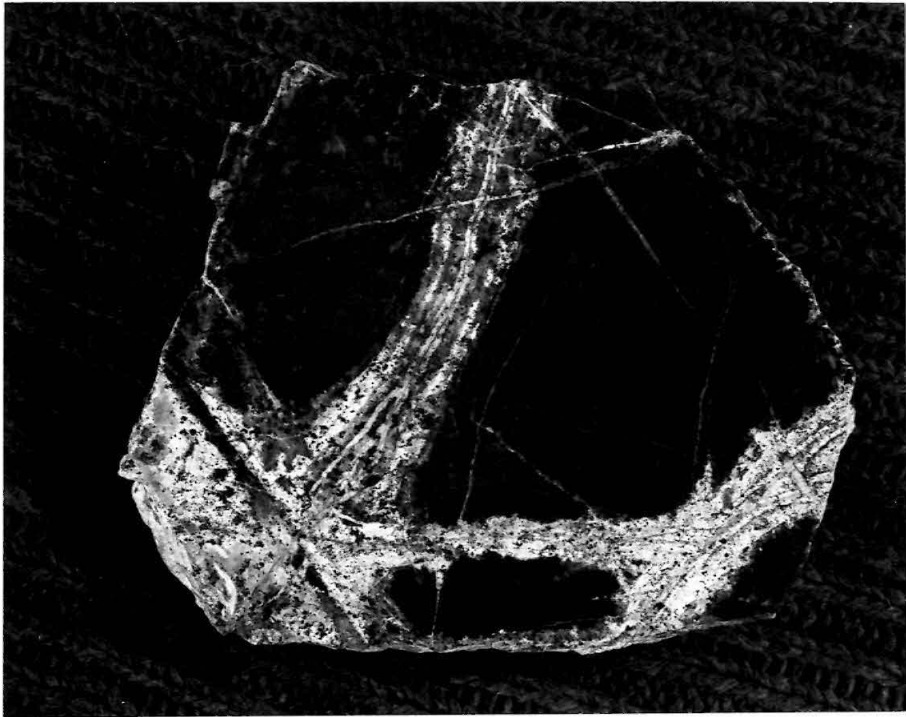
Skarn in the zone in contact with pyroxenite contains 40 to 70 volume percent idocrase which gives the rock its characteristic yellow-green color. The contact between the green skarn zone and the brown melilite skarn zone is sharp and generally planar at most localities. Idocrase occurs to the exclusion of melilite in the green skarn zone but idocrase is found locally in the brown skarn. Where it occurs outside of the green skarn zone, idocrase is developed along fractures that cut the melilite skarn (Plate 1, Figure 1). These fractures can usually be traced back into the green skarn zone. This vein-like replacement of melilite by idocrase suggests that the idocrase-melilite zone boundary did not propagate through the rock as a planar front, but developed by the coalescence of a network of idocrase veinlets. Where such a gradational contact occurs, the spatial relationships between the green skarn and brown skarn zones reflect the probable time sequence of development of the green skarn.

The gradational contact between green skarn and brown skarn in the core of a large skarn xenolith in the fine-grained gabbro clearly shows the progressive replacement of melilite by idocrase (Plate 1, Figure 2). Idocrase developed along intersecting fractures forms a latticework of veinlets which enclose polygonal areas of melilite skarn. Wide idocrase veinlets overlap at points of intersection and round off the corners of the enclosed melilite polygons. As the contact with the main mass of green skarn is approached, the residual "eyes" of melilite become smaller until they are completely engulfed by idocrase.

Plate 1. Idocrase replacement of melilite along fractures in skarn.

Figure 1. Idocrase veinlets in melilite skarn, sample CM-86. Sample is 85 x 110 mm.

Figure 2. Latticework of idocrase veinlets in melilite skarn, surrounded by idocrase skarn in core of xenolith. The contact between idocrase skarn and melilite skarn propagated inward by coalescence of idocrase veinlets growing outward from intersecting fractures. Sample CM-86 is from this outcrop. Penny gives scale.



The spatial relationships between the green skarn and brown skarn zones at gradational contacts provide strong evidence for the origin of idocrase through reaction of melilite with an aqueous fluid flowing along fractures in brown skarn. Textural evidence in thin section suggests that idocrase formed by pseudomorphic replacement of melilite.

Where melilite and idocrase occur in the same thin section, their grain habits are identical. Idocrase is distinguished from melilite by its anomalous birefringent colors, berlin blue, brilliant purple or brown. In some rocks it is isotropic. Although it may be colorless and clear in plane light, idocrase usually has a dusty brown appearance. Its sweeping extinction and lack of a well-defined interference figure suggest that idocrase forms polycrystalline or fibrous replacement of individual melilite grains.

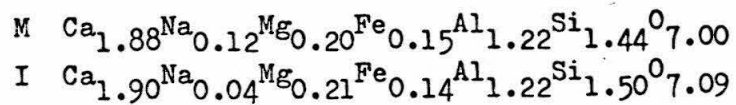
Unequivocal petrographic evidence for pseudomorphism of melilite by idocrase is shown by partial and complete replacement of euhedral prisms of melilite by fibrous idocrase in calcite-spurrite skarn sample CM-6-6MB (Plate 2, Figures 1 and 2). Figures 1 and 2 of Plate 3 are photomicrographs of one side of an idocrase veinlet developed along a fracture in melilite skarn. Note that the very finely divided opaque in idocrase enhances the relict (001) cleavage planes of the host melilite. In all samples examined in which both idocrase and melilite occur, idocrase pseudomorphs accurately preserve the crystal habit of melilite characteristic of that rock. The habit of idocrase in melilite-free rocks is identical to that of melilite in rocks with the same assemblage of calc-silicate phases. On the

Plate 2. Partial and complete pseudomorphs of fibrous idocrase after euhedral crystals of melilite.

Figure 1. Plane light. Three rectangular melilite crystals in center of field have been partially replaced by fibrous idocrase. Sample CM-6-6MB. Field of view is 1.2 x 1.6 mm.

Figure 2. Crossed nicols, same field as Figure 1. Idocrase is in extinction.

Anhydrous mineral formulae for melilite (M) and idocrase (I) from this sample are:



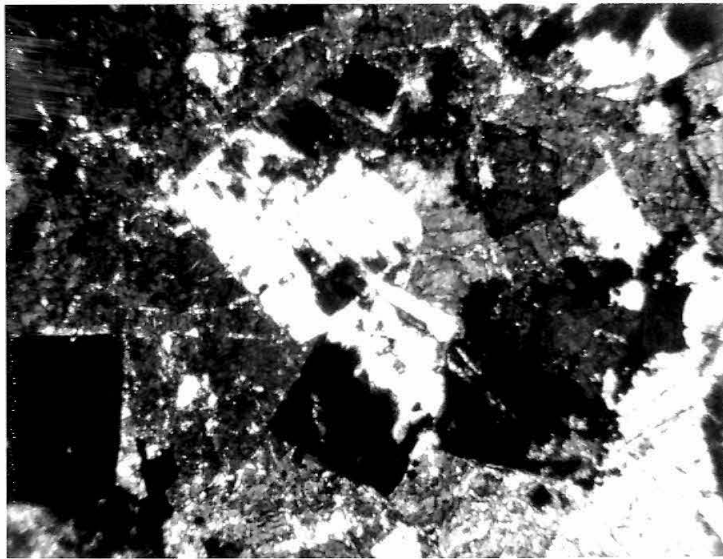
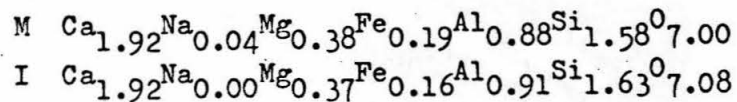


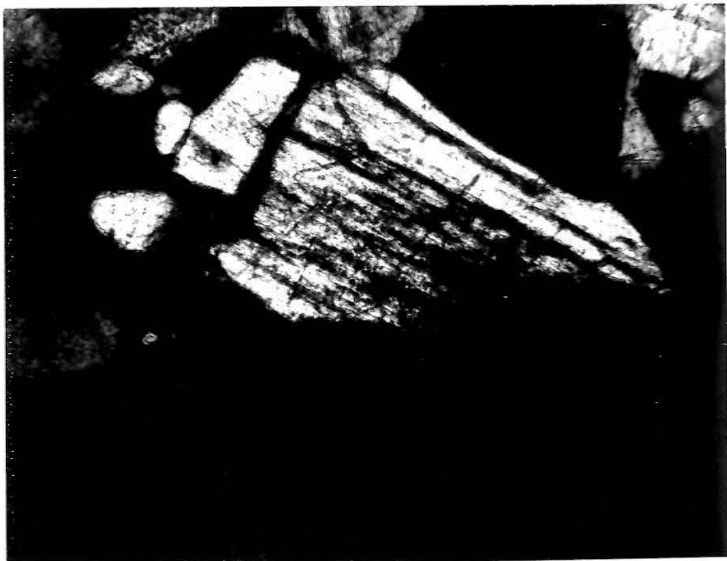
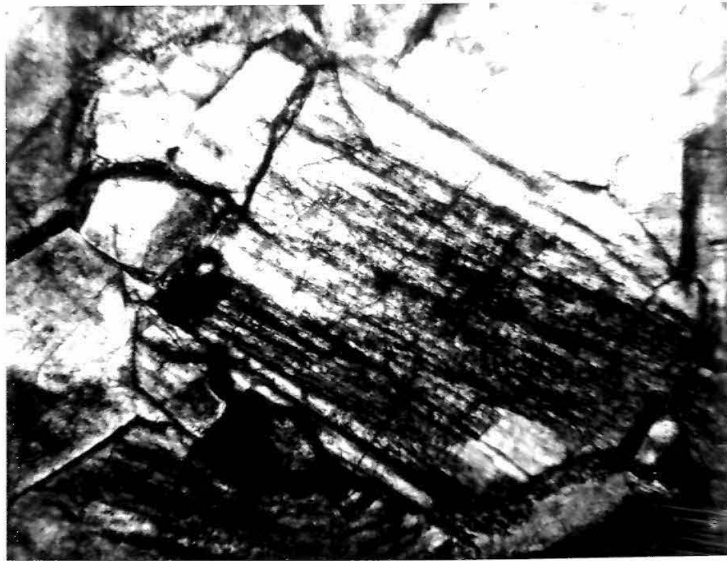
Plate 3. Replacement of melilite by idocrase along edge of idocrase veinlet in melilite skarn.

Figure 1. Plane light. Lower half of melilite grain in center of field has been replaced by fibrous idocrase. Very finely divided opaque enhances the relict (001) cleavage of the host melilite. Sample CM-86. Field of view 0.58 x 0.85 mm.

Figure 2. Crossed nicols, same field as Figure 1. Planar front of idocrase replacement cuts across melilite grain boundaries. Idocrase in extinction across lower half of field.

Anhydrous mineral formulae for melilite (M) and idocrase (I) from this sample are:





basis of the textural evidence presented it is concluded that melilite was a primary phase in all idocrase-bearing skarn assemblages and that all idocrase in the skarn is pseudomorphous after melilite.

In order to characterize the reaction leading to the pseudomorphic replacement, 16 pairs of coexisting idocrase and melilite were analyzed with the electron microprobe. These analyses are listed in Table C-2. Mineral formulae of idocrase have been computed on the basis of 5 cations per formula rather than the customary 50 (Warren and Modell, 1931; Machatschki, 1932; Barth, 1963; Ito and Arem, 1970) to facilitate direct comparison with analyses of coexisting melilite. Within a single thin section, concentrations of the major elements in idocrase vary between 2 and 5 percent of the amount present. As was found for melilite, there is no consistent pattern of chemical zonation within single grains.

Comparison of the anhydrous mineral formulae of coexisting mineral pairs shows a close and consistent correspondence between proportion of each element in idocrase and melilite. The only exception is sodium which is depleted by a factor of 2 to 50 in idocrase relative to melilite. To systematically portray this relationship, the atom fraction of each cation in coexisting melilite and idocrase from each of the pairs have been plotted against each other in Figures 3 through 8. A line of slope = 1 on diagrams of this type represents equal partitioning of the cation between the two phases. Although there is some scatter, particularly for iron and magnesium, the major elements are equally partitioned between coexisting melilite and idocrase over the full range of solid solution

Figure 3. Atom fraction of calcium in coexisting melilite and idocrase from 16 samples of skarn. Dotted line represents equal partitioning of calcium between the two phases.

COEXISTING MELILITE AND IDOGRASE FROM SKARN, CHRISTMAS MOUNTAINS, TEXAS

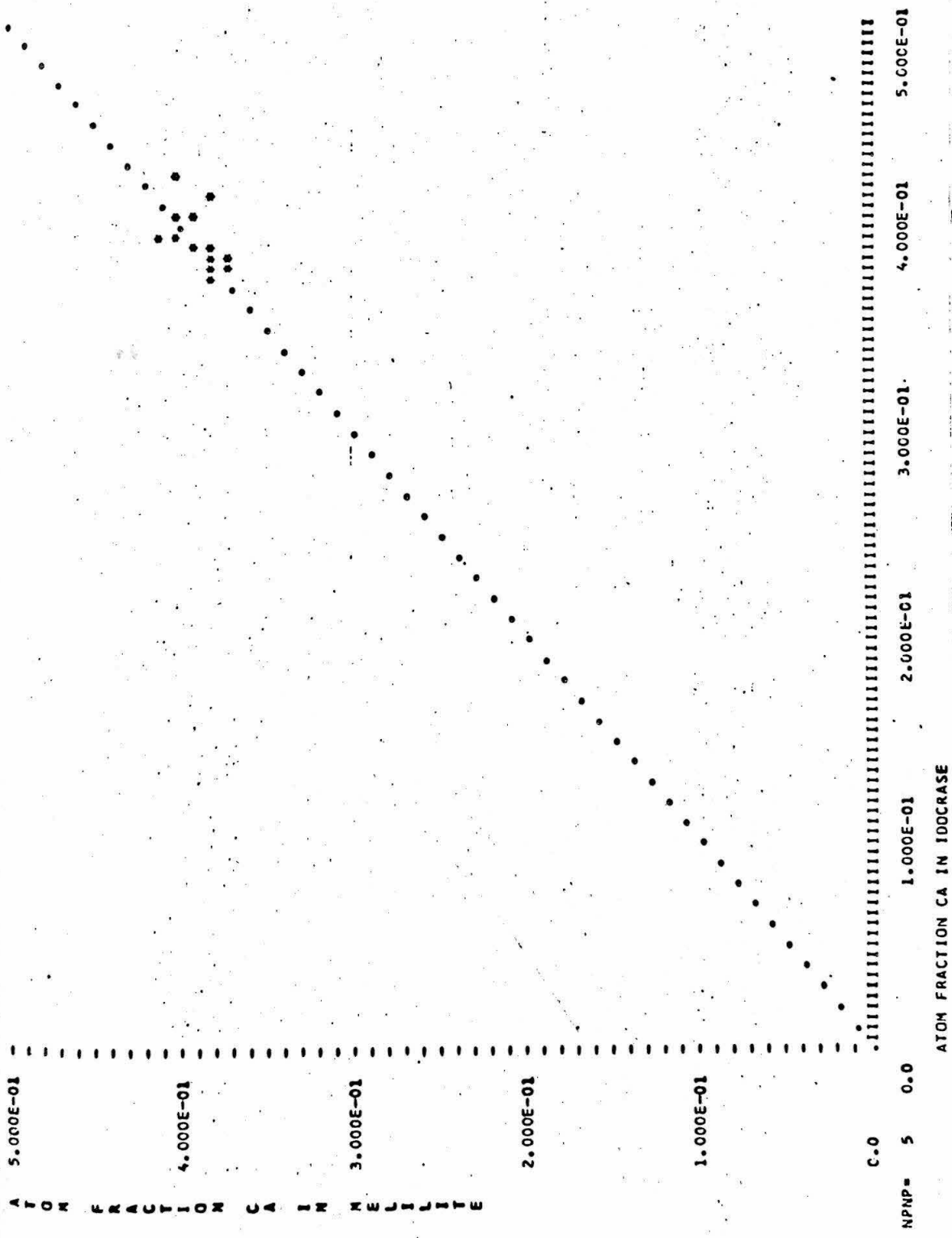


Figure 4. Atom fraction of silicon in coexisting melilite and idocrase from 16 samples of skarn. Dotted line represents equal partitioning of silicon between the two phases.

COEXISTING MELILITE AND IDOGRASE FROM SKARN, CHRISTMAS MOUNTAINS, TEXAS

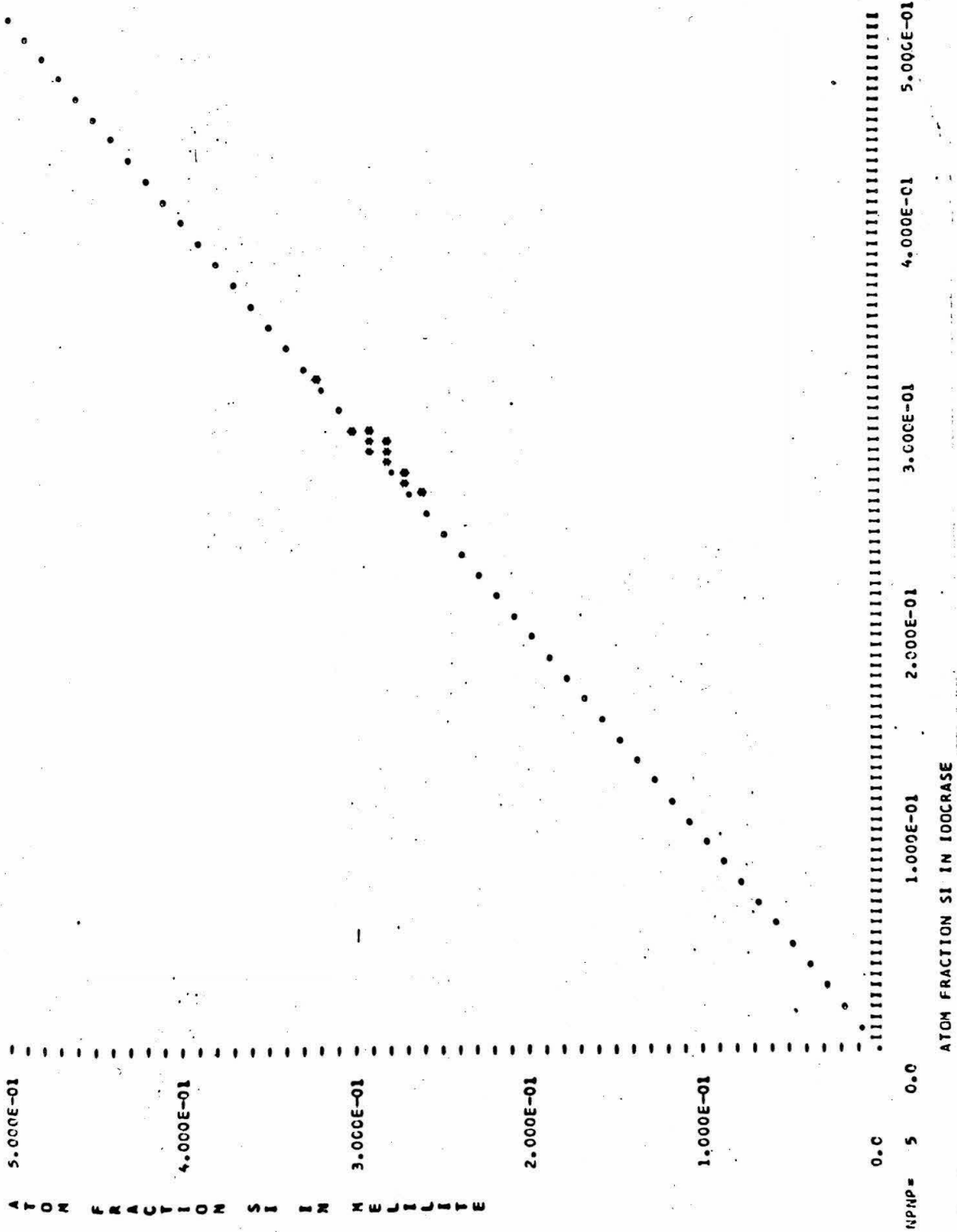
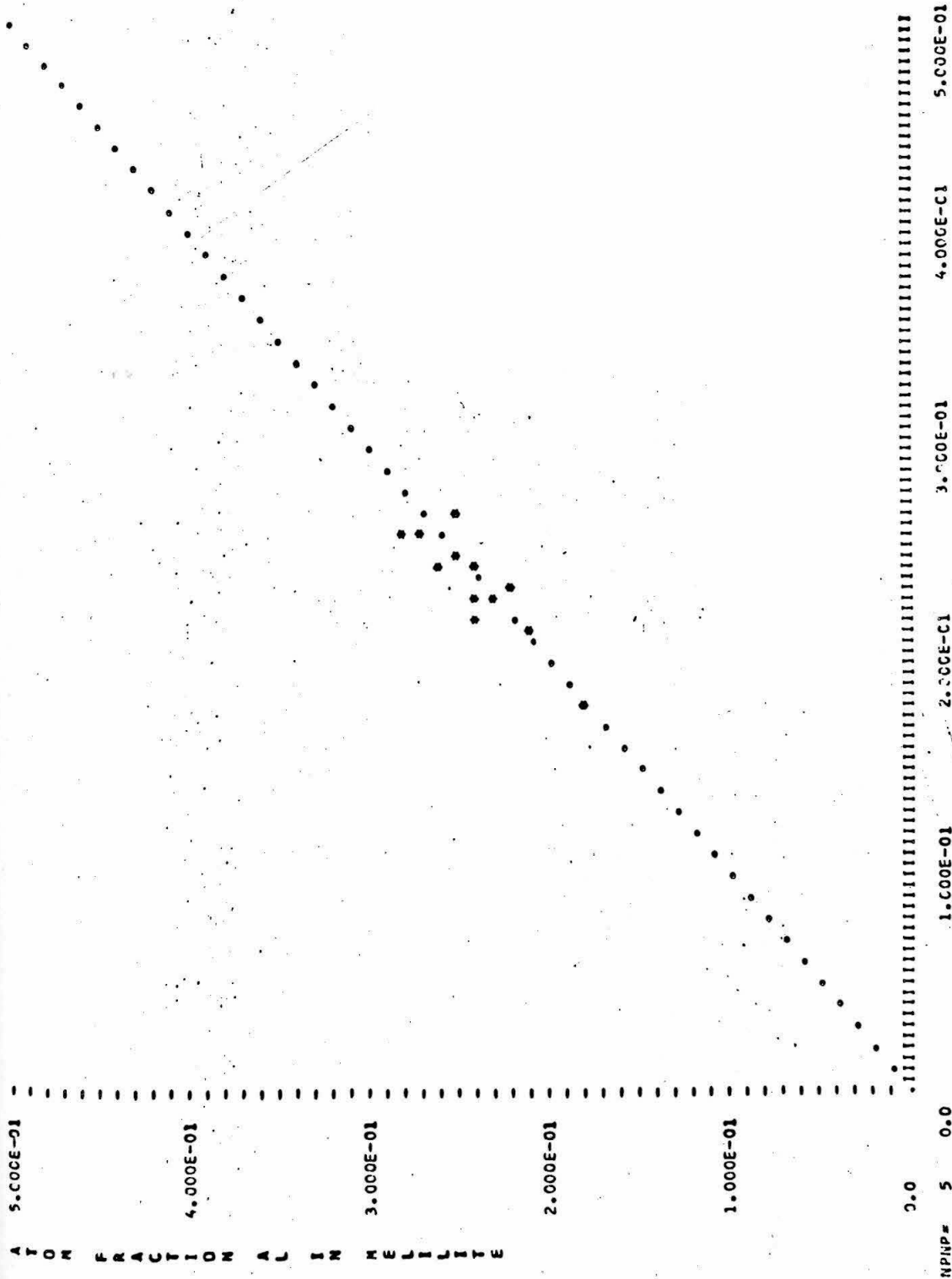


Figure 5. Atom fraction of aluminum in coexisting melilite and idocrase from 16 samples of skarn. Dotted line represents equal partitioning of aluminum between the two phases.

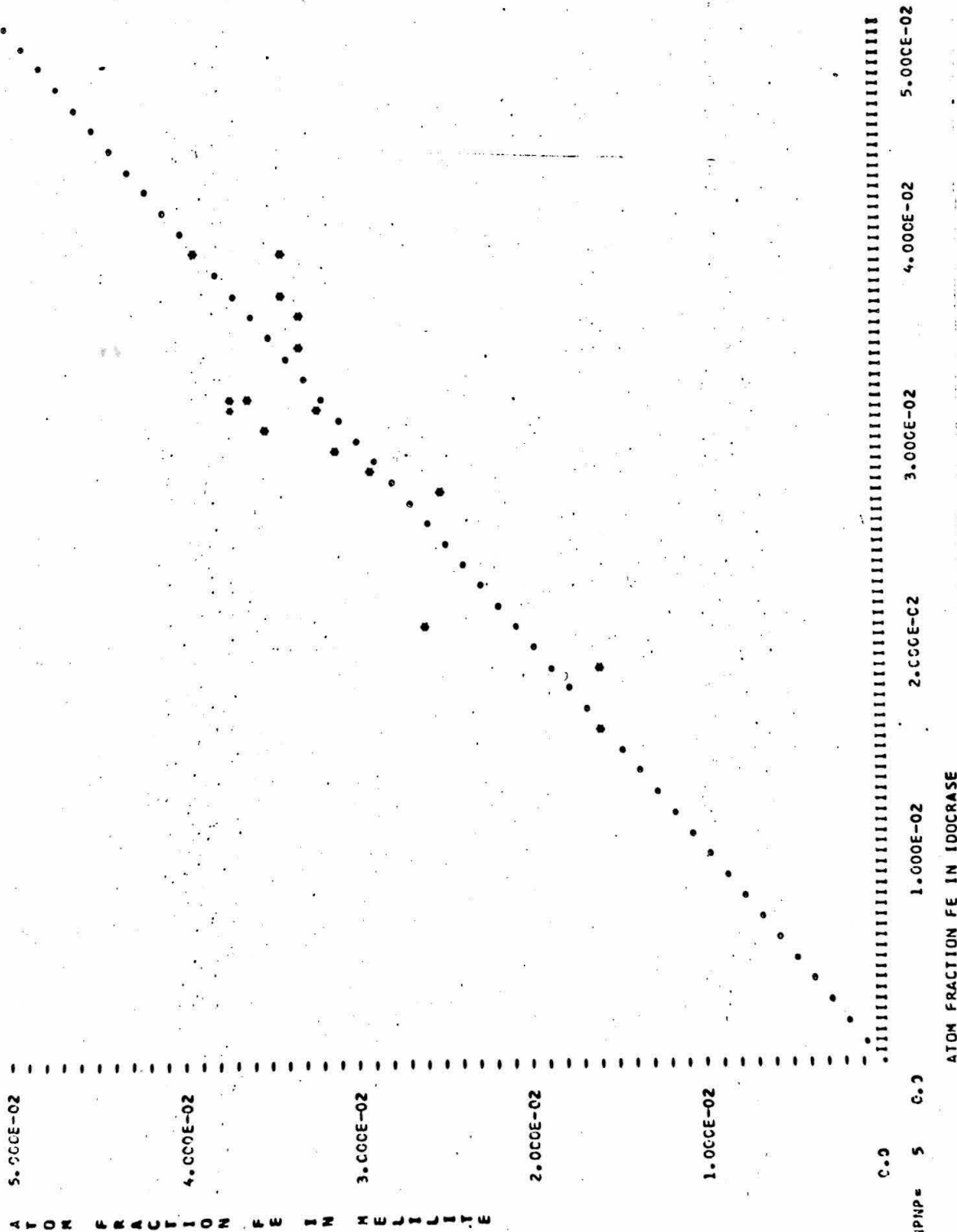
COEXISTING MELILITE AND IDOCRASE FROM SKARN, CHRISTMAS MOUNTAINS, TEXAS



ATOM FRACTION AL IN IDOCRASE

Figure 6. Atom fraction of iron in coexisting melilite and idocrase from 16 samples of skarn. Dotted line represents equal partitioning of iron between the two phases.

COEXISTING MELILITE AND IDOGRASE FROM SKARN, CHRISTMAS MOUNTAINS, TEXAS



MPNP= 5 6.0

Figure 7. Atom fraction of magnesium in coexisting melilite and idocrase from 16 samples of skarn. Dotted line represents equal partitioning of magnesium between the two phases.

COEXISTING MELILITE AND IDOGRASE FROM SKARN, CHRISTMAS MOUNTAINS, TEXAS

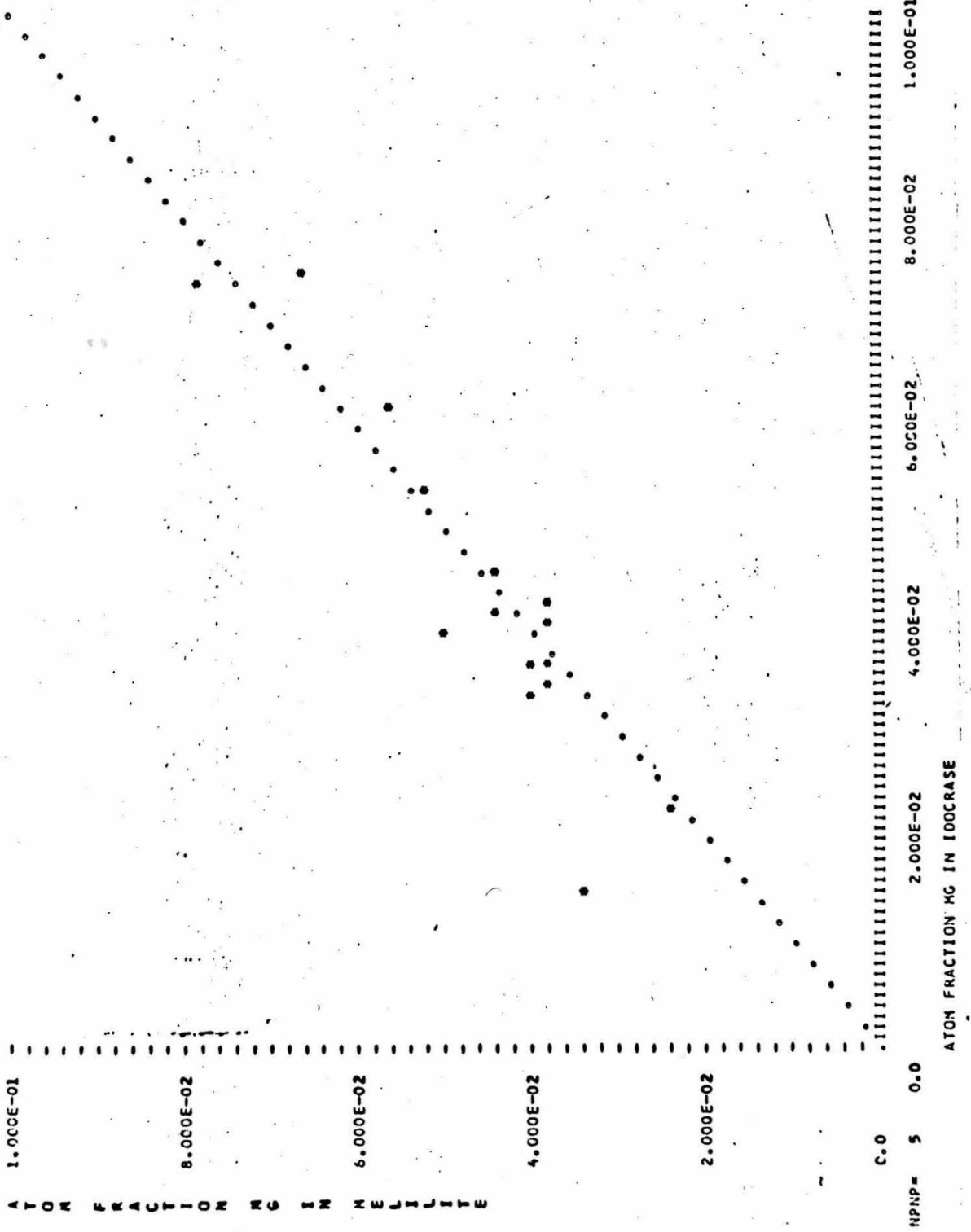


Figure 8. Atom fraction of sodium in coexisting melilite and idocrase from 16 samples of skarn. Dotted line represents equal partitioning of sodium between the two phases.



represented. This clearly shows that the reaction leading to pseudomorphic replacement of melilite by idocrase involves an essentially isochemical hydration.

Reconniassance hydrothermal experiments outlining the pressure-temperature stability fields of melilite (Christie, 1961) and idocrase (Ito and Arem, 1970) confirm the possibility of producing idocrase by the hydration of melilite. Christie (1961, p. 257-58) found that melilite ranging in composition from  $AK_{70}GE_{30}$  to  $GE_{100}$  formed a mixture of idocrase and hydrogarnet when heated with water to temperatures of 450 to 600°C at pressures of 4.8 to 6.7 kilobars. Using gels corresponding in composition to possible formulae of stoichiometric idocrase, Ito and Arem (1970, p. 884-87) established a P-T boundary separating the field of stability of idocrase from that of melilite +  $H_2O$ . The P-T coordinates of the dehydration reaction are sensitive to gel composition, and range from 600 to 700°C over the pressure interval 500 to 2500 bars. The presence of minor amounts of wollastonite and monticellite with melilite in the dehydration products of the gels of idocrase composition probably results from the fact that the compositions chosen have ratios of Si:Al:Mg that do not fit the stoichiometry of melilite. Ito and Arem (1970, p. 885) produced idocrase by heating synthetic melilite with water within the idocrase field of their P-T diagram. Their experiments did not confirm the presence of hydrogarnet as a hydration product of melilite.

The following model, based on field, petrographic and chemical evidence presented above, is proposed for the progressive development

of idocrase skarn by isochemical hydration of melilite. Flow of an aqueous fluid along fractures in melilite skarn results in hydration of melilite adjacent to the fracture. Because a zone of idocrase skarn always separates melilite skarn from pyroxenite, the fluid was probably magmatic in origin. Diffusion of water down the chemical potential gradient established across the idocrase zone and reaction with melilite at the zone boundary cause the zone to grow outward, perpendicular to the fracture. The idocrase zone will continue to widen so long as melilite is available and fluid is flowing in the fracture. Sodium diffusing into the fracture, is carried away by the flowing fluid. Complete replacement of melilite skarn by idocrase results from the coalescence of idocrase veinlets developed along a network of intersecting fractures. The faithful preservation of the external habit and internal cleavage of melilite by idocrase and the lack of disruption of the original skarn fabric indicates that pseudomorphism took place without a change in volume.

#### Calc-silicate Phases

Solid phases from the system  $\text{CaO-SiO}_2\text{-CO}_2$  found in the skarn are:

WOLLASTONITE	$\text{CaSiO}_3$
RANKINITE	$\text{Ca}_3\text{Si}_2\text{O}_7$
KILCHOANITE	$\text{Ca}_3\text{Si}_2\text{O}_7$
LARNITE	$\text{Ca}_2\text{SiO}_4$
SPURRITE	$\text{Ca}_5\text{Si}_2\text{O}_8\text{CO}_3$
TILLEYITE	$\text{Ca}_5\text{Si}_2\text{O}_7(\text{CO}_3)_2$
CALCITE	$\text{CaCO}_3$

One or two of these minerals are present in all melilite or idocrase skarn assemblages. The stoichiometric calc-silicate phase or phases present in such an assemblage reflect the ratio of CaO to SiO<sub>2</sub> in excess over that combined with Al<sub>2</sub>O<sub>3</sub>, MgO and FeO to form melilite. In this sense, they reflect the relative silica saturation of the assemblage. Each mineralogic zone in the skarn is characterized by the presence of one of the calc-silicate phases. The sequence of mineral zones across skarn from pyroxenite to marble, both at the main contact and in the large xenoliths, is wollastonite, rankinite, spurrite, calcite.

Electron microprobe analyses of calc-silicate phases from skarn are listed in Table C-3. Each of the analyzed calc-silicate minerals from the skarn closely approaches the ideal stoichiometric composition of the pure phase. Although iron is a minor constituent of wollastonite and rankinite and sodium occurs in larnite and spurrite, in no case does the sum of the impurities exceed one mole percent. Wollastonite from pyroxenite (analysis 1) contains 2.5 mole percent impurities.

Two polymorphs of Ca<sub>3</sub>Si<sub>2</sub>O<sub>7</sub>, rankinite and kilchoanite, are found in the skarn, but rankinite is the main rock-forming mineral of this composition. Aggregates of kilchoanite occur as monomineralic patches and veinlets in rankinite-melilite skarn, where it appears to post-date the main assemblage. Individual kilchoanite grains have very irregular, serrated boundaries. Kilchoanite from the Christmas Mountains is similar in habit and optical properties to that from the type locality described by Agrell (Agrell and Gay, 1961; Agrell, 1965). It is distinguished from rankinite by its extreme dispersion

( $r > v$ ), which causes most sections to extinguish ultra-blue or ultra-brown, and by its dusty appearance in plane light. Electron microprobe analyses of rankinite and kilchoanite from section CM-8-3 (analyses 3 and 4, Table C-3) confirm their compositional identity, even to the extent that minor elements are partitioned equally between them.

Although tilleyite forms the outer zone in contact with marble in the calc-silicate nodules in the contact aureole, spurrite coexists with calcite in skarn at the marble contact. Tilleyite has been found with spurrite in skarn at only one locality along the gabbro contact. At this locality, "veins" of tilleyite with minor amounts of idocrase, Ti-Zr garnet and magnetite cut idocrase skarn. The veins originate in the tilleyite zone in contact with marble but are developed only along fractures in skarn. The lack of appropriate mineral assemblages and textures rule out a magmatic origin for the veins (Wyllie and Haas, 1966). The presence of tilleyite rather than spurrite and the fact that idocrase is pseudomorphous after euhedral melilite suggest that the veins developed from a carbon dioxide-rich fluid flowing along the fractures.

#### Calcium-Magnesium Orthosilicates

Four minerals on the orthosilicate join in the system CaO-MgO-FeO-SiO<sub>2</sub> are found in the skarn. They are:

LARNITE	$\text{Ca}_2\text{SiO}_4$
PHASE "T"	$\text{Ca}_{1.75}(\text{Mg,Fe})_{0.25}\text{SiO}_4$
MERWINITE	$\text{Ca}_{1.50}(\text{Mg,Fe})_{0.50}\text{SiO}_4$
MONTICELLITE	$\text{Ca}(\text{Mg,Fe})\text{SiO}_4$

Of the four, only merwinite has been found at more than one locality. Electron microprobe analyses of monticellite, merwinite and "T" are listed in Table C-4. All three phases show significant solid solution of iron. As is true of the larnite with which it coexists, phase "T" has a small, but significant content of sodium.

This is the first reported natural occurrence of phase "T". It occurs in two assemblages,

SPURRITE + LARNITE + "T" + MELILITE + PEROVSKITE + MAGNETITE

RANKINITE + LARNITE + "T" + MELILITE + PEROVSKITE + MAGNETITE

Phase "T" was first synthesized by Gutt (1961, 1965) in a phase equilibrium study of the join  $\text{Ca}_2\text{SiO}_4$ - $\text{Ca}_3\text{MgSi}_2\text{O}_8$ . Further work by Schlaudt and Roy (1966) showed that the assemblage  $\text{Ca}_2\text{SiO}_4$  + "T" is stable relative to  $\text{Ca}_2\text{SiO}_4$  + merwinite between 979 and 1381°C at one atmosphere pressure. Phase "T" is colorless in plane light, shows no twinning or cleavage and has  $2V(+) = 30^\circ$ .

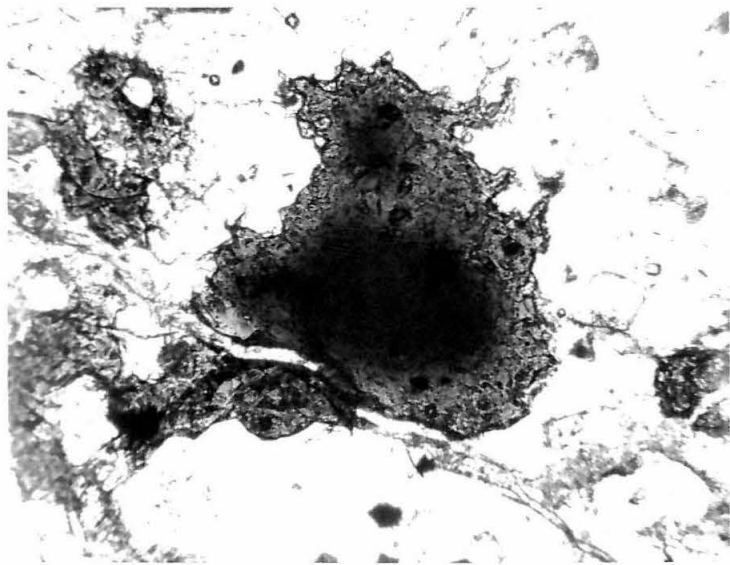
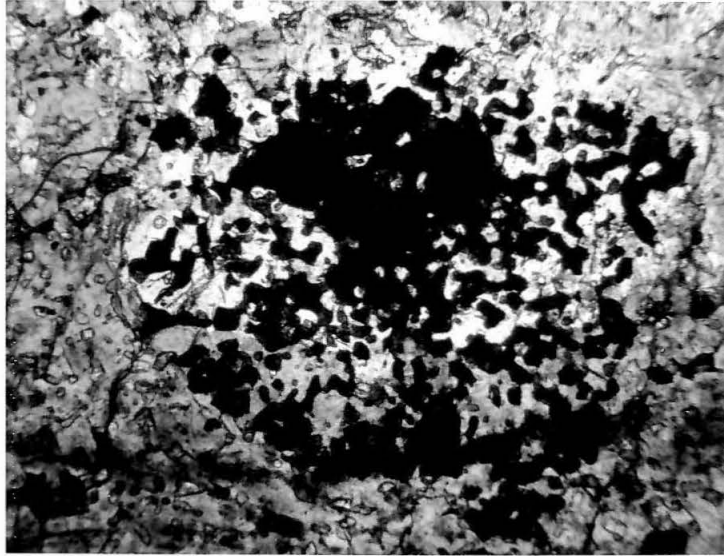
#### Titanian-Zirconian Garnet

Titanian-zirconian andradite garnet that is yellow to yellow-brown in thin section, is a minor but characteristic phase of nearly all assemblages of the skarn. It is always anhedral and commonly is interstitial to melilite. In some cases, numerous individual grains of garnet are concentrated to form what appear to be large, spongy porphyroblasts in which the volume percentage of melilite "inclusions" exceeds that of the host garnet (Plate 4, Figure 1). In section CM-103-6A from the rim of a large skarn xenolith, garnets with deep purple cores are rimmed by yellow-brown or very pale pink garnet (Plate 4, Figure 2). Poikiloblastic inclusions of perovskite crowd

Plate 4. Titanian-Zirconian garnet from skarn

Figure 1. Poikiloblastic garnet in wollastonite-melilite skarn, sample CM-103-6B. Plane light, field 2.3 x 3.0 mm.

Figure 2. Zoned garnet with honey-yellow rim and deep purple core, sample CM-103-6A. Analyses of similar garnet from this sample are given in Table 2. Plane light, field 0.58 x 0.85 mm.



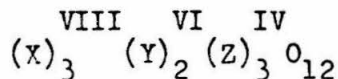
the rims of these garnets, but do not occur in their cores. Garnets from the small skarn xenoliths in pyroxenite and from skarn within 1 cm of the pyroxenite contact are colorless to very-pale pink grossular-andradite solid solutions.

Electron microprobe analyses of garnets from skarn are listed in Table C-5. Because concentrations of Si, Ti and Zr are highly variable, both within single grains and from grain to grain within a single thin section, the values tabulated represent the single point analysis which gave the median value for the formula proportion of silicon of all points analyzed in that section. The range of variation of the formula proportions of Si, Ti and Zr and the number of spot analyses are also listed. Variations in the proportions of other cations are small and no consistent pattern of zonation in Si, Ti and Zr was found. Total iron was corrected as ferric iron in the computation of oxide concentrations from X-ray intensities by inserting the difference between the oxide summation and 1.0 as excess oxygen in each iteration (Bence and Albee, 1968, p. 393). The mineral formulae are based on a cation sum equal to 8.0. The oxygen content computed to balance the electrostatic charge of the cations ranges from 11.96 to 12.20 oxygen atoms per formula unit of 8.0 metal atoms. The small excess of oxygen over the required 12.0 per formula unit shows that the assumption that the bulk of the iron is trivalent and that titanium is tetravalent is essentially correct.

Analyzed garnets that are colorless to pale pink are grossular-andradite solid solutions in which aluminum and iron vary antithetically. The yellow-brown garnets that are characteristic of the skarn are

titanian and titanian-zirconian andradites in which Ti, Zr and Si vary over a broad range. Ca, Mg, Al and Fe show relatively little variation. Because titanium and zirconium appear to be negatively correlated with silicon, the formula proportions of Ti, Zr and Ti + Zr have been plotted against the silicon deficiency, defined as 3.0-formula proportion Si, in order to systematize the nature of the solid solution (Figures 9, 10 and 11). The linear relationships between the formula proportions of Ti, Zr and especially Ti + Zr and the silicon deficiency suggest that titanium and zirconium chemically substitute for silicon.

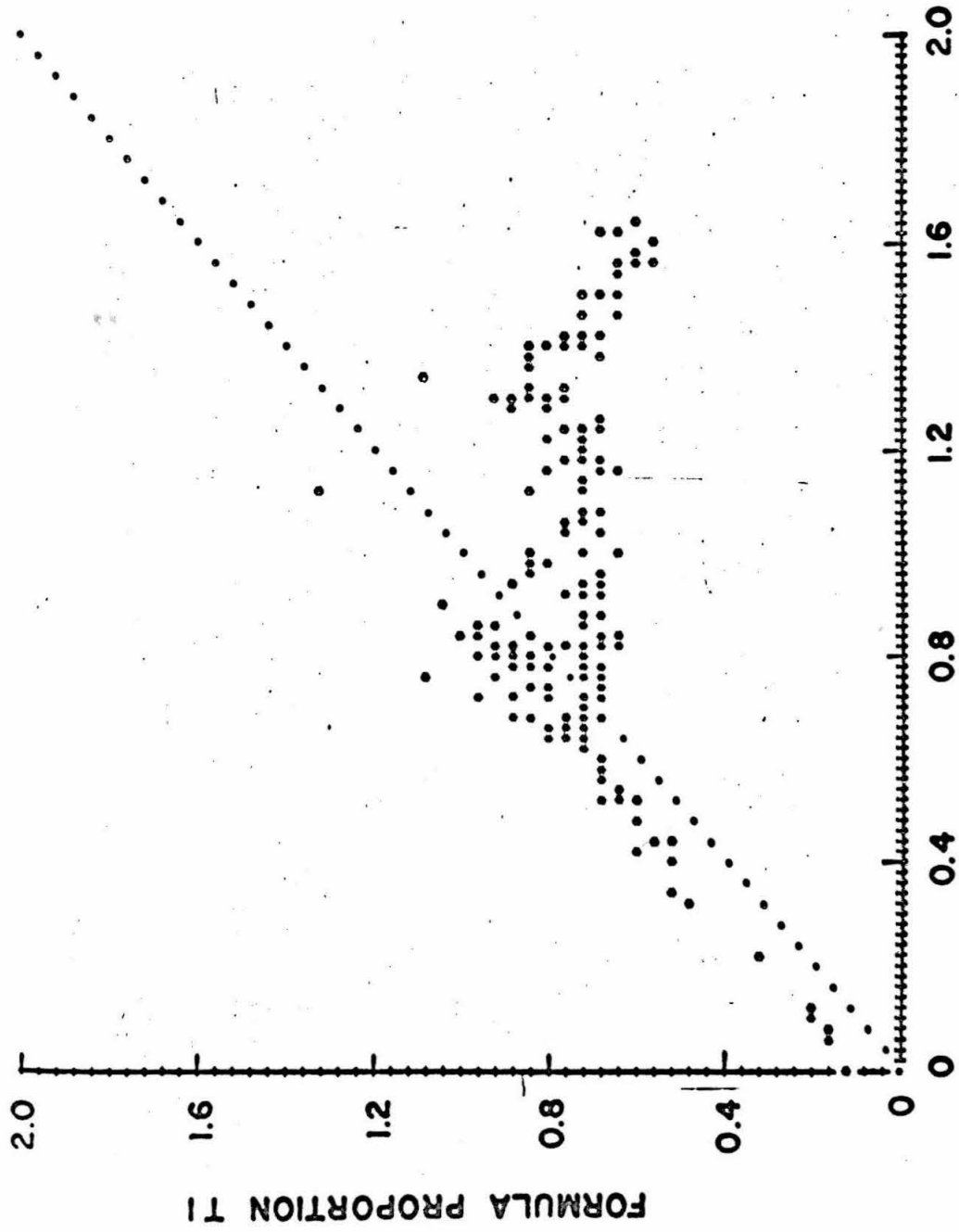
The crystal chemistry of titanian and zirconian andradite has been the subject of a great deal of discussion. Although the valence and site occupancy for most cations which substitute in the garnet structure are well known (Celler, 1967), those of titanium and zirconium are not well understood. The structural formula of garnet may be written:



where the Roman superscripts refer to the oxygen coordination number for the cations on each site. The tetrahedral (Z) site is completely occupied by silicon in most garnets, however titanium-rich garnets always contain fewer than 3.0 atoms of silicon per formula unit. The central question is that of whether titanium and zirconium structurally substitute for silicon on the tetrahedral site or for ferric iron on the octahedral (Y) site, with ferric iron filling the silicon deficiency on the Z site. That is, should the structural formula of titanian andradite be written

Figure 9. Formula proportion of titanium plotted against the tetrahedral silicon deficiency in garnet from skarn. Based on 196 point analyses of garnet from 28 samples of skarn.

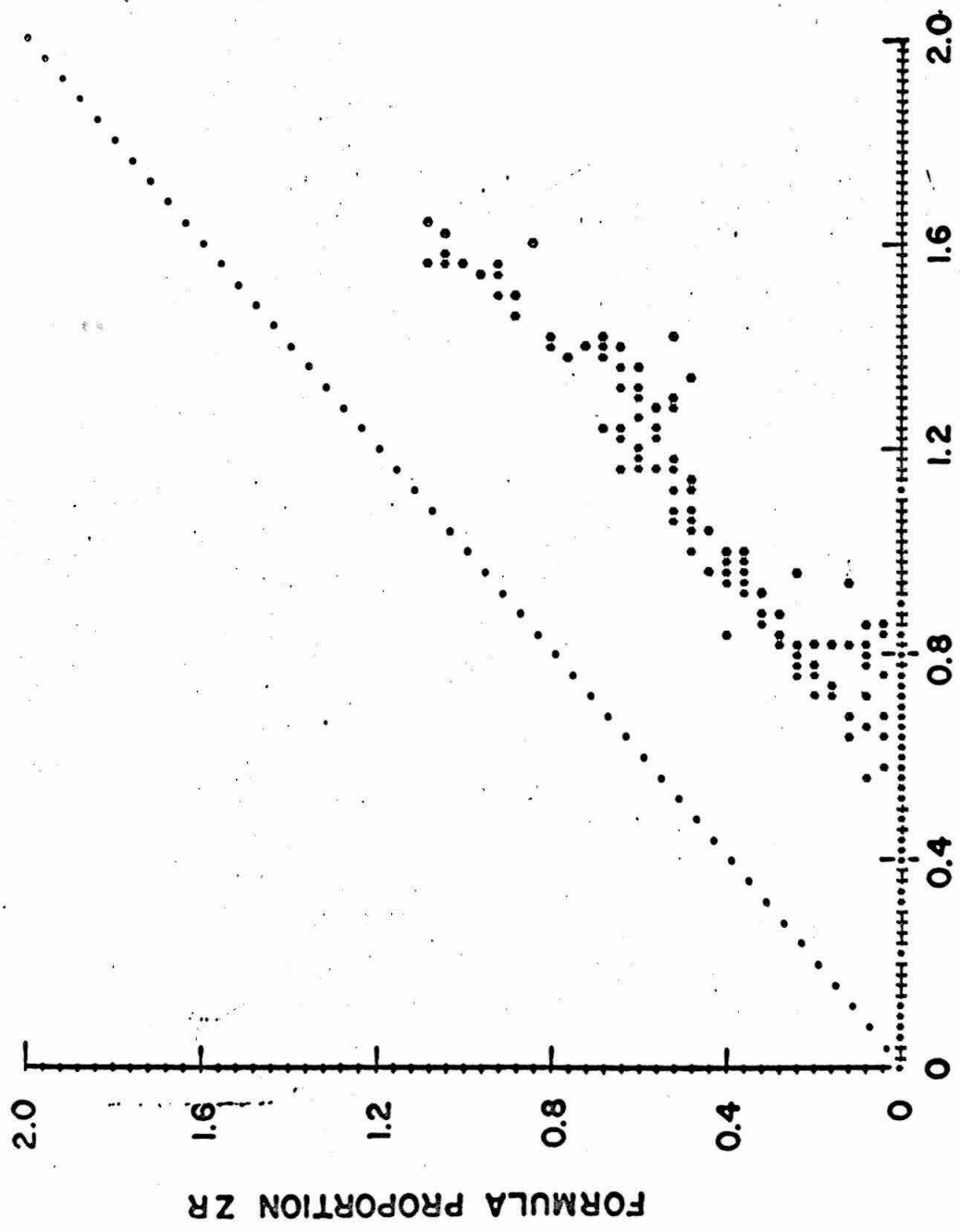
GARNET FROM SKARN, CHRISTMAS MOUNTAINS, TEXAS



3.0-FORMULA PROPORTION S1

Figure 10. Formula proportion of zirconium plotted against the tetrahedral silicon deficiency in garnet from skarn. Based on 196 point analyses of garnet from 28 samples of skarn.

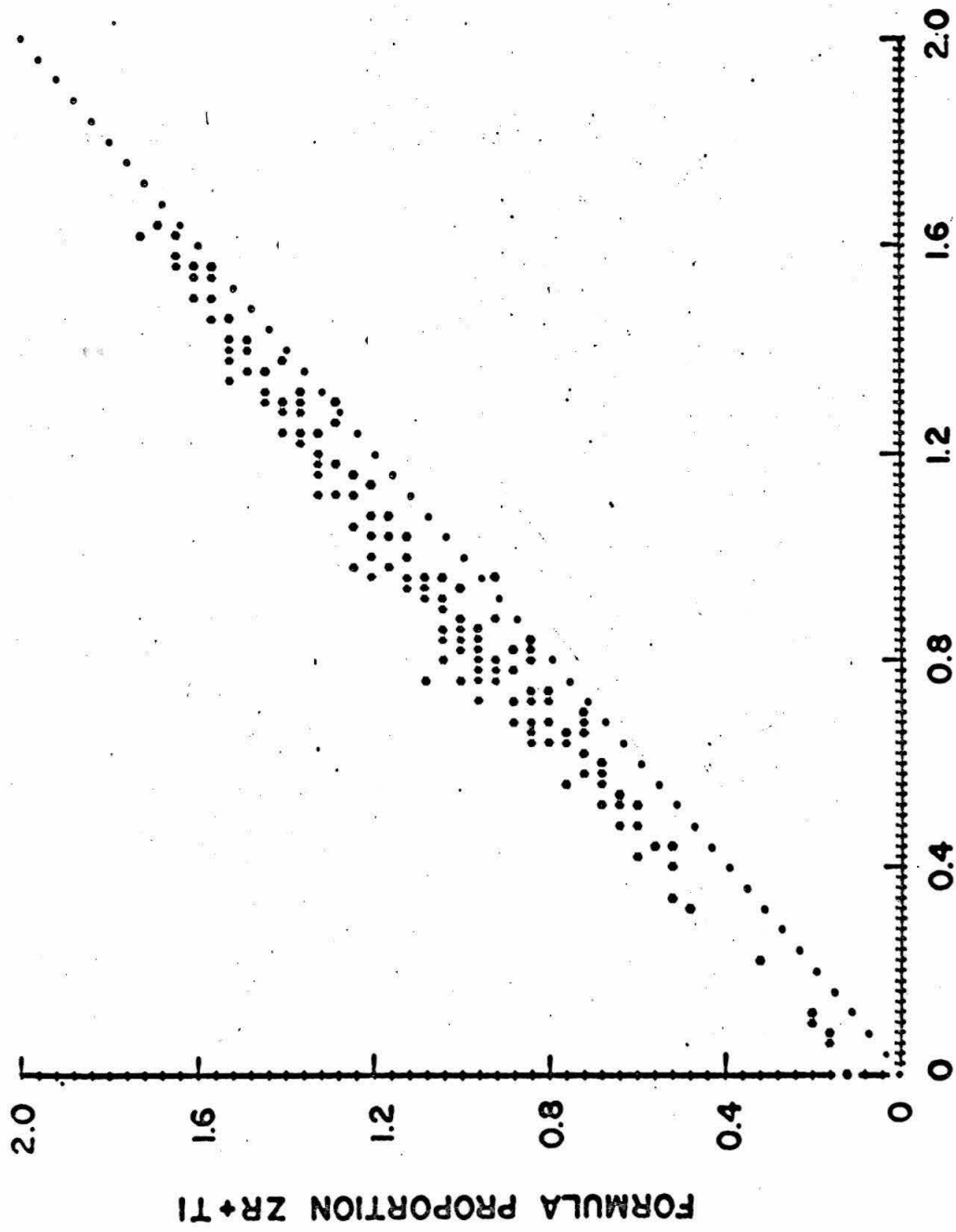
GARNET FROM SKARN, CHRISTMAS MOUNTAINS, TEXAS



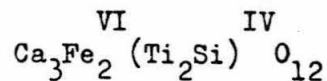
3.0-FORMULA PROPORTION Si

Figure 11. Formula proportions of zirconium and titanium plotted against the tetrahedral silicon deficiency in garnet from skarn. Based on 196 point analyses of garnet from 28 samples of skarn.

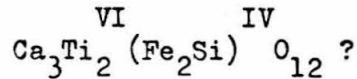
GARNET FROM SKARN, CHRISTMAS MOUNTAINS, TEXAS



3.0-FORMULA PROPORTION SI



or



The approaches to the solution to this problem have taken many forms, which include (1) establishment of a systematic negative correlation between cations in solid solutions covering a wide range of composition (Isaacs, 1968; Howie and Woolley, 1968; Gomes, 1969; Dowty, 1971), (2) optical absorption measurements in the visible and infra-red to characterize possible electronic transitions (Manning, 1967; Howie and Woolley, 1968; Manning and Harris, 1970; Moore and White, 1971; Dowty, 1971), (3) Mössbauer spectroscopy to determine site occupancy and oxidation state (Burns and Burns, 1971; Dowty, 1971), (4) X-ray single crystal structure refinement of chemically analyzed garnets to determine site occupancy (Dowty and Appleman, 1970) and mineral synthesis to determine the extent of miscibility of titanium and zirconium in silicate garnet (Ito and Frondel, 1967; Huckenholz, 1969). The reader is referred to Dowty (1971) for a critical review of the problem. Although equivocal, optical absorption and Mössbauer spectra suggest that part of the silicon deficiency is balanced by tetrahedrally coordinated ferric and ferrous iron (Moore and White, 1971; Burns and Burns, 1971; Dowty, 1971). In nearly all such cases, there is sufficient aluminum to fill the Z position, but the spectral measurements do not rule out the possibility that some of the titanium may occupy the tetrahedral site. Unsuccessful attempts to synthesize silicate garnets with more than two atoms of Ti per formula

unit (Ito and Frondel, 1967; Huckenholz, 1969) suggest that Ti is restricted to the octahedral site. It is possible, however, that up to 2 atoms of Ti may substitute for Si on Z but that the distortion caused by the entry of the large Ti atoms into the tetrahedral site disrupts the garnet structure at concentrations greater than this.

The plot of the formula proportion of Ti + Zr against the silicon deficiency (Figure 11) shows that Ti + Zr just balance the silicon deficiency with a consistent excess of 0.1 to 0.2 atoms per formula unit. The negative correlation between titanium and silicon in garnet has been cited as evidence that titanium occupies the tetrahedral site in the structure (Howie and Woolley, 1968; Gomes, 1969). However, as emphasized by Dowty (1971, p. 1988), such a negative correlation between Ti + Zr and Si in no way proves that titanium and zirconium substitute structurally for silicon. It is merely a consequence of the fact that the number of cations in the garnet formula must total to a constant sum. With this in mind, it is possible to gain some insight into possible site occupancy of the analyzed garnets from the relationships between titanium, zirconium and silicon.

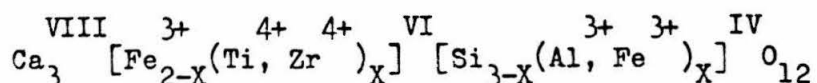
A simple approach to the prediction of site occupancy is to consider the relative ionic sizes expressed as the ratio of the cation radius ( $R_c$ ) to the radius of divalent oxygen ( $R_o = 1.40 \text{ \AA}$ ). If the ions are treated as hard spheres, the radius ratio ( $R_c/R_o$ ) determines the type of cation-oxygen coordination polyhedron that is likely to be formed. A tetrahedron is predicted for

$$0.22 < R_c/R_o < 0.41$$

and an octahedron is predicted for

$$0.41 < R_c/R_o < 0.73.$$

As is shown on Figure 9, titanium balances the silicon deficiency only up to 0.8 atoms per formula unit. Thus for a silicon deficiency of 0.8 or less, there is sufficient Ti 4+ ( $R_c/R_o = 0.49$ ) to substitute for Si 4+ ( $R_c/R_o = 0.30$ ) on the tetrahedral site. However, Al 3+ ( $R_c/R_o = 0.36$ ) and Fe 3+ ( $R_c/R_o = 0.46$ ) may also enter the Z position. Substitution of either Al 3+, Fe 3+ or Ti 4+ for Si 4+ requires a large distortion of the oxygen tetrahedron. It would seem reasonable, from a geometric point of view, to fill the tetrahedral site with the smallest available cations. Zr 4+ ( $R_c/R_o = 0.57$ ) is probably too large to be stable in tetrahedral coordination with oxygen. Thus, where the silicon deficiency is greater than 0.8, Al 3+ and/or Fe 3+ must occupy the tetrahedral site. Ti 4+ may occupy the Z position up to 0.8 atoms per formula unit, but since all analyzed garnets have Al + Fe in excess of the amount needed to balance the silicon deficiency, it is argued on geometrical grounds that Al 3+ and Fe 3+ rather than Ti 4+ occupy the tetrahedral site. Ti 4+ and Zr 4+ would then be octahedrally coordinated with oxygen. The ideal structural formula that describes garnets from the skarn is



The consistent close approach to 12.0 of the number of oxygen atoms needed to balance the electrostatic charge of 8.0 cations in the garnet formula justifies the assumption that all iron is

trivalent and all titanium is tetravalent. However, formulae computed from spot analyses of the deep purple cores of yellow-brown garnets from wollastonite-idocrase skarn (CM-103-6A) from the large xenolith consistently show an oxygen excess, implying that some of the iron and/or titanium is in a lower oxidation state than that assumed (Table 2). The oxygen excess results from an excess of tetravalent cations and a corresponding deficiency of trivalent and divalent cations. Comparison of analyses 1 and 2 in Table 2, representing a purple core and its corresponding yellow rim, shows no significant differences in composition. This compositional similarity between core and rim along with the oxygen excess in the core suggests that the purple color of the core may be due to mixed oxidation states of titanium and/or iron. Optical absorption spectra of pink titanian andradite from San Benito County, California (Manning and Harris, 1970; Dowty, 1971) suggest that some of the octahedrally coordinated titanium is trivalent. Isaacs (1968) measured a large reducing capacity for garnet from San Benito County which was attributed to the presence of essentially all of the titanium in the trivalent state. Charge balance calculations for the purple garnet cores from the skarn allow 25 percent of the titanium to be assigned as trivalent. This assignment also results in there being 3 divalent, 2 trivalent and 3 tetravalent cations per formula unit.

#### Perovskite and Magnetite

Perovskite and magnetite, like garnet, are characteristic but minor phases of the skarn. Perovskite occurs as minute purple

TABLE 2

ELECTRON MICROPROBE ANALYSES OF GARNET FROM SKARN CM-103-6A				
FORMULA PROPORTIONS BASED ON CATION SUM = 8.0				
	PURPLE CORE		YELLOW RIM	
Si 4+	2.29	2.29	2.33	2.33
Zr 4+	0.01	0.01	0.02	0.02
Ti 4+	0.95	0.73	0.77	0.67
Ti 3+	—	0.22	—	0.10
Al 3+	0.60	0.60	0.46	0.46
Fe 3+	1.22	1.14	1.39	1.39
Fe 2+	—	0.08	—	—
Mn 2+	0.02	0.02	0.01	0.01
Mg 2+	0.04	0.04	0.05	0.05
Ca 2+	2.86	2.86	2.98	2.98
Oxygen	12.15	12.00	12.05	12.00

octahedra in assemblages with rankinite, spurrite or calcite. Where it coexists with wollastonite, perovskite forms anhedral, drop-like grains. Large, subhedral, polysynthetically-twinned grains of perovskite occur with spurrite. Electron microprobe analyses of perovskite show it to be of fairly uniform composition in all assemblages and that its composition closely approaches that of the ideal formula,  $\text{CaTiO}_3$ . Two representative analyses are listed in Table C-6.

Magnetite occurs as anhedral grains, that commonly are interstitial to melilite. It is optically homogeneous and shows no evidence of exsolution of ulvospinel or oxidation to ilmenite. Although a systematic electron microprobe study of the magnetite in skarn was not done, reconnaissance analyses show that it contains between 1 and 8 mole percent of the ulvospinel end-member. The low titanium content of the magnetites in skarn which coexist with perovskite are in sharp contrast to those of magnetite in gabbro which coexist with ilmenite and contain 10 to 60 mole percent ulvospinel. There appear to be systematic compositional differences between magnetite from the main contact and that from the xenolith. That from the main contact is enriched in titanium whereas that from the xenolith is enriched in magnesium. Representative magnetite analyses are listed in Table C-6.

## MINERAL ASSEMBLAGES

Mineral assemblages in zoned skarn from the main contact traverse and xenolith traverse are listed in Tables 3 and 4. To a first approximation, the mineralogy of the skarn may be described by solid phases in the system  $\text{CaO-FeO-MgO-Al}_2\text{O}_3\text{-SiO}_2\text{-CO}_2$ . The ubiquitous accessory minerals garnet, perovskite and magnetite rarely exceed 3 volume percent. Ferrous iron and magnesium may be combined as a single component for the purpose of graphical portrayal of the 6 component system on a tetrahedron without loss of generality because in most rocks, melilite is the only phase in which these components occur. In those assemblages in which melilite coexists with merwinite, monticellite or phase "T", no crossing tie-line relationships arise that are attributable to this simplification.

All mineral assemblages from the two traverses (with the exception of CM-108, assemblages 10 and 14, discussed below) are plotted on Figure 12 on which the composition of melilite has been projected from Al onto the Ca-(Fe+Mg)-Si face of the simplified skarn tetrahedron. Tie-lines joining phases on the face of the tetrahedron with melilite are shown vanishing to a point to aid in visualization of the three possible four-phase volumes involving melilite, merwinite and two adjacent phases on the Ca-Si join. Phases joined by tie-lines represent assemblages compatible over a range of P, T and  $u_{\text{CO}_2}$ . The lack of crossing tie-lines suggests that the assumptions used in the construction of the diagram are reasonable and that to the extent that the

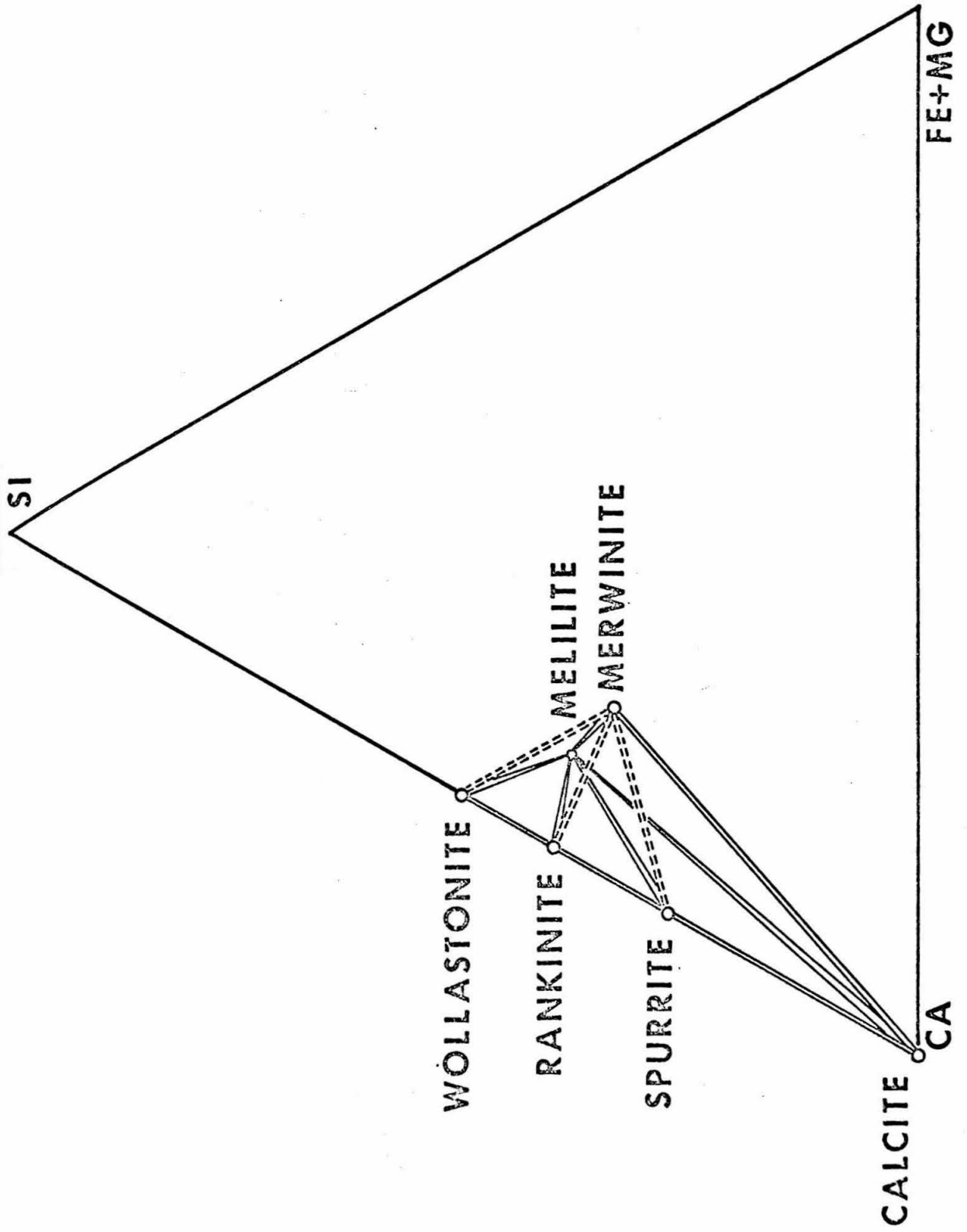
TABLE 3  
 MINERAL ASSEMBLAGES IN SKARN  
 MAIN CONTACT WITH SUE PEAKS FORMATION

Distance From Pyroxenite (CM)	0-4	4-15	15-25	25-42	42-74	74-140	
CALCITE							x x
SPURRITE				x	x		x
RANKINITE				x			
WOLLASTONITE	x	x	x				
MERWINITE							x
MELILITE			x	x	x	x	x
IDOCRASE	x	x					
TI-ZR GARNET	x	x	x	x	x	x	x
PEROVSKITE		x	x	x	x	x	x
MAGNETITE	x	x	x	x	x	x	x

TABLE 4  
 MINERAL ASSEMBLAGES IN SKARN  
 XENOLITH OF SANTA ELENA LIMESTONE

Distance From Pyroxenite (CM)	0-5	5-55	55-75	75-90
CALCITE				x
SPURRITE			x	x
RANKINITE		x		
WOLLASTONITE	x	x		
MELILITE		x	x	x
IDOCRASE	x			
TI-ZR GARNET	x	x	x	x
PEROVSKITE	x	x	x	x
MAGNETITE	x	x	x	x

Figure 12. Perspective view of the simplified skarn tetrahedron  $\text{Ca}-(\text{Fe}+\text{Mg})-\text{Al}-\text{Si}$  viewed normal to the  $\text{Ca}-(\text{Fe}+\text{Mg})-\text{Si}$  face, showing two and three-phase assemblages in skarn. Phases joined by dashed tie-lines have not been found in coexistence. The absence of 4-phase assemblages indicates the skarn compositions lie on planes and joins within the tetrahedron.



bulk compositional range of the skarn is sensitive to changes in P, T and  $u_{\text{CO}_2}$ , conditions of metamorphism were the same both in the xenolith and at the main contact. Within a skarn band, different mineral assemblages result from metamorphism of different bulk compositions.

The mineral assemblage of each skarn zone is compatible with the assemblages at each of its contacts, while the assemblages bounding it on either side are incompatible. Thus, each point along a traverse across the skarn may be treated as a local equilibrium system. The establishment of local equilibrium at each point along the gradient in bulk composition across a skarn band produced a series of mineral zones analogous to those involving stoichiometric phases in the zoned calc-silicate nodules. The main difference between the zoned nodules and the zoned skarn is the presence in the latter of phases capable of extensive solid solution in addition to the stoichiometric calc-silicate minerals.

Each monomineralic zone in the calc-silicate nodules represents a "special" bulk composition in the system  $\text{CaO-SiO}_2\text{-CO}_2$ , in that it consists of fewer than the maximum number of solid phases that may co-exist in equilibrium with  $\text{CO}_2$ . Similarly, the mineral assemblages of the skarn represent "special" bulk compositions within the simplified skarn system  $\text{CaO-(FeO+MgO)-Al}_2\text{O}_3\text{-SiO}_2$ . Although a general composition within the simplified skarn tetrahedron is represented by a four-phase assemblage, skarn assemblages consist of either two or three phases in the simple system. Merwinite has not been found with either

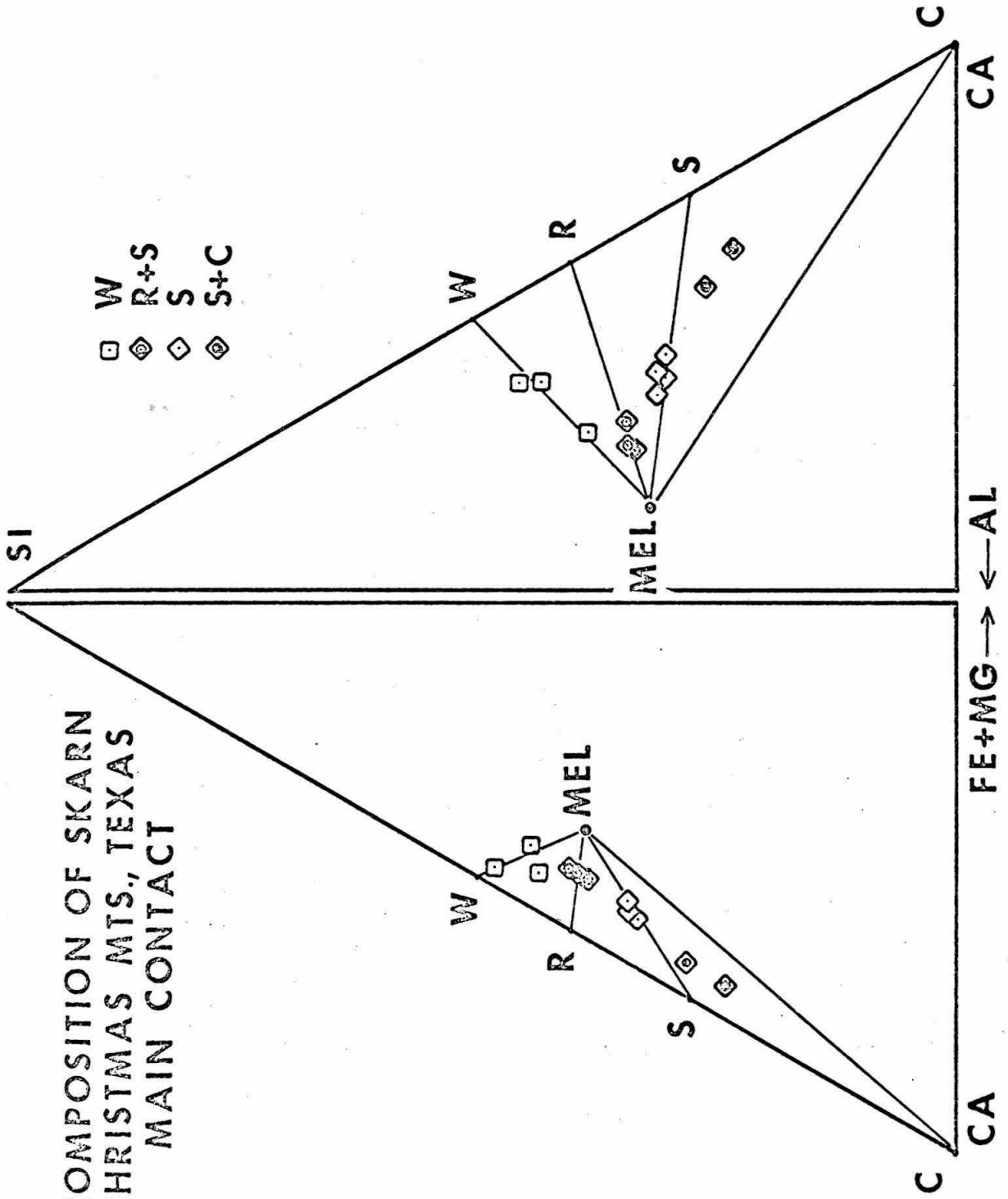
rankinite or wollastonite and, although it occurs in rocks with calcite and melilite, merwinite and spurrite have not been observed to be in mutual contact. Merwinite commonly occurs as drop-like inclusions in melilite which, in turn, is in contact with either calcite or spurrite. The presence of two- and three-phase assemblages requires that the bulk composition of the skarn be confined to joins and planes within the simple skarn tetrahedron. The sequence of mineral zones developed in skarn along a traverse from marble to pyroxenite is encountered within the tetrahedron along a line joining calcite with the wollastonite-melilite join and lying within the plane calcite-wollastonite-melilite. The bulk composition leaves this plane only within the volume calcite-spurrite-melilite-merwinite.

Bulk chemical compositions of individual samples of skarn were determined by electron microprobe analysis of glass discs made by fusing equal parts by weight of pulverized skarn and lithium tetraborate at 1000°C in carbon crucibles in an electric muffle furnace. The analyses are listed in Table C-7. To test the inferred relationship between rock composition and mineral assemblage, the analytical results, recast as atom fraction of cations, have been plotted on the Ca-Si-(Fe+Mg) and Ca-Si-Al faces of the simplified skarn tetrahedron (Figures 13 and 14). The calc-silicate phases are joined by tie-lines with a point representing the mean composition of melilite determined for the traverse.

For skarn from both the main contact and the xenolith, the bulk compositions of rocks with two-phase assemblages in the simple system plot on or close to the appropriate two-phase joins. The bulk composi-

-Figure 13. Bulk composition of skarn samples from main contact traverse projected onto Ca-(Fe+Mg)-Si and Ca-Al-Si faces of the simplified skarn tetrahedron. Projected composition of melilite is average for traverse. Mineral assemblage symbols as on Figure 1.

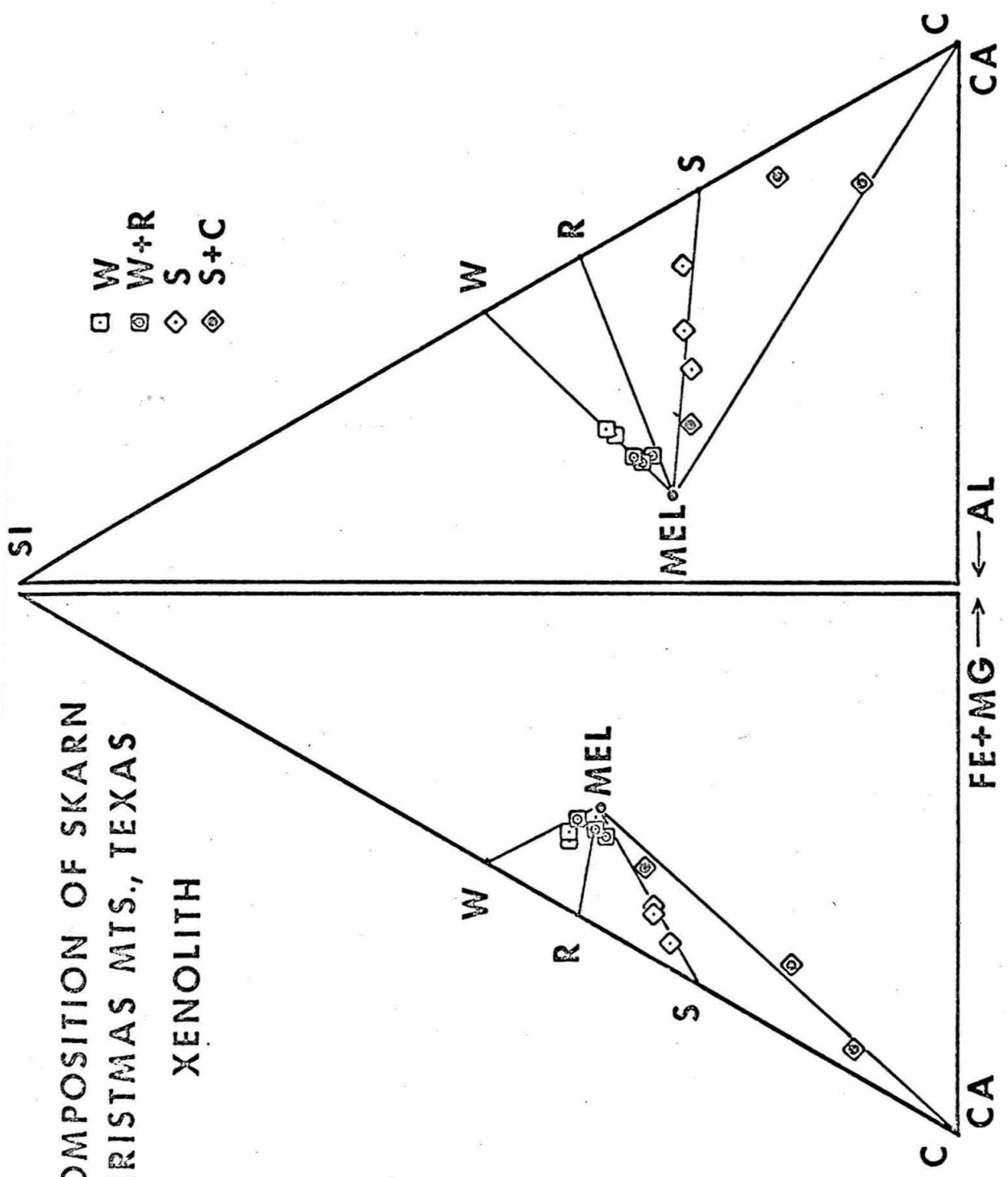
COMPOSITION OF SKARN  
CHRISTMAS MTS., TEXAS  
MAIN CONTACT



FE+MG → ← AL

Figure 14. Bulk composition of skarn samples from xenolith traverse projected onto Ca-(Fe+Mg)-Si and Ca-Al-Si faces of the simplified skarn tetrahedron. Projected composition of melilite is average for traverse. Mineral assemblage symbols as on Figure 1.

COMPOSITION OF SKARN  
CHRISTMAS MTS., TEXAS  
XENOLITH



- W
- W+R
- ◇ S
- ◊ S+C

tions of rocks with three-phase assemblages generally plot within the appropriate three-phase triangle but, with the exception of those with the assemblage calcite+spurrite+mellite, they plot close to one of the bounding two-phase joins with melilite. The striking feature of the distribution of skarn compositions within the tetrahedron is that rather than showing a continuous variation of bulk composition across the adjoining three-phase triangles, the compositions of the skarns are grouped along the two-phase joins with melilite.

An understanding of the genesis of the series of "special" compositions recorded by the zoned skarn may be approached along the same lines as those of the model developed to illustrate the growth of the zoned calc-silicate nodules from the contact aureole. The restriction of skarn compositions to joins and planes within the simple skarn tetrahedron suggests that the growth of a skarn zone is initiated by reaction between incompatible phases with diffusion down the resulting chemical potential gradients causing the zone to widen. To test the applicability of the reaction-diffusion model, the initial configuration of reactants and the specific sequence of mineral reactions which lead to the observed assemblages must be determined. First, however, the local equilibrium hypothesis requires further testing.

#### COMPOSITIONAL GRADIENTS

The assumption of local equilibrium on which the growth model is based, requires that the gradients of the chemical potentials of all transported species be continuous from point to point across the series of skarn zones. The compatibility of mineral assemblages of adjacent zones is a necessary condition for local equilibrium. However, because

solid solutions are involved in all of the assemblages, continuity of the gradients of the chemical potentials requires that the gradients in the composition of the solid solutions be continuous. The only compositional discontinuities consistent with continuity in the gradient of the chemical potentials are those resulting from miscibility gaps in the phases. Neither melilite nor garnet have miscibility gaps in the range of composition recorded in the skarn.

#### Melilite

The composition of melilite, recast as formula proportion of cations, is plotted as a function of distance from the pyroxenite contact for the main contact traverse on Figure 15 and for the xenolith traverse on Figure 16. Where pseudomorphism of melilite by idocrase is complete in wollastonite skarn, the composition of idocrase was plotted. Although the samples may not be sufficiently closely spaced, there do not appear to be any discontinuities in the composition of melilite either within the calc-silicate zones or at zone boundaries.

The gradients of Si and Al in melilites from the xenolith cross between the spurrite and spurrite-calcite zones, but Si and Al contents of melilite coexisting with calcite + spurrite are similar both in the xenolith and at the main contact, suggesting that they may be controlled by the calc-silicate assemblage of the marble. The reversal in slope of the Mg gradient across the same contact in the xenolith may reflect the same control. Melilite and idocrase in the wollastonite zone from both traverses show a sharp increase in Si and a complementary decrease in Al as the pyroxenite contact is approached. Although this appears to require discontinuities in the gradients of Si and Al along the main

Figure 15. Formula proportion of major cations in melilite from skarn of the main contact traverse plotted as a function of position in skarn relative to contact with pyroxenite. Points at 2.5 and 5 cm are idocrase, pseudomorphous after melilite, in wollastonite skarn. The contact between skarn and marble is at 74 cm. Mineral assemblage symbols as in Figure 1.

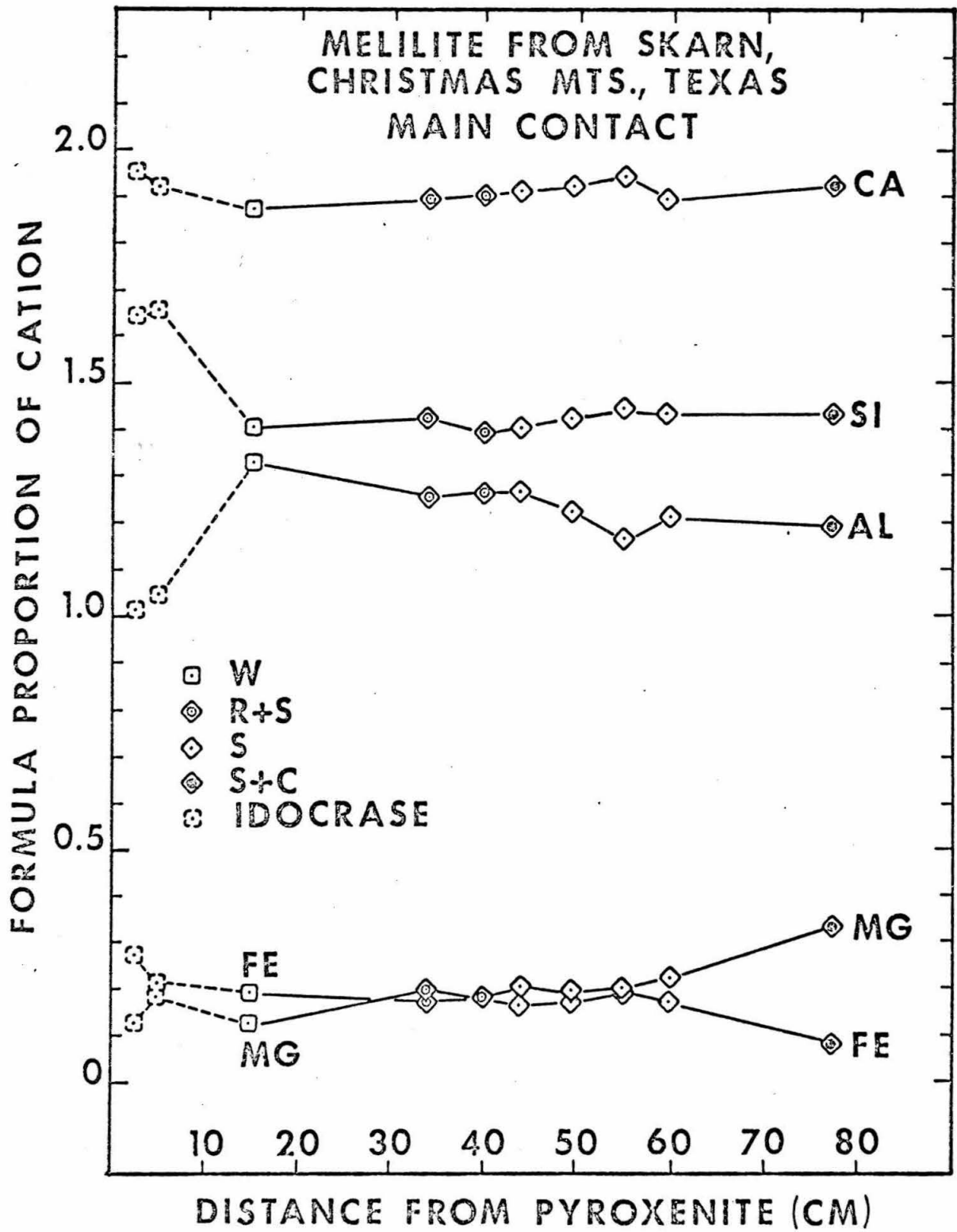
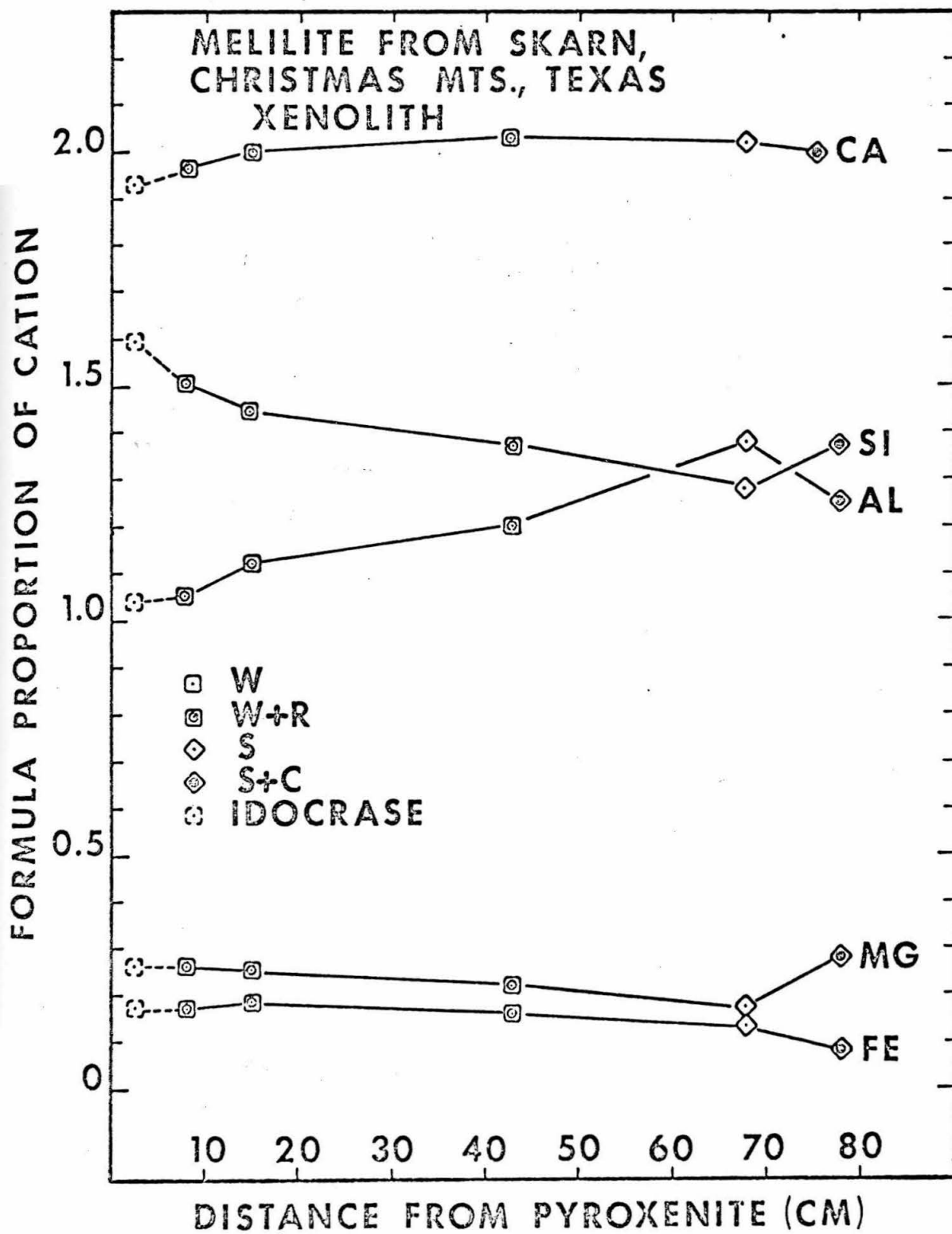


Figure 16. Formula proportion of major cations in melilite from skarn of the xenolith traverse plotted as a function of position in skarn relative to contact with pyroxenite. Point at 2.5 cm is idocrase, pseudomorphous after melilite, in wollastonite skarn. The contact between skarn and marble is at 86 cm. Mineral assemblage symbols as in Figure 1.



contact traverse, the gradient is smooth in the xenolith. The Si and Al contents of idocrase from within 2 cm of the pyroxenite on both traverses are essentially the same.

The compositions of idocrase at the contact with pyroxenite are similar both in the xenolith and at the main contact, as are the compositions of melilite at the contact with marble, but compositional variation within the skarn is markedly different along the two traverses. These differences are readily apparent on a triangular plot of atomic Al-Fe-Mg (Figure 17). At the main contact, the ratio  $Fe/(Fe+Mg)$  in melilite decreases along the traverse from pyroxenite to marble, while the ratio  $Al/(Al+Si)$  shows a small but steady decrease. In the xenolith, the ratio  $Al/(Al+Si)$  shows a strong steady increase at constant  $Fe/(Fe+Mg)$  from the wollastonite zone to the calcite-spurrite zone, where the ratio decreases while  $Fe/(Fe+Mg)$  decreases. Compositions of melilite from skarn derived from Santa Elena Limestone, both at the intrusive contact and in xenoliths plot on the trend established for the xenolith, while melilite from impure beds of Sue Peaks Limestone, metamorphosed by the intrusion plot on the main contact trend. This suggests that differences in gradients of melilite composition across the skarn are controlled by the composition of the host limestone. Along both traverses, however, the gradients of the composition of melilite appear to be continuous.

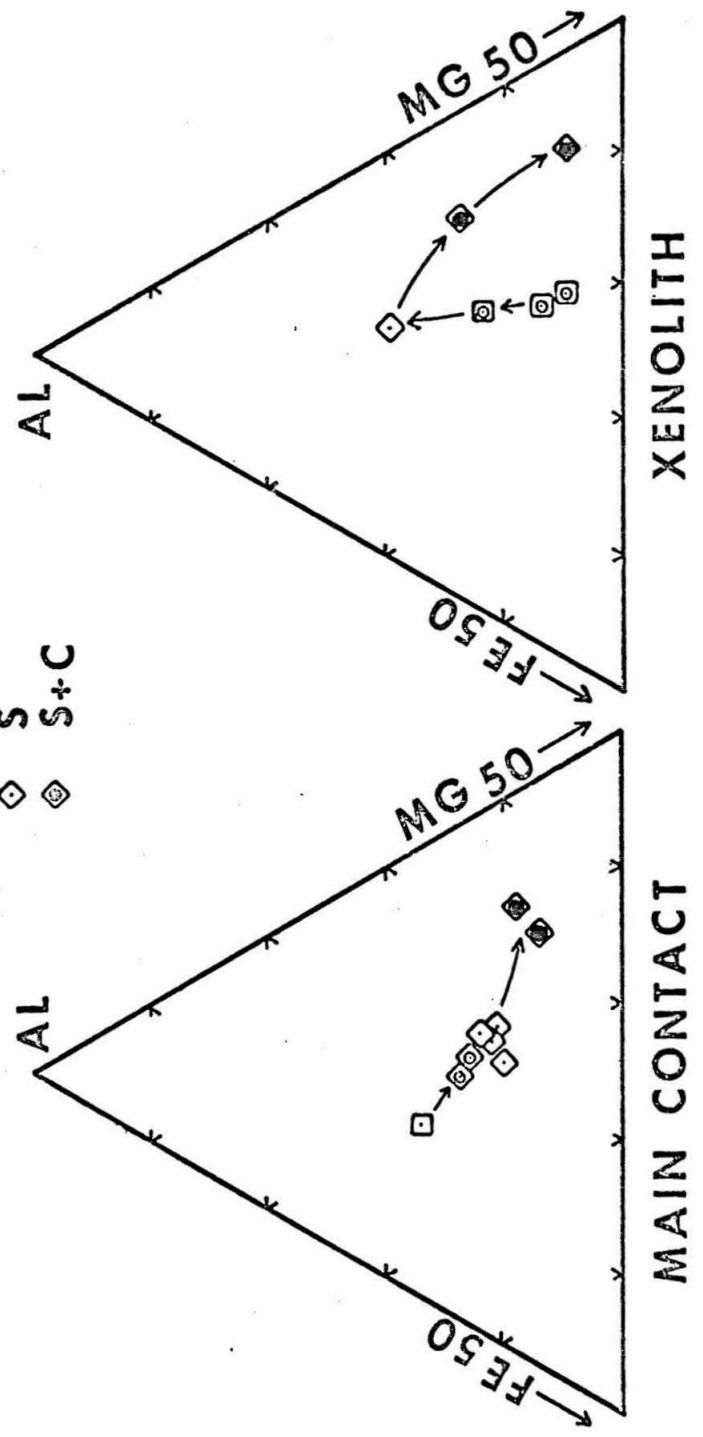
#### Garnet

Although it is not volumetrically important, variation in the composition of garnet with position in the skarn is of interest because

Figure 17. Molecular proportion of aluminum, magnesium and iron in melilite from skarn. Arrows outline trend of composition with position in skarn. Mineral assemblage symbols as in Figure 1.

# MELLILITE FROM SKARN CHRISTMAS MTS., TEXAS

- W
- ◻ W+R
- ◻ R+S
- ◻ S
- ◻ S+C



it is a solid solution involving silicon, hence it may serve as an index of the chemical potential of  $\text{SiO}_2$ . The composition of garnet, recast as formula proportion of cations, is plotted as a function of distance from the pyroxenite contact for the main contact traverse on Figure 18 and for the xenolith traverse on Figure 19. Calcium and magnesium show no significant variation and were not plotted. The main feature of these plots is the striking decrease in silicon content of the garnets from a maximum in the wollastonite zone of the skarn to a minimum in the calcite-spurrite marble. The details of the variation in silicon in garnet across the main contact traverse are balanced by corresponding increases in the zirconium content. A similar antithetic relationship exists between silicon and titanium in garnets from the xenolith. Within the wollastonite zone, the titanium content of the garnet initially decreases along the xenolith traverse whereas it increases along the main contact traverse. In both cases, variation in titanium is opposite in direction to that of silicon. The antithetic variation between aluminum and iron within the wollastonite zones of both traverses corresponds to an increase in the ratio of andradite to grossular components in the garnets with increasing distance from the pyroxenite.

As was the case for similar plots for melilite, the spacing of samples makes it difficult to test for the existence of discontinuities in the gradient compositions at zone boundaries in the skarn. Variations in the proportions of Al and Fe appear to follow smooth curves but the

Figure 18. Formula proportion of major cations in garnet from skarn of the main contact traverse plotted as a function of position in skarn relative to the contact with pyroxenite. The contact between skarn and marble is at 74 cm. Mineral assemblage symbols as in Figure 1.

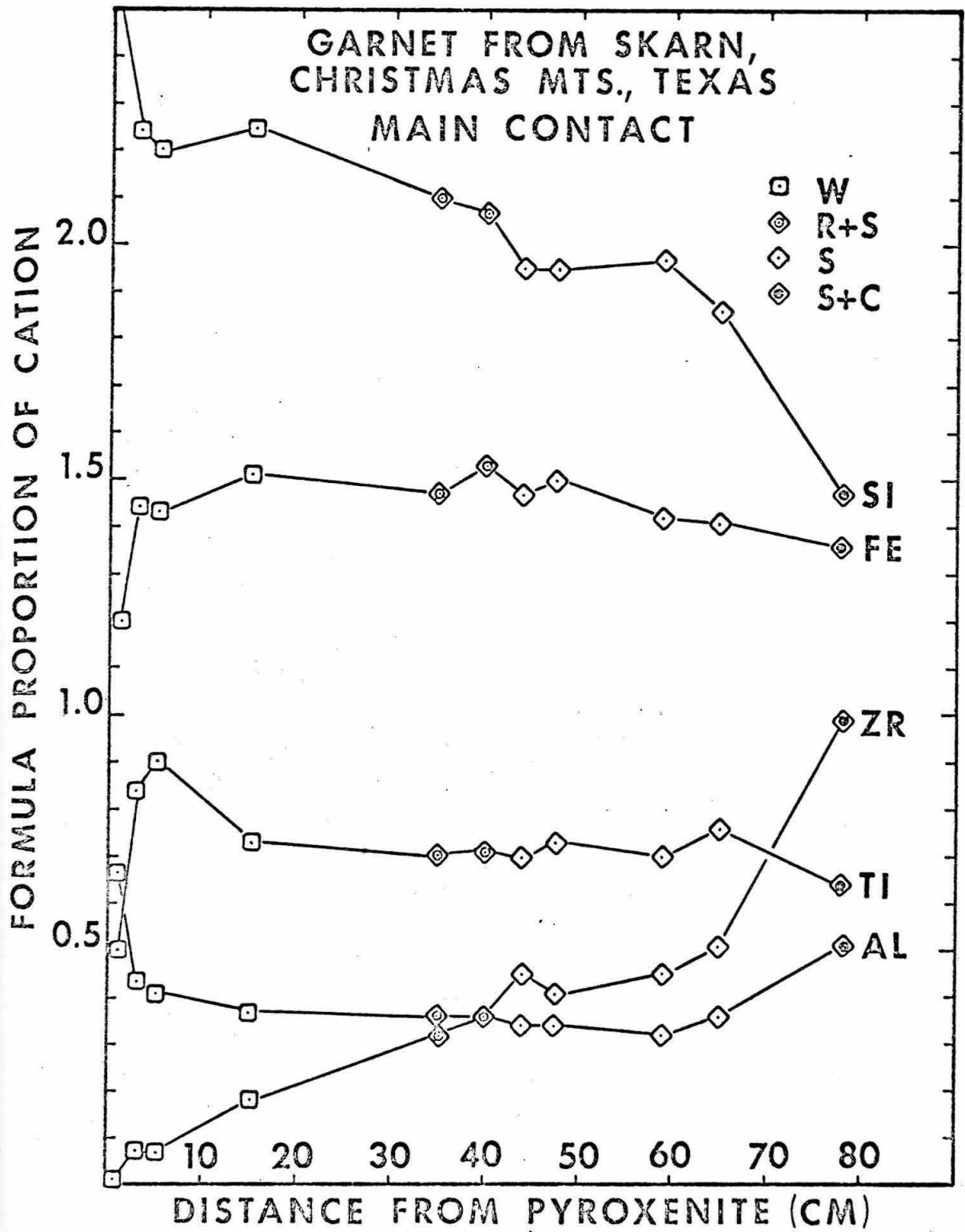
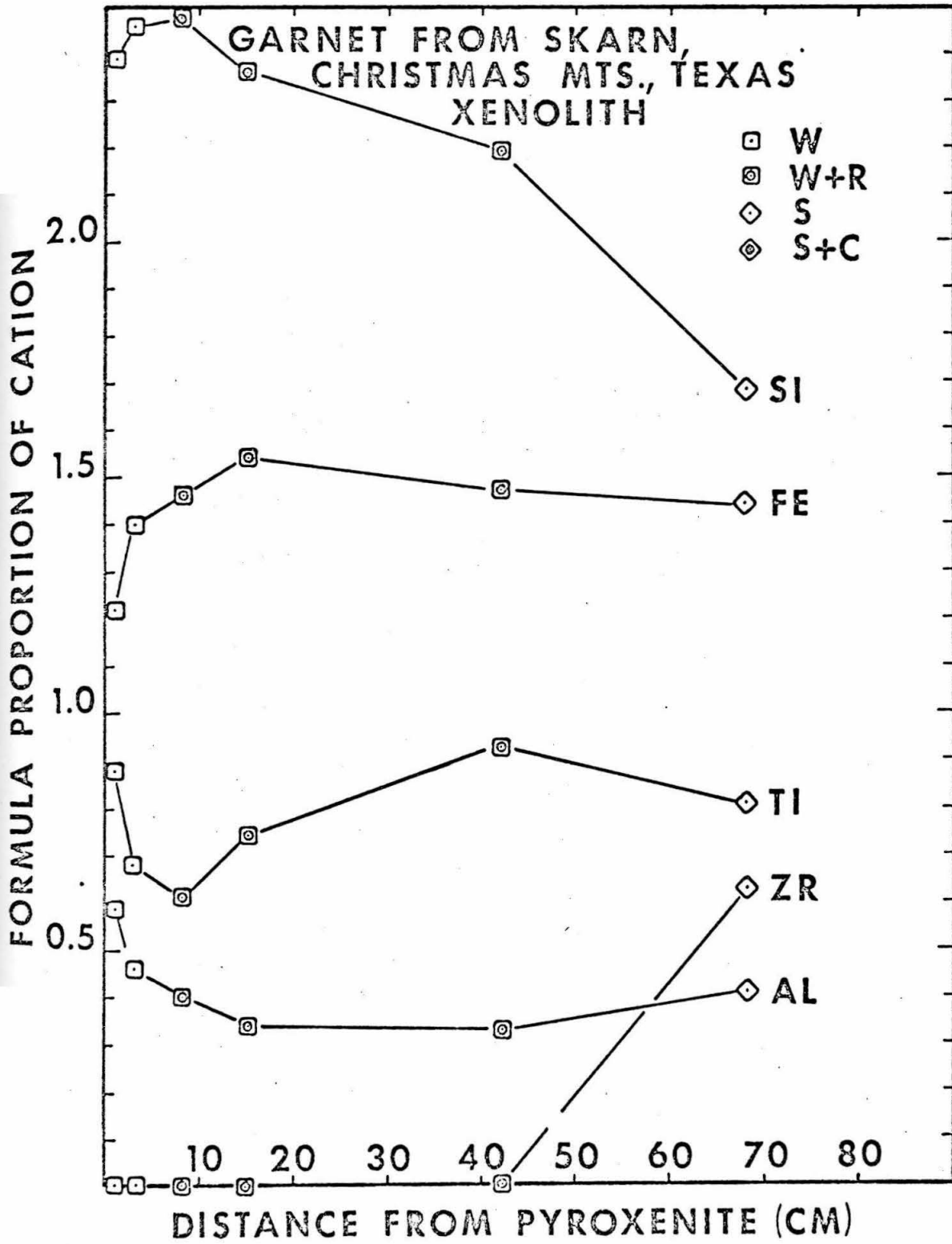


Figure 19. Formula proportion of major cations in garnet from skarn of the xenolith traverse plotted as a function of position in skarn relative to the contact with pyroxenite. The contact between skarn and marble is at 86 cm.

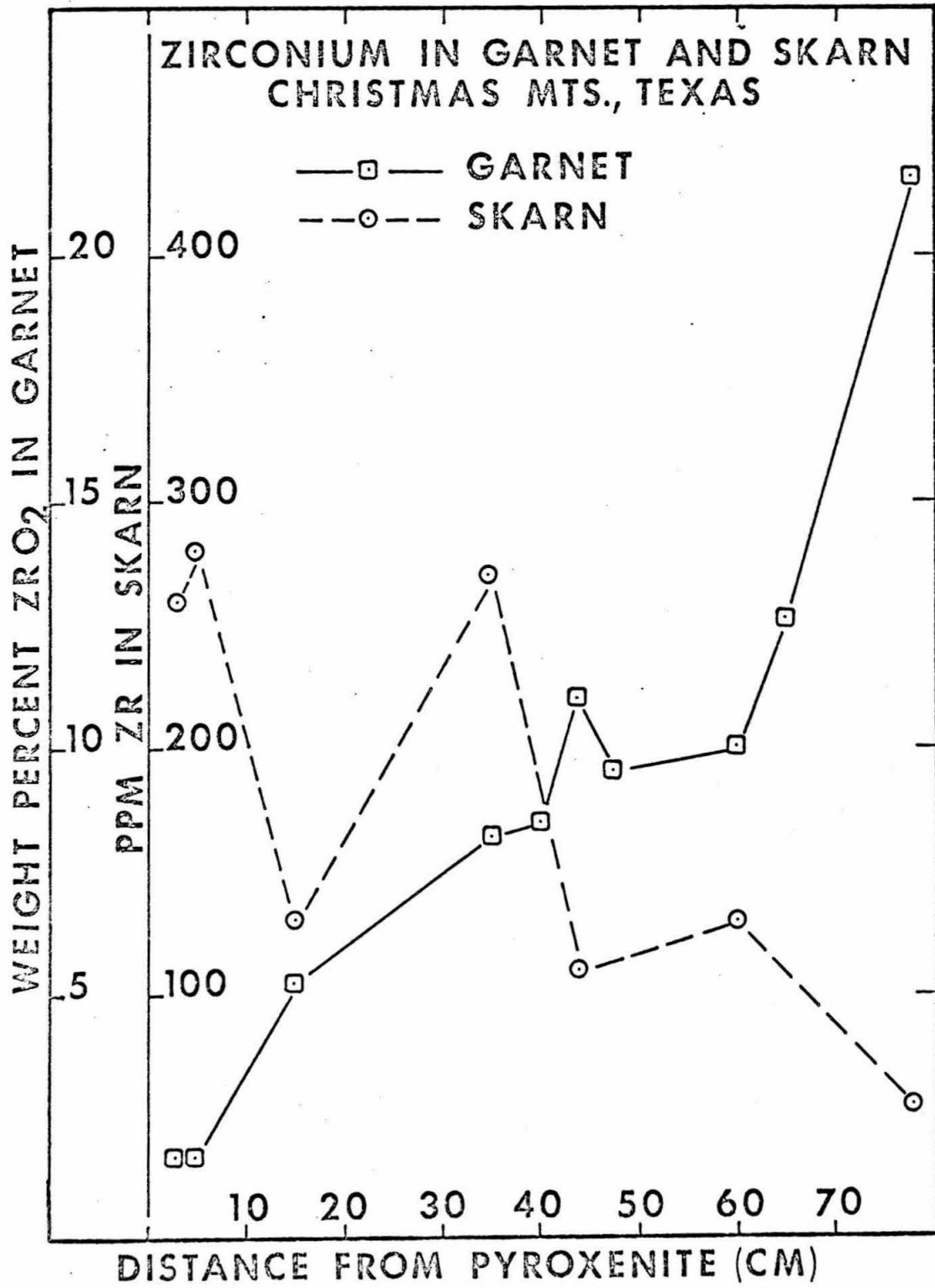


possibility of discontinuities in the gradients of Si, Ti and Zr cannot be ruled out on the basis of the median values plotted. Cation proportions of Si, Ti and Zr vary over wide ranges within garnets from a single thin section. Because these ranges overlap for adjacent samples, it is considered unlikely that discontinuities in the gradients of these cations are present.

The question naturally arises as to the cause of the antithetic relation between Si and Ti + Zr in garnet and of the relationship between garnet composition and that of the bulk rock. Do high concentrations of titanium and zirconium in garnet reflect high concentrations of these elements in the bulk rock or does the chemical potential of silica, as determined by the calc-silicate assemblage, control the silicon content of garnet with titanium and/or zirconium merely filling the silicon deficiency?

To test the hypothesis that the zirconium content of garnet reflects that of the bulk rock and to determine the source of the zirconium, semiquantitative estimates of the concentration of zirconium in limestone, skarn, pyroxenite, gabbro and syenite were determined by optical emission spectroscopy (Table C-8). Concentrations of zirconium in garnet and skarn from the main contact traverse are plotted against distance from the pyroxenite contact in Figure 20. Although the bulk skarn data are characterized by a great deal of scatter, they do show an overall decrease from about 270 ppm Zr within 10 cm of the pyroxenite to about 60 ppm Zr in calcite-spurrite marble.  $ZrO_2$  in garnet shows a steady increase from about 2 to 22 weight percent across the same interval. Clearly the zirconium content of garnet

Figure 20. Weight percent  $ZrO_2$  in garnet from skarn and parts per million zirconium in bulk skarn plotted as a function of position in skarn, relative to contact with pyroxenite for the main contact traverse. Contact between skarn and marble is at 74 cm.



does not reflect that of the bulk rock. The gradient in Zr across the skarn indicates that a significant proportion of the zirconium in the skarn was metasomatically introduced from the gabbro. No mineral other than garnet contains significant concentrations of zirconium. To balance the high zirconium content of the rock with the low zirconium content of the garnet and vice versa, the modal proportion of garnet in skarn varies from about 2 volume percent in the wollastonite zone to less than 0.1 percent in the calcite-spurrite marble.

Comparison of the gradient of silicon content of garnet across the main contact traverse (Figure 18) with the gradient of silica content of the bulk skarn along the same traverse (Figure 23) shows a close and consistent correspondence between the number of atoms of silicon per formula unit of garnet and the concentration of silica in the rock in which it occurs. A similar relationship holds for the xenolith traverse (Figures 19 and 24). The stoichiometric calc-silicate phases that characterize each mineral assemblage also show a consistent relationship to the silica content of the skarn. The phase or phases present reflect the ratio of CaO to SiO<sub>2</sub> present in excess over combination with Al<sub>2</sub>O<sub>3</sub>, FeO and MgO to form melilite. In the model developed to illustrate the growth of the zoned calc-silicate nodules it was shown that reactions between stoichiometric calc-silicates at zone boundaries buffered the chemical potential of silica ( $\mu_{\text{SiO}_2}$ ) and that these equilibria controlled  $\mu_{\text{SiO}_2}$  within monomineralic zones. It is suggested that the calc-silicate phases play a similar role in the skarn. Equilibria controlling  $\mu_{\text{SiO}_2}$  may be more complex, however, due to the presence of melilite in which

aluminum may substitute for silicon by the coupled mechanism  $AlAl = (Mg, Fe)Si$ . It has been argued above that the composition of melilite is controlled by the bulk composition of the host limestone and magma involved in its genesis.

It is proposed that the gradient of the silicon deficiency in garnet across the zoned skarn reflects the gradient of the chemical potential of silica as controlled by the calc-silicate assemblages. Thus titanium and zirconium enter garnet to balance the silicon deficiency and to bring the sum of the tetravalent cations to 3.0. The occurrence of perovskite in nearly all assemblages with Ti-Zr garnet indicates that the local environment was saturated with titanium. The increase in the ratio of zirconium to titanium in garnet with decreasing silica content of the bulk rock suggests that garnet shows a preference of zirconium over titanium at low values of  $u_{SiO_2}$ .

To test the hypothesis that the silicon deficiency of garnet reflects the chemical potential of silica in the assemblage as controlled by the coexisting stoichiometric calc-silicate phases, garnet compositions plotted in terms of atomic Ca-Si-(Ti+Zr), joined by tie-lines with the coexisting calc-silicate minerals, are shown on Figures 21 and 22. If the silicon deficiency of garnet is a function  $u_{SiO_2}$ , which is controlled only by the stoichiometric calc-silicate phases in the assemblage, its value should be fixed in assemblages with two calc-silicate phases plus garnet and may vary in assemblages with one calc-silicate plus garnet. However, the silicon deficiency in a two-phase assemblage may only vary between the limits imposed by the three-phase assemblages on either side along the Ca-Si join.

Figure 21. Molecular proportion of calcium, silicon and zirconium + titanium in garnet from skarn of main contact traverse. Tie-lines join composition of garnet with coexisting calc-silicate phase or phases.

GARNET FROM SKARN  
CHRISTMAS MTS., TEXAS  
MAIN CONTACT

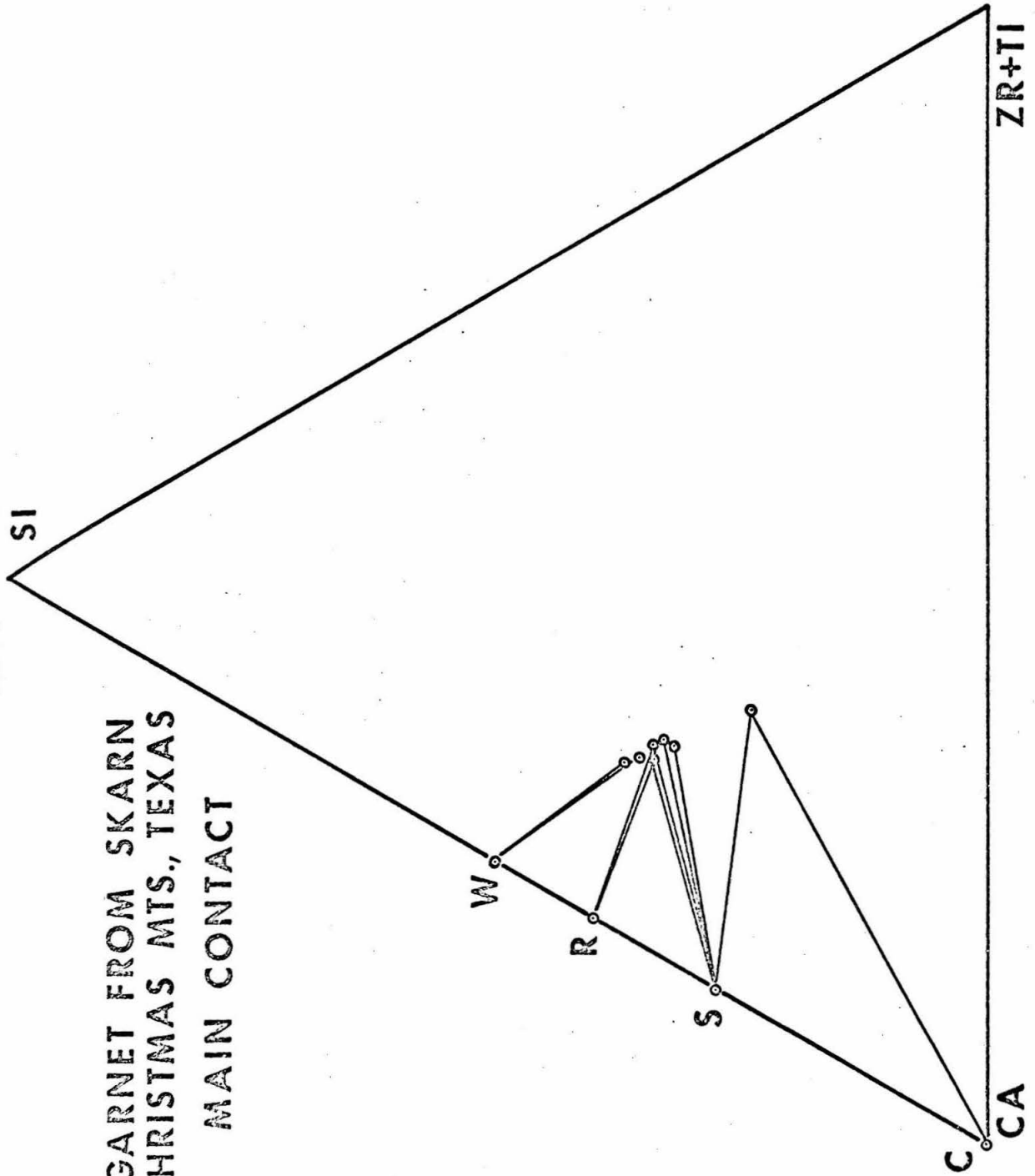
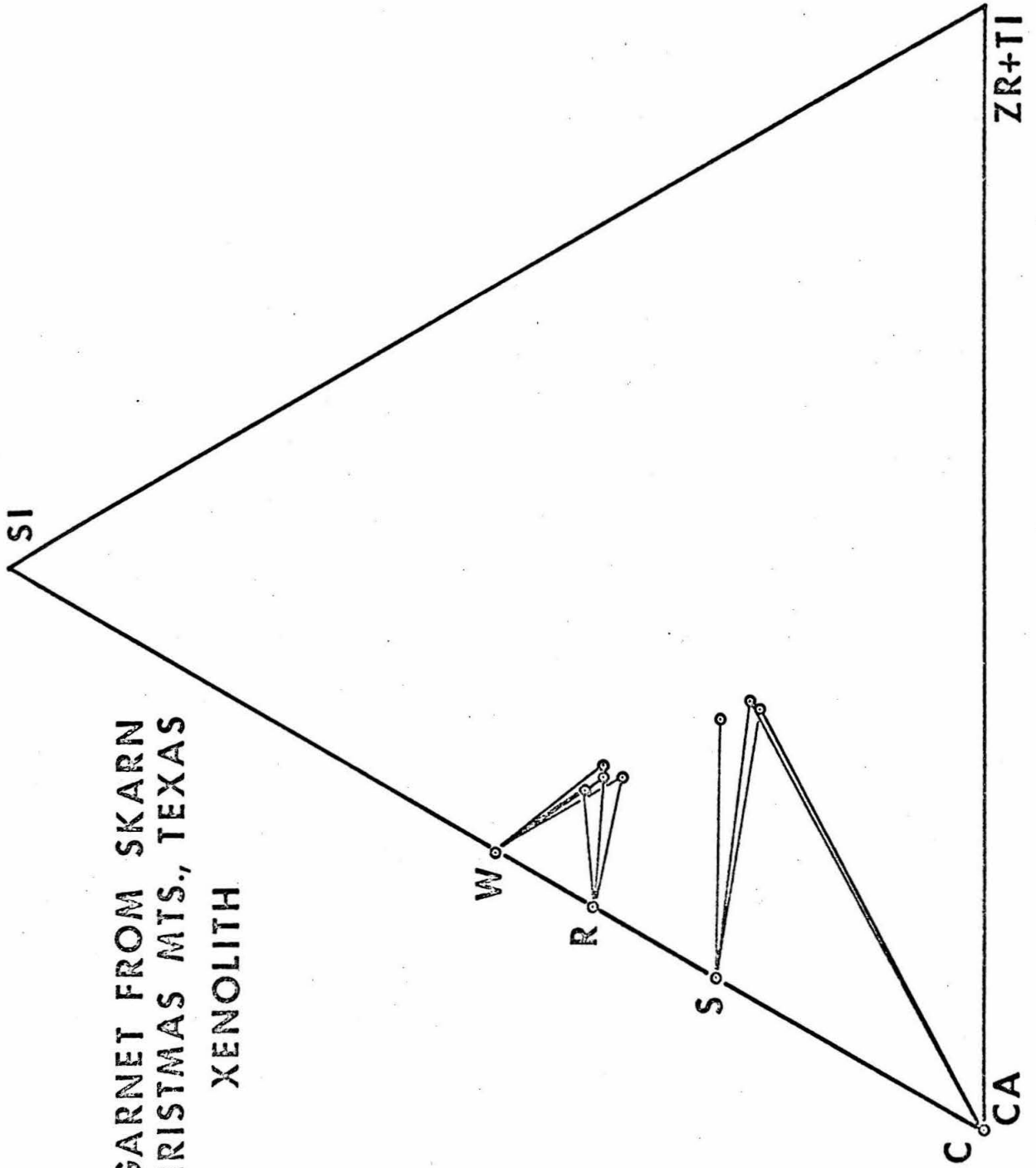


Figure 22. Molecular proportion of calcium, silicon and zirconium + titanium in garnet from skarn of xenolith traverse. Tie-lines join composition of garnet with coexisting calc-silicate phase or phases.

GARNET FROM SKARN  
CHRISTMAS MTS., TEXAS  
XENOLITH



Garnet-bearing assemblages from the main contact traverse fit the model quite well but those from the xenolith show a number of crossing tie-lines for assemblages with wollastonite and rankinite. Comparison of the gradients of aluminum and silicon in melilite across the wollastonite and wollastonite-rankinite zones of the xenolith shows that the ratio of Si to Al rapidly changes with distance across these zones, thus introducing an additional degree of freedom.

The limited range in silicon deficiency across the wollastonite and spurrite zones of the main contact traverse and the apparent step in the silicon deficiency at the boundary between the rankinite-spurrite and spurrite zones suggests that the gradient of  $\mu_{\text{SiO}_2}$  is relatively flat across the wollastonite and spurrite zones and that it steepens only near the zone boundaries. However, the utility of the silicon deficiency of garnet as a precise measure of  $\mu_{\text{SiO}_2}$  in local assemblages is limited by the large variation in the silicon deficiency within single garnet grains.

Gradients of the compositions of both melilite and garnet appear to be continuous across the zoned skarn, both in the xenolith and at the main contact. The lack of compositional discontinuities in the solid solutions at the boundaries of the calc-silicate zones indicates that the gradients of the chemical potentials of the transported species are continuous across zone boundaries. Thus, a necessary condition for the application of the principle of local equilibrium to the interpretation of the mineral assemblages in the zoned skarn is fulfilled (Thompson, 1959, p. 430). Because continuity of compositional

gradients in the solid solutions imply continuity of the gradients of the chemical potentials in the transport medium, Korzhinskii (1965, p. 198; 1968, p. 227; 1970, p. 114) has suggested that this is a useful criterion for the identification of diffusion as the mechanism of mass transport. Thus, although an aqueous fluid of magmatic origin may have passed outward through the skarn, there is no evidence that it played a significant role in the metasomatic development of the skarn.

#### Bulk Composition

Although composition-distance plots for diffusion without chemical reaction are smooth curves, those for systems involving chemical reaction may show discontinuities where reactions involve phases of fixed composition. The discontinuous gradients of bulk composition across the zoned calc-silicate nodules result from reaction between stoichiometric phases and consequent diffusion. Because the bulk composition of the rock can be controlled by mineral reactions, composition-distance plots can provide information about possible reactions leading to the present distribution of elements across the zoned skarn.

The chemical compositions of the analyzed skarn samples are plotted as a function of distance from the pyroxenite contact for the main contact traverse on Figure 23 and for the xenolith traverse on Figure 24. Composition-distance plots for both traverses are similar. The concentrations of silica and iron decrease monotonically from pyroxenite to marble while that of calcium increases across the same interval. The concentration of alumina rises to a broad maximum in the rankinite zone, then decreases toward the marble. The culmination of alumina can be

Figure 23. Weight percent of major oxides in skarn from main contact traverse plotted as a function of distance from contact with pyroxenite. Contact between skarn and marble is at 74 cm. Integrated bulk composition of the skarn was obtained by graphical integration of the area under the curve for each oxide. Mineral assemblage symbols as in Figure 1.

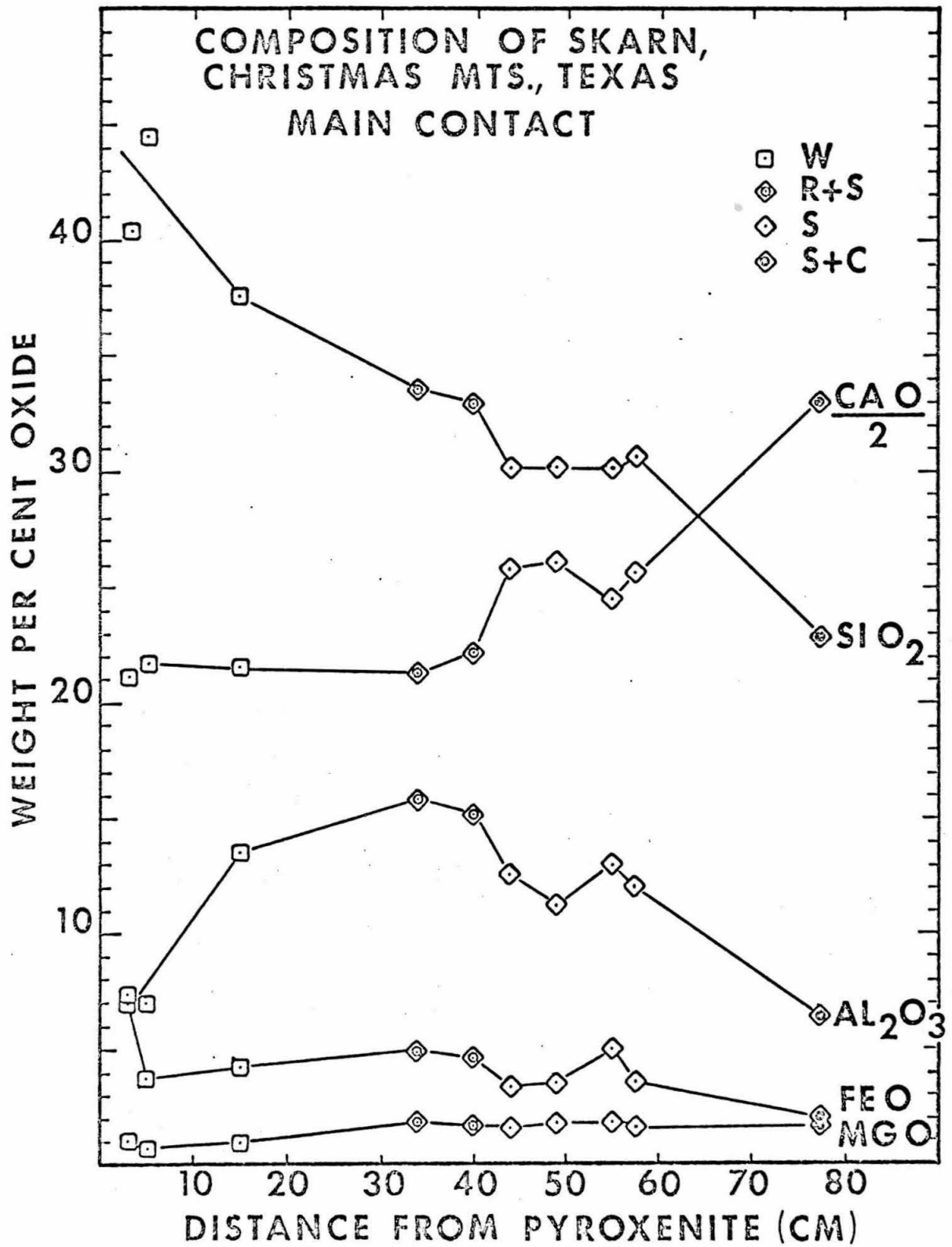
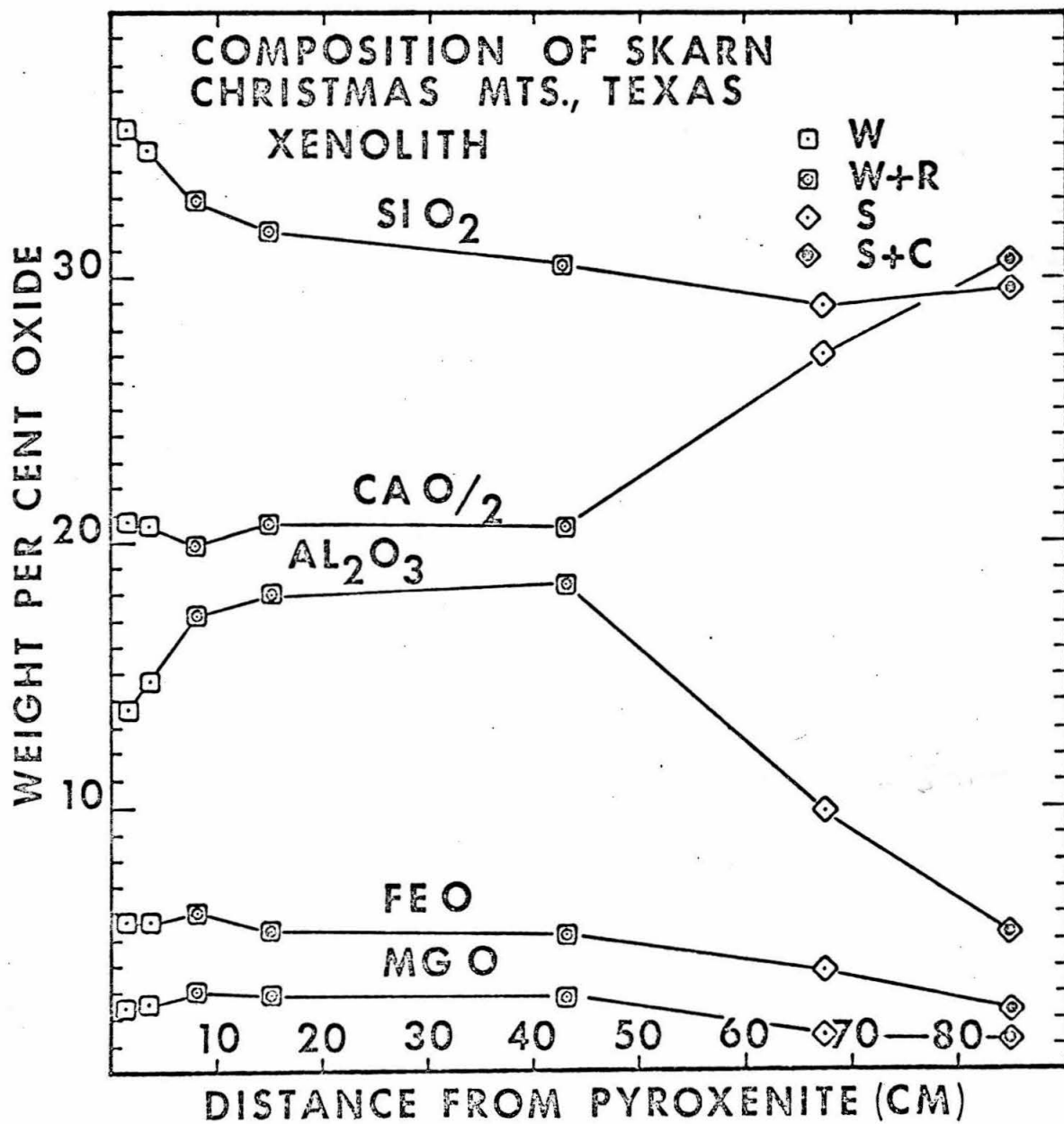


Figure 24. Weight percent of major oxides in skarn from xenolith traverse plotted as a function of distance from contact with pyroxenite. Contact between skarn and marble is at 86 cm. Integrated bulk composition of skarn was obtained by graphical integration of the area under the curve for each oxide. Mineral assemblage symbols as in Figure 1.

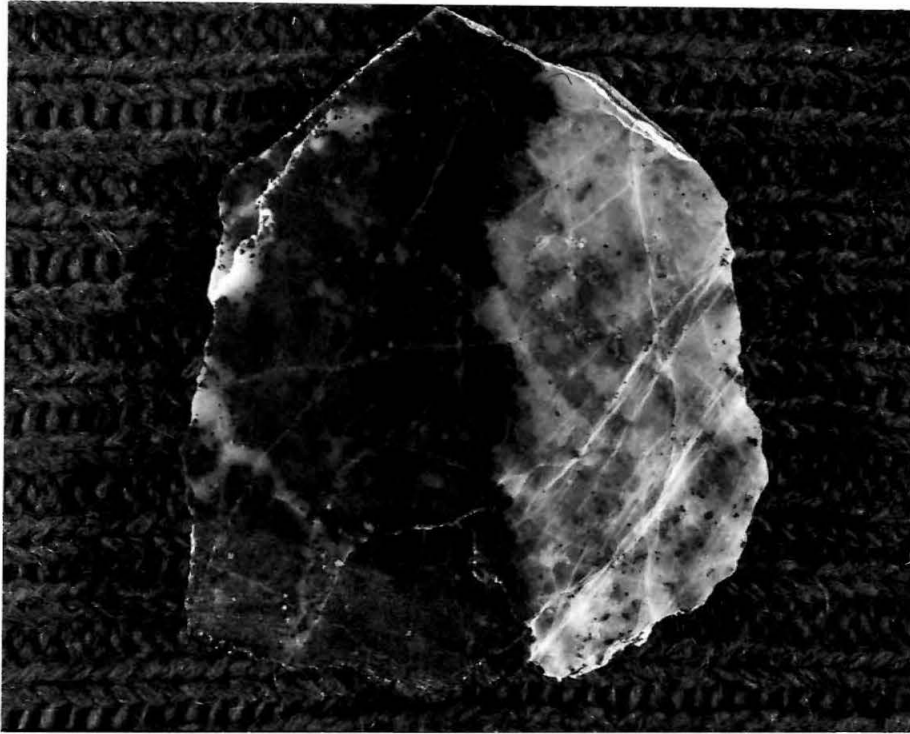


attributed primarily to variation in the modal abundance of melilite which reaches a maximum in this zone, and secondarily to the steep gradient in alumina content in idocrase and melilite across the wollastonite zone.

The sharp, planar contact between melilite-rich brown skarn and essentially melilite-free white skarn, which marks the outer limit of metasomatically introduced alumina, is not well developed on either of the sampled traverses. In the xenolith, the brown skarn-white skarn contact is a sharp front, but it has a very irregular, lobate form. The analyzed sample at 67 cm, which contains the contact, is a mixture of the two rock types. The development of calcite-spurrite-melilite skarn in beds of impure Sue Peaks limestone within 20 meters of the intrusive contact shows that there is sufficient alumina present to form melilite by isochemical metamorphism. There are two discontinuities in the modal proportion of melilite along the main contact traverse, both of which coincide with the boundaries of calc-silicate zones. The first, between 40 and 43 cm, involves a decrease from about 70 to 55 volume percent melilite at the contact between the rankinite-spurrite and spurrite skarn zones. These two transitions are reflected in sharp discontinuities in the gradients of calcium, silica and alumina. The second discontinuity, at 74 cm, coincides with the contact between spurrite skarn and spurrite-calcite marble. The modal proportion of melilite decreases from about 55 to 35 volume percent across this contact.

A sharp, planar contact between melilite-rich brown skarn and melilite-free white skarn, developed from relatively pure Del Carmen limestone at the intrusive contact, is shown in Plate 5. Analyses

Plate 5. Planar contact between brown melilite skarn and white spurrite skarn, sample CM-6-6M. Chemical analyses of melilite skarn and spurrite skarn from this sample are listed in Table C-7 (Appendix). Sample is 65 x 80 mm.



6-6MB and 6-6MA (Table C-7) are of melilite skarn and spurrite skarn from either side of the contact in the sample shown in Plate 5. The contact is characterized by major discontinuities in the concentrations of calcium, aluminum, magnesium and iron and probably represents the outer limit of metasomatic transport of these elements.

Melilite is the most abundant mineral in the skarn, hence the main features of the composition-distance plots result from changes in its modal abundance and chemical composition. The sharp discontinuity in the modal proportion of melilite at the brown skarn-white skarn contact probably is the result of a melilite-producing reaction between plagioclase and pyroxene of the gabbro and calcite. It will be shown below that the compositional range of the Sue Peaks Limestone overlaps those of calcite-spurrite-melilite skarn and spurrite-melilite skarn. The contact is 74 cm from the main-contact traverse and possibly represents an original sedimentary contact, sharpened by reaction and diffusion. The discontinuity at 40 to 43 cm may be interpreted as the outer limit of "metasomatic" melilite and corresponds to the brown skarn-white skarn contact in skarn developed from the Del Carmen and Santa Elena limestones.

Mineralogic boundaries between the calc-silicate zones are sharp. Although rankinite coexists with wollastonite in the xenolith, and with spurrite at the main contact, the second phase is not modally abundant. The sequence of calc-silicate zones across the skarn is analogous to the series of monomineralic zones of the calc-silicate nodules. This similarity suggests that the zonation is the result of a sequence of

TABLE C-2 (CONTINUED)  
 ELECTRON MICROPROBE ANALYSES OF MELILITE AND IDOCRASE FROM SKARN  
 CHRISTMAS MOUNTAINS, TEXAS

Sample Mineral	103-6A I	103-6B M	103-6B I	103-5 M	103-5 I	103-4 M	103-4 I
SiO <sub>2</sub>	32.25	32.13	30.33	30.87	29.08	29.66	28.29
TiO <sub>2</sub>	0.04	0.02	0.05	0.01	0.0	0.02	0.04
Al <sub>2</sub> O <sub>3</sub>	17.91	18.99	18.36	20.40	20.23	22.14	21.15
FeO	4.22	4.26	4.34	4.56	3.86	4.12	3.78
MnO	0.10	0.08	0.08	0.07	0.02	0.05	0.03
MgO	3.52	3.74	3.67	3.54	2.70	3.15	3.09
CaO	36.60	39.16	36.70	39.97	38.08	41.04	37.07
Na <sub>2</sub> O	0.02	0.58	0.01	0.18	0.02	0.24	0.07
TOTAL	94.66	98.98	93.54	99.59	93.99	100.42	93.52

FORMULA PROPORTION BASED ON CATION SUM = 5.0

Si 4+	1.59	1.50	1.51	1.44	1.44	1.37	1.40
Al 3+	1.04	1.05	1.08	1.12	1.18	1.40	1.24
Fe 2+	0.17	0.17	0.18	0.18	0.16	0.16	0.16
Mg 2+	0.26	0.26	0.27	0.25	0.20	0.22	0.23
Ca 2+	1.93	1.96	1.96	2.00	2.02	2.03	1.97
Na +	0.01	0.05	0.00	0.02	0.0	0.02	0.01
OXYGEN	7.11	7.00	7.05	6.99	7.03	6.96	7.02
N	5	5	4	6	2	6	2

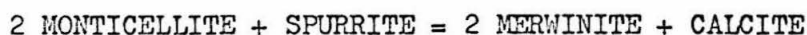
I = idocrase, M = melilite

to 1030°C (Figure 3, Chapter 4). The inferred presence of the facies type defined by the coexistence of rankinite + tilleyite in calc-silicate nodules in the aureole within 16 meters of the gabbro contact restricts the composition of the fluid phase in the vicinity of a growing nodule to one in which the mole fraction of CO<sub>2</sub> was greater than 0.6 (Figure 5, Chapter 4). The minimum temperature at 16 meters, at the peak of metamorphism, was that of the isobaric invariant point [C,L] on the T-X<sub>CO<sub>2</sub></sub> plane, 920°C at 325 bars and X<sub>CO<sub>2</sub></sub> = 0.6. Such direct evidence for the lower limits of temperature and fluid phase composition are not available for the skarn, but plausible estimates can be made based on information from the outer aureole. The minimum temperature in the skarn at the contact must have been greater than or equal to that at 16 meters, 920°C. The temperature at the contact must closely approach that of the magma because the set of mineral assemblages in the skarn at the main contact and in the xenolith define the same facies type. Simple heat conduction calculations show that the time required for the temperature at the center of a tabular, cylindrical or spherical limestone xenolith with a half-width or radius of one meter to rise to a value equal to that of the surrounding magma is of the order of a few years (Lovering, 1938; Carslaw and Jaeger, 1959, p. 102) while the time required for complete crystallization of the magma is of the order of thousands of years (Carslaw and Jaeger, 1959, p. 288-89). At the minimum possible contact temperature, 920°C, the facies type defined by the coexistence of rankinite + spurrite requires that the mole fraction of CO<sub>2</sub> has been greater than 0.2. Were the temperature higher, the ab-

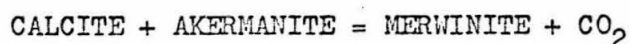
sence of larnite in the skarn requires that the fluid phase be correspondingly enriched in  $\text{CO}_2$ . The maximum temperature in the skarn did not exceed  $1030^\circ\text{C}$ , the high temperature stability limit of coexistence of rankinite + spurrite in the presence of pure  $\text{CO}_2$  at pressures of 335 to 355 bars.

Calcite, merwinite and melilite coexist in calc-silicate marble within 140 cm of the pyroxenite at the main contact and in the marble core of a large skarn xenolith in fine-grained gabbro located 75 meters W.N.W. of the xenolith from which the traverse samples were taken. Merwinite occurs as round, drop-like grains within subhedral prisms of melilite and as subhedral grains in contact with calcite. Within melilite, the modal proportion of merwinite ranges between 5 and 30 volume percent.

The pressure-temperature coordinates of two reactions which define the low temperature limit of coexistence of calcite + merwinite have been experimentally determined. The equilibrium temperature of the reaction.



is  $820^\circ\text{C}$  at 60 bars and is little effected by pressure (Walter, 1965). However, the equilibrium temperature of the decarbonation reaction



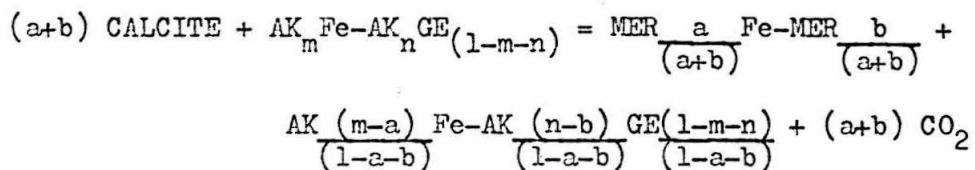
is strongly pressure dependent (Shmulovich, 1969). The decarbonation reaction lies within the stability field of tilleyite, just to the high pressure side of reaction (C,L,R,W) which defines the high pressure stability limit of spurrite. Within probable limits of experimental error, the two univariant reactions involving merwinite meet at an

invariant point within the spurrite field at 820°C and 70 bars (Walter, 1965, p. 69).

The presence of merwinite as inclusions in melilite suggests that the merwinite-forming reaction in the marble was similar to the reaction studied by Shmulovich (1969). However, the melilite in the skarn is a solid solution with 44 to 64 mole percent gehlenite. Although the coexistence of calcite + merwinite + melilite may represent divariant equilibrium in P-T-X<sub>CO<sub>2</sub></sub>, the three-phase assemblage may result from reaction of calcite with a melilite solid solution to form merwinite + gehlenite,

$$n \text{ CALCITE} + \text{AK}_n \text{GE}_{(1-n)} = n \text{ MERWINITE} + (1-n) \text{ GEHLINITE} + n \text{ CO}_2,$$

or by a similar reaction involving cation exchange of iron and magnesium between melilite and merwinite,



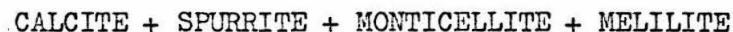
The ratio Fe/(Fe+Mg) in merwinite from marble is 0.1. If merwinite formed by either reaction involving melilite solid solution, both the aluminum content and the ratio Fe/(Fe+Mg) should be greater in melilite coexisting with calcite + merwinite than in melilite coexisting with calcite alone. The composition of melilite coexisting with calcite + merwinite (AK<sub>33</sub>Fe-AK<sub>08</sub>GE<sub>59</sub>, CM-8-7A) is essentially the same as that of melilite coexisting with calcite (AK<sub>33</sub>Fe-AK<sub>10</sub>GE<sub>57</sub>, CM-8-17). However, the modal proportion of merwinite inclusions in melilite in CM-8-7A is about 5 volume percent, suggesting that the amount of reaction was not great.

The experimentally determined curve for the decarbonation reaction involving calcite, akermanite and merwinite lies just within the stability field of tilleyite (Shmulovich, 1969). Because the merwinite-free assemblage calcite + spurrite + melilite occurs in marble between 140 and 2040 cm from the pyroxenite contact, while the same assemblage with merwinite is found in the interval 74 to 140 cm, the merwinite-forming reaction must lie within the stability field of spurrite. Due to the contribution of the entropy of mixing in melilite, equilibria involving calcite, melilite and merwinite will take place at higher temperatures than that involving calcite, akermanite and merwinite. For equilibrium between calcite, melilite of composition  $AK_{50}GE_{50}$  and merwinite, Shmulovich (1969) has computed an equilibrium temperature  $65^{\circ}C$  above that of the experimentally determined curve at 160 bars. Thus solid solution in melilite can displace the reaction curve into the spurrite field.

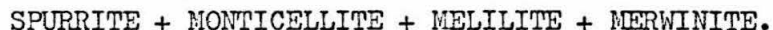
A striking feature of the set of mineral assemblages that make up the skarn is the absence of four-phase assemblages involving merwinite, melilite, rankinite and either wollastonite or spurrite. If temperatures were sufficiently high to allow reaction between calcite and melilite solid solutions of the compositional range found in skarn, 13 to 27 mole percent akermanite, the lack of merwinite in the skarn assemblages raises the possibility that calcite and melilite did not coexist during growth of the skarn. Two field observations suggest that this in fact may have been the case. In skarn developed from the relatively pure Del Carmen and Santa Elena limestones, the zone of melilite-

rich spurrite skarn is separated from marble by an essentially monomineralic zone of spurrite. All merwinite assemblages occur in impure marble, where they are the demonstrable result of essentially isochemical metamorphism. Thus the merwinite-producing reaction did not contribute to the metasomatic growth of the skarn.

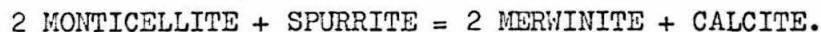
Merwinite occurs in impure marble in the core of the large skarn xenolith studied in detail. Sample CM-108 appears to be made up of two four-phase assemblages,



and



The assemblages are plotted on the simplified skarn tetrahedron on Figure 25. The bulk of the rock is made up of the calcite assemblage while the merwinite assemblage is restricted to localized patches in the marble. Merwinite is always separated from calcite by an optically-continuous rim of either monticellite or spurrite (Plate 6, Figure 1). Merwinite is never found as inclusions in melilite, although the two phases are found in mutual contact. The textural incompatibility of calcite and merwinite suggests that they are involved in the reaction.



Although the facies type defined by the two local four-phase assemblages is stable on the low temperature side of this reaction, vermicular intergrowths of spurrite and monticellite (Plate 6, Figure 2) suggest that the assemblages in CM-108 are the result of retrograde metamorphism of the assemblage

Figure 25. Perspective view of simplified skarn tetrahedron viewed normal to Ca-(Fe+Mg)-Si face, showing two four-phase assemblages involving spurrite, melilite and monticellite in sample CM-108.

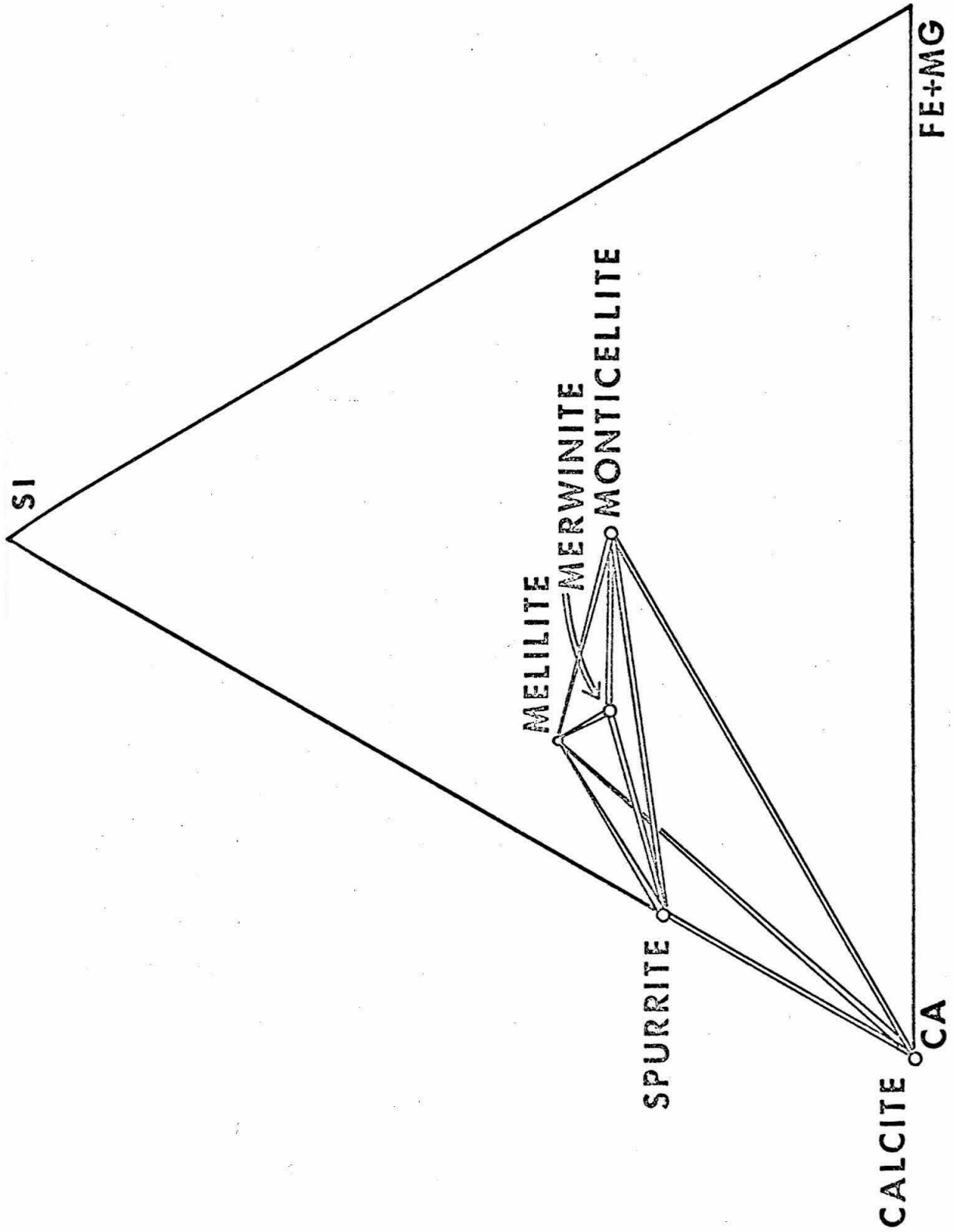
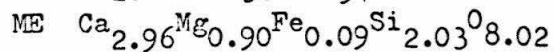
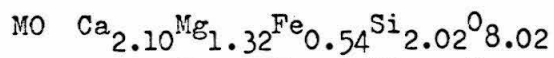


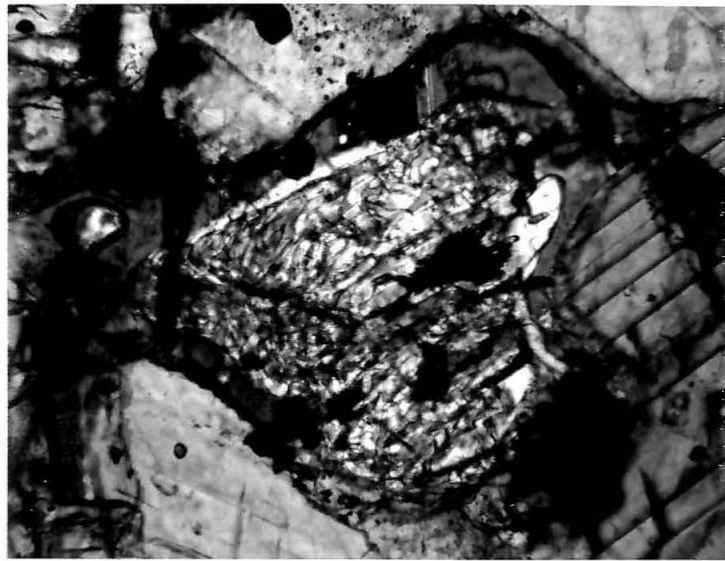
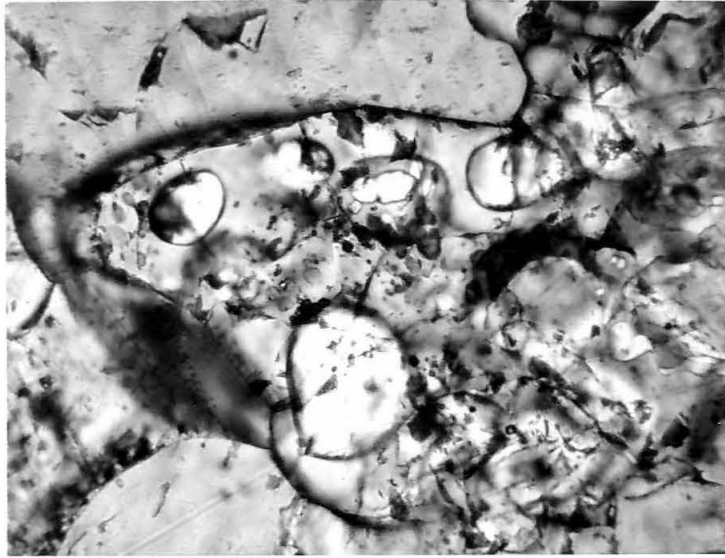
Plate 6. Products of the reaction MONTICELLITE +  
SPURRITE = MERWINITE + CALCITE

Figure 1. Round grains of merwinite enclosed by single grain of monticellite in calcite matrix, sample CM-108. Crossed nicols, field 0.36 x 0.47 mm.

Figure 2. Vermicular intergrowth of spurrite + monticellite separated from calcite by rim of spurrite, sample CM-108. Plane light, field 0.58 x 0.85 mm.

Mineral formulae of monticellite (MO) and merwinite (ME) from this sample are:





## CALCITE + SPURRITE + MELILITE + MERWINITE.

Although the equilibrium temperature of the reaction is insensitive to pressure ( $dP/dT = -90 \text{ bars}/^{\circ}\text{C}$ ), it is metastable in the presence of pure  $\text{CO}_2$  at pressures greater than that of the invariant point involving the phases calcite, spurrite, akermanite, monticellite, merwinite and  $\text{CO}_2$  at  $820^{\circ}\text{C}$  and 70 bars (Walter, 1965). The hydration of melilite to idocrase in the rim of the xenolith indicates the presence of an  $\text{H}_2\text{O}$ -rich fluid when temperature dropped below about  $700^{\circ}\text{C}$ . Because the invariant point involves decarbonation reactions, the pressure at which it occurs is a function of the mole fraction of  $\text{CO}_2$  in the fluid phase. The coordinates of the invariant point on an isobaric  $T-X_{\text{CO}_2}$  section can be determined by computation of the point of intersection of the decarbonation reaction studied by Shmulovich (1969) with the reaction studied by Walter (1965), using the methods described by Greenwood (1967) and Anderson (1970). At a pressure of 300 bars, the invariant point is at  $820^{\circ}\text{C}$  and  $X_{\text{CO}_2} = 0.2$ . The textural evidence that the mineral assemblages in CM-108 result from retrogradation of the assemblage calcite + merwinite rigorously indicates that the temperature in the core of the xenolith exceeded  $820^{\circ}\text{C}$ , regardless of the composition of the fluid present during the peak of metamorphism.

Skarn rimming a 15 to 20 meter wide septum of marble between coarse-grained and fine-grained gabbro contains two four-phase assemblages involving larnite and phase "T",

## RANKINITE + LARNITE + PHASE "T" + MELILITE

and

LARNITE + SPURRITE + PHASE "T" + MELILITE,

which result from metamorphism under the highest temperatures recorded in the skarn. Both assemblages are plotted on the simplified skarn tetrahedron on Figure 26. The lower limit of stability of phase "T" is defined by the reaction



which should have a very steep slope on a P-T diagram. The coexistence of larnite + phase "T" indicates that the temperature exceeded 980°C (Schlaudt and Roy, 1966). If pure CO<sub>2</sub> were present, the coexistence of spurrite + larnite requires that the temperature have been greater than 1030°C. If metamorphism took place near the lower limit of temperature, the mole fraction of CO<sub>2</sub> in the fluid phase cannot have exceeded 0.6. The high temperature assemblages recorded in the skarn from the septum are the result of polymetamorphism and intrusion into marble preheated by the first intrusion.

#### BULK COMPOSITION OF LIMESTONE AND SKARN

##### Integrated Bulk Composition of Skarn

The bulk chemical composition of a series of skarn zones can be computed by graphical integration of the area under the curves on a composition-distance plot. The integrated bulk compositions of skarn from the main contact and xenolith traverses, computed by graphical integration of the curves for each oxide on Figures 23 and 24 are listed in Table 5. The bulk densities were determined by graphical integration of density-distance plots for each traverse. The integrated compositions

Figure 26. Perspective view of simplified skarn tetrahedron viewed normal to Ca-(Fe+Mg)-Si face, showing two four-phase assemblages involving larnite, melilite and phase "T" in sample CM-273-5.

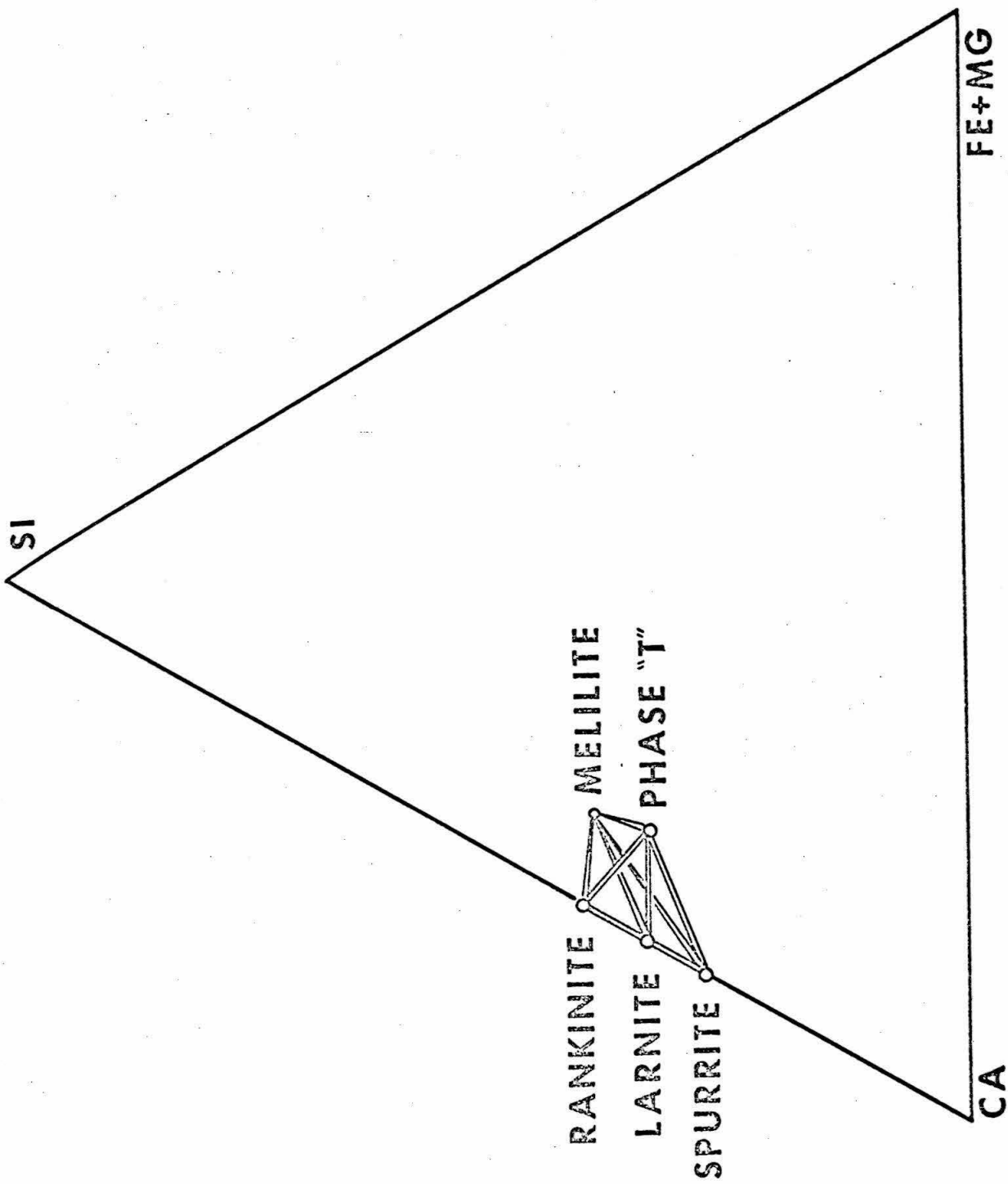


TABLE 5

---

INTEGRATED BULK COMPOSITION OF SKARN  
CHRISTMAS MOUNTAINS, TEXAS

---

	<u>Main Contact</u>	<u>Xenolith</u>
SiO <sub>2</sub>	33.4	30.5
TiO <sub>2</sub>	0.7	1.0
Al <sub>2</sub> O <sub>3</sub>	12.1	14.3
FeO	3.9	4.6
MgO	1.3	2.3
CaO	47.6	46.5
Na <sub>2</sub> O	0.3	0.2
TOTAL	99.3	99.4
<hr/>		
Density	3.07 gm/cm <sup>3</sup>	3.10 gm/cm <sup>3</sup>

---

of the two skarns are strikingly similar, despite the fact that the compositions of the Sue Peaks and Santa Elena limestones and of the porphyritic and fine-grained gabbros involved in their genesis are very different. The integrated compositions of both skarns plot within the rankinite-spurrite-melilite field in the simplified skarn tetrahedron. Thus, in addition to the paragenetic evidence that the conditions of metamorphism were essentially the same in the xenolith and at the main contact, the similarity of metasomatic products suggests that the mechanics of growth of the two skarns were essentially the same.

#### Bulk Composition of Limestone

Electron microprobe analyses of three samples of Sue Peaks limestone and of two samples of skarn derived from isochemical metamorphism of Sue Peaks Limestone are listed in Table C-9. Samples CM-336-1D and CM-336-1L represent the dark-gray, tan weathering and the light-gray, rusty-brown weathering lithologic components of the Sue Peaks limestone, respectively. The analysis of the dark-gray fraction of the Sue Peaks limestone plots within the calcite-spurrite-melilite field of the simplified skarn tetrahedron while those of the light-gray fraction plot near the spurrite-melilite join. Compositions of skarn from the spurrite zone of the main contact traverse overlap those of the unmetamorphosed Sue Peaks limestone.

Semiquantitative spectrographic analyses of a sample of Santa Elena limestone and of Del Carmen marble are listed in Table C-9. Samples CM-336-1D and CM-336-1L, analyzed by electron microprobe, were used as standards. Although the analyses of two samples do not provide adequate

information about the range of composition of the massive limestones, they do indicate very low initial concentrations of iron, alumina and silica.

#### GROWTH MODEL

##### The Reaction-Diffusion Model

Mineralogic zones in skarn at the contact between pyroxenite and marble truncate bedding in the marble. Thus, although the skarn mineral assemblages can be produced by isochemical metamorphism of impure limestone, skarn at the intrusive contact is the result of metasomatic introduction of material from the gabbro. The compatibility of mineral assemblages of adjacent skarn zones and the apparent continuity of the gradients of composition of melilite and garnet across the zoned skarn show that the principle of local equilibrium is applicable at each point along a traverse across the skarn and that the gradients of the chemical potentials of the transported species are continuous functions across zone boundaries. Continuity of the chemical potential gradients is a necessary condition for mass transport by diffusion. Note that mass transport by filtration of a flowing fluid (infiltration metasomatism) results in discontinuities in the gradients of the chemical potentials at zone boundaries which are manifested as discontinuities in the compositional gradients of the solid solutions and incompatibility of mineral assemblages of adjacent zones.

Any model for mass transport in the genesis of the skarn must account for the "special" compositions of the skarn mineral zones. The similarity of the sequence of skarn zones, characterized by stoichiometric

calc-silicate phases, to the monomineralic zones of the calc-silicate nodules suggests that the reaction-diffusion model used to describe growth of the nodules may be applicable to the metasomatic growth of the skarn. Because mass transport involves diffusion down chemical potential gradients produced by reactions to form specific mineral assemblages, it is the mineral reactions, not the relative diffusion rates of the various chemical species that exercise primary control of the composition of the mineral zones. Metasomatic growth of the skarn by the reaction-diffusion model must involve reactions to produce a zone of melilite plus wollastonite, separating calcite from the igneous reactants. Note that a reaction which produces wollastonite will suffice to generate all other calc-silicate zones because wollastonite and calcite will react to form spurrite which in turn will react with wollastonite to form rankinite. In order to utilize the reaction-diffusion model, the identity of the initial phases involved in reactions leading to the metasomatic growth of the skarn must be determined.

The sequence of lithologies developed across the intrusive contact is gabbro, pyroxenite, skarn, marble. The pyroxenite is magmatic in origin, resulting from the direct interaction of gabbroic magma with limestone and, although cumulate in origin, it existed in a mobile state, capable of flow and intrusion. Possible reactions leading to skarn formation may have involved solid limestone and either gabbroic magma or pyroxenite. The contact between pyroxenite and skarn is sharp, with little evidence for extensive reaction between the two. There is, however, a zone of skarn at the contact, 1 to 5 cm in width, in which the relict outlines of euhedral clinopyroxene and sphene, characteris-

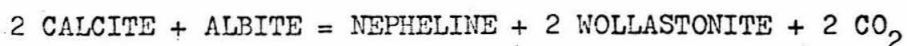
tic of the pyroxenite, are preserved in aggregates of idocrase + andradite + wollastonite and andradite + perovskite, respectively. Apatite, a characterizing accessory mineral of the pyroxenite is found in skarn only within the narrow zone at the contact with the relict pyroxenite texture, thus indicating very limited reaction between skarn and solid pyroxenite. On the basis of field and textural relationships at the intrusive contact it is suggested that skarn is the result of direct reaction between gabbroic magma and solid limestone and that the pyroxenite represents an accumulation of clinopyroxene precipitated in response to reaction between magma and limestone.

Reaction between gabbroic magma and limestone involves two processes, (1) decarbonation reactions between calcite and magma and/or crystals in equilibrium with magma, and (2) crystallization of phases with which the magma is saturated, to supply energy for the endothermic decarbonation reactions. Because the chemical potential of a component is equal in all phases in mutual equilibrium, its value is a characteristic of the system, not of the phases or their physical states. Thus, to describe reaction between gabbroic magma and limestone, reactions may be written between calcite and minerals that may crystallize from the magma, but the actual phases participating in the reaction may be either the magma or the solids in equilibrium with it. Products of a decarbonation reaction may (1) remain in solution in the magma, (2) crystallize from the magma, but remain suspended in it, or (3) recrystallize in the solid state within the carbonate of the wallrock or xenolith involved in the reaction. The only constraint imposed by the condition that the

phases be in equilibrium is that the chemical potential of each component be uniform throughout the system.

Gabbros of the Christmas Mountains complex are characterized by 60 to 70 volume percent plagioclase and 20 to 30 volume percent clinopyroxene. Although there is no direct evidence for determination of possible solidus phases at the time of intrusion, alkali gabbro at chilled contacts of laccoliths and sills in the Big Bend Region commonly have phenocrysts of plagioclase and more rarely, clinopyroxene as well. It is probable that the gabbroic magmas in the Christmas Mountains were saturated with both plagioclase and clinopyroxene at the time of emplacement. To test the model for development of the skarn and pyroxenite by reaction between gabbroic magma and limestone, we may begin by writing decarbonation reactions between calcite and plagioclase and between calcite and clinopyroxene and compare the product phases with those that make up the pyroxenite and skarn.

Possible decarbonation reactions between calcite and the end-members of the plagioclase solid solution series are



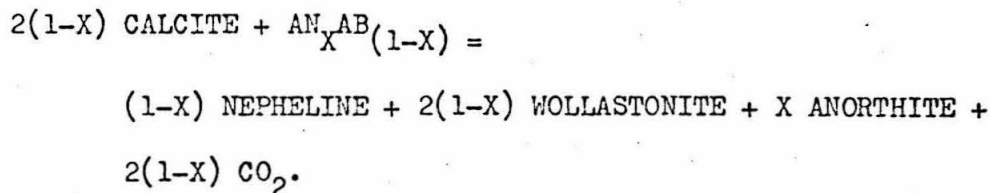
and



These may be combined into a general reaction between plagioclase and calcite



The breakdown of plagioclase may proceed in steps, however, with the albite component breaking down before anorthite by the reaction

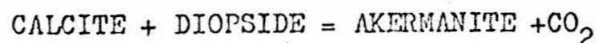


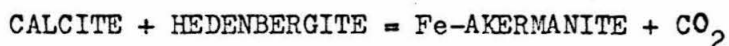
Anorthite may subsequently react with calcite to form gehlenite + wollastonite by the reaction above, but the rare occurrence of anorthite in pyroxenite suggest that it, as well as nepheline and wollastonite go into solution in the melt. Although exceedingly rare in pyroxenite, plagioclase has two modes of occurrence in pyroxenite with distinctive textures and compositions. The most widespread mode of occurrence of plagioclase is as isolated single crystals, with corroded margins, that are completely enveloped by large, euhedral grains of nepheline. This textural relationship suggests that plagioclase was involved in a resorption reaction with the magma. Compositions of plagioclase in this paragenesis overlap those of plagioclase from the gabbro ( $\text{AN}_{30}\text{-AN}_{70}$ ). Anorthite ( $\text{AN}_{80}\text{-AN}_{96}$ ) occurs locally in the assemblage anorthite + wollastonite + nepheline + clinopyroxene in a thin (< 1 cm), discontinuous zone separating nepheline pyroxenite from skarn. Individual grains of anorthite do not show any evidence for reaction. Although it is a product of each of the hypothetical reactions between calcite and plagioclase, wollastonite is restricted in occurrence to a few localities where it is found in pyroxenite within 30 cm of skarn. In

nepheline pyroxenite, wollastonite invariably occurs as elongate bladed crystals which have a skeletal habit with rounded margins, suggestive of reaction with magma or the enveloping nepheline.

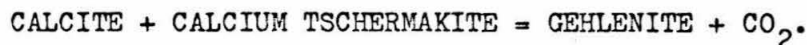
The products of the reaction of anorthite with calcite are simple analogues of the dominant mineral phases of the skarn, melilite and a stoichiometric calc-silicate. As will be shown below, the akermanite and iron akermanite components of the melilite solid solution can be produced by reaction between clinopyroxene and calcite. Although melilite and wollastonite are minerals characteristic of the skarn, nepheline is the dominant alkali-aluminosilicate phase of the pyroxenite. Its textural relationships to euhedral clinopyroxene and the occurrence of dikes of calcium-rich nepheline syenite intrusive into pyroxenite and skarn suggest that nepheline remains in solution in the magma and crystallizes late in the solidification of the pyroxenite. The corroded outlines of individual grains of plagioclase and wollastonite may be interpreted as due to partial resorption by the magma. Thus, initial reaction between gabbroic magma and limestone produced a "desilicated" liquid capable of crystallizing nepheline, anorthite, wollastonite and clinopyroxene. The melt is desilicated in that the ratio of silicon to other cations is less than that in the original magma. This is the result of solution of CaO and does not necessarily imply selective transport of silicon out of the local system.

Possible decarbonation reactions involving calcite and clinopyroxene are

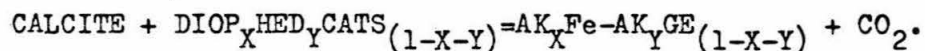




and



A combined reaction between calcite and a clinopyroxene solid solution may be written



At 430 bars, the first reaction runs to the right at 890°C in the presence of pure CO<sub>2</sub> (Walter, 1963). Although the contribution of calcium tschermakite to the total gehlenite content of the melilite in the skarn is probably small compared to that of plagioclase, clinopyroxene is the main source of iron and magnesium. Thus the ratio of Fe/(Fe+Mg) of melilite in skarn should be equal to that of the clinopyroxene involved in the decarbonation reaction.

Although melilite and clinopyroxene are mutually compatible in the absence of calcite, clinopyroxene is never found in skarn and melilite is never found in either pyroxenite or in any of its alkali-rich differentiates. Although plagioclase shows textural evidence for reaction with magma, clinopyroxene in pyroxenite shows no evidence for reaction either with magma or with any solid phase. It is nearly always euhedral and, where zoning can be distinguished optically, zone boundaries are parallel to the faces of the crystal. Any decarbonation reaction involving clinopyroxene cannot have involved the solid clinopyroxene in the nepheline pyroxenite. In fact, to obtain energy necessary for the solution reactions between magma and limestone to take place, clinopyroxene probably was crystallized from the melt.

The highly irregular modal distribution of clinopyroxene in pyroxenite suggests that pyroxenite represents a crystal mesh of euhedral clinopyroxenes "cemented" together by a late-crystallizing alkali-rich residual magma of nepheline syenite composition. Decarbonation reactions written between calcite and end-member molecules of plagioclase and clinopyroxene are endothermic with reaction enthalpies of 20 to 30 kilocalories per mole of calcite at 1300°K (computed from thermochemical data of Robie and Waldbaum, 1968). The energy required for the decarbonation reactions involving magma and calcite can be supplied by crystallization of the phases with which the magma is saturated, thus liberating the enthalpy of fusion (Bowen, 1928, p. 175-91). Clinopyroxene concentrated in the pyroxenite was probably crystallized in response to reaction between magma and carbonate. The enthalpy of fusion of diopside, 24.3 kcal/mole (Bowen, 1928, p. 178), is comparable in magnitude to the enthalpies of the decarbonation reactions, but opposite in sign when diopside crystallizes from a melt. Thus for each mole of CO<sub>2</sub> evolved by reaction between calcite and magma, approximately one mole of clinopyroxene was crystallized to supply the energy necessary for the endothermic decarbonation reaction.

The melilite calc-silicate skarn forms a reaction rim separating chemically incompatible gabbroic magma and limestone. A crucial question in the genesis of the skarn is that of the time of formation of the reaction rim relative to the time of complete crystallization of the pyroxenite. The scalloped contact between pyroxenite and skarn is suggestive of extensive solution of wallrock by magma. Because the

mineral assemblages of the nepheline pyroxenite and the skarn are compatible, reaction must have involved limestone, not skarn. Because the energy necessary for endothermic reaction between magma and limestone is provided by crystallization of the "heat equivalent" of clinopyroxene, the amount of solution reaction is limited by the concentration of potential clinopyroxene in the original magma plus that taken into solution from the carbonate. It is thus likely that a significant amount of pyroxenite was crystallized before formation of the zone of melilite-wollastonite skarn. Where impure limestone, such as that of the Sue Peaks Formation, is involved, melilite may form by isochemical recrystallization. In this case, the melilite reaction rim is formed at the outset and magmatic reaction consists of selective solution of calcite.

Once a zone of melilite-wollastonite skarn is formed between limestone and either anorthite-rich pyroxenite or desilicated gabbroic magma, the skarn will grow by reactions at its contacts so long as anorthite and/or clinopyroxene are available either in the melt or as solid phases. The chemical potential of aluminum is controlled in the melilite skarn by equilibria between anorthite, wollastonite and melilite at the pyroxenite contact and between calcite and melilite at the marble contact. Similarly, equilibria between clinopyroxene + melilite and either calcite + melilite or spurrite + melilite control the chemical potentials of iron and magnesium. Equilibria between wollastonite + rankinite, rankinite + spurrite and spurrite + calcite exercise primary control over the chemical potentials of calcium and silicon as did similar equilibria in the calc-silicate nodules.

The skarn consists essentially of a zone of melilite superimposed on a series of mineral zones defined by the presence of a stoichiometric calc-silicate mineral. The "special" bulk compositions of each of the skarn zones are the direct result of the specific mineral reactions between gabbroic magma and limestone. Reaction between calcite and clinopyroxene of a wide range of composition will produce a single solid phase, melilite. Similarly, reaction between calcite and plagioclase will produce melilite + wollastonite + nepheline. Because melilite is capable of extensive solid solution of iron, magnesium and aluminum, it is the stable reaction product for a wide range of mixtures of plagioclase, clinopyroxene and calcite. At the temperature of reaction between magma and limestone, wollastonite and calcite are incompatible. The calc-silicate zones result from reaction between calcite and wollastonite to form spurrite which in turn reacted with wollastonite to form rankinite. Thus the calc-silicates in each zone are compatible with those of the adjacent zones at each of the zone boundaries.

Because melilite is formed by reaction involving clinopyroxene and plagioclase, its composition should reflect the ratio of  $Fe/(Fe+Mg)$  of clinopyroxene in pyroxenite and the overall ratio of clinopyroxene to anorthite in the desilicated gabbroic magma. The ratio of  $Fe/(Fe+Mg)$  of clinopyroxene from pyroxenite surrounding the large skarn xenolith (CM-111B) ranges from 0.4 to 0.6. The ratio of  $Fe/(Fe+Mg)$  in melilite from wollastonite, wollastonite-rankinite and spurrite skarn from the xenolith is uniform and equal to 0.4. The ratio of  $Fe/(Fe+Mg)$  in melilite from skarn of the main contact traverse shows a continuous

variation from 0.7 at the pyroxenite contact to 0.2 in marble. Although most clinopyroxene in the adjacent pyroxenite is iron-rich ( $\text{Fe}/(\text{Fe}+\text{Mg}) = 0.6$ ), the ratio of  $\text{Fe}/(\text{Fe}+\text{Mg})$  of zoned crystals ranges from 0.2 in the core to 0.6 on the rim. The progressive iron enrichment of melilite as the pyroxenite contact is approached closely matches the zoning in clinopyroxene from core to rim, indicating that melilite continuously re-equilibrated with the composition of the outermost zone of the clinopyroxene during growth of the skarn and simultaneous crystallization of the nepheline pyroxenite. The aluminum content of idocrase, pseudomorphic after melilite, is similar in skarn at the pyroxenite contact from both traverses. However, while the gradient of aluminum in melilite and idocrase across the xenolith has a uniform slope, the slope of the gradient of aluminum in melilite and idocrase is quite steep within 15 cm of the pyroxenite contact on the main contact traverse. The progressive enrichment of silicon over aluminum in melilite and idocrase as the pyroxenite contact is approached may be the result of the elimination of anorthite from pyroxenite by reaction with calcite to form gehlenite, so that in the late stages of skarn growth, the composition of melilite is dominated by the composition of clinopyroxene.

#### Mass Balance Calculations

The relative gains and losses of material in the metasomatic development of skarn can be computed from the integrated composition of the skarn and the initial composition of the limestone. In order to compute the magnitude of the gains and losses of material in the metasomatic growth to the skarn, a specific reference state of the system

must be chosen and all gains and losses computed relative to this reference state (Thompson, 1959, p. 428-29). Possible reference states are a constant volume of rock or a fixed mass of CaO. Relative gains and losses are computed by subtraction of the mass of each oxide in the limestone from the mass of the same oxide in the skarn.

Mass balance calculations for growth of the skarn from limestone have been made by computing gains and losses relative to a fixed volume of limestone, set equal to a prism of rock  $1 \text{ cm}^2$  in cross-section with a length equal to the thickness of the skarn (Table 6), and relative to a fixed mass of CaO (Table 7). Mass balance calculations have been made using both lithologic components of the Sue Peaks Limestone to outline the range of possible exchanges in genesis of the skarn at the main contact.

The magnitude of the gains and losses for each skarn-limestone combination are similar for both models. As might have been expected, the exchanges are greater for conversion of the relatively pure Santa Elena Limestone to skarn than for conversion of the silica- and alumina-rich Sue Peaks Limestone to skarn. Despite the differences in initial limestone composition, both skarns require substantial additions of silicon, aluminum, iron and titanium. There is an excess of magnesium and sodium in Sue Peaks Limestone over that in skarn, but these elements were added to the Santa Elena Limestone. Note that had the more magnesian Del Carmen marble been used in the calculation, there would have been an excess of magnesium.

TABLE 6

---

 MASS BALANCE CALCULATION FOR GROWTH OF SKARN
 

---

## CONSTANT VOLUME MODEL

	Main Contact Traverse		Xenolith Traverse	
Width of Skarn	74	cm <sup>3</sup>	86	cm <sup>3</sup>
Volume Element	74	cm <sup>3</sup>	86	cm <sup>3</sup>
Density of Skarn	3.07	gm/cm <sup>3</sup>	3.10	gm/cm <sup>3</sup>
Mass of Skarn	227.2	gm	266.6	gm
Density of Limestone	2.7	gm/cm <sup>3</sup>	2.7	gm/cm <sup>3</sup>
Mass of Limestone	199.8	gm	232.20	gm
Net Change in Mass	+27.4	gm	+34.4	gm

---

	WT%	MASS (gm)	WT%	MASS (gm)	ΔMASS (gm)
--	-----	-----------	-----	-----------	------------

---

## MAIN CONTACT TRAVERSE

	Skarn	Limestone	336-1L		
SiO <sub>2</sub>	33.6	76.3	31.5	62.9	+13.4
TiO <sub>2</sub>	0.7	1.6	0.4	0.8	+ 0.8
Al <sub>2</sub> O <sub>3</sub>	12.2	27.7	11.0	22.0	+ 5.7
FeO	3.9	8.9	2.6	5.2	+ 3.7
MgO	1.3	2.9	3.3	6.6	- 3.7
CaO	48.0	109.1	50.8	101.5	+ 7.6
Na <sub>2</sub> O	0.3	0.7	0.4	0.8	- 0.1
TOTAL	100.0	227.2	100.0	199.8	+27.4

---

TABLE 6 (CONTINUED)

MASS BALANCE CALCULATION FOR GROWTH OF SKARN					
CONSTANT VOLUME MODEL					
	WT%	MASS (gm)	WT%	MASS (gm)	$\Delta$ MASS (gm)
MAIN CONTACT TRAVERSE					
	Skarn		Limestone	336-1D	
SiO <sub>2</sub>	33.6	76.3	23.5	47.1	+29.2
TiO <sub>2</sub>	0.7	1.6	0.3	0.6	+ 1.0
Al <sub>2</sub> O <sub>3</sub>	12.2	27.7	9.0	18.0	+ 9.7
FeO	3.9	8.9	2.0	4.0	+ 4.9
MgO	1.3	2.9	2.0	4.0	- 1.1
CaO	48.0	109.1	62.8	125.3	-16.2
Na <sub>2</sub> O	0.3	0.7	0.4	0.8	- 0.1
TOTAL	100.0	227.2	100.0	199.8	+27.4
XENOLITH TRAVERSE					
	Skarn		Limestone	335-2	
SiO <sub>2</sub>	30.7	81.8	7.1	16.5	+65.3
TiO <sub>2</sub>	1.0	2.7	0	0	+ 2.7
Al <sub>2</sub> O <sub>3</sub>	14.4	38.4	1.4	3.2	+35.2
FeO	4.6	12.3	0.1	0.2	+12.1
MgO	2.3	6.1	2.4	5.6	+ 0.5
CaO	46.8	124.8	89.0	206.7	-81.9
Na <sub>2</sub> O	0.2	0.5	0	0	+ 0.5
TOTAL	100.0	266.6	100.0	232.2	+34.4

TABLE 7

MASS BALANCE CALCULATION FOR GROWTH OF SKARN					
FIXED MASS OF CaO MODEL					
	WT%	MASS (gm)	WT%	MASS (gm)	Δ MASS (gm)
MAIN CONTACT TRAVERSE					
	SKARN		LIMESTONE		336-1L
SiO <sub>2</sub>	33.6	70.0	31.5	62.0	+ 8.0
TiO <sub>2</sub>	0.7	1.5	0.4	0.8	+ 0.7
Al <sub>2</sub> O <sub>3</sub>	12.2	25.4	11.0	21.7	+ 3.7
FeO	3.9	8.1	2.6	5.1	+ 3.0
MgO	1.3	2.7	3.3	6.5	- 3.8
CaO	48.0	100.0	50.8	100.0	0
Na <sub>2</sub> O	0.3	0.6	0.4	0.8	- 0.2
TOTAL	100.0	208.3	100.0	196.9	+11.4
	SKARN		LIMESTONE		336-1D
SiO <sub>2</sub>	33.6	70.0	23.5	36.4	+33.6
TiO <sub>2</sub>	0.7	1.5	0.3	0.5	+ 1.0
Al <sub>2</sub> O <sub>3</sub>	12.2	25.4	9.0	14.3	+11.1
FeO	3.9	8.1	2.0	3.2	+ 4.9
MgO	1.3	2.7	2.0	3.2	- 0.5
CaO	48.0	100.0	62.8	100.0	0
Na <sub>2</sub> O	0.3	0.6	0.4	0.6	0
TOTAL	100.0	208.3	100.0	158.2	+50.1
XENOLITH TRAVERSE					
	SKARN		LIMESTONE		335-2
SiO <sub>2</sub>	30.5	65.6	7.1	8.0	+57.6
TiO <sub>2</sub>	1.0	2.2	0	0	+ 2.2
Al <sub>2</sub> O <sub>3</sub>	14.3	30.8	1.4	1.6	+29.2
FeO	4.6	9.9	0.1	0.1	+ 9.8
MgO	2.3	5.0	2.4	2.7	+ 2.3
CaO	46.5	100.0	89.0	100.0	0
Na <sub>2</sub> O	0.2	0.4	0	0	+ 0.4
TOTAL	100.0	213.9	100.0	112.4	+101.5

Computation of the chemical exchanges necessary to convert limestone to skarn are useful estimating the scale of interaction between carbonate and magma or solid rock, but they provide little information about the specific rocks or magmas involved.

If the bulk composition of the skarn is the result of reaction between limestone and gabbroic magma, it should be possible to approximate the integrated bulk composition of the skarn by a linear combination of the compositions of the magma and limestone involved. Although the phaneritic gabbros analyzed do not represent magmatic liquids, they probably closely approach the composition of the mixture of magma plus crystals involved in the reactions with limestone. As a reconnaissance check of the mixing hypothesis, analyses of the porphyritic gabbro, Sue Peaks Limestone and the integrated bulk composition of the main contact skarn have been plotted on the Ca-Si-(Fe+Mg) and Ca-Si-Al faces of the simplified skarn tetrahedron (Figures 27 and 28). Similar plots of analyses of fine-grained gabbro, Del Carmen and Santa Elena limestones and the bulk composition of the xenolith skarn are shown in Figures 29 and 30. The remarkably close fit to a line for the main contact data on both sections confirms the applicability of the mixing hypothesis for the elements portrayed on the diagrams. Although the data for the xenolith show considerable scatter, the validity of the mixing model is confirmed.

A crude estimate of the proportions of magma and limestone involved in the reaction can be obtained by application of the lever rule to a specific combination of analyzed limestone and gabbro and the integrated bulk composition of skarn. The composition of the skarn at the main contact may be approximated by mixing 25 moles of porphyritic gabbro

Figure 27. Molecular proportion of calcium, iron + magnesium and silicon of individual samples of porphyritic gabbro and Sue Peaks Limestone and of integrated bulk composition of skarn from main contact traverse.

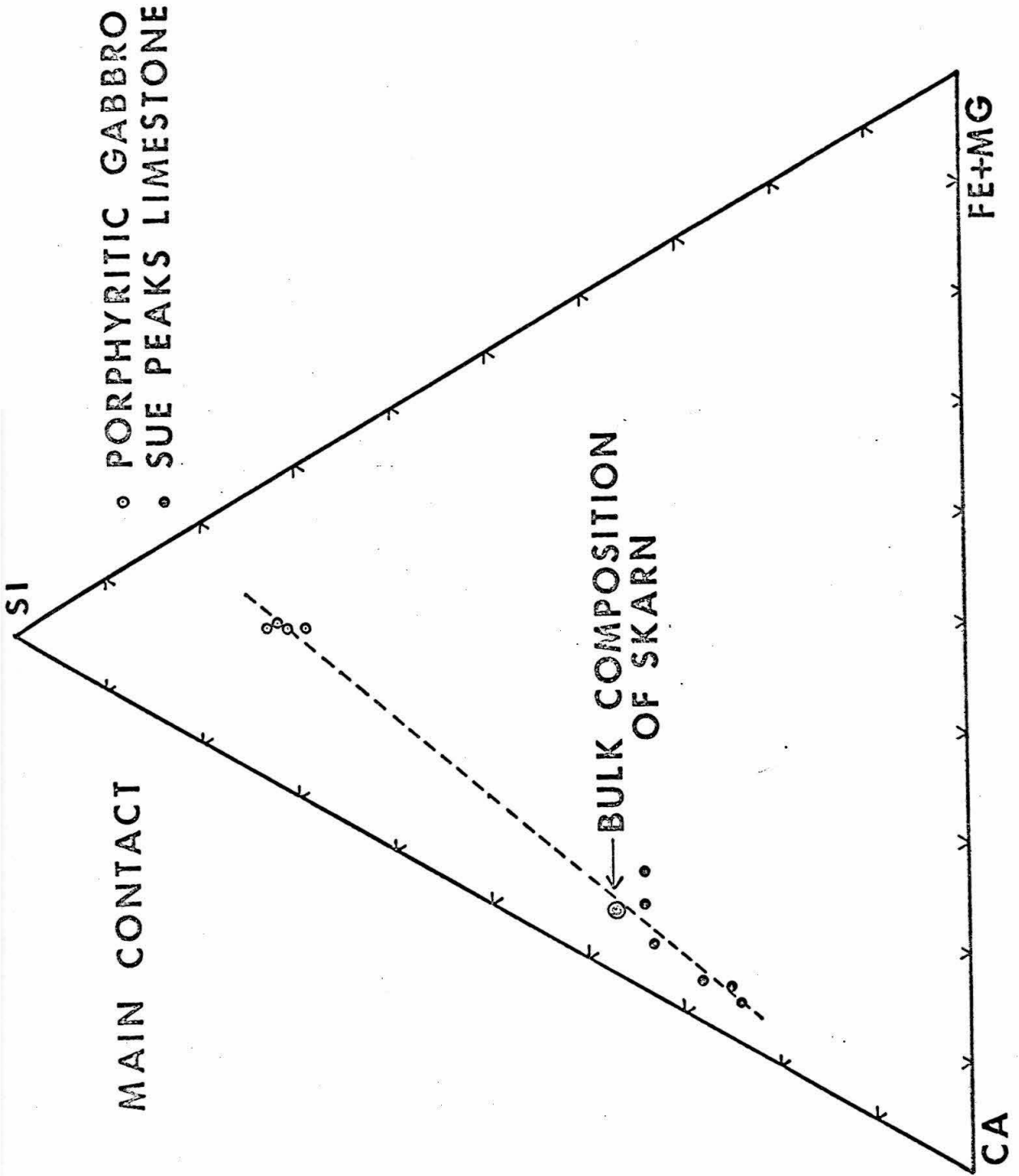


Figure 28. Molecular proportion of calcium, aluminum and silicon of individual samples of porphyritic gabbro and Sue Peaks Limestone and of integrated bulk composition of skarn from main contact traverse.

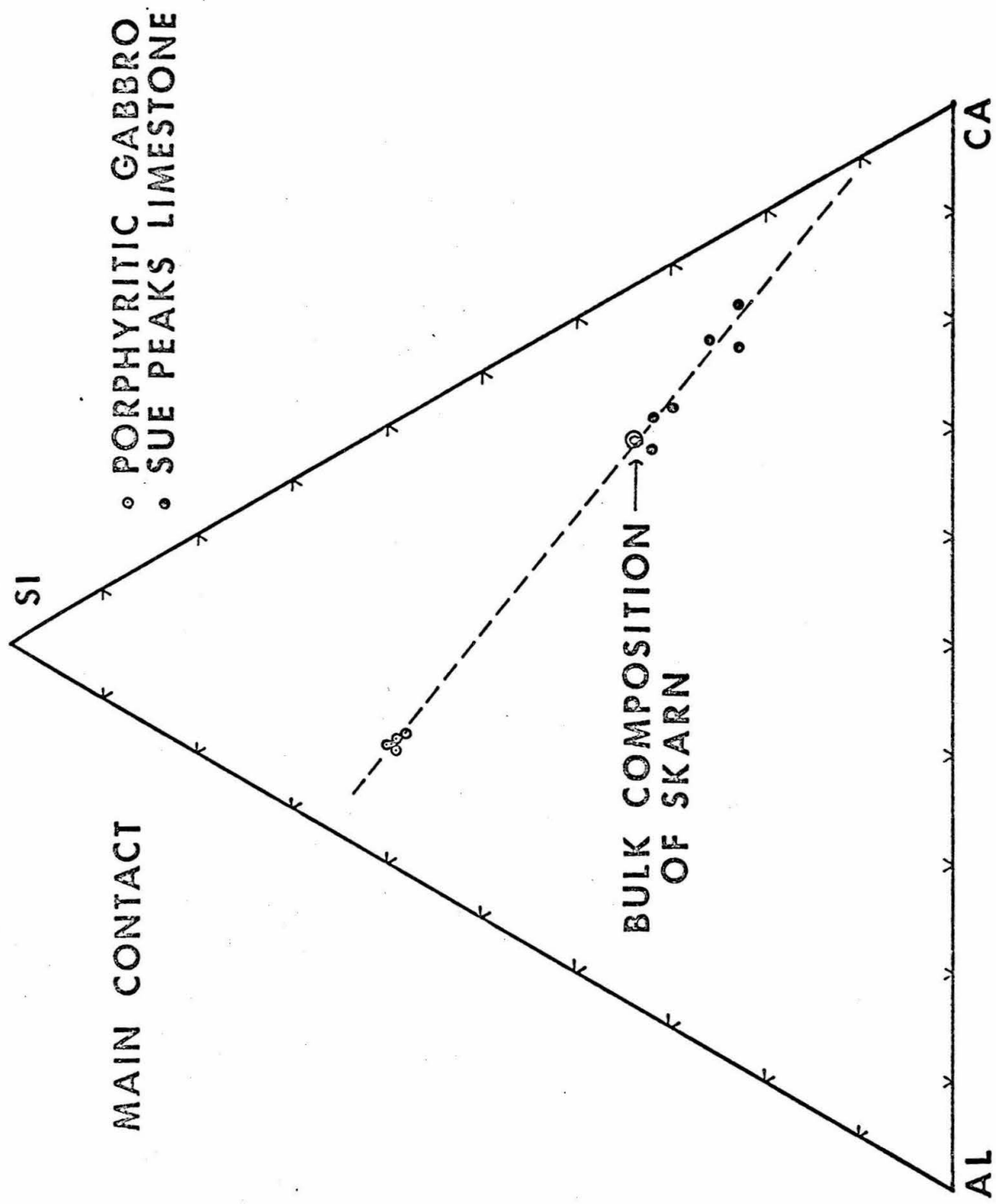


Figure 29. Molecular proportion of calcium, iron + magnesium and silicon of individual samples of fine-grained gabbro, Del Carmen Limestone and Santa Elena Limestone and of integrated bulk composition of skarn from the xenolith traverse.

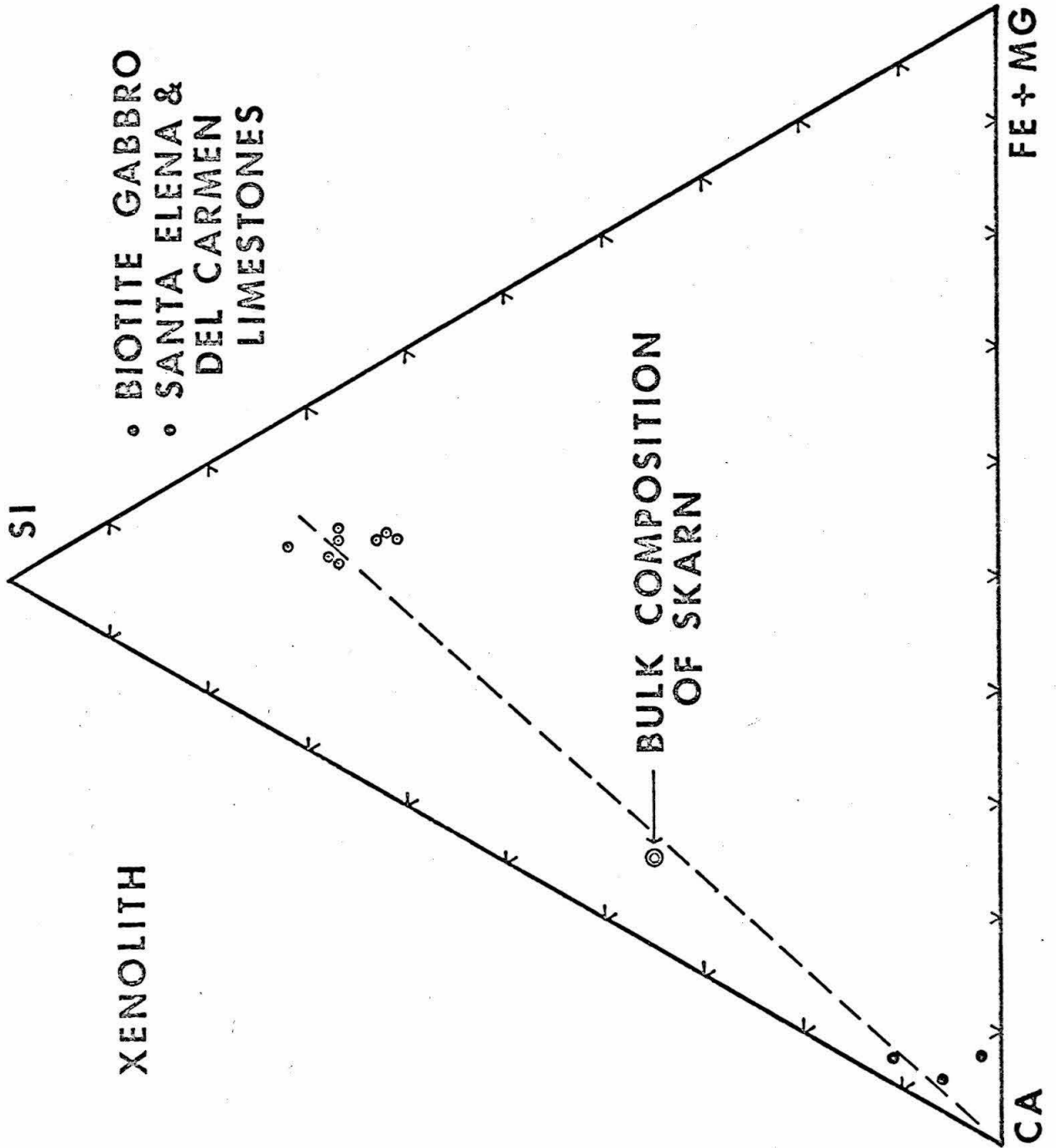
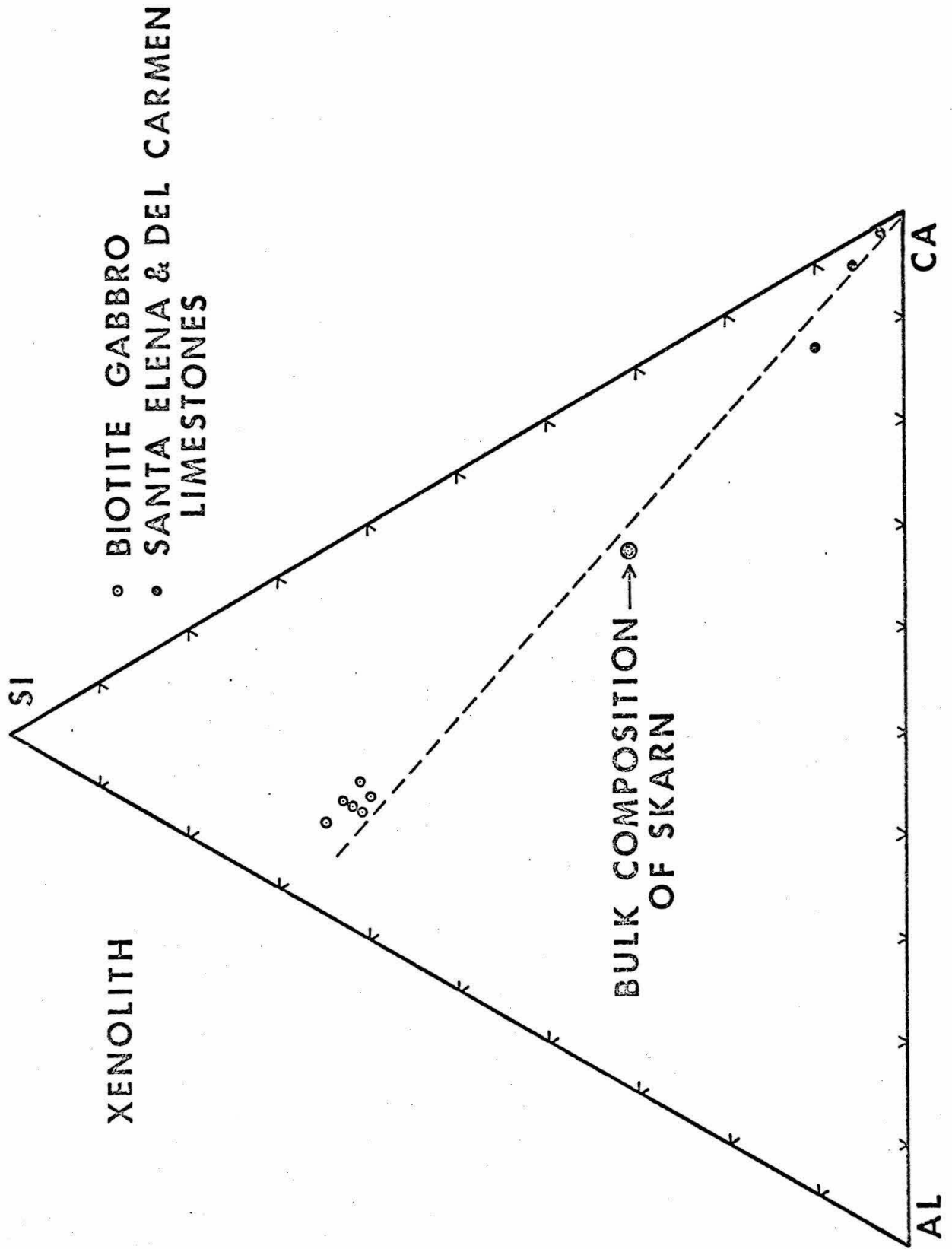


Figure 30. Molecular proportion of calcium, aluminum and silicon of individual samples of fine-grained gabbro, Del Carmen Limestone and Santa Elena Limestone and of integrated bulk composition of skarn from the xenolith traverse.



(CM-39-3) with 75 moles of the dark-gray fraction of the Sue Peaks limestone (CM-336-1D) or by mixing 5 moles of the same gabbro with 95 moles of the light-gray fraction of the Sue Peaks limestone (CM-336-1L). The integrated bulk composition of the xenolith skarn may be generated by mixing 48 moles of fine-grained gabbro (CM-109-5) with 52 moles of Santa Elena limestone (CM-335-2).

#### SUMMARY

Mineralogically zoned calc-silicate skarn occurs as a narrow band that separates pyroxenite and marble along the intrusive contact between gabbro and limestone and as a rim on marble-cored xenoliths in gabbro. The most widely developed mineral assemblages in skarn consist of melilite or idocrase pseudomorphic after melilite, one or two of the phases wollastonite, rankinite, spurrite and calcite and accessory Ti-Zr garnet, perovskite and magnetite. Each mineralogic zone in skarn is characterized by the presence of one of the stoichiometric calc-silicate phases. The sequence of zones, from pyroxenite to marble, is wollastonite, rankinite, spurrite, calcite. The series mineral zones developed across a band of skarn is analogous to the set of monomineralic zones in calc-silicate nodules from the inner part of the aureole, the main difference being the presence in skarn of additional phases capable of solid solution. Proof that the mineralogic zonation in skarn is the result of metasomatic introduction of material from the gabbro and not the isochemical metamorphism of a bedded sediment is demonstrated by the observations that (1) the sequence of mineral zones is the same in skarn formed

in each of the three carbonate units, (2) the zoning is parallel to the intrusive contact which is discordant to bedding in marble and (3) mineralogy and sequences of zones are the same on all sides of skarn xenoliths in gabbro.

To a first approximation, the mineral phases of the skarn may be described by solid phases in the system  $\text{CaO-FeO-MgO-Al}_2\text{O}_3\text{-SiO}_2\text{-CO}_2$  and may be represented graphically in a tetrahedron with Ca, Fe+Mg, Al and Si as apices. The lack of crossing tie-lines when all skarn assemblages are plotted in the simple skarn tetrahedron shows that to the extent that the facies type so defined is sensitive to changes in P, T and  $u_{\text{CO}_2}$ , conditions of metamorphism were the same both in the xenolith and at the intrusive contact, and that the different mineral assemblages represent products of metamorphism of different bulk compositions. The mineral assemblage of each skarn zone is compatible with the assemblages at each of its contacts, while the assemblages bounding it on either side are incompatible. Metamorphism of a general composition within the simple skarn tetrahedron under conditions of trivariant equilibrium in P, T and  $u_{\text{CO}_2}$  should result in a four-phase assemblage. However, the series of mineral assemblages in a skarn band are represented by a sequence of two-phase joins and adjacent three-phase planes in the tetrahedron. Hence, each skarn zone represents a "special" bulk composition within the simple system. The close analogy between the mineral assemblages of the zoned skarn and the monomineralic zones of the calc-silicate nodules suggests that the reaction-diffusion model used to describe the

metasomatic growth of the calc-silicate nodules may be applicable to the genesis of the skarn.

The assumption of local equilibrium on which the growth model is based requires that the gradients of the chemical potentials of all transported species be continuous from point to point across the series of skarn zones. The compatibility of mineral assemblages of adjacent zones and the continuity of gradients of composition of melilite and garnet solid solutions across the skarn are consistent with the local equilibrium hypothesis and verify that diffusion was the dominant mechanism of mass transport.

The formula proportions of titanium and zirconium in garnet vary antithetically with that of silicon and the formula proportion of silicon in garnet from skarn systematically decreases from pyroxenite to marble. The formula proportion of silicon in garnet is directly proportional to the concentration of silicon in bulk skarn while the formula proportion of zirconium in garnet varies inversely with the concentration of zirconium in skarn. By analogy with the calc-silicate nodules, the chemical potential of silicon in each skarn zone was controlled by the assemblage of coexisting stoichiometric calc-silicate phases. Thus the formula proportion of silicon in garnet is a direct measure of the chemical potential of silicon from point to point in the skarn. Titanium and zirconium enter garnet to fill the silicon deficiency.

Although composition-distance plots for diffusion without chemical reaction are smooth curves, those for systems involving chemical reaction may show discontinuities where reactions involve

phases of fixed composition. Because mass transport involves diffusion down chemical potential gradients produced by reactions to form specific mineral assemblages, it is the mineral reactions, not the relative diffusion rates of the various chemical species that exercise primary control of the bulk composition of the mineral zones. Concentration-distance plots for skarn from the intrusive contact and from the xenolith show that the concentrations of silicon and iron decrease from pyroxenite to marble while the concentration of calcium increases across the same interval. The concentration of aluminum increases to a broad maximum in the rankinite zone then decreases toward marble. Mass balance calculations show that relative either to a fixed volume of rock or to a fixed mass of CaO, silicon, aluminum, iron and titanium were added to limestone to form skarn. A striking feature of the distribution of skarn compositions plotted in the simple skarn tetrahedron is that rather than show a continuous variation in composition across adjoining three-phase triangles, the compositions of skarn samples are grouped along the two-phase tie-lines joining melilite and stoichiometric calc-silicate phases.

On the basis of field, textural, mineralogical and chemical relationships at the intrusive contact it is concluded that the zoned calc-silicate skarn is the result of direct reaction between gabbroic magma and solid limestone and that the pyroxenite represents an accumulation of clinopyroxene precipitated in response to reaction between magma and limestone. Reaction between gabbroic magma and

limestone involves two processes, (1) decarbonation reactions between calcite and magma and/or crystals in equilibrium with magma, and (2) crystallization of phases with which the magma is saturated, to supply energy for the endothermic decarbonation reactions.

The skarn consists essentially of a zone of melilite superimposed on a series of mineral zones defined by the presence of a stoichiometric calc-silicate mineral. The "special" bulk compositions of each of the skarn zones are the direct result of specific mineral reactions between gabbroic magma, saturated with plagioclase and clinopyroxene, and limestone. Reaction between calcite and clinopyroxene of a wide range of composition will produce a single solid phase, melilite. Similarly, reaction between calcite and plagioclase will produce melilite + wollastonite + nepheline. At the temperature of initial reaction between magma and limestone, wollastonite and calcite are incompatible. The calc-silicate zones result from reaction between wollastonite and calcite to form spurrite which in turn reacted with wollastonite to form rankinite.

## REFERENCES

- Adkins, W. S., 1928, Handbook of Texas Cretaceous fossils: Univ. Texas Bull., 2838, 385 p.
- Agrell, S. O., 1965, Polythermal metamorphism of limestones at Kilchoan, Ardnamurchan: Mineralog. Mag., v. 34 (Tilley Volume), p. 1-15.
- \_\_\_\_\_, and Gay, P., Kilchoanite, a polymorph of rankinite: Nature, v. 189, p. 743.
- Albee, A. L., 1965, A petrogenetic grid for the Fe-Mg silicates of pelitic schists: Am. Jour. Sci., v. 263, p. 512-36.
- \_\_\_\_\_, and Ray, L., 1970, Correction factors for electron probe microanalysis of silicates, oxides, carbonates, phosphates and sulphates: Anal. Chem., v. 42, p. 1408-14.
- Anderson, G. M., 1970, Some thermodynamics of dehydration equilibria: Am. Jour. Sci., v. 269, p. 392-401.
- Barth, T. F. W., 1963, Contribution to the mineralogy of Norway. No. 22, Vesuvianite from Kirstiansand, other occurrences in Norway, the general formula of vesuvianite: Norsk. Geol. Tidsskr., v. 43, p. 457-72.
- Bence, A. E., and Albee, A. L., 1968, Empirical correction factors for the electron microanalysis of silicates and oxides: Jour. Geology, v. 76, p. 382-403.
- Bloomer, R. R., 1949, Geology of the Christmas and Rosillos Mountains, Brewster County, Texas: unpublished Ph.D. dissertation, Texas Univ., 82 p.
- Böse, E., 1913, Algunas faunas del Cretacico superior de Coahuila y regiones limitrofes: Inst. Geol. Mexico, Bull. 30, 56 p.
- Bowen, N. L., 1928, The evolution of the igneous rocks: Princeton, N.J., Princeton University Press, 332 p., reprinted by Dover Publications, Inc., 1956.
- \_\_\_\_\_, 1940, Progressive metamorphism of siliceous limestone and dolomite: Jour. Geology, v. 48, p. 225-74.
- \_\_\_\_\_, 1945, Phase equilibria bearing on the origin and differentiation of alkaline rocks: Am. Jour. Sci., v. 243-A (Daly Volume), p. 75-89.

- Buddington, A. F., and Lindsley, D. H., 1964, Iron-titanium oxide minerals and their synthetic equivalents: *Jour. Petrology*, v. 5, p. 310-57.
- Burnham, C. W., 1959, Contact metamorphism of magnesian limestone at Crestmore, California: *Geol. Soc. Am. Bull.*, v. 70, p. 879-920.
- Burns, R. G., and Burns, V. M., 1971, Study of the crystal chemistry to titaniferous garnets by Mössbauer spectroscopy: (ABS.) *Geol. Soc. Am. Abstracts with Programs.*, v. 3, p. 519-20.
- Carmichael, I. S. E., Nicholls, J., and Smith, A. L., 1970, Silica activity in igneous rocks: *Am. Mineralogist*, v. 55, p. 246-63.
- Carslaw, H. S., and Jaeger, J. C., 1959, *Conduction of heat in solids*: New York, Oxford University Press, 510 p.
- Chodos, A. A., and Albee, A. L., 1971, Quantitative microprobe analysis and data reduction using an on-line mini computer: (ABS.) *Proc. Sixth National Conference on electron probe analysis*, Electron Probe Society of America, p. 1512.
- Christie, O. H. J., 1961, On sub-solidus relations of silicates. 1. The lower breakdown temperature of the akermanite-gehlenite mixed crystal series at moderate water pressure: *Norsk. Geol. Tidsskr.*, v. 41, p. 255-270.
- Clabaugh, S. E., 1953, Contact metamorphism in the Christmas Mountains, Brewster County, Texas: (ABS.) *Geol. Soc. Am. Bull.*, v. 64, p. 1408.
- Daly, R. A., 1910, Origin of the alkaline rocks: *Geol. Soc. Am. Bull.*, v. 21, p. 87-118.
- Denbigh, K., 1966, *The principles of chemical equilibrium*: London, Cambridge University Press, 494 p.
- Dowty, E., 1971, Crystal chemistry of titanian and zirconian garnet: I. Review and spectral studies: *Am. Mineralogist*, v. 56, p. 1983-2009.
- \_\_\_\_\_, and Appleman, 1970, X-ray refinement and Mössbauer study of Ti-Zr garnets: tetrahedral Fe 2+?: (ABS.) *Geol. Soc. Am. Abstracts with Programs*, v. 2, p. 541.
- Flanagan, F. J., 1969, U. S. Geological Survey Standards - II. First compilation of data for the new U.S.G.S. rocks: *Geochim. et Cosmochim. Acta*, v. 33, p. 81-120.

- Geller, S., 1967, Crystal chemistry of the garnets: *Zeitschr. Kristallographie*, v. 125, p. 1-47.
- Gomes, C. deB., 1969, Electron microprobe analysis of zoned melanites: *Am. Mineralogist*, v. 54, p. 1654-61.
- Greenwood, H. J., 1967, Mineral equilibria in the system  $MgO-SiO_2-H_2O-CO_2$  in Abelson, P. H., ed., *Researches in Geochemistry*, v. 2: New York, John Wiley and Sons, p. 542-67.
- Gutt, W., 1961, A new calcium magnesiosilicate: *Nature*, v. 190, p. 339-40.
- \_\_\_\_\_, 1965, The system dicalcium silicate-merwinite: *Nature*, v. 207, p. 184-85.
- Harker, R. I., 1959, The synthesis and stability of tilleyite,  $Ca_5Si_2O_7(CO_3)_2$ : *Am. Jour. Sci.* v. 257, p. 656-67.
- \_\_\_\_\_, and Tuttle, O. F., 1956, Experimental data on the  $P(CO_2)$ -T curve for the reaction: calcite + quartz = wollastonite + carbon dioxide: *Am. Jour. Sci.*, v. 254, p. 239-56.
- Hoffman, A., 1962, Chromatographic theory of infiltration metasomatism and its application to feldspars: *Am. Jour. Sci.*, v. 272, p. 69-90.
- Howie, R. A., and Wooley, A. R., 1968, The role of titanium and the effect of  $TiO_2$  on the cell-size, refraction index, and specific gravity in the andradite-melanite-schorlomite series: *Mineralog. Mag.*, v. 36, p. 775-90.
- Huckenholz, H. G., 1969, Synthesis and stability of Ti-andradite: *Am. Jour. Sci.*, v. 267-A (Schairer Volume), p. 209-32.
- Isaacs, T., 1968, Titanium substitutions in andradites: *Chem. Geol.*, v. 3, p. 219-22.
- Ito, J., and Frondel, C., 1967, Synthetic zirconium and titanium garnets: *Am. Mineralogist*, v. 52, p. 773-81.
- \_\_\_\_\_, and Arem, J., 1970, Idocrase: synthesis, phase relations and crystal chemistry: *Am. Mineralogist*, v. 55, p. 880-912.
- Jaeger, J. C., 1959, Temperatures outside a cooling intrusive sheet: *Am. Jour. Sci.*, v. 257, p. 44-54.
- \_\_\_\_\_, 1964, Thermal effects of intrusions: *Rev. Geophysics*, v. 2, p. 443-66.

- Jenkins, E. C., 1959, Hypabyssal rocks associated with the Christmas Mountains gabbro, Brewster County, Texas: unpublished M. A. thesis, Texas Univ., 117 p.
- Kennedy, W. Q., 1959, The formation of a diffusion reaction skarn by pure thermal metamorphism: *Mineralog. Mag.*, v. 32, p. 26-31.
- Korzhinskii, D. S., 1949, The phase rule and systems with fully mobile components: *Doklady Akad. Nauk SSSR*, v. 64, p. 361-64 (in Russian).
- \_\_\_\_\_, 1950, Phase rule and geochemical mobility of the elements: *Internat. Geol. Cong.*, 18th Great Britain, 1948, Rept. pt. 2, Sec. A., p. 50-57.
- \_\_\_\_\_, 1959, *Physiochemical basis of the analysis of the paragenesis of minerals (English Translation)*: New York, Consultants Bureau, Inc., 142 p.
- \_\_\_\_\_, 1965, The theory of systems with perfectly mobile components and processes of mineral formation: *Am. Jour. Sci.*, v. 263, p. 193-205.
- \_\_\_\_\_, 1966, On thermodynamics of open systems and the phase rule (a reply to D. F. Weill and W. S. Fyfe): *Geochim. et Cosmochim. Acta*, v. 30, p. 829-35.
- \_\_\_\_\_, 1967, On thermodynamics of open systems and the phase rule (a reply to the second critical paper of D. S. Weill and W. S. Fyfe): *Geochim. et Cosmochim. Acta*, v. 31, p. 1177-80.
- \_\_\_\_\_, 1968, The theory of metasomatic zoning: *Mineral. Deposita*, v. 3, p. 222-31.
- \_\_\_\_\_, 1970, *Theory of metasomatic zoning (English Translation)*: Oxford, Clarendon Press, 162 p.
- Kushiro, I., 1960, Si-Al relations in clinopyroxenes from igneous rocks: *Am. Jour. Sci.*, v. 258, p. 548-54.
- \_\_\_\_\_, 1962, Clinopyroxene solid solutions I., the  $\text{CaAl}_2\text{SiO}_6$  component: *Japan. Jour. Geol. Geogr.*, v. 33, p. 213-220.
- LeBas, M. J., 1962, The role of Aluminum in igneous clinopyroxenes with relation to their parentage: *Am. Jour. Sci.*, v. 260, p. 267-88.
- Lonsdale, J. T., 1940, Igneous rocks of the Terlingua-Solitario Region, Texas: *Geol. Soc. Am. Bull.*, v. 51, p. 1539-1626.
- Lovering, T. S., 1938, Temperatures in a sinking xenolith: *Trans. Am. Geophys. Union*, 19th Ann. Meeting, p. 274-77.

- Matchatschki, F., 1932, Zur Formel des Vesuvian: Zeitschr. Kristallographie, v. 81, p. 148-52.
- Majumdar, A. J., and Roy, R., 1956, Fugacities and free energies of CO<sub>2</sub> at high pressure and temperatures: Geochim. et Cosmochim. Acta, v. 10, p. 311-15.
- Manning, P. G., 1967, The optical absorption spectra of some andradites and the identification of the  ${}^6A_1 - {}^4A_1, {}^4E(G)$  transition in octahedrally bonded Fe 3+: Can. Jour. Earth Sci., v. 4, p. 1039-47.
- \_\_\_\_\_, and Harris, D. C., 1970, Optical absorption and electron microprobe studies of some high-Ti andradites: Can. Mineralogist, v. 10, p. 260-71.
- Maxwell, R. A., Lonsdale, J. T., Hazzard, R. T., and Wilson, J. A., 1967, Geology of the Big Bend National Park, Brewster County, Texas: Univ. Texas, Bur. Econ. Geology, Pub. 6711, 320 p.
- Moore, R. K., and White, W. B., 1971, Intervalence electron transfer effects in the spectra of melanite garnets: Am. Mineralogist, v. 56, p. 826-40.
- Mueller, R. F., 1967, Mobility of the elements in metamorphism: Jour. Geol., v. 75, p. 565-82.
- Orville, P. M., and Greenwood, H. J., 1965, Determination of  $\Delta H$  of reaction from experimental pressure-temperature curves: Am. Jour. Sci., v. 263, p. 678-83.
- Reiss, H., 1965, Methods of thermodynamics: New York, Blaisdell, 217 p.
- Robie, R. A., and Waldbaum, D. R., 1968, Thermodynamic properties of minerals and related substances at 298.15°K (25.0°C) and one atmosphere (1.013 bars) pressure and at higher temperatures: U. S. Geol. Surv. Bull. 1259.
- Schairer, J. F., and Yoder, H. S., 1960, The system fosterite-nepheline-diopside: Carnegie Inst. Wash. Year Book 59, p. 70-71.
- Shmulovich, K. I., 1969, Stability of merwinite in the system CaO-MgO-SiO<sub>2</sub>-CO<sub>2</sub>: Dokkady Akad. Nauk. SSSR, v. 184, p. 1177-79.
- Swadley, W C, 1958, Petrology of the Christmas Mountains gabbro, Brewster County, Texas: unpublished M. A. thesis, Texas Univ., 67 p.

- Thompson, J. B., Jr., 1957, The graphical analysis of mineral assemblages in pelitic schists: *Am. Mineral.*, v. 42, p. 842-58.
- \_\_\_\_\_, 1959, Local equilibrium in metasomatic processes, in Abelson, P. H., ed., *Researches in Geochemistry*, v. 1: New York, John Wiley and Sons, p. 427-57.
- \_\_\_\_\_, 1970, Geochemical reaction and open systems: *Geochim. et Cosmochim. Acta*, v. 34, p. 529-51.
- Tilley, C. E., 1929, On larnite (calcium orthosilicate, a new mineral) and its associated minerals from the limestone contact-zone of Scawt Hill, Co. Antrim: *Mineralog. Mag.*, v. 22, p. 77-86.
- \_\_\_\_\_, 1951a, A note on the progressive metamorphism of siliceous limestones and dolomites: *Geol. Mag.*, v. 89, p. 175-78.
- \_\_\_\_\_, 1951b, The zoned contact skarns of the Broadford area, Skye: a study of boron-fluorite metasomatism in dolomites: *Mineralog. Mag.*, v. 29, p. 621-66.
- \_\_\_\_\_, 1952, Some trends of basaltic magma in limestone syntaxis: *Am. Jour. Sci.*, v. 250-A (Bowen Volume), p. 529-45.
- \_\_\_\_\_, and Alderman, A. R., 1934, Progressive metasomatism of the flint nodules of the Scawt Hill contact zone: *Mineralog. mag.*, v. 23, p. 513-18.
- \_\_\_\_\_, and Harwood, H. F., 1931, The dolerite-chalk contact of Scawt Hill, Co. Antrim. The production of basic alkali-rocks by the assimilation of limestone by basaltic magma: *Mineralog. Mag.*, v. 22, p. 439-68.
- Tuttle, O. F., and Harker, R. I., 1957, Synthesis of spurrite and the reaction wollastonite + calcite = spurrite + carbon dioxide: *Am. Jour. Sci.*, v. 255, p. 226-34.
- Vance, J. A., 1969, On synneusis: *Contr. Mineralogy and Petrology*, v. 24, p. 7-29.
- Verhoogen, J., 1962, Distribution of titanium between silicates and oxides in igneous rocks: *Am. Jour. Sci.*, v. 260, p. 211-20.
- Walter, L. S., 1963, Experimental studies on Bowen's decarbonation series I: P-T univariant equilibria of the "monticellite" and "akermanite" reactions: *Am. Jour. Sci.*, v. 261, p. 488-500.

- Walter, L. S., 1965, Experimental studies on Bowen's decarbonation series III: P-T univariant equilibrium of the reaction: spurrite + monticellite = merwinite + calcite and analysis of assemblages found at Crestmore, California: *Am. Jour. Sci.*, v. 263, p. 64-77.
- Warren, B. E., and Modell, D. I., 1931, The structure of vesuvianite  $\text{Ca}_{10}\text{Al}_4(\text{Mg,Fe})_2\text{Si}_9\text{O}_{18}(\text{OH})_4$ : *Zeitschr. Kristallographie*, v. 78, p. 422-32.
- Watkinson, D. H., and Wyllie, P. J., 1969, Phase equilibrium studies bearing on the limestone-assimilation hypothesis: *Geol. Soc. Am. Bull.*, v. 80, p. 1565-76.
- Weill, D. F., and Fyfe, W. S., 1964, A discussion of the Korzhinskii and Thompson treatment of thermodynamic equilibrium in open systems: *Geochim. et Cosochim. Acta*, v. 28, p. 565-76.
- \_\_\_\_\_, and \_\_\_\_\_, 1967, On equilibrium thermodynamics of open systems and the phase rule (a reply to D. S. Korzhinskii): *Geochim. et Cosmochim. Acta*, v. 31, p. 1167-76.
- Wyllie, P. J., and Haas, J. L., Jr., 1966, The system  $\text{CaO-SiO}_2\text{-CO}_2\text{-H}_2\text{O}$  II - the petrogenetic model: *Geochim. et Cosmochim. Acta*, v. 30, p. 525-43.
- Zen, E., 1963, Components, phases and criteria of chemical equilibrium in rocks: *Am. Jour. Sci.*, v. 261, p. 929-42.
- \_\_\_\_\_, 1966, Construction of pressure-temperature diagrams for multicomponent systems after the method of Schreinemakers—a geometric approach: *U. S. Geol. Surv. Bull.* 1225, 56 p.
- Zharikov, V. A., and Shmulovich, K. I., 1969, High temperature mineral equilibria in the system  $\text{CaO-SiO}_2\text{-CO}_2$ : *Geokhimiya*, n. 9, p. 1039-56.

APPENDIX A

METHODS OF ELECTRON MICROPROBE ANALYSIS

## ELECTRON MICROPROBE ANALYSIS OF MINERALS

All electron microprobe analyses of minerals were made of grains in situ in polished thin section. All analyses of minerals from igneous and contaminated igneous rocks were performed with an Applied Research Laboratories (ARL) model EMX electron microprobe while those of minerals from skarn were performed both with the ARL and with a Materials Analysis Company (MAC) model 5-SA-3 electron microprobe interfaced with a DEC PDP-8/L computer. Operating conditions for both instruments were 15 KV accelerating potential and 0.05 microamp sample current, measured on brass. Beam current drift was compensated by counting X-rays generated for a fixed flux of electrons with the ARL and by taking the ratio of X-ray counts to beam current averaged over a fixed counting time with the MAC. Primary standards used for analyses of all phases were oxides, synthetic silicates and well-characterized natural minerals. Oxide concentrations were computed from X-ray intensity ratios by the method of Bence and Albee (1968) using binary oxide correction factors computed by Albee and Ray (1970). Three elements were analyzed simultaneously with the ARL. Data for complete analysis of a point were accumulated in three to five runs made on successive days. Output from the probe was punched on paper tape that was processed by an IBM 360/75 to edit data and compute X-ray intensity ratios relative to the standards (K-values). Oxide concentrations and mineral formulae were computed with a separate program. Data collection and reduction was done on-line with the MAC using a program written in FOCAL-8 by A. A. Chodos (Chodos and Albee, 1971). Elements were analyzed sequentially, three at a time, and

oxide concentrations were computed before moving the sample from the point of analysis.

#### ELECTRON MICROPROBE ANALYSIS OF ROCKS

Rock samples were homogenized for analysis by electron microprobe by fusion with  $\text{Li}_2\text{B}_4\text{O}_7$ . Samples of rock, weighing 10 to 250 gm, were pulverized in a Spex shatterbox. Approximately 2 gm of rock powder was mixed with an equal weight of Baker and Adamson  $\text{Li}_2\text{B}_4\text{O}_7$  in a Spex mixer-mill and fused for 5 to 15 minutes in a carbon crucible in an electric muffle furnace at  $1000^\circ$  to  $1100^\circ\text{C}$ . The fused sample was cast on an aluminum plate held at  $250^\circ\text{C}$  and the resulting glass disc was annealed at that temperature for several hours. The glass disc, 20 mm in diameter and 5 mm thick, was mounted in a 1 inch O.D. brass ring with epoxy and the surface was polished for analysis with the electron microprobe.

Glass discs were prepared from the U.S. Geological Survey standard granite (G-2), granodiorite (GSP-1), andesite (AGV-1) and basalt (BCR-1) described by Flanagan (1969). Three discs were made of each rock by fusion of carefully weighed mixtures of rock powder and flux dried at  $110^\circ\text{C}$  for 24 hours before weighing. Discs were made with the compositions 3 gm rock + 1 gm flux (designated 3R/1F in Tables A-1 through A-8), 2 gm rock + 1 gm flux (2R/2F) and 1 gm rock + 3 gm flux (1R/3F). Electron microprobe analyses of these carefully prepared standards provided a test for the accuracy and precision of the method and allowed computation of empirical correction factors for the interaction of  $\text{Li}_2\text{B}_4\text{O}_7$  and radiation of the analyzed elements.

Three blanks, made by fusion of 4 gm of flux, were analyzed by electron microprobe to determine the concentration of impurities in the glass. The mean values, as weight percent are:

SiO <sub>2</sub>	0.030
TiO <sub>2</sub>	0.004
Al <sub>2</sub> O <sub>3</sub>	0.052
FeO	0.010
MgO	0.009
CaO	0.042
Na <sub>2</sub> O	0.009
K <sub>2</sub> O	0.014
P <sub>2</sub> O <sub>5</sub>	<u>0.022</u>
	0.192 TOTAL IMPURITY

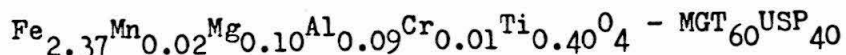
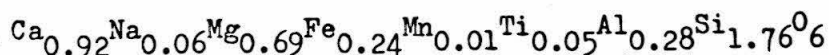
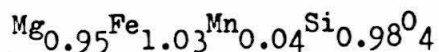
Glass discs made from igneous and contaminated rocks were analyzed with the ARL microprobe. X-ray intensity ratios were determined by averaging results of 20 ten second analyses distributed over the surface of the sample. Glass discs made from skarn were analyzed with the MAC microprobe. X-ray intensity ratios were determined by slowly moving the sample under beam while accumulating counts for 60 seconds. Operating conditions and standards used with both instruments were identical to those listed above.

Oxide concentrations were computed from X-ray intensity ratios by the method of Bence and Albee (1968). To account for the interaction of between Li<sub>2</sub>B<sub>4</sub>O<sub>7</sub> and the radiation of the elements analyzed, the difference between the oxide summation and 1.0 was entered as excess oxygen in each iteration. Convergence to a difference less than 0.003

pyroxenite was probably crystallized in response to reaction between magma and carbonate. The enthalpy of fusion of diopside, 24.3 Kcal/mole (Bowen, 1928, p. 178), is comparable in magnitude to the enthalpy of the decarbonation reaction, but opposite in sign when diopside crystallizes from a melt. Thus for each mole of calcite taken into solution by the magma, approximately one mole of clinopyroxene was crystallized to supply the energy necessary for the endothermic decarbonation reaction. The amount of limestone that may be assimilated by a given volume of gabbroic magma is limited by the concentration of potential clinopyroxene in uncontaminated magma.

#### The Olivine Reaction

Olivine in pyroxenite and nepheline gabbro derived from porphyritic gabbro is restricted in occurrence to the cores of large grains of titanite where it is rimmed by vermicular magnetite (Plate 3, Figure 1). The former presence of olivine in these rocks is marked by vermicular magnetite in the core of zoned grains of titanite (Plate 3, Figure 2). Compositions of coexisting olivine, titanite and magnetite from the assemblage of Plate 3, Figure 1 (CM-8-1A) are



The composition of titanite in contact with olivine is the most magnesian in the rock. Although composition of olivine in this and

Table A-1  
U.S.G.S. SILICATE ROCK STANDARDS

	140999	140120	140220	140221	140222	140320	140321	0	0	C
0	C.C	0.0	0.0	C.0	0.0	0.0	0.0	0	0	C
S102	69.769	69.133	69.591	69.228	69.475	69.579	70.243			
T102	0.535	0.449	0.465	0.518	0.499	0.490	0.483			
ZR02	C.C	0.0	0.0	C.0	0.0	0.0	0.0			
AL203	15.473	15.785	15.547	15.691	15.653	15.790	15.387			
V203	C.C	0.0	0.0	0.0	0.0	C.0	0.0			
CR203	C.C	0.0	0.0	C.0	0.0	0.0	0.0			
FE203	C.C	0.0	0.0	C.0	0.0	C.0	0.0			
FEO	2.512	2.477	2.545	2.502	2.558	2.482	2.388			
MNO	0.037	0.058	0.065	0.0	0.0	0.023	0.019			
MGO	0.788	0.799	0.762	0.790	0.748	0.784	0.750			
CAO	2.004	2.104	2.064	2.102	2.053	1.979	1.908			
BAU	C.C	0.0	0.0	0.0	0.0	0.0	0.0			
NA2O	4.191	4.358	4.278	4.403	4.367	4.199	4.168			
K2O	4.543	4.553	4.490	4.568	4.473	4.498	4.449			
P2O5	0.142	0.283	0.195	0.198	0.174	0.177	0.205			
TOTAL	100.000	100.000	100.000	100.000	100.000	100.000	100.000	C.0	0.0	C.C
140999	USGS GRANITE G-2	F. J. FLANAGAN AVG.								
140120	USGS GRANITE G-2	1R/3F GL NOV-DEC 1970								
140220	USGS GRANITE G-2	2R/2F GL NOV-DEC 1970								
140221	USGS GRANITE G-2	2R/2F GL NOV-DEC 1970								
140222	USGS GRANITE G-2	2R/2F GL NOV-DEC 1970								
140320	USGS GRANITE G-2	3R/1F GL NOV-DEC 1970								
140321	USGS GRANITE G-2	3R/1F GL NOV-DEC 1970								



Table A-3

U.S.G.S. SILICATE ROCK STANDARDS

	142120	142220	142221	142222	142320	142322	0	0	0
C	0.0	0.0	0.0	0.0	0.0	0.0	0	0	0
SI02	60.506	60.857	60.574	60.469	60.620	60.544			
TI02	1.110	1.058	1.029	1.092	1.069	1.067			
ZR02	0.0	0.0	0.0	0.0	0.0	0.0			
AL203	17.473	17.096	17.658	17.743	17.298	17.278			
V203	0.0	0.0	0.0	0.0	0.0	0.0			
CR203	0.0	0.0	0.0	0.0	0.0	0.0			
FE203	0.0	0.0	0.0	0.0	0.0	0.0			
FEU	6.278	6.439	6.290	6.316	6.296	6.356			
MNO	0.100	0.080	0.0	0.0	0.115	0.202			
MGO	1.530	1.443	1.468	1.444	1.577	1.543			
CAO	5.109	5.012	5.001	5.074	5.112	5.104			
BAO	0.0	0.0	0.0	0.0	0.0	0.0			
NA2O	4.445	4.455	4.452	4.390	4.405	4.403			
K2O	2.972	2.988	2.957	2.931	2.966	2.961			
P2O5	0.499	0.572	0.570	0.542	0.543	0.542			
TOTAL	100.000	100.000	100.000	100.000	100.000	100.000	0.0	0.0	0.0
142999	USGS ANDESITE AGV-1	F.J. FLANAGAN AVG.							
142120	USGS ANDESITE AGV-1	1R/3F GL NOV-DEC 1970							
142220	USGS ANDESITE AGV-1	2R/2F GL NOV-DEC 1970							
142221	USGS ANDESITE AGV-1	2R/2F GL NOV-DEC 1970							
142222	USGS ANDESITE AGV-1	2R/2F GL NOV-DEC 1970							
142320	USGS ANDESITE AGV-1	3R/1F GL NOV-DEC 1970							
142322	USGS ANDESITE AGV-1	3R/1F GL NOV-DEC 1970							

Table A-4

U.S.G.S. SILICATE ROCK STANDARDS

	143120	143220	143221	143222	143223	143320	143322	0	0
0	C.0	0.0	C.0	0.0	0.0	0.0	0.0	0.0	0
S102	54.847	55.204	55.102	55.054	55.230	55.988	55.857	55.857	0
T102	2.344	2.282	2.306	2.288	2.300	2.300	2.293	2.293	0
ZR02	0.0	0.0	0.0	0.0	0.0	0.0	0.0	0.0	0
AL203	13.658	13.717	13.791	13.824	13.893	14.071	14.041	14.041	0
V203	0.0	0.0	0.0	0.0	0.0	0.0	0.0	0.0	0
CR203	0.0	0.0	0.0	0.0	0.0	0.0	0.0	0.0	0
FE203	0.0	0.0	0.0	0.0	0.0	0.0	0.0	0.0	0
FE0	12.394	12.559	12.545	12.690	12.626	11.077	11.107	11.107	0
MNO	0.179	0.207	0.200	0.0	0.0	0.184	0.333	0.333	0
MGO	3.346	3.366	3.346	3.370	3.321	3.497	3.518	3.518	0
CAO	7.089	7.100	7.090	7.137	7.056	7.212	7.191	7.191	0
BAO	C.C	0.0	0.0	0.0	0.0	0.0	0.0	0.0	0
NA20	3.378	3.399	3.448	3.458	3.444	3.509	3.503	3.503	0
K20	1.717	1.732	1.730	1.730	1.720	1.777	1.773	1.773	0
P205	0.370	0.434	0.443	0.449	0.410	0.386	0.385	0.385	0
TOTAL	100.000	100.000	100.000	100.000	100.000	100.000	100.000	100.000	C.C
143999	USGS BASALT BCR-1	F.J. FLANAGAN AVG.							
143120	USGS BASALT BCR-1	1R/3F GL	NOV-DEC 1970						
143220	USGS BASALT BCR-1	2R/2F GL	NOV-DEC 1970						
143221	USGS BASALT BCR-1	2R/2F GL	NOV-DEC 1970						
143222	USGS BASALT BCR-1	2R/2F GL	NOV-DEC 1970						
143223	USGS BASALT BCR-1	2R/2F GL	NOV-DEC 1970						
143320	USGS BASALT BCR-1	3R/1F GL	NOV-DEC 1970						
143322	USGS BASALT BCR-1	3R/1F GL	NOV-DEC 1970						

Table A-5  
U.S.G.S. ANALYZED ROCK STANDARDS

	140000	140100	140200	140210	140220	140230	140300
WEIGHT PER CENT OXIDES							
O	0.0	C.C	C.C	0.0	0.0	0.0	0.0
SiO2	69.894	70.203	70.380	70.198	70.048	70.894	71.008
TiO2	0.536	0.535	0.478	0.618	0.474	0.341	0.542
ZrO2	0.0	0.0	0.0	0.0	0.0	0.0	0.0
Al2O3	15.501	15.916	15.323	15.478	15.333	15.159	15.596
V2O3	0.0	0.0	0.0	0.0	0.0	0.0	0.0
Cr2O3	C.C	C.C	0.0	0.0	C.C	0.0	0.0
Fe2O3	C.C	C.C	0.0	0.0	0.0	0.0	0.0
FEO	2.516	2.454	2.589	2.535	2.689	2.544	2.421
MNO	0.0	0.0	0.0	0.0	0.0	0.0	0.0
MGO	0.790	0.737	0.715	0.704	0.740	0.701	0.641
CAO	2.008	2.150	2.134	2.039	2.095	2.268	1.984
BAD	C.C	C.C	0.0	0.0	0.0	0.0	0.0
NA2O	4.198	4.354	4.514	4.623	4.581	4.337	3.880
K2O	4.556	3.648	3.867	3.805	4.039	3.757	3.824
P2O5	0.0	0.0	0.0	0.0	0.0	0.0	0.0
TOTAL	100.000	99.999	100.000	100.000	100.000	100.000	99.998

FORMULA PROPORTION CATIONS

	140000	140100	140200	140210	140220	140230	140300
FORMULA PROPORTION CATIONS							
O	0.0	0.0	0.0	0.0	0.0	0.0	0.0
Si4+	64.748	65.057	65.167	64.954	64.797	65.753	66.104
Ti4+	0.373	0.373	0.333	0.430	0.330	0.238	0.379
Zr4+	0.0	0.0	0.0	0.0	0.0	0.0	0.0
Al3+	16.923	17.382	16.721	16.878	16.715	16.569	17.220
V 3+	0.0	0.0	0.0	0.0	0.0	0.0	0.0
CR3+	0.0	0.0	0.0	0.0	0.0	0.0	0.0
FE3+	C.C	0.0	0.0	0.0	0.0	0.0	0.0
FE2+	1.948	1.901	2.004	1.961	2.079	1.972	1.884
MN2+	0.0	0.0	0.0	0.0	0.0	0.0	0.0
MG2+	1.091	1.018	0.987	0.971	1.020	0.969	0.889
CA2+	1.993	2.135	2.117	2.022	2.077	2.254	1.979
BA2+	C.C	0.0	0.0	0.0	0.0	0.0	0.0
NA +	7.539	7.822	8.103	8.293	8.215	7.798	7.003
K +	5.385	4.313	4.568	4.492	4.767	4.446	4.542
P 5+	C.C	0.0	0.0	0.0	0.0	0.0	0.0
OXYGEN	167.120	168.052	167.525	167.430	166.993	168.154	169.321

F.J. FLANAGAN AVG.  
 7-?? JUL 29631 AUG 1 1971  
 ???? JUL 29631 AUG 1 1971

140000	USGS GRANITE G-2
140100	USGS GRANITE G-2
140200	USGS GRANITE G-2
140210	USGS GRANITE G-2
140220	USGS GRANITE G-2
140230	USGS GRANITE G-2
140300	USGS GRANITE G-2



Table A-7  
U.S.G.S. ANALYZED ROCK STANDARDS

	142200	142210	142220	142230	142240	142300
WEIGHT PER CENT OXIDES						
O	C.C.	C.C.	0.0	C.C.	C.C.	0.0
SiO2	60.871	60.477	60.341	60.625	60.809	60.888
TiO2	1.116	1.039	1.044	1.135	1.015	1.367
ZrO2	0.0	0.0	0.0	0.0	0.0	0.0
Al2O3	17.554	18.287	18.302	18.377	18.199	17.775
V2O5	0.0	0.0	0.0	0.0	0.0	0.0
CR2O3	0.0	0.0	0.0	0.0	0.0	0.0
FE2O3	0.0	0.0	0.0	0.0	0.0	0.0
FEO	6.316	6.246	6.484	6.283	6.251	6.249
MNO	0.0	0.0	0.0	0.0	0.0	0.0
MGO	1.539	1.531	1.614	1.445	1.468	1.504
CAO	5.140	5.140	5.408	5.035	5.035	5.058
BAO	0.0	0.0	0.0	0.0	0.0	0.0
NA2O	4.472	4.530	4.578	4.390	4.497	4.324
K2O	2.990	2.747	2.791	2.709	2.726	2.833
P2O5	0.0	0.0	0.0	0.0	0.0	0.0
TOTAL	100.000	100.000	100.000	100.000	100.000	100.000

FORMULA PROPORTION CATIONS

	142200	142210	142220	142230	142240	142300
O	0.0	0.0	0.0	0.0	0.0	0.0
Si4+	55.381	55.942	55.739	56.185	56.292	56.511
Ti4+	0.777	0.723	0.725	0.791	0.766	0.954
Zr4+	0.0	0.0	0.0	0.0	0.0	0.0
Al3+	19.161	19.935	19.924	20.071	19.854	19.442
V 3+	0.0	0.0	0.0	0.0	0.0	0.0
CR3+	0.0	0.0	0.0	0.0	0.0	0.0
FE3+	0.0	0.0	0.0	0.0	0.0	0.0
FE2+	4.890	4.830	4.608	5.007	4.837	4.848
MN2+	0.0	0.0	0.0	0.0	0.0	0.0
Mg2+	2.125	2.111	2.197	1.996	2.025	2.080
CA2+	5.101	5.095	5.353	5.000	4.994	5.030
BA2+	0.0	0.0	0.0	0.0	0.0	0.0
NA +	8.030	8.124	8.198	7.888	8.071	7.780
K +	3.533	3.242	3.256	3.203	3.220	3.355
P 5+	0.0	0.0	0.0	0.0	0.0	0.0
OXYGEN	160.957	160.949	160.698	161.465	161.280	161.618
F.J. FLANAGAN AVG.						
142000	USGS ANDESITE AGV-1	????	???	JUL 29631 AUG 1 1971		
142100	USGS ANDESITE AGV-1	????	???	JUL 29631 AUG 1 1971		
142200	USGS ANDESITE AGV-1	????	???	JUL 29631 AUG 1 1971		
142210	USGS ANDESITE AGV-1	????	???	JUL 29631 AUG 1 1971		
142220	USGS ANDESITE AGV-1	????	???	JUL 29631 AUG 1 1971		
142230	USGS ANDESITE AGV-1	????	???	JUL 29631 AUG 1 1971		
142240	USGS ANDESITE AGV-1	????	???	JUL 29631 AUG 1 1971		
142300	USGS ANDESITE AGV-1	????	???	JUL 29631 AUG 1 1971		

Table A-8

U.S.G.S. ANALYZED ROCK STANDARDS

	143100	143150	143200	143210	143220	143230	143300
	WEIGHT PER CENT OXIDES						
O	0.0	0.0	0.0	0.0	0.0	0.0	0.0
SiO2	55.628	55.021	55.384	54.898	55.875	55.379	57.004
TiO2	2.291	2.249	2.324	2.180	2.430	2.363	2.378
ZrO2	0.0	0.0	0.0	0.0	0.0	0.0	0.0
Al2O3	14.003	14.501	14.273	14.773	14.143	13.904	14.128
V2O3	0.0	0.0	0.0	0.0	0.0	0.0	0.0
Cr2O3	0.0	0.0	0.0	0.0	0.0	0.0	0.0
Fe2O3	0.0	0.0	0.0	0.0	0.0	0.0	0.0
FeO	12.463	12.412	12.692	12.743	12.322	12.740	10.807
MnO	0.0	0.0	0.0	0.0	0.0	0.0	0.0
MgO	3.364	3.455	3.327	3.338	3.120	3.523	3.347
CaO	7.128	7.053	7.019	6.915	7.078	7.063	7.273
NaO	0.0	0.0	0.0	0.0	0.0	0.0	0.0
Na2O	3.397	3.663	3.488	3.510	3.441	3.513	3.439
K2O	1.727	1.643	1.593	1.643	1.591	1.516	1.622
P2O5	0.0	0.0	0.0	0.0	0.0	0.0	0.0
TOTAL	100.000	99.999	100.000	100.000	100.000	100.000	100.000
	FORMULA PROPORTION CATIONS						
O	0.0	0.0	0.0	0.0	0.0	0.0	0.0
Si4+	52.623	51.867	52.374	51.847	52.910	52.366	53.781
Ti4+	1.629	1.594	1.652	1.548	1.730	1.680	1.687
Zr4+	0.0	0.0	0.0	0.0	0.0	0.0	0.0
Al3+	15.611	16.110	15.906	16.442	15.783	15.494	15.708
V3+	0.0	0.0	0.0	0.0	0.0	0.0	0.0
Cr3+	0.0	0.0	0.0	0.0	0.0	0.0	0.0
Fe3+	0.0	0.0	0.0	0.0	0.0	0.0	0.0
Fe2+	9.855	9.781	9.962	10.060	9.754	10.070	8.523
Mn2+	0.0	0.0	0.0	0.0	0.0	0.0	0.0
Mg2+	4.743	4.854	4.689	4.698	4.403	4.965	4.706
Ca2+	7.225	7.124	7.112	6.998	7.182	7.156	7.352
Na+	0.0	0.0	0.0	0.0	0.0	0.0	0.0
K+	6.230	6.694	6.395	6.427	6.317	6.440	6.290
P5+	2.084	1.976	1.910	1.980	1.922	1.829	1.952
OXYGEN	157.900	157.180	157.927	157.413	158.411	157.658	159.200
143000	USGS BASALT BCR-1						
143100	USGS BASALT BCR-1						
143200	USGS BASALT BCR-1						
143210	USGS BASALT BCR-1						
143220	USGS BASALT BCR-1						
143230	USGS BASALT BCR-1						
143300	USGS BASALT BCR-1						
143000	F.J. FLANAGAN AVG.						
143100	????	????	????	????	????	????	????
143200	????	????	????	????	????	????	????
143210	????	????	????	????	????	????	????
143220	????	????	????	????	????	????	????
143230	????	????	????	????	????	????	????
143300	????	????	????	????	????	????	????

APPENDIX B

ELECTRON MICROPROBE ANALYSES OF  
IGNEOUS ROCKS AND MINERALS

TABLE B-1  
ANALYZED IGNEOUS ROCKS  
CHRISTMAS MOUNTAINS, TEXAS

	Olivine	Clinopyroxene	Amphibole	Biotite	Magnetite	Ilmenite	"Opaque"	Plagioclase	Alkali Feldspar	Nepheline	Analcite	Apatite	Clinozoisite	Chlorite
COARSE-GRAINED OLIVINE-TITANAUGITE GABBRO														
CM-6-2	1	20	..	2	x	..	10	65	..	..	..	1	..	..
CM-33-14	1	20	..	3	x	x	6	64	3	..	2	1	..	..
CM-39-6	3	30	..	1	x	x	7	57	2	..	..	1	..	..
CM-77A	2	30	..	3	x	..	7	51	5	..	..	2	..	..
CM-80CG	( )	15	..	5	x	x	4	70	..	..	..	1	2	3
CM-139	( )	15	..	15	-	-	7	50	5	..	..	1	3	4
CM-144	( )	20	..	5	x	x	10	57	3	..	..	1	2	2
CM-298	( )	25	..	5	-	-	10	57	3	..	..	1	..	2
FINE-GRAINED BIOTITE-TITANAUGITE GABBRO														
CM-80FG	..	10	..	15	x	..	15	60	..	..	..	2	..	..
CM-109-5	..	25	..	3	x	..	7	69	..	..	..	1	..	..
CM-136	( )	10	..	10	x	x	5	60	..	..	..	3	..	10
CM-276	( )	10	20	5	x	x	5	55	..	..	..	4	..	1
CM-53H	..	17	2	2	-	-	3	75	..	..	..	1	..	..
CM-83	..	30	..	10	-	-	10	48	..	..	..	2	..	..
CM-283	..	10	5	10	-	-	10	60	..	..	..	2	..	..
CM-293	..	10	..	10	-	-	10	68	..	..	..	2	..	..
PORPHYRITIC OLIVINE-BIOTITE-TITANAUGITE GABBRO														
CM-69	3	10	..	4	x	x	8	54	14	4	2	1	..	..
CM-39-1H	1	9	..	8	x	x	8	58	12	2	1	1	..	..
CM-39-3	2	10	..	4	-	-	4	63	10	3	2	2	..	..
AUGITE SYENITE														
CM-81	..	5	..	1	x	..	2	10	80	..	..	1	..	..
CM-288A	..	7	..	..	-	-	3	15	75	..	..	1	..	..
CM-294A	..	10	5	..	x	..	7	20	56	..	..	2	..	..
CM-315	..	6	1	10	x	x	3			..	1	1	..	..
CM-39-1	..	3	2	3	x	..	1	..	90	..	..	1	..	..
CM-53D	..	3	2	..	..	..	2	10	80	..	2	1	..	..

TABLE B-2

ELECTRON MICROPROBE ANALYSES OF IGNEOUS ROCKS  
CHRISTMAS MOUNTAINS, TEXAS  
COARSE-GRAINED, OLIVINE-BIOTITE-TITANAUGITE GABBRO

	298	144	77A	33-14	39-6	80-CG	139B
SiO <sub>2</sub>	46.12	47.29	47.73	47.73	47.74	48.02	48.57
TiO <sub>2</sub>	4.85	3.77	3.28	2.63	5.14	3.07	3.19
Al <sub>2</sub> O <sub>3</sub>	18.64	18.79	18.82	21.49	19.03	19.64	20.10
FeO*	9.87	10.13	9.78	7.71	6.77	9.15	7.67
MgO	4.04	3.91	3.46	2.90	4.89	3.77	4.18
CaO	11.74	10.31	11.48	12.28	12.15	10.61	10.67
Na <sub>2</sub> O	3.36	4.13	3.79	3.58	3.40	3.93	3.90
K <sub>2</sub> O	1.08	1.08	1.05	0.95	0.66	1.14	1.30
P <sub>2</sub> O <sub>5</sub>	0.30	0.59	0.61	0.73	0.22	0.67	0.42
TOTAL	100.00	100.00	100.00	100.00	100.00	100.00	100.00

C.I.P.W. NORM -- MOLE PERCENT

Or	6.43	6.41	6.27	5.61	3.93	6.76	7.67
Ab	19.67	25.38	24.17	23.83	26.21	26.39	25.40
An	33.00	29.68	31.45	39.88	34.85	32.65	33.42
Wo	..	..	..	..	..	..	..
Ac	..	..	..	..	..	..	..
Di	19.17	14.23	17.48	13.13	19.33	12.55	13.29
Hy	..	..	..	..	..	..	..
Ol	7.75	10.65	8.66	7.31	5.39	10.55	9.21
Lc	..	..	..	..	..	..	..
Ne	6.51	7.12	6.08	5.04	2.63	5.40	5.69
Ka	..	..	..	..	..	..	..
La	..	..	..	..	..	..	..
Mo	..	..	..	..	..	..	..
Il	6.84	5.27	4.60	3.68	7.19	4.28	4.43
Ap	0.63	1.24	1.29	1.52	0.46	1.41	0.88
Ns	..	..	..	..	..	..	..

\*Total iron determined as FeO

TABLE B-3

ELECTRON MICROPROBE ANALYSES OF IGNEOUS ROCKS  
CHRISTMAS MOUNTAINS, TEXAS  
FINE-GRAINED BIOTITE - TITANAUGITE GABBRO

	276	109-5	83	53H	293	136	283	80FG
SiO <sub>2</sub>	45.40	45.62	46.57	47.68	48.34	48.63	49.03	51.63
TiO <sub>2</sub>	4.19	4.10	4.40	3.21	3.31	3.42	2.99	2.56
Al <sub>2</sub> O <sub>3</sub>	15.90	15.28	15.11	18.42	16.71	17.76	18.31	17.53
FeO* <sup>3</sup>	11.99	12.64	12.74	9.98	11.08	10.65	9.83	9.38
MgO	4.50	4.21	3.82	2.99	3.62	4.23	3.18	2.93
CaO	10.30	11.30	10.76	9.86	8.72	8.42	9.08	7.05
Na <sub>2</sub> O	4.33	3.91	4.03	5.86	5.13	4.48	4.75	5.27
K <sub>2</sub> O	1.57	1.65	1.42	1.49	1.82	1.60	1.73	2.67
P <sub>2</sub> O <sub>5</sub>	1.82	1.29	1.15	0.51	1.27	0.81	1.10	0.98
TOTAL	100.00	100.00	100.00	100.00	100.00	100.00	100.00	100.00

C.I.P.W. NORM -- MOLE PERCENT

Or	9.38	9.89	8.55	8.73	10.78	9.45	10.25	15.68
Ab	21.92	17.19	23.24	19.57	28.13	30.44	30.16	34.65
An	19.49	19.55	19.27	19.37	17.22	23.68	23.54	16.24
Wo	..	..	..	..	..	..	..	..
Ac	..	..	..	..	..	..	..	..
Di	16.05	23.00	21.95	20.68	14.22	10.30	11.45	9.81
Hy	..	..	..	..	..	..	..	..
Ol	13.02	10.77	10.17	6.56	11.59	13.73	10.59	10.55
Lc	..	..	..	..	..	..	..	..
Ne	10.39	11.06	8.14	19.60	10.79	5.93	7.52	7.49
Ka	..	..	..	..	..	..	..	..
La	..	..	..	..	..	..	..	..
Mo	..	..	..	..	..	..	..	..
Il	5.90	5.80	6.24	4.43	4.62	4.77	4.17	3.55
Ap	3.85	2.73	2.44	1.06	2.66	1.69	2.31	2.03
Ns	..	..	..	..	..	..	..	..

\*Total iron determined as FeO

TABLE B-4

ELECTRON MICROPROBE ANALYSES OF IGNEOUS ROCKS  
CHRISTMAS MOUNTAINS, TEXAS  
PORPHYRITIC OLIVINE-BIOTITE-TITANAUGITE GABBRO

	39-3	69	39-1
SiO <sub>2</sub>	49.26	49.29	50.04
TiO <sub>2</sub>	2.12	2.31	1.95
Al <sub>2</sub> O <sub>3</sub>	20.79	20.34	21.08
FeO* <sub>3</sub>	8.09	8.00	7.38
MgO	2.56	2.42	2.19
CaO	9.15	8.60	8.74
Na <sub>2</sub> O	5.10	5.77	5.55
K <sub>2</sub> O	1.93	2.28	2.16
P <sub>2</sub> O <sub>5</sub>	1.00	0.99	0.91
TOTAL	100.00	100.00	100.00

## C.I.P.W. NORM—MOLE PERCENT

Or	11.32	13.31	12.58
Ab	27.21	24.82	27.55
An	27.91	22.57	25.88
Wo	..	..	..
Ac	..	..	..
Di	8.48	10.49	8.84
Hy	..	..	..
Ol	9.19	7.80	7.61
Lc	..	..	..
Ne	10.89	15.77	12.98
Ka	..	..	..
La	..	..	..
Mo	..	..	..
Il	2.93	3.18	2.68
Ap	2.07	2.04	1.88
Ns	..	..	..

\*Total iron determined as FeO

TABLE B-5

ELECTRON MICROPROBE ANALYSES OF IGNEOUS ROCKS  
CHRISTMAS MOUNTAINS, TEXAS  
SYENITE

	294A	315	81	288A	53D	39-1D
SiO <sub>2</sub>	55.93	56.79	58.71	61.43	54.83	60.77
TiO <sub>2</sub>	1.15	1.54	0.71	0.56	1.25	0.83
Al <sub>2</sub> O <sub>3</sub>	17.00	18.96	16.69	17.75	20.07	18.02
FeO*	9.22	5.64	8.32	6.05	5.59	4.03
MgO	1.12	1.31	0.66	0.40	0.86	0.55
CaO	4.30	3.40	3.21	2.57	3.24	1.84
Na <sub>2</sub> O	7.08	6.40	6.68	6.53	6.85	6.56
K <sub>2</sub> O	3.80	5.53	4.77	4.54	7.08	7.24
P <sub>2</sub> O <sub>5</sub>	0.40	0.43	0.25	0.17	0.23	0.16
TOTAL	100.00	100.00	100.00	100.00	100.00	100.00

C.I.P.W. NORM -- MOLE PERCENT

Or	22.10	31.96	27.78	26.36	40.53	41.66
Ab	38.64	34.30	43.32	55.62	15.43	37.51
An	3.33	6.53	1.45	5.65	3.02	..
Wo	..	..	..	..	..	..
Ac	..	..	..	..	..	..
Di	12.08	5.80	10.13	4.64	8.90	6.28
Hy	..	..	..	..	..	..
Ol	7.10	5.31	6.34	5.41	3.43	2.48
Lc	..	..	..	..	..	..
Ne	14.35	13.14	9.48	1.21	26.54	9.97
Ka	..	..	..	..	..	..
La	..	..	..	..	..	..
Mo	..	..	..	..	..	..
Il	1.58	2.09	0.98	0.76	1.69	1.12
Ap	0.82	0.87	0.51	0.35	0.46	0.33
Ns	..	..	..	..	..	..

\*Total iron determined as FeO

Figure B-1 Electron microprobe analyses of igneous rocks plotted on Harker variation diagrams

- a.  $\text{Al}_2\text{O}_3$  against  $\text{SiO}_2$
- b.  $\text{TiO}_2$  against  $\text{SiO}_2$
- c. Total iron as FeO against  $\text{SiO}_2$
- d. MgO against  $\text{SiO}_2$
- e. CaO against  $\text{SiO}_2$
- f.  $\text{Na}_2\text{O}$  against  $\text{SiO}_2$
- g.  $\text{K}_2\text{O}$  against  $\text{SiO}_2$
- h.  $\text{P}_2\text{O}_5$  against  $\text{SiO}_2$

IGNEOUS ROCKS, CHRISTMAS MOUNTAINS, TEXAS

7.500E 01

WEIGHT 2

2.000E 01

ALZ 03

1.500E 01

1.000E 01

5.000E 00

G.C

5 3.500E 01

4.500E 01

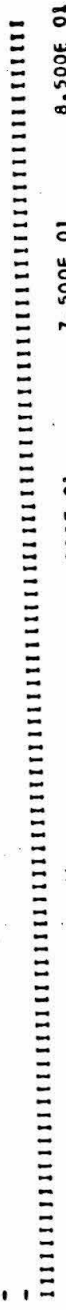
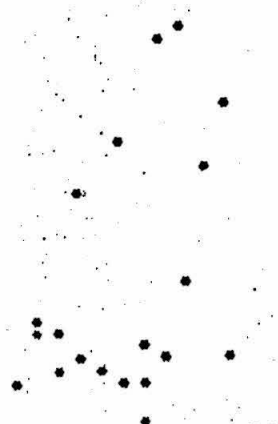
5.500E 01

6.500E 01

7.500E 01

8.500E 01

WEIGHT & SIZE



IGNEOUS ROCKS, CHRISTMAS MOUNTAINS, TEXAS

1.000E 01

WEIGHT %

8.000E 00

TIO2

6.000E 00

4.000E 00

2.000E 00

0.0

|||||

W.P.P. = 5 3.500E 01

4.500E 01

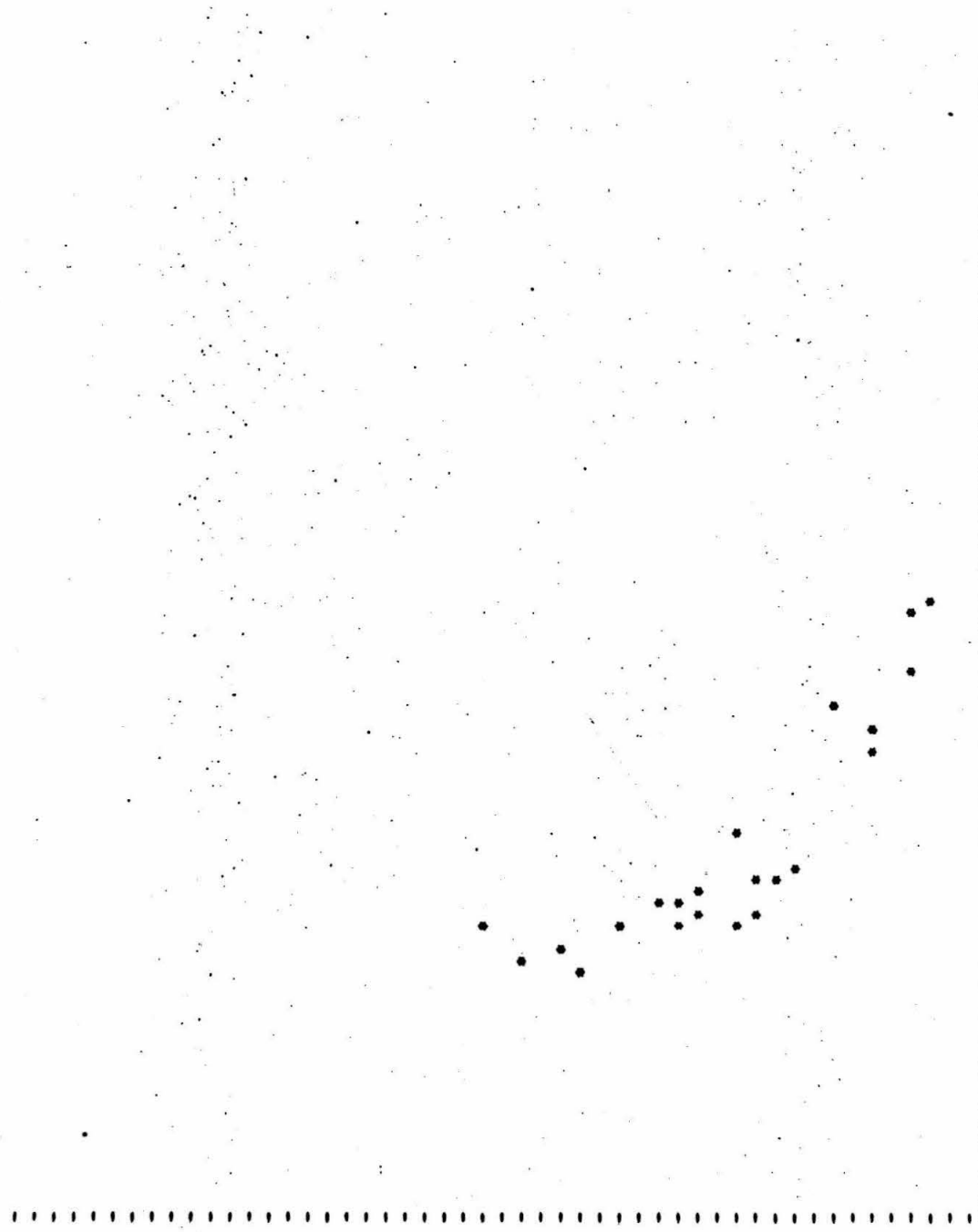
5.500E 01

6.500E 01

7.500E 01

8.500E 01

HEIGHT % SiO2



IGNEOUS ROCKS, CHRISTMAS MOUNTAINS, TEXAS

2.500E 01

WEIGHT %

2.000E 01

FeO

1.500E 01

1.000E 01

5.000E 00

0.0

5 3.500E 01

8.500E 01

7.500E 01

6.500E 01

5.500E 01

4.500E 01

WEIGHT % SiO2



IGNEOUS ROCKS, CHRISTMAS MOUNTAINS, TEXAS

2.500E 01

X  
E  
I  
G  
M  
T  
Z

2.000E 01

N  
G  
O

1.500E 01

1.000E 01

5.000E 00

0.0

HPN# 5 3.500E 01

4.500E 01

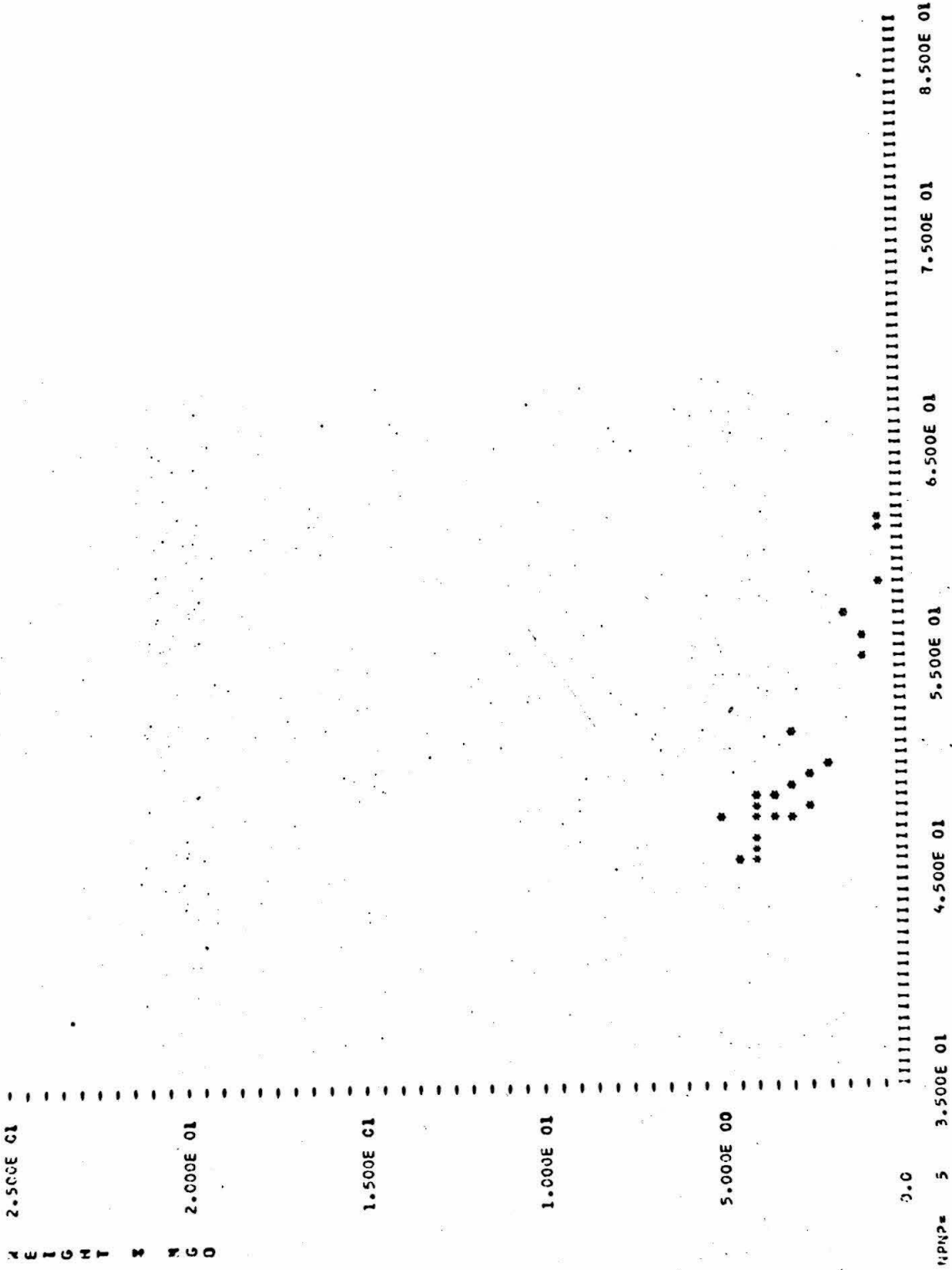
5.500E 01

6.500E 01

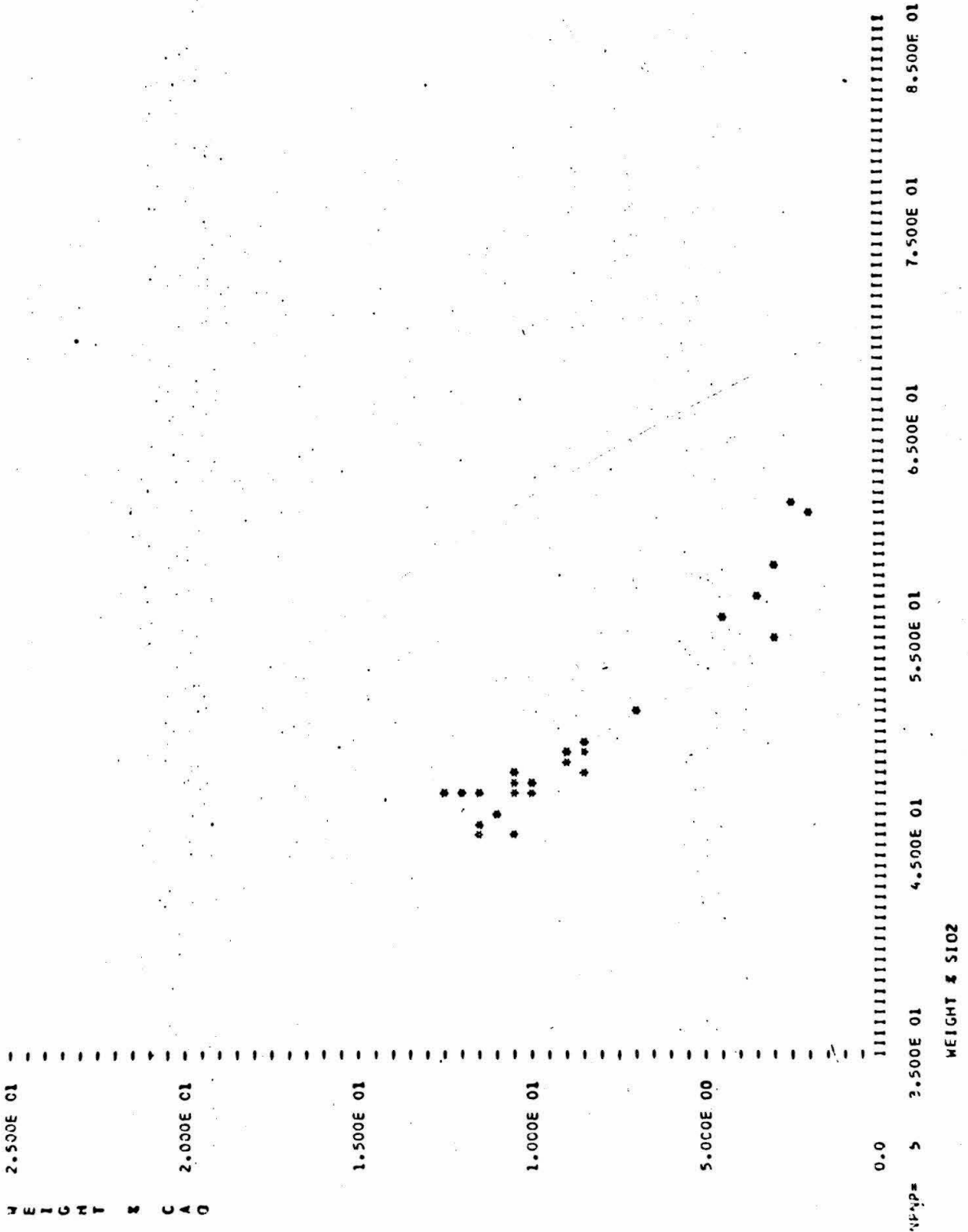
7.500E 01

8.500E 01

WEIGHT X S102



IGNEOUS ROCKS, CHRISTMAS MOUNTAINS, TEXAS



IGNEOUS ROCKS, CHRISTMAS MOUNTAINS, TEXAS

1.000E C1

HEIGHT 3  
N  
A  
Z  
O

8.000E C0

6.000E 00

4.000E 00

2.000E 00

0.0



NPWP= 5

3.500E 01 4.500E 01 5.500E 01 6.500E 01 7.500E 01 8.500E 01

WEIGHT 3 S102

IGNEOUS ROCKS, CHRISTMAS MOUNTAINS, TEXAS

1.000E 01

H  
E  
I  
G  
H  
T  
Z  
K  
2  
0

8.000E 00

6.000E 00

4.000E 00

2.000E 00

0.0

PIP# 5

3.500E 01

4.500E 01

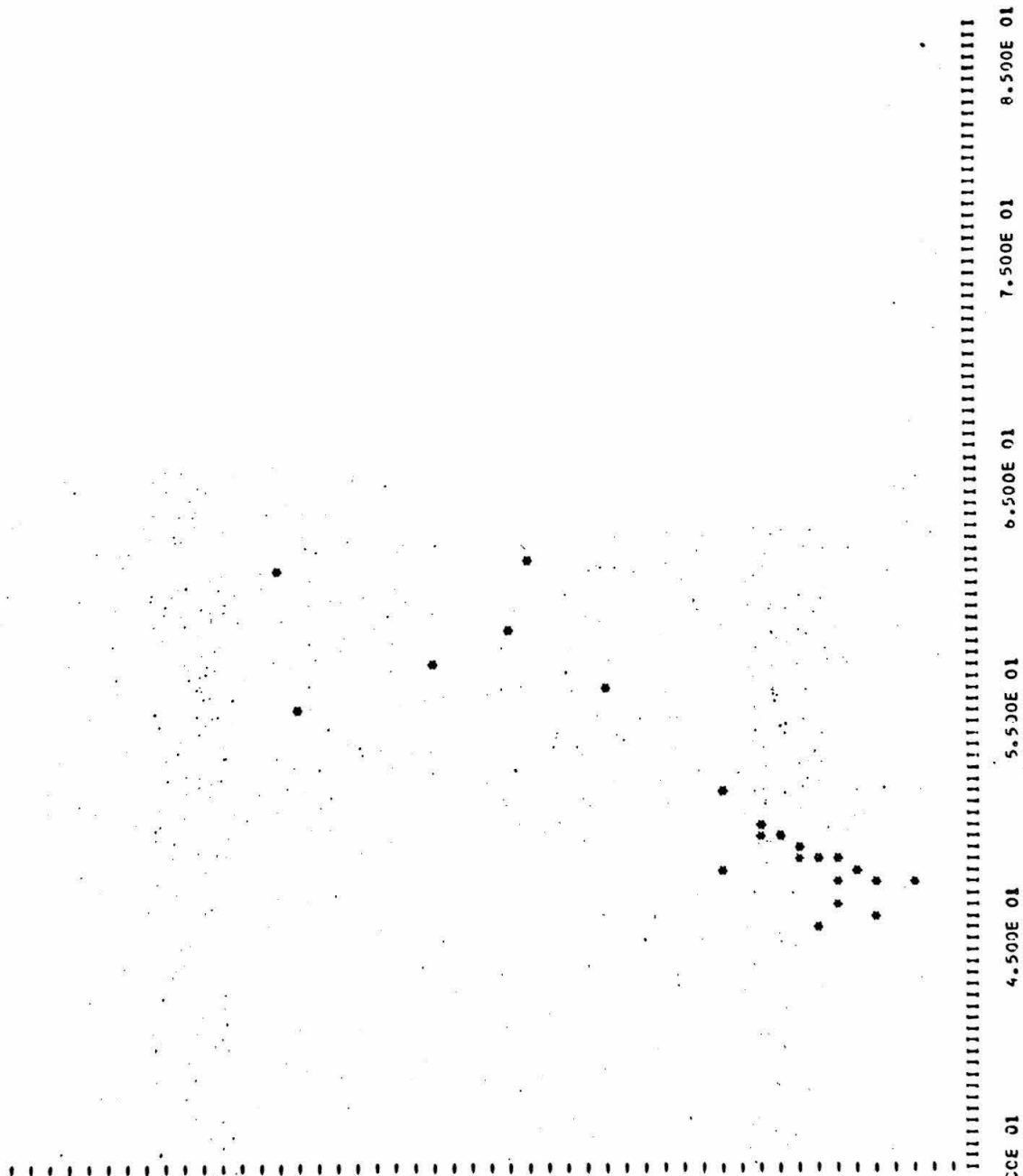
5.500E 01

6.500E 01

7.500E 01

8.500E 01

WEIGHT % SiO2



IGNEOUS ROCKS, CHRISTMAS MOUNTAINS, TEXAS

5.000E 00

WEIGHT

4.000E 00

3.000E 00

2.000E 00

1.000E 00

0.0

||||| 3.500E 01 4.500E 01 5.500E 01 6.500E 01 7.500E 01 8.500E 01

WEIGHT % S102

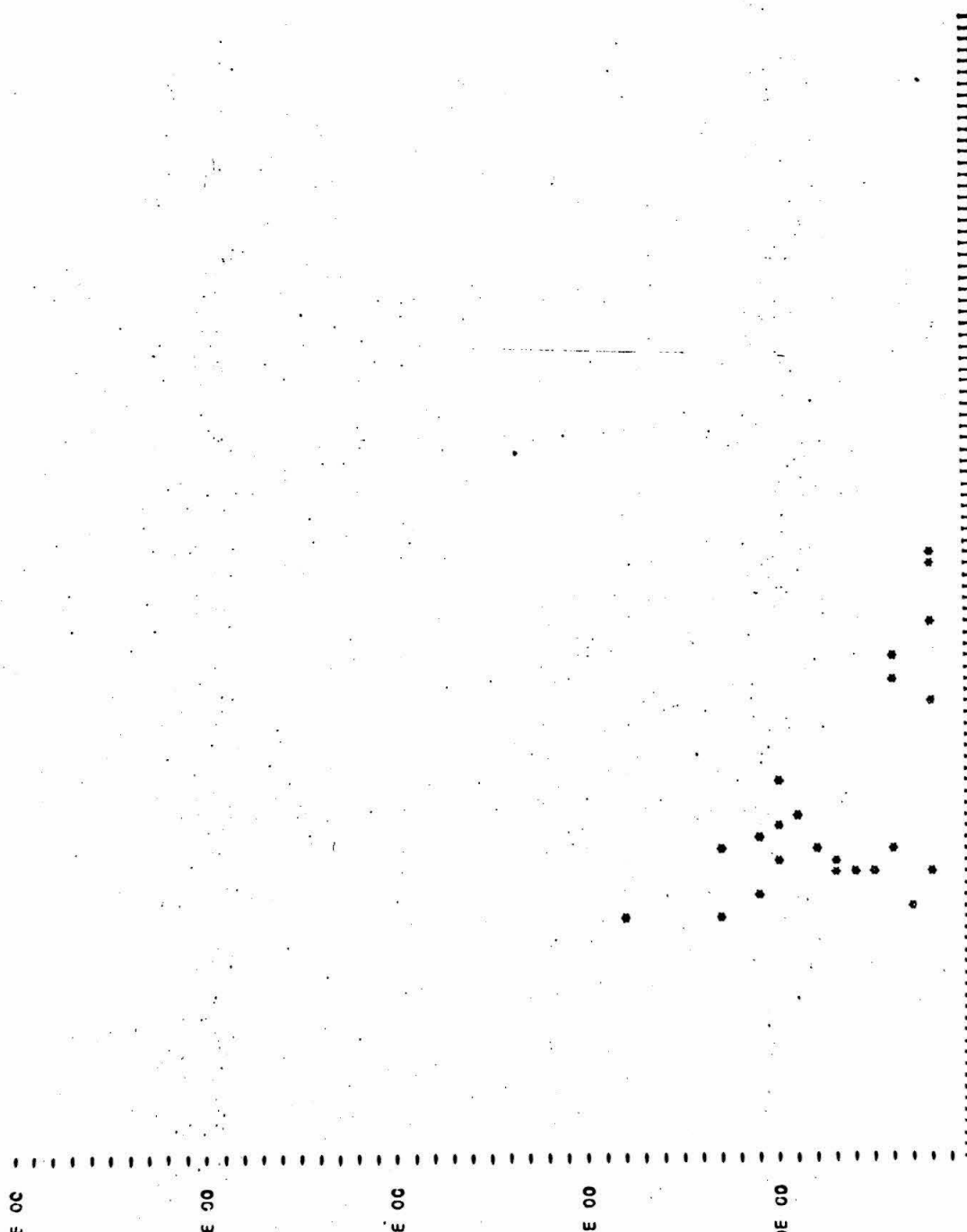
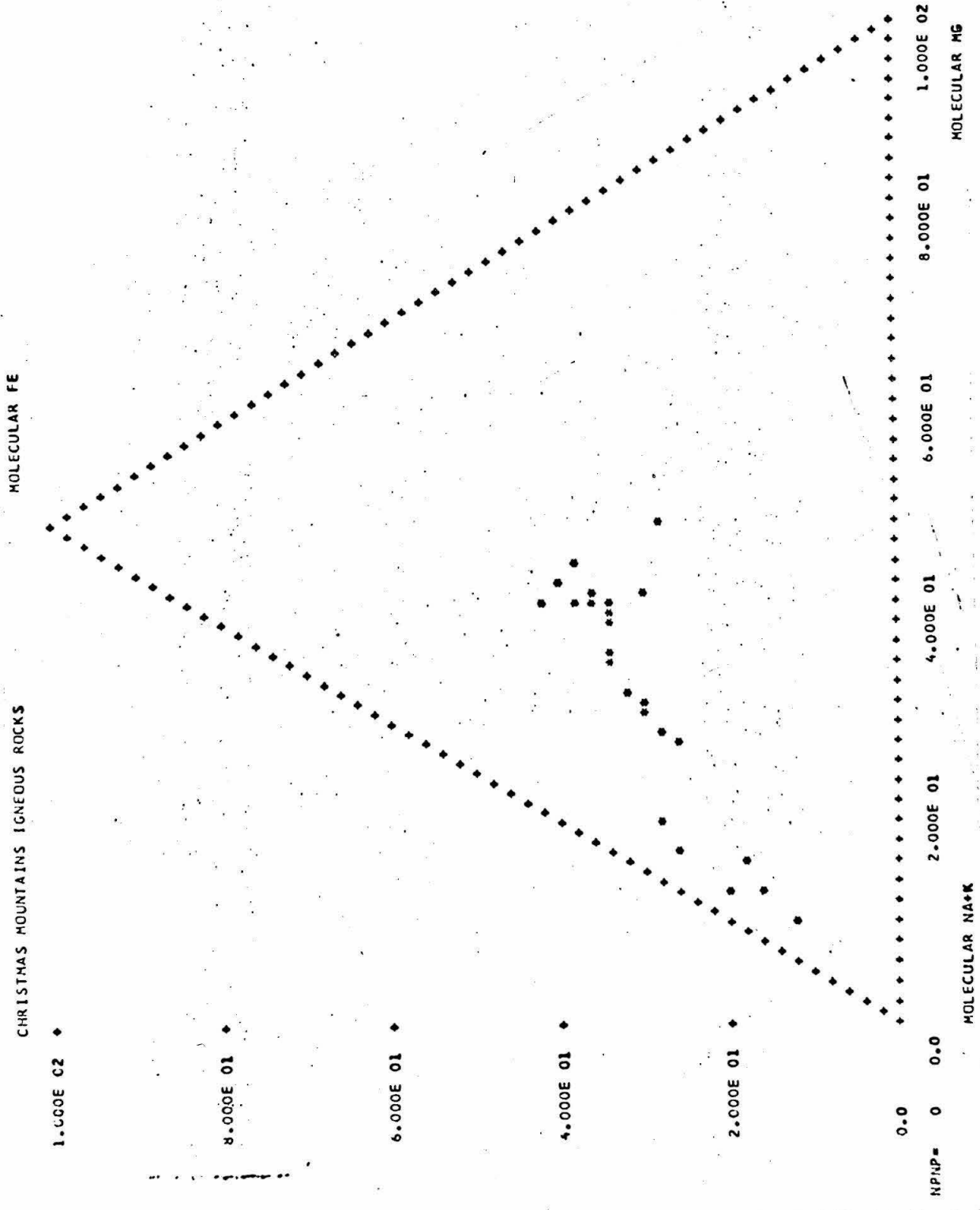


Figure B-2 Electron microprobe analyses of igneous rocks, plotted as molecular proportions of total alkalies, total iron and magnesium.



MOLECULAR FE

CHRISTMAS MOUNTAINS IGNEOUS ROCKS

1.000E 02

8.000E 01

6.000E 01

4.000E 01

2.000E 01

0.0

NP1P= 0 0.0

1.000E 02

8.000E 01

6.000E 01

4.000E 01

2.000E 01

MOLECULAR MG

MOLECULAR NA+K

Figure B-3 Electron microprobe analyses of igneous rocks plotted as molecular proportions of calcium, sodium and potassium.

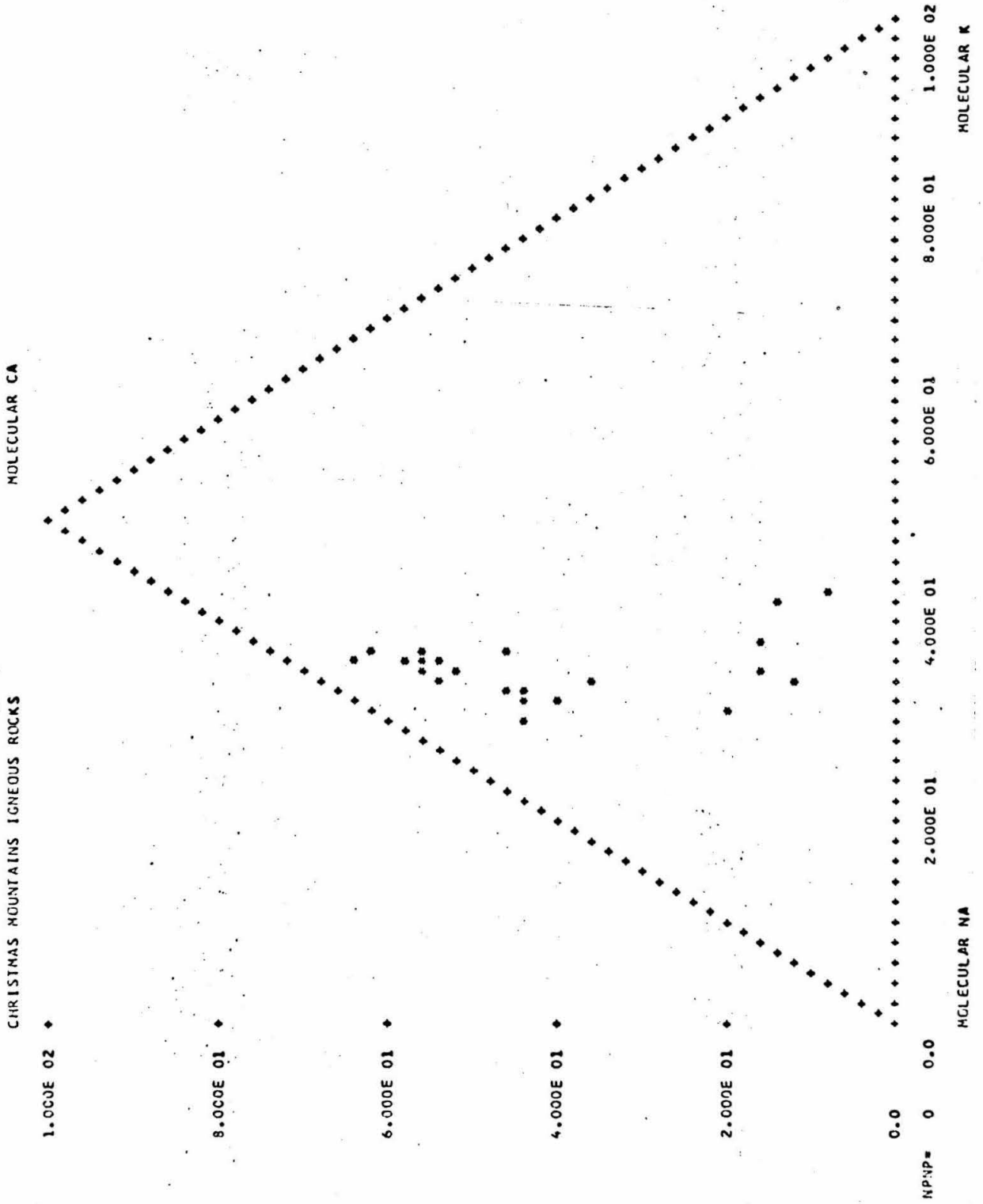


TABLE B-6  
ANALYZED IGNEOUS ROCKS  
CHRISTMAS MOUNTAINS, TEXAS

	OLIVINE	CLINO- PYROXENE	AMPHIBOLE	BIOTITE	GARNET	MAGNETITE	ILMENITE	"OPAQUE"	SPHENE	PEROVSKITE	PLAGIOCLASE	ALKALI FELDSPAR	NEPHELINE	ANALCITE	WOLLASTONITE	APATITE
CONTAMINATED ROCKS DERIVED FROM COARSE-GRAINED GABBRO																
CM-6-3B	..	50	..	..	..	..	..	..	3	..	..	..	35	..	10	2
CM-29A	2	50	..	..	..	x	x	1	1	..	..	5	32	1	7	1
CM-29B	..	70	..	..	..	x	..	1	2	..	2	..	22	..	2	1
CM-33-6	..	55	..	..	..	x	..	1	2	..	..	..	30	..	10	2
CM-33-11	..	80	..	5	..	x	x	7	..	..	2	..	4	1	..	1
CM-33-13	3	40	..	10	..	x	x	15	..	..	16	..	16	..	..	1
CM-29-70	..	30	..	2	..	x	..	1	3	..	2	35	25	..	..	2
CM-28	..	x	..	..	..	..	..	x	x	..	..	x	x	..	x	x
CONTAMINATED ROCKS DERIVED FROM FINE-GRAINED GABBRO																
CM-85D	..	85	..	..	..	..	..	3	..	..	6	..	1	..	..	5
CM-111FG	..	75	..	..	..	x	..	1	1	..	15	4	4	..	..	1
CM-111CG	..	50	..	..	..	x	..	1	2	..	..	25	17	..	..	5
CM-303-1A	..	30	..	..	..	..	..	..	..	..	30	..	8	..	30	1
CM-320	2	7	5	1	..	x	x	4	..	..	10	50	20	..	..	1
CM-141-4	..	25	..	..	..	..	..	2	5	..	..	50	7	..	10	1
CM-141-8	..	40	..	..	..	..	..	1	2	..	..	42	10	..	..	5
CM-340	..	15	..	..	5	..	..	2	3	1	..	..	70	..	2	2
CONTAMINATED ROCKS DERIVED FROM PORPHYRITIC GABBRO																
CM-33-12	2	32	tr	tr	..	x	x	4	..	..	40	..	20	..	..	1
CM-40-4	2	20	..	1	..	-	-	6	..	..	45	..	25	..	..	1
CM-40-6	..	40	..	..	..	..	..	1	1	..	27	15	15	..	..	1
CM-40-7	2	35	..	..	..	..	..	1	1	..	35	5	15	5	..	1
CM-41-6	1	20	..	..	..	x	..	4	1	..	65	..	5	3	..	2
CM-8-9	2	40	..	..	..	x	x	6	..	..	30	5	15	..	..	2
CM-8-1B	1	60	..	..	..	x	..	1	10	..	..	20	..	5	..	3
CM-40-8	..	80	..	..	..	-	-	2	1	..	..	..	15	..	..	2
CM-41-2	1	55	..	..	..	x	..	1	1	..	..	15	30	3	3	2
CM-62CB	..	x	..	..	..	..	..	..	..	..	..	x	..	..	x	..

TABLE B-6 (CONTINUED)  
ANALYZED IGNEOUS ROCKS  
CHRISTMAS MOUNTAINS, TEXAS

CONTAMINATED ROCKS DERIVED FROM COARSE-GRAINED GABBRO

- CM-6-3B WOLLASTONITE-NEPHELINE PYROXENITE  
Collected 1 meter from contact with skarn in Del Carmen Limestone. Sample contains small xenoliths of skarn that were analyzed separately (CM-6-3BX, Table C-7).
- CM-29A OLIVINE-WOLLASTONITE-NEPHELINE PYROXENITE  
CM-29B ANORTHITE-WOLLASTONITE-NEPHELINE PYROXENITE  
CM-29-70 AUGITE-NEPHELINE SYENITE  
Pyroxenite samples were collected within 1 meter of contact with skarn in Del Carmen Limestone. Sample CM-29B contains small skarn xenoliths that were analyzed separately (CM-29BX, Table C-7). ANORTHITE in CM-29B is restricted to zone 2 mm in width, at contact with skarn xenolith. Sample CM-29-70 is from dike, 15 cm in width, intruded along pyroxenite-skarn contact.
- CM-33-6 WOLLASTONITE-NEPHELINE PYROXENITE  
Collected 30 cm from contact with skarn in Del Carmen Limestone
- CM-33-11 PLAGIOCLASE-NEPHELINE-BIOTITE PYROXENITE  
CM-33-13 OLIVINE-BIOTITE-NEPHELINE GABBRO  
Collected 2 m and 3 m, respectively, from contact with skarn in Del Carmen Limestone
- CM-28 WOLLASTONITE-NEPHELINE SYENITE  
Dike intrusive into pyroxenite at contact with skarn in Del Carmen Limestone

CONTAMINATED ROCKS DERIVED FROM FINE-GRAINED GABBRO

- CM-85D PLAGIOCLASE PYROXENITE  
Sample of 2.5 cm wide dike intrusive into idocrase-wollastonite skarn in xenolith
- CM-111FG NEPHELINE-PLAGIOCLASE PYROXENITE  
CM-111CG NEPHELINE-ALKALI FELDSPAR PYROXENITE  
Pyroxenite in contact with skarn at north contact of xenolith (Figure 2, Chapter 5). CM-111FG is from 1-2.5 cm wide zone of fine-grained pyroxenite in direct contact with skarn. CM-111CG is coarse-grained leucocratic pyroxenite sampled 3-13 cm from skarn contact.

TABLE B-6 (CONTINUED)  
ANALYZED IGNEOUS ROCKS  
CHRISTMAS MOUNTAINS, TEXAS

CM-303-1A NEPHELINE-DIOPSIDE-ANORTHITE-WOLLASTONITE ROCK  
Collected at contact with skarn in Santa Elena Limestone

CM-320 BIOTITE-OLIVINE-KAERSUTITE-AUGITE-NEPHELINE SYENITE  
Coarse-grained syenite intrusive into fine-grained gabbro, 5 m from skarn.

CM-141-4 WOLLASTONITE-TITANAUGITE-NEPHELINE SYENITE

CM-141-8 TITANAUGITE-NEPHELINE SYENITE

Both samples from dikes intrusive into skarn xenolith.

CM-340 WOLLASTONITE-GARNET-TITANAUGITE-NEPHELINE SYENITE

Dike 10 cm wide, intrusive and idocrase skarn. Sample from float

CONTAMINATED ROCKS DERIVED FROM PORPHYRITIC GABBRO

CM-33-12 OLIVINE-NEPHELINE GABBRO

Sample from 30 cm dike intrusive into pyroxenite derived from coarse-grained gabbro, 3 m from skarn.

CM-40-4 OLIVINE-NEPHELINE GABBRO

CM-40-6 NEPHELINE GABBRO

CM-40-7 OLIVINE-NEPHELINE GABBRO

CM-40-8 NEPHELINE PYROXENITE

Samples collected from 2.5 m wide dike intrusive into Santa Elena Limestone. Septum of skarn, 2 m thick separates derivatives of porphyritic gabbro from pyroxenite derived from coarse-grained gabbro. Samples collected at following points in dike, measured from contact with skarn septum: 40-4 200 cm, 40-6 75 cm, 40-7 40 cm and 40-8, 6 cm.

41-6 OLIVINE-NEPHELINE GABBRO

41-2 OLIVINE-WOLLASTONITE-NEPHELINE PYROXENITE

Samples collected from same dike as CM-40-n, but dike 1.5 m wide at this locality. Sample CM-41-6 collected 15 cm below contact with skarn that is in contact with marble. Sample CM-41-2 collected 5 cm from contact with skarn of the septum.

CM-8-1B OLIVINE-ALKALI FELDSPAR PYROXENITE

CM-8-9 OLIVINE-NEPHELINE GABBRO

Collected from dike 1 m thick, intruded into Sue Peaks Limestone (Figure 1, Chapter 5). CM-8-1A collected in contact with skarn. CM-8-9 collected 45 cm below skarn contact.

TABLE B-6 (CONTINUED)  
ANALYZED IGNEOUS ROCKS  
CHRISTMAS MOUNTAINS, TEXAS

CM-62CB WOLLASTONITE SYENITE  
Dike intrusive into skarn in Sue Peaks Limestone

TABLE B-7

ELECTRON MICROPROBE ANALYSES OF IGNEOUS ROCKS  
CHRISTMAS MOUNTAINS, TEXAS  
CONTAMINATED ROCKS DERIVED FROM COARSE-GRAINED GABBRO

	33-6	29A	29B	33-11	28	29-70
SiO <sub>2</sub>	44.47	44.57	45.68	45.73	48.57	52.26
TiO <sub>2</sub>	3.20	2.09	2.54	3.46	1.53	1.29
Al <sub>2</sub> O <sub>3</sub>	13.11	15.33	13.73	11.05	18.58	18.92
FeO*	10.38	7.46	8.78	11.65	4.85	4.96
MgO	4.05	4.30	4.66	6.80	1.04	1.79
CaO	17.98	16.62	17.49	15.70	15.64	7.44
Na <sub>2</sub> O	3.72	5.01	3.93	2.33	5.06	5.37
K <sub>2</sub> O	1.95	2.84	1.78	2.04	4.06	7.30
P <sub>2</sub> O <sub>5</sub>	1.14	1.78	1.41	1.24	0.67	0.67
TOTAL	100.00	100.00	100.00	100.00	100.00	100.00

C.I.P.W. NORM—MOLE PERCENT

Or	..	..	5.87	12.24	21.46	41.10
Ab	..	..	..	1.64	..	..
An	13.45	10.79	14.61	13.94	15.75	5.83
Wo	2.46	..	2.28	..	14.43	..
Ac	..	..	..	..	..	..
Di	46.02	39.67	45.87	45.60	16.26	20.77
Hy	..	..	..	..	..	..
Ol	..	..	..	7.31	..	0.14
Lc	9.32	13.24	3.71	..	1.73	0.81
Ne	20.23	26.62	21.17	11.75	26.89	28.23
Ka	..	..	..	..	..	..
La	0.41	2.55	..	..	..	..
Mo	..	0.59	..	..	..	..
Il	4.50	2.87	3.55	4.90	2.10	1.75
Ap	2.40	3.67	2.94	2.63	1.39	1.36
Ns	..	..	..	..	..	..

\*Total iron determined as FeO

TABLE B-8

ELECTRON MICROPROBE ANALYSES OF IGNEOUS ROCKS  
CHRISTMAS MOUNTAINS, TEXAS  
CONTAMINATED ROCKS DERIVED FROM FINE-GRAINED GABBRO

	85D	111FG	303-1A	141-8	320	111CG	141-4
SiO <sub>2</sub>	39.02	46.60	47.74	47.80	48.69	50.37	52.13
TiO <sub>2</sub>	3.13	2.14	1.04	1.56	3.30	1.47	1.92
Al <sub>2</sub> O <sub>3</sub>	4.82	12.56	14.96	13.69	16.15	16.34	14.40
FeO* <sup>3</sup>	14.90	10.00	5.41	8.00	12.24	5.96	6.21
MgO	7.47	4.18	1.73	3.97	3.03	3.54	0.91
CaO	24.80	17.42	25.54	14.98	8.25	12.00	13.67
Na <sub>2</sub> O	0.86	3.83	2.45	5.49	5.05	4.18	5.61
K <sub>2</sub> O	0.04	1.40	0.80	2.24	2.16	4.70	4.61
P <sub>2</sub> O <sub>5</sub>	4.96	1.87	0.33	2.27	1.13	1.44	0.54
TOTAL	100.00	100.00	100.00	100.00	100.00	100.00	100.00

C.I.P.W. NORM—MOLE PERCENT

Or	..	8.36	4.76	13.08	12.87	27.44	26.99
Ab	..	4.63	1.83	6.85	27.93	5.01	10.33
An	9.62	13.08	27.81	6.07	15.12	11.84	0.50
Wo	..	0.44	27.42	0.15	..	..	15.95
Ac	..	..	..	..	..	..	..
Di	53.85	48.52	23.73	41.87	14.89	30.18	18.71
Hy	..	..	..	..	..	..	..
Ol	5.29	..	..	..	11.57	1.27	..
Lc	0.18	..	..	..	..	..	..
Ne	4.86	18.01	12.27	25.12	10.61	19.27	23.76
Ka	..	..	..	..	..	..	..
La	..	..	..	..	..	..	..
Mo	10.80	..	..	..	..	..	..
Il	4.56	3.01	1.46	2.15	4.63	2.02	2.66
Ap	10.84	3.95	0.71	4.70	2.38	2.98	1.11
Ns	..	..	..	..	..	..	..

\*Total iron determined as FeO

TABLE B-9

ELECTRON MICROPROBE ANALYSES OF IGNEOUS ROCKS  
CHRISTMAS MOUNTAINS, TEXAS  
CONTAMINATED ROCKS DERIVED FROM PORPHYRITIC GABBRO

	40-8	8-9	41-2	8-1A	40-6A	40-7	33-12	40-4	41-6
SiO <sub>2</sub>	43.44	44.84	44.86	45.18	46.89	47.12	47.32	47.95	48.47
TiO <sub>2</sub>	2.74	3.28	2.50	5.49	2.64	1.74	2.96	2.50	2.01
Al <sub>2</sub> O <sub>3</sub>	10.78	14.04	10.65	9.24	16.54	19.76	19.00	20.33	21.89
FeO*	12.57	13.90	11.41	10.77	8.92	6.54	7.54	8.62	7.39
MgO	4.86	3.51	4.43	3.50	3.12	2.64	3.99	2.54	1.49
CaO	19.65	13.80	17.84	19.76	15.49	15.88	14.20	9.83	11.06
Na <sub>2</sub> O	2.84	3.38	3.81	1.90	3.40	3.81	3.50	4.68	5.04
K <sub>2</sub> O	1.27	1.63	2.47	2.36	1.80	1.73	1.48	2.54	2.04
P <sub>2</sub> O <sub>5</sub>	1.85	1.62	2.03	1.81	1.20	0.78	0.91	1.01	0.61
TOTAL	100.00	100.00	100.00	100.00	100.00	100.00	100.00	100.00	100.00

C.I.P.W. NORM -- MOLE PERCENT

Or	..	9.85	..	14.47	10.74	10.19	8.73	14.91	11.96
Ab	..	9.80	..	3.93	7.82	5.14	11.98	18.48	17.46
An	13.19	18.76	4.72	10.14	24.78	31.61	31.71	26.87	30.83
Wo	..	..	0.52	12.33	..	1.77	..	..	..
Ac	..	..	..	..	..	..	..	..	..
Di	50.87	32.41	53.42	38.95	35.87	29.92	26.14	12.08	15.69
Hy	..	..	..	..	..	..	..	..	..
Ol	0.06	8.29	..	..	0.73	..	5.04	8.08	3.61
Lc	6.15	..	11.79	..	..	..	..	..	..
Ne	15.62	12.75	20.75	8.29	13.80	17.34	11.64	14.01	16.41
Ka	..	..	..	..	..	..	..	..	..
La	..	..	0.25	..	..	..	..	..	..
Mo	6.28	..	..	..	..	..	..	..	..
Il	3.90	4.67	3.52	7.95	3.71	2.41	2.87	3.46	2.78
Ap	3.94	3.46	4.29	3.94	2.54	1.62	1.90	2.11	1.26
Ns	..	..	..	..	..	..	..	..	..

\*Total iron determined as FeO

Figure B-4 Electron microprobe analyses of contaminated igneous rocks plotted on Harker variation diagrams

- a.  $\text{Al}_2\text{O}_3$  against  $\text{SiO}_2$
- b.  $\text{TiO}_2$  against  $\text{SiO}_2$
- c. Total iron As FeO against  $\text{SiO}_2$
- d. MgO against  $\text{SiO}_2$
- e. CaO against  $\text{SiO}_2$
- f.  $\text{Na}_2\text{O}$  against  $\text{SiO}_2$
- g.  $\text{K}_2\text{O}$  against  $\text{SiO}_2$
- h.  $\text{P}_2\text{O}_5$  against  $\text{SiO}_2$

IGNEOUS ROCKS, CHRISTMAS MOUNTAINS, TEXAS--CONTAMINATED

2.500E 01

W E I G H T 3

2.000E 01

A L O 3

1.500E 01

1.000E 01

5.000E 00

0.C

HPHP= 5

3.500E 01

4.500E 01

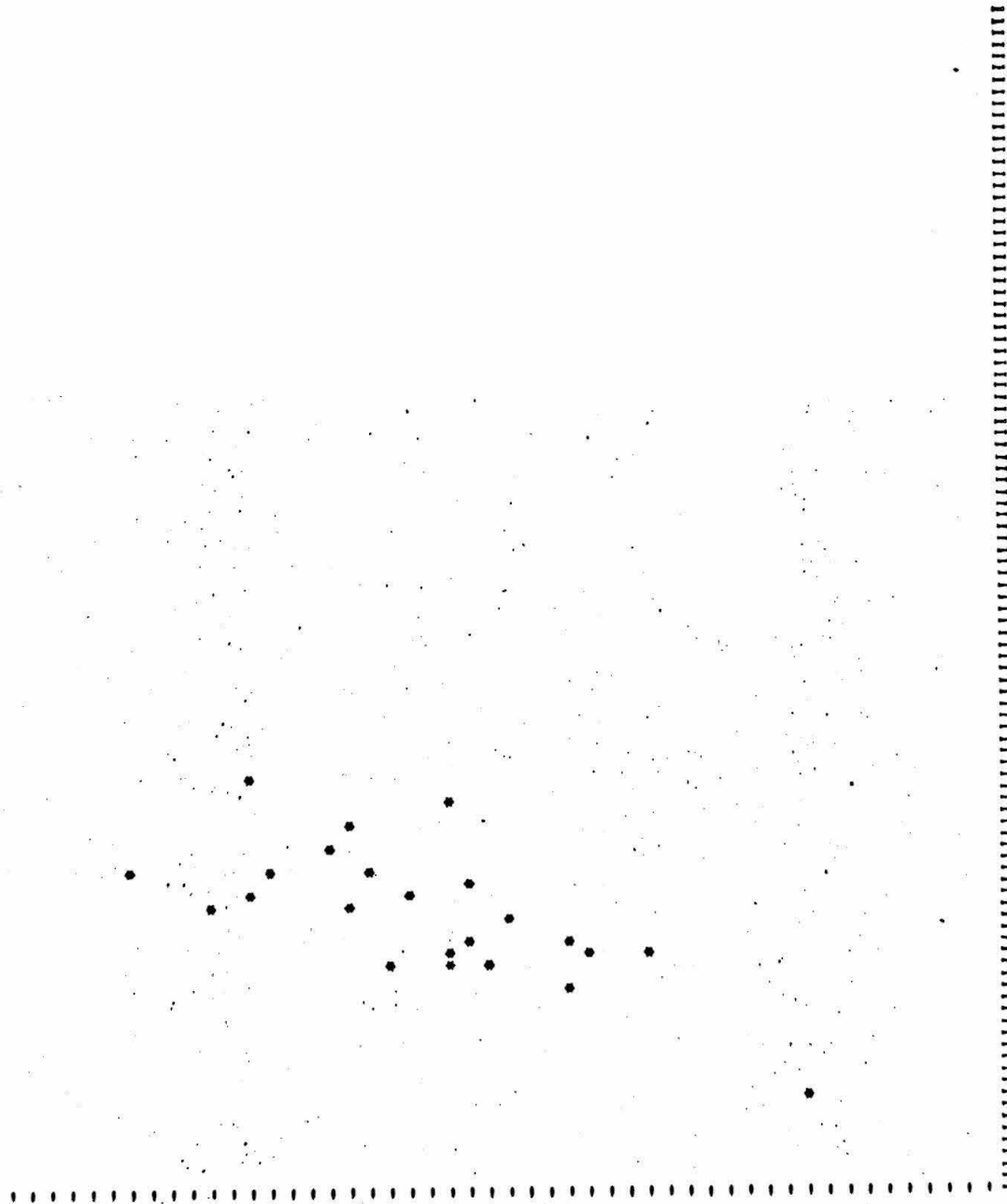
5.500E 01

6.500E 01

7.500E 01

8.500E 01

WEIGHT % S102



IGNEOUS ROCKS, CHRISTMAS MOUNTAINS, TEXAS--CONTAMINATED

W 1.000E 01

C  
I  
G  
H  
T  
Z  
T  
I  
D  
D  
Z

8.000E 00

6.000E 00

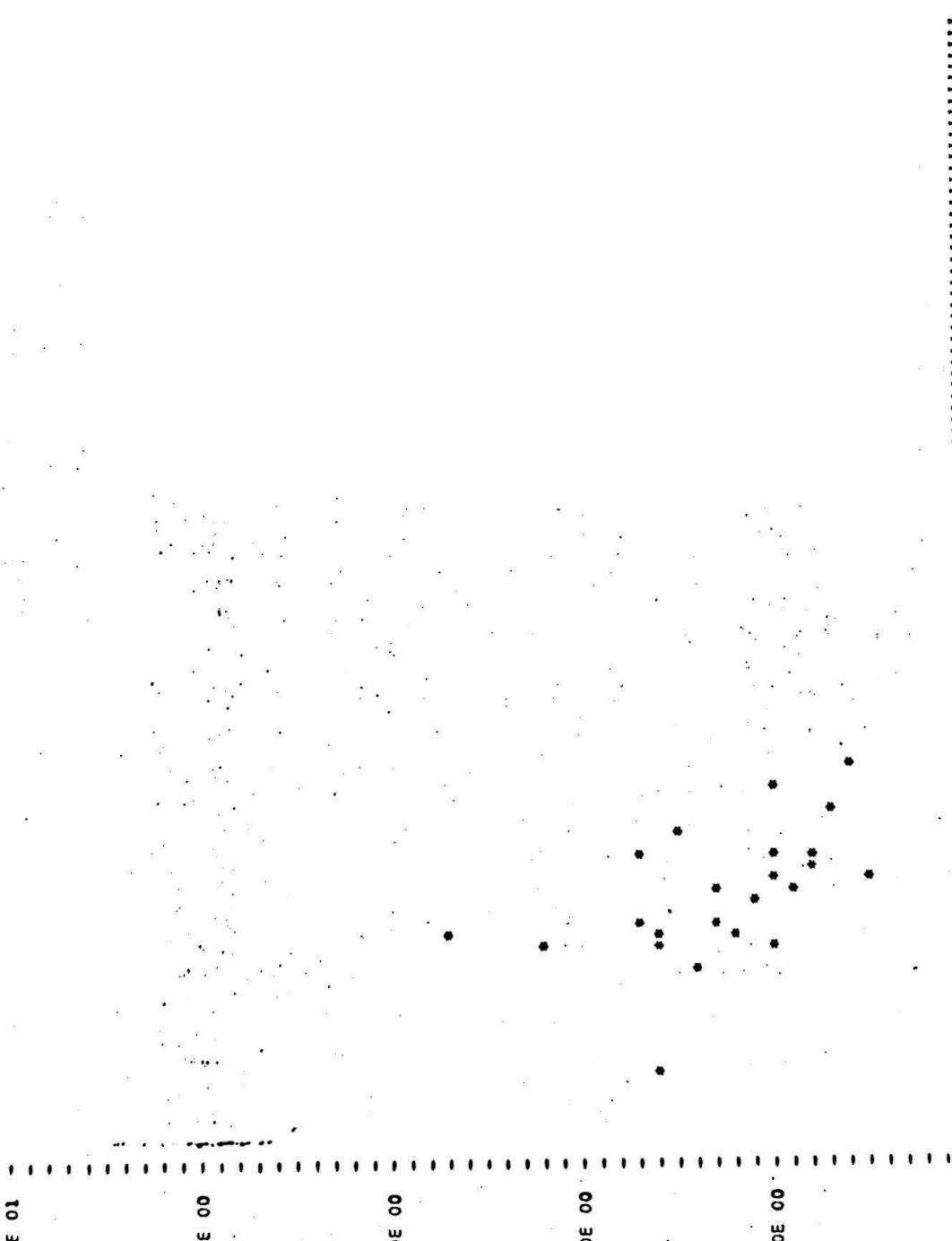
4.000E 00

2.000E 00

0.0

HP/P= 5 3.500E 01 4.500E 01 5.500E 01 6.500E 01 7.500E 01 8.500E 01

WEIGHT % S102



IGNEOUS ROCKS, CHRISTMAS MOUNTAINS, TEXAS--CONTAMINATED

2.500E C1

WEIGHT %

2.000E 01

FE O

1.500E 01

1.000E 01

5.000E 00

0.0

MPAP= 5

3.500E 01

4.500E 01

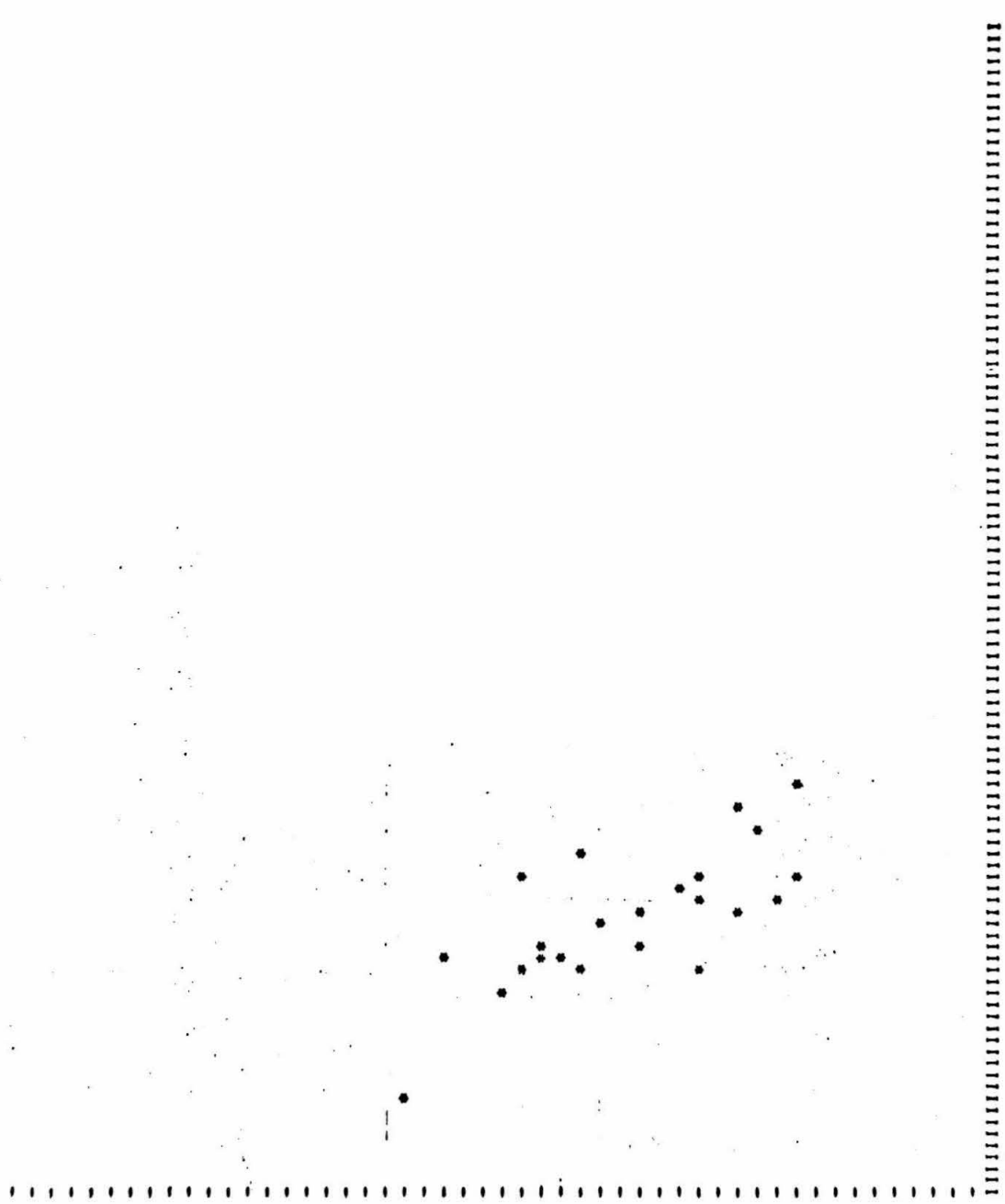
5.500E 01

6.500E 01

7.500E 01

8.500E 01

WEIGHT % ST02



IGNEOUS ROCKS, CHRISTMAS MOUNTAINS, TEXAS--CONTAMINATED

M 2.500E C1

E  
I  
G  
M  
Y  
Z

M 2.000E 01

M  
G  
O

1.500E 01

1.000E 01

5.000E 00

0.0

HP# 5 3.500E 01

4.500E 01

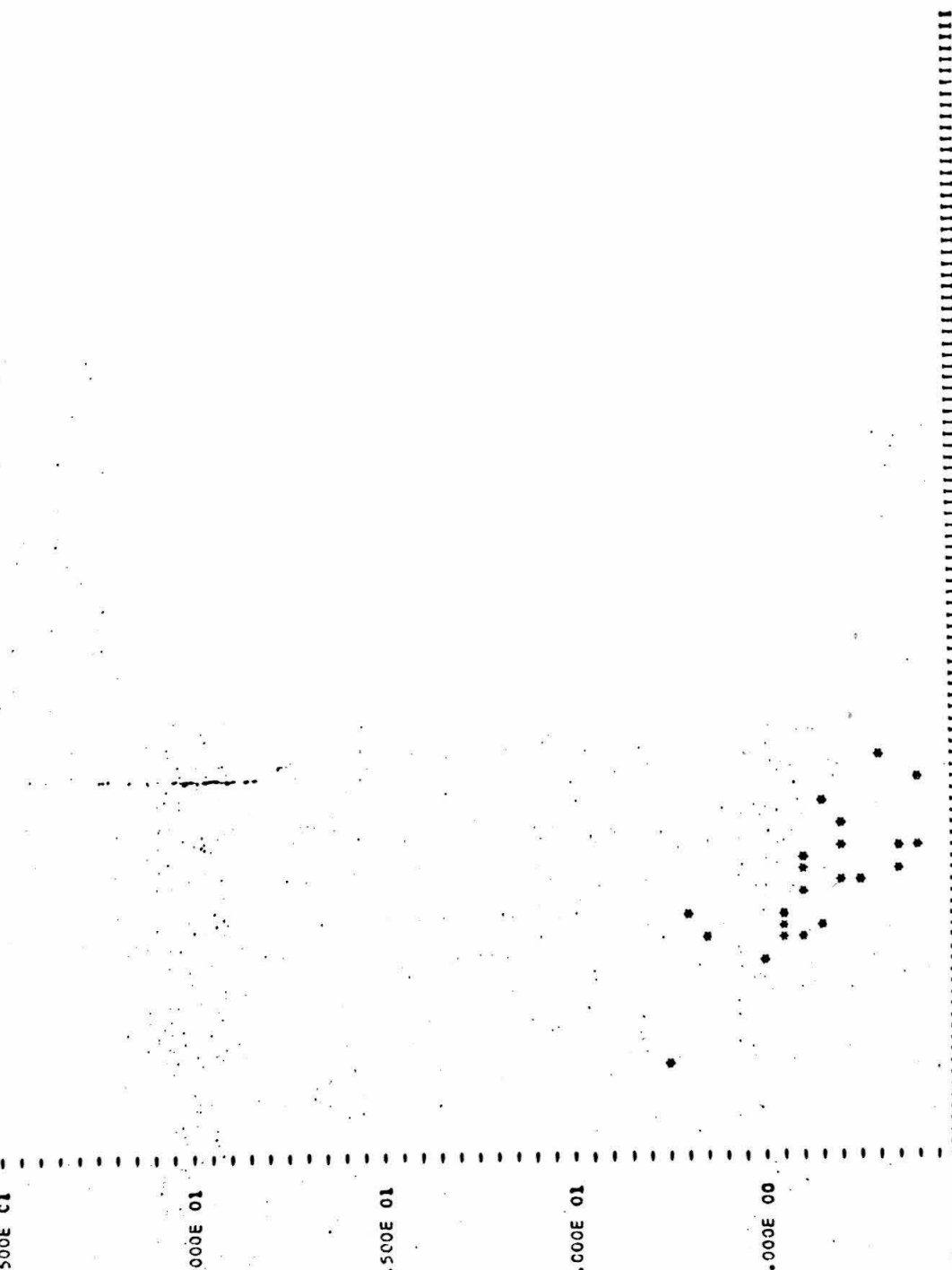
5.500E 01

6.500E 01

7.500E 01

8.500E 01

WEIGHT & SI02



IGNEOUS ROCKS, CHRISTMAS MOUNTAINS, TEXAS--CONTAMINATED

2.500E 01

E I C M T 3

2.000E 01

C A O

1.500E 01

1.000E 01

5.000E 00

0.0

MFNP# 6

3.500E 01

4.500E 01

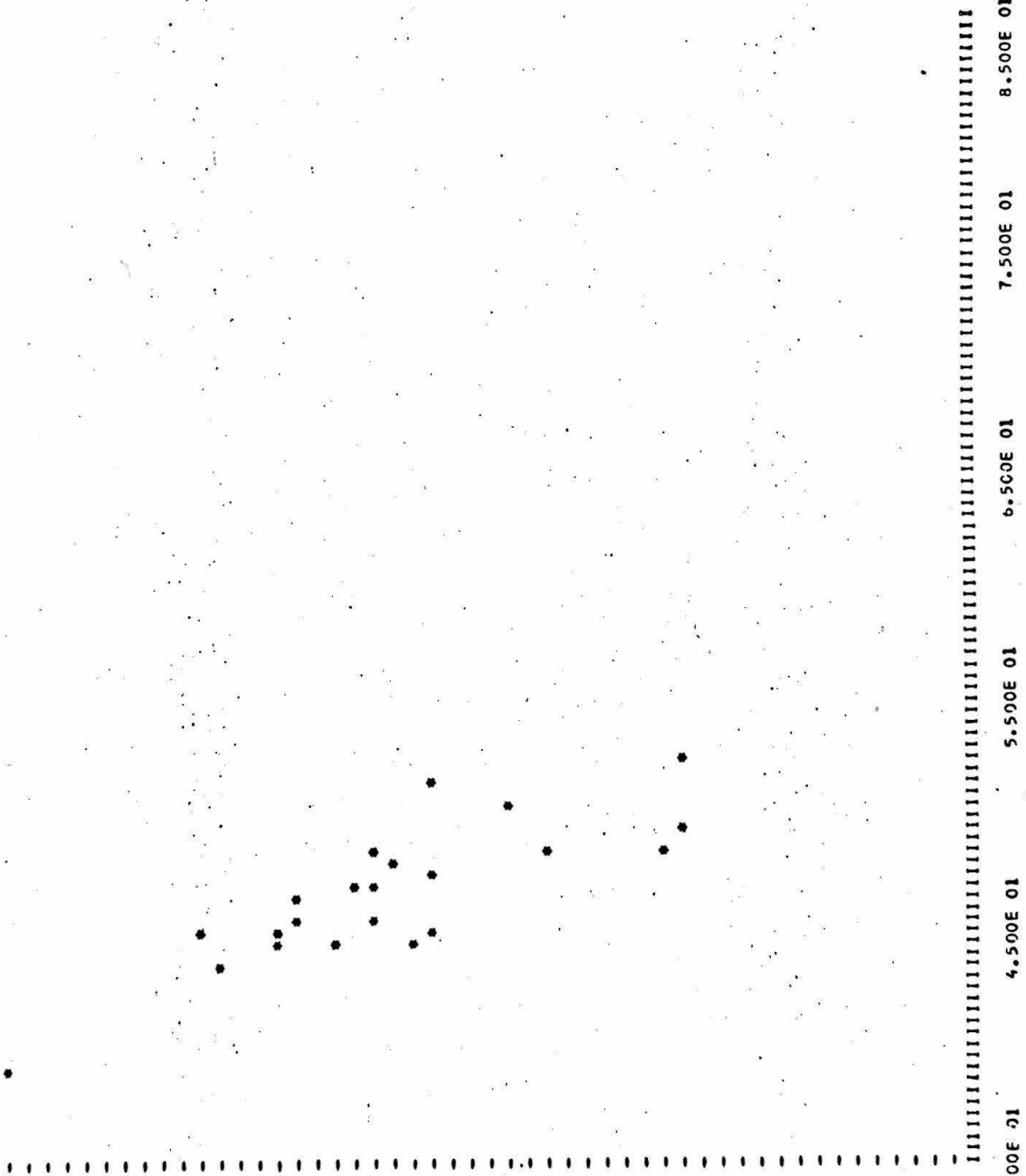
5.500E 01

6.500E 01

7.500E 01

8.500E 01

WEIGHT X S102



IGNEOUS ROCKS, CHRISTMAS MOUNTAINS, TEXAS--CONTAMINATED

1 1.000E 01  
2  
3  
4  
5  
6  
7  
8  
9  
0  
N A 8.000E 00  
2 0

6.000E 00

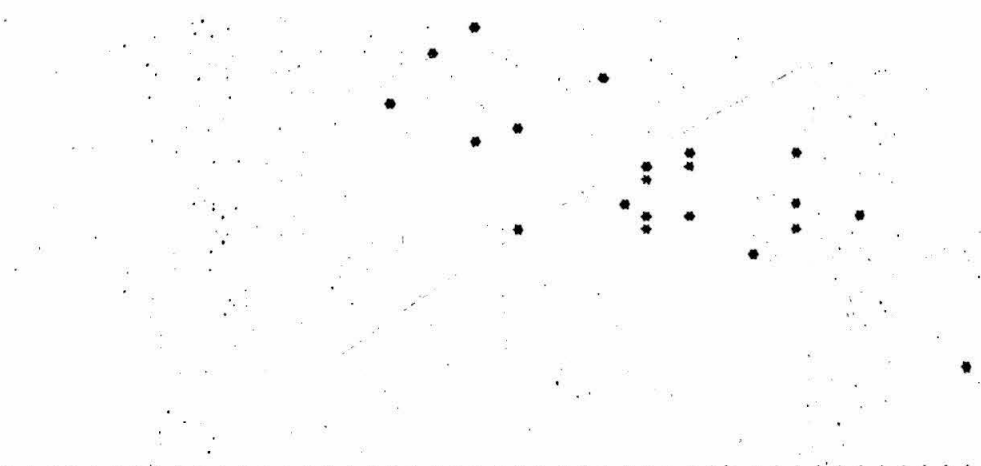
4.000E 00

2.000E 00

0.0

HP'P= 5 3.500E 01 4.500E 01 5.500E 01 6.500E 01 7.500E 01 8.500E 01

WEIGHT & SIC2





IGNEOUS ROCKS, CHRISTMAS MOUNTAINS, TEXAS--CONTAMINATED



5.000E 00  
 4.000E 00  
 3.000E 00  
 2.000E 00  
 1.000E 00  
 0.0

MFP= 5 3.500E 01 4.500E 01 5.500E 01 6.500E 01 7.500E 01 8.500E 01  
 WEIGHT X 102

Figure B-5 Electron microprobe analyses of contaminated igneous rocks, plotted as molecular proportions of total alkalis, total iron and magnesium.



Figure B-6 Electron microprobe analyses of contaminated igneous rocks plotted as molecular proportions of calcium, sodium and potassium.

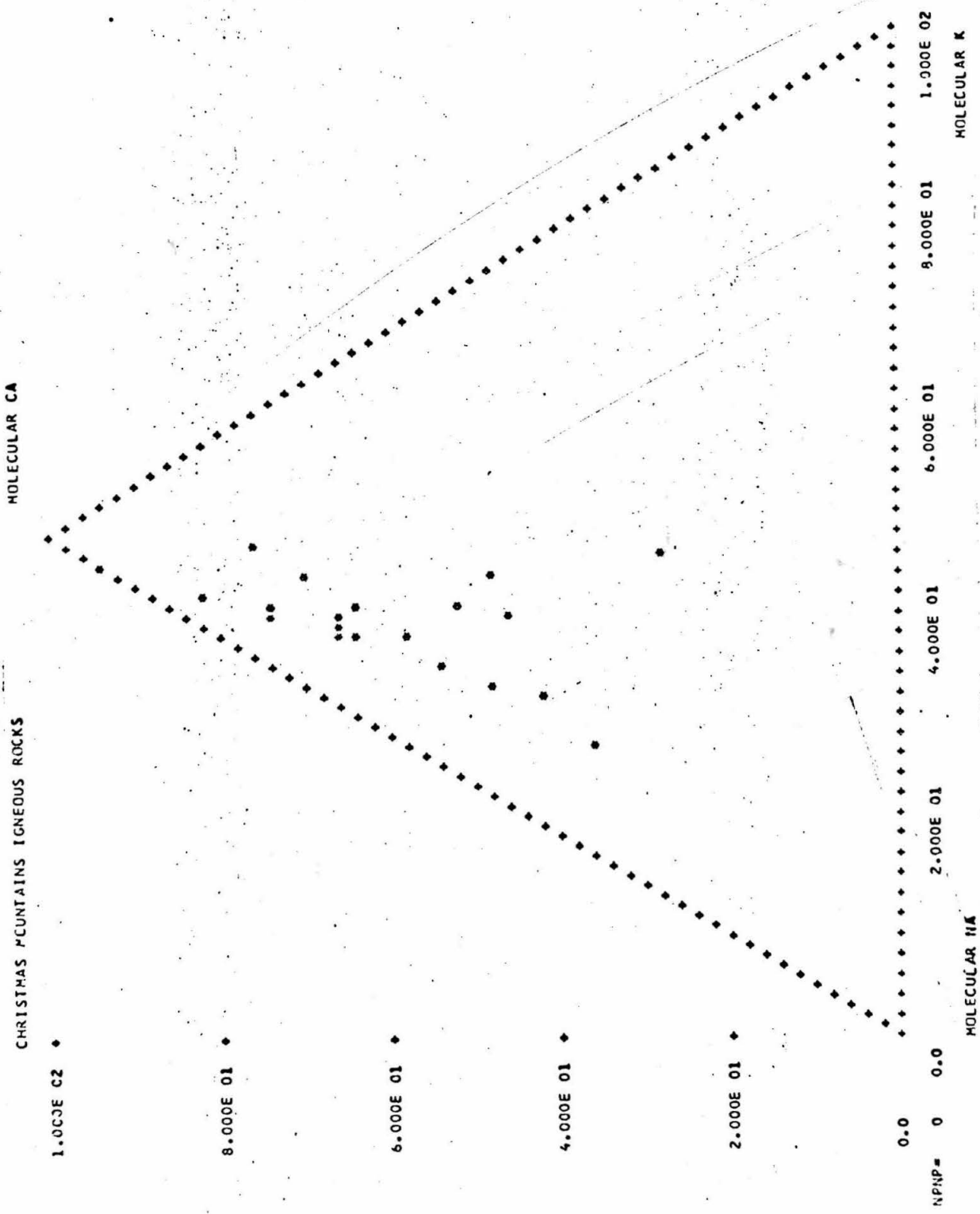




Table B-10

MINERALS FROM IGNEOUS ROCKS, CHRISTMAS MOUNTAINS, TEXAS

184000 188000 174000 186000 187000 174000  
WEIGHT PER CENT OXIDES

	C.O	0.0	C.O	0.0	C.O	0.0	C.O	0.0	C.O	0.0
S102	35.505	34.423	36.660	35.971	36.432	35.267				
TI02	0.014	0.065	0.0	0.074	0.072	0.0				
ZR02	0.0	0.0	0.0	0.0	0.0	0.0				
AL2O3	0.016	0.051	0.0	0.0	0.0	0.053				
V2O3	0.0	0.0	0.0	0.0	0.0	0.0				
CR2O3	0.0	0.0	0.0	0.0	0.0	0.0				
FE2O3	41.188	43.401	31.857	37.347	31.950	39.556				
MNO	1.395	1.655	0.979	1.164	0.961	1.034				
MGO	24.148	22.308	32.193	27.569	32.172	25.001				
CAO	0.0	0.0	0.0	0.0	0.0	0.0				
BAO	0.0	0.0	0.0	0.0	0.0	0.0				
NA2O	0.0	0.0	0.0	0.0	0.0	0.0				
K2O	0.0	0.0	0.0	0.0	0.0	0.0				
P2O5	0.0	0.0	0.0	0.0	0.0	0.0				

TOTAL 102.265 101.903 101.689 102.225 101.586 100.911

FORMULA PROPORTION CATIONS

O	0.0	0.0	0.0	0.0	0.0	0.0
S14+	0.994	0.979	0.981	0.986	0.976	0.993
T14+	0.000	0.001	0.0	0.002	0.001	0.0
ZR4+	0.0	0.0	0.0	0.0	0.0	0.0
AL3+	0.001	0.002	0.0	0.0	0.0	0.002
V.3+	0.0	0.0	0.0	0.0	0.0	0.0
CR3+	0.0	0.0	0.0	0.0	0.0	0.0
FE3+	0.0	0.0	0.0	0.0	0.0	0.0
FE2+	0.964	1.032	0.713	0.856	0.716	0.931
MN2+	0.033	0.040	0.022	0.027	0.022	0.025
MG2+	1.008	0.946	1.294	1.130	1.285	1.049
CA2+	0.0	0.0	0.0	0.0	0.0	0.0
BA2+	0.0	0.0	0.0	0.0	0.0	0.0
NA+	0.0	0.0	0.0	0.0	0.0	0.0
K+	0.0	0.0	0.0	0.0	0.0	0.0
P.5+	0.0	0.0	0.0	0.0	0.0	0.0
OXYGEN	3.995	3.981	3.981	3.987	3.978	3.994

184000 CM-41-6 OL-NE-OR GABBR0 OLIVINE NOVEMBER 1970  
 186000 CM-320 OL-CPX-AMP-NE SYN OLIVINE NOVEMBER 1970  
 176000 CM-8-18 PYROXENITE OLIVINE SEPT-OCT 1970  
 186000 CM-8-9 PLAG PYROXENITE OLIVINE NOVEMBER 1970  
 187000 CM-41-2 NEPH PYROXENITE OLIVINE NOVEMBER 1970  
 174000 CM-33-13 PYROXENITE OLIVINE SEPT-OCT 1970



Table B-11

MINERALS FROM IGNEOUS ROCKS, CHRISTMAS MOUNTAINS, TEXAS

	1631CC	164100	173100	1601CC	165100	169100	170100
	WEIGHT PER CENT OXIDES						
O	0.0	0.0	0.0	0.0	0.0	0.0	0.0
SiO2	50.652	52.193	48.246	50.994	52.500	49.088	50.173
TiO2	1.370	1.451	2.277	1.115	1.020	0.465	0.588
ZrO2	0.0	0.0	0.0	0.0	0.0	0.0	0.0
Al2O3	2.390	2.939	5.063	2.342	1.482	1.390	1.419
V2O3	0.0	0.0	0.0	0.0	0.0	0.0	0.0
Cr2O3	0.075	0.031	0.000	0.084	0.041	0.041	0.039
FeO	9.290	8.969	9.582	10.017	14.966	18.510	15.974
MnO	0.300	0.290	0.213	0.267	0.758	0.861	0.551
MgO	13.123	12.917	11.347	12.458	8.964	7.353	8.533
CaO	22.020	22.357	22.671	22.418	20.207	21.177	21.893
Na2O	0.0	0.0	0.0	0.0	0.0	0.0	0.0
K2O	0.668	0.833	0.800	0.763	2.055	1.041	0.949
P2O5	0.0	0.0	0.0	0.0	0.0	0.0	0.0
TOTAL	99.888	101.980	100.289	100.456	101.993	99.926	100.118

FORMULA PROPORTION CATIONS

O	0.0	0.0	0.0	0.0	0.0	0.0	0.0
Si4+	1.893	1.909	1.805	1.901	1.959	1.907	1.927
Ti4+	0.038	0.040	0.064	0.031	0.029	0.014	0.017
Zr4+	0.0	0.0	0.0	0.0	0.0	0.0	0.0
Al3+	0.105	0.127	0.223	0.103	0.065	0.064	0.064
V3+	0.0	0.0	0.0	0.0	0.0	0.0	0.0
Cr3+	0.002	0.001	0.003	0.002	0.001	0.001	0.001
Fe3+	0.0	0.0	0.0	0.0	0.0	0.0	0.0
Fe2+	0.290	0.274	0.300	0.312	0.467	0.601	0.513
Mn2+	0.009	0.009	0.007	0.008	0.024	0.028	0.018
Mg2+	0.731	0.704	0.633	0.692	0.499	0.426	0.488
Ca2+	0.882	0.876	0.909	0.895	0.808	0.881	0.901
Na+	0.048	0.059	0.058	0.055	0.149	0.078	0.071
K+	0.0	0.0	0.0	0.0	0.0	0.0	0.0
P5+	0.0	0.0	0.0	0.0	0.0	0.0	0.0
OXYGEN	5.361	5.984	5.953	5.957	5.947	5.914	5.941
163100	CM-69	PLAG	PORPHYRY	PYROXENE	SEPT-OCT	1970	
164100	CM-39-1	PLAG	PORPHYRY	PYROXENE	SEPT-OCT	1970	
173100	CM-33-12	PLAG	PORPHYRY	PYROXENE	SEPT-OCT	1970	
167100	CM-39-6	SYENITE	DIKE	PYROXENE	SEPT-OCT	1970	
165100	CM-39-1	SYENITE	DIKE	PYROXENE	SEPT-OCT	1970	
169100	CM-91	SYENITE	CG	PYROXENE	SEPT-OCT	1970	
170100	CM-294A	SYENITE	FG	PYROXENE	SEPT-OCT	1970	

Table B-11

MINERALS FROM IGNEOUS ROCKS, CHRISTMAS MOUNTAINS, TEXAS

	182100	182150	183100	183150	185100	188100	189100	184100	187100
WEIGHT PER CENT OXIDES									
O	0.0	0.0	0.0	0.0	0.0	0.0	0.0	0.0	0.0
SiO2	49.552	43.771	48.347	48.795	49.890	51.621	51.680	48.476	46.199
TiO2	1.517	3.619	0.897	2.381	0.787	0.717	1.075	2.111	2.323
ZrO2	0.0	0.0	0.0	0.0	0.0	0.0	0.0	0.0	0.0
Al2O3	2.920	8.673	2.513	5.373	1.272	2.388	2.209	4.369	5.392
V2O3	0.0	0.0	0.0	0.0	0.0	0.0	0.0	0.0	0.0
CR2O3	0.0	0.0	0.0	0.0	0.0	0.0	0.0	0.0	0.0
FE2O3	0.0	0.0	0.0	0.0	0.0	0.0	0.0	0.0	0.0
FE0	15.705	13.243	22.914	10.329	21.646	9.325	8.602	13.238	13.041
MNO	0.432	0.253	0.470	0.286	0.638	0.376	0.411	0.380	0.383
MGO	8.190	7.857	3.796	11.414	4.937	12.959	13.305	9.502	9.252
CAO	22.045	23.139	20.782	22.785	18.579	22.604	22.076	22.538	22.605
BAO	0.0	0.0	0.0	0.0	0.0	0.0	0.0	0.0	0.0
NA2O	1.155	0.589	1.480	0.771	3.271	0.806	1.421	0.777	0.827
K2O	0.040	0.016	0.035	0.017	0.038	0.023	0.032	0.022	0.033
P2O5	0.0	0.0	0.0	0.0	0.0	0.0	0.0	0.0	0.0
TOTAL	101.536	101.161	101.235	101.150	101.280	100.819	100.814	101.414	100.035

FORMULA PROPORTION CATIONS

O	0.0	0.0	0.0	0.0	0.0	0.0	0.0	0.0	0.0
Si4+	1.874	1.657	1.869	1.815	1.915	1.908	1.898	1.822	1.757
Ti4+	0.043	0.103	0.026	0.067	0.023	0.020	0.030	0.060	0.066
Zr4+	0.0	0.0	0.0	0.0	0.0	0.0	0.0	0.0	0.0
Al3+	0.130	0.387	0.116	0.192	0.058	0.104	0.096	0.193	0.242
V3+	0.0	0.0	0.0	0.0	0.0	0.0	0.0	0.0	0.0
CR3+	0.0	0.0	0.0	0.0	0.0	0.0	0.0	0.0	0.0
FE3+	0.0	0.0	0.0	0.0	0.0	0.0	0.0	0.0	0.0
FE2+	0.497	0.419	0.748	0.321	0.695	0.288	0.264	0.416	0.415
MN2+	0.014	0.008	0.016	0.009	0.018	0.012	0.013	0.012	0.012
MG2+	0.462	0.443	0.221	0.633	0.282	0.714	0.728	0.532	0.524
CA2+	8.894	0.939	0.870	9.908	0.764	8.895	8.869	9.907	9.921
BA2+	0.0	0.0	0.0	0.0	0.0	0.0	0.0	0.0	0.0
NA+	0.085	0.043	0.112	0.056	0.243	0.058	0.101	0.057	0.061
K+	0.002	0.001	0.002	0.001	0.002	0.001	0.001	0.001	0.002
P5+	0.0	0.0	0.0	0.0	0.0	0.0	0.0	0.0	0.0
OXYGEN	5.939	5.931	5.916	5.949	5.844	5.951	5.924	5.949	5.913

178100	CM-29-7C	NE-CPX SYENITE	PYROXENE	NOVEMBER 1970
182100	CM-141-4	NE-MO-CPX SYENT	PYROXENE	NOVEMBER 1970
183150	CM-141-4	NE-MO-CPX SYENT	PYROXENE	NOVEMBER 1970
183150	CM-141-8	NE-CPX SYENITE	PYROXENE	NOVEMBER 1970
183150	CM-141-8	NE-CPX SYENITE	PYROXENE	NOVEMBER 1970
185100	CM-62CA	MO-CPX SYENITE	PYROXENE	NOVEMBER 1970
188100	CM-323	UL-CPX-AMP-NE SYN	PYROXENE	NOVEMBER 1970
189100	CM-3C5	CPX SYENITE	PYROXENE	NOVEMBER 1970
184100	CM-41-6	OL-NE-OR	PYROXENE	NOVEMBER 1970
187100	CM-41-2	NEPH. PYROXENITE	PYROXENE	NOVEMBER 1970

Table B-11

MINERALS FROM IGNEOUS ROCKS, CHRISTMAS MOUNTAINS, TEXAS

	174100	172100	174100	176100	176150	177100	180100	181100	186100
WEIGHT PER CENT OXIDES									
O	0.0	0.0	0.0	0.0	0.0	0.0	0.0	0.0	0.0
SiO2	44.589	50.669	49.899	47.779	52.449	43.680	46.504	45.299	48.815
TiO2	2.844	1.329	2.848	1.697	1.039	3.856	2.136	2.253	1.921
ZrO2	0.0	0.0	0.0	0.0	0.0	0.0	0.0	0.0	0.0
Al2O3	7.153	2.824	3.854	4.005	0.571	8.477	5.414	6.761	5.019
V2O5	0.0	0.0	0.0	0.0	0.0	0.0	0.0	0.0	0.0
Cr2O3	0.0	0.032	0.082	0.027	0.084	0.0	0.0	0.0	0.0
Fe2O3	0.0	0.0	0.0	0.0	0.0	0.0	0.0	0.0	0.0
FeO	14.374	9.427	8.431	15.930	29.103	13.376	15.186	16.708	12.522
MnO	0.240	0.247	0.210	0.317	0.124	0.296	0.393	0.311	0.396
MgO	7.210	12.395	13.047	7.545	1.141	7.549	8.064	6.687	10.103
CaO	22.815	22.372	22.162	22.398	3.521	23.669	22.182	22.970	22.561
Na2O	0.0	0.0	0.0	0.0	0.0	0.0	0.0	0.0	0.0
Na2O	0.706	0.865	0.718	0.852	12.088	0.677	1.056	0.651	0.832
K2O	0.0	0.0	0.0	0.011	0.0	0.032	0.022	0.019	0.032
P2O5	0.0	0.0	0.0	0.0	0.0	0.0	0.0	0.0	0.0
TOTAL	100.047	100.167	100.415	100.561	99.120	101.014	100.957	101.659	101.201

365

FORMULA PROPORTION CATIONS

O	0.0	0.0	0.0	0.0	0.0	0.0	0.0	0.0	0.0
Si5+	1.714	1.892	1.851	1.833	1.983	1.659	1.765	1.725	1.830
Ti4+	0.085	0.037	0.057	0.049	0.030	0.110	0.061	0.064	0.054
Zr5+	0.0	0.0	0.0	0.0	0.0	0.0	0.0	0.0	0.0
Al3+	0.324	0.124	0.168	0.181	0.025	0.379	0.242	0.303	0.178
V3+	0.0	0.0	0.0	0.0	0.0	0.0	0.0	0.0	0.0
Cr3+	0.001	0.001	0.002	0.001	0.003	0.0	0.0	0.0	0.0
Fe3+	0.0	0.0	0.0	0.0	0.0	0.0	0.0	0.0	0.0
Fe2+	0.462	0.294	0.261	0.511	0.920	0.425	0.482	0.532	0.392
Mn2+	0.008	0.010	0.007	0.010	0.004	0.010	0.013	0.010	0.013
Mg2+	0.413	0.394	0.431	0.431	0.008	0.427	0.456	0.379	0.565
Ca2+	0.949	0.900	0.981	0.920	0.143	0.939	0.902	0.937	0.906
Na+	0.0	0.0	0.0	0.0	0.0	0.0	0.0	0.0	0.0
Na+	0.053	0.054	0.052	0.063	0.886	0.050	0.078	0.048	0.060
K+	0.001	0.0	0.0	0.001	0.0	0.002	0.001	0.001	0.002
P5+	0.0	0.0	0.0	0.0	0.0	0.0	0.0	0.0	0.0
OXYGEN	5.935	5.927	5.964	5.940	5.583	5.933	5.908	5.916	5.942

144100 CM-6-38 MO-NF PYROXENITE PYROXENE JUNE 1969  
 171100 CM-33-6 PYROXENITE PYROXENE SEPT-OCT 1970  
 172100 CM-33-11 PYROXENITE PYROXENE SEPT-OCT 1970  
 174100 CM-33-13 PYROXENITE PYROXENE SEPT-OCT 1970  
 176100 CM-9-18L FELD PYROXENITE PYROXENE JUNE 1969  
 176150 CM-9-18 PYROXENITE PYROXENE SEPT-OCT 1970  
 177100 CM-298 MO-PLAG-NE PYRXNT PYROXENE NOVEMBER 1970  
 182100 CM-1113 NF-OP-PLAG PYRXNT PYROXENE NOVEMBER 1970  
 181100 CM-373-1A MO-PLAG PYRXNT PYROXENE NOVEMBER 1970  
 183100 CM-9-9 PLAG PYROXENITE PYROXENE NOVEMBER 1970

Table B-12

MINERALS FROM IGNEOUS ROCKS, CHRISTMAS MOUNTAINS, TEXAS

	165200	167200	170200	173200	188200	189200
	0.0	1.301	2.795	1.973	0.939	1.100
SiO2	42.639	40.792	37.852	39.990	39.137	39.513
TiO2	4.163	5.577	1.887	2.375	6.073	4.695
ZrO2	0.0	0.0	0.0	0.0	0.0	0.0
Al2O3	11.310	10.697	10.325	10.339	11.758	11.569
V2O3	0.0	0.0	0.0	0.0	0.0	0.0
Cr2O3	0.0	0.0	0.0	0.0	0.0	0.0
Fe2O3	0.0	0.0	0.0	0.0	0.0	0.0
FeO	14.358	15.424	28.146	21.888	17.954	18.737
MnO	0.539	0.238	0.888	0.632	0.228	0.368
MgO	11.661	10.273	3.374	7.567	8.146	8.257
CaO	11.232	11.324	10.208	10.770	11.634	11.323
Na2O	0.0	0.0	0.0	0.0	0.0	0.0
Na2O	3.072	3.146	2.892	2.886	2.352	2.578
K2O	1.429	1.156	1.632	1.581	1.778	1.796
P2O5	0.0	0.0	0.0	0.0	0.0	0.0
TOTAL	100.402	98.699	97.205	98.027	99.061	98.900

366

FORMULA PROPORTION CATIONS

	165200	167200	170200	173200	188200	189200
O	0.0	1.313	3.072	2.040	0.962	1.124
Si4+	6.273	6.171	6.024	6.199	6.010	6.189
Ti4+	0.460	0.634	0.228	0.277	0.701	0.541
Zr4+	0.0	0.0	0.0	0.0	0.0	0.0
Al3+	1.961	1.907	1.959	1.889	2.128	2.089
V3+	0.0	0.0	0.0	0.0	0.0	0.0
Cr3+	0.0	0.0	0.0	0.0	0.0	0.0
Fe3+	0.0	0.0	0.0	0.0	0.0	0.0
Fe2+	1.766	1.959	3.788	2.836	2.305	2.400
Mn2+	0.267	0.121	0.421	0.083	0.030	0.055
Mg2+	2.557	2.316	0.810	1.748	1.864	1.885
Ca2+	1.771	1.836	1.761	1.789	1.914	1.859
Na+	0.0	0.0	0.0	0.0	0.0	0.0
Na+	0.876	0.923	0.903	0.867	0.700	0.766
K+	0.268	0.223	0.335	0.313	0.348	0.351
P5+	0.0	0.0	0.0	0.0	0.0	0.0
OXYGEN	23.142	23.186	22.683	22.830	23.251	23.080
165200	CM-39-1	SVENITE DIKE	AMPHIBOL	SEPT-NOV 1970		
167200	CM-276	GABBRU-FG	AMPHIBOL	SEPT-NOV 1970		
169200	CM-B1	SVENITE-CG	AMPHIBOL	SEPT-NOV 1970		
170200	CM-294A	SVENITE-FG	AMPHIBOL	SEPT-NOV 1970		
173200	CM-33-12	PLAG PORPHYRY	AMPHIBOL	SEPT-NOV 1970		
188200	CM-320	DL-CPX-AMP-NE SYN	AMPHIBOL	NOVEMBER 1970		
189200	CM-305	CPX SVENITE	AMPHIBOL	NOVEMBER 1970		

Table B-13

MINERALS FROM IGNEOUS ROCKS, CHRISTMAS MOUNTAINS, TEXAS

	144200	171200	177200	181200	182200
	0.0	0.0	0.0	0.0	0.0
SiO2	51.195	51.229	51.614	51.783	52.235
TiO2	0.115	0.204	0.083	0.167	0.110
ZrO2	0.0	0.0	0.0	0.0	0.0
Al2O3	0.027	0.062	0.073	0.076	0.060
V2O3	0.0	0.0	0.0	0.0	0.0
Cr2O3	0.0	0.050	0.0	0.0	0.0
FeO	1.921	1.850	1.809	1.832	1.891
MnO	0.265	0.313	0.337	0.287	0.390
MgO	0.276	0.303	0.191	0.362	0.130
CaO	45.979	45.881	46.323	46.476	46.140
Na2O	0.0	0.0	0.0	0.0	0.0
K2O	0.014	0.021	0.014	0.025	0.070
P2O5	0.038	0.0	0.217	0.018	0.030
	0.0	0.0	0.0	0.0	0.0
TOTAL	99.800	99.914	100.461	101.027	101.150

367

	FORMULA PROPORTION CATIONS				
O	0.0	0.0	0.0	0.0	0.0
Si4+	0.995	0.995	0.997	0.994	1.003
Ti4+	0.002	0.003	0.001	0.002	0.002
Zr4+	0.0	0.0	0.0	0.0	0.0
Al3+	0.001	0.001	0.002	0.002	0.001
V3+	0.0	0.0	0.0	0.0	0.0
Cr3+	0.0	0.001	0.0	0.0	0.0
Fe3+	0.0	0.0	0.0	0.0	0.0
Fe2+	0.031	0.030	0.029	0.029	0.030
Mn2+	0.004	0.005	0.006	0.005	0.006
Mg2+	0.008	0.009	0.005	0.010	0.004
Ca2+	0.958	0.955	0.959	0.956	0.950
Na+	0.001	0.0	0.001	0.001	0.003
K+	0.030	0.0	0.000	0.000	0.001
P5+	0.0	0.0	0.0	0.0	0.0
OXYGEN	2.997	2.999	2.999	2.997	3.004

	144200	171200	177200	181200	182200
CM-6-3B	MO-NE PYROXENITE	MO-NE PYROXENITE	MO-NE PYROXENITE	MO-NE PYROXENITE	MO-NE PYROXENITE
171200	CM-33-6	MO-NE PYROXENITE	MO-NE PYROXENITE	MO-NE PYROXENITE	MO-NE PYROXENITE
177200	CM-29B	MO-PLAG-NE PYRXNT	MO-PLAG-NE PYRXNT	MO-PLAG-NE PYRXNT	MO-PLAG-NE PYRXNT
181200	CM-203-1A	MO-PLAG PYRXNT	MO-PLAG PYRXNT	MO-PLAG PYRXNT	MO-PLAG PYRXNT
182200	CM-141-4	MO-NE-PX SYEN	MO-NE-PX SYEN	MO-NE-PX SYEN	MO-NE-PX SYEN

Table B-14

MINERALS FROM IGNEOUS ROCKS, CHRISTMAS MOUNTAINS, TEXAS

	157400	158400	159400	161400	175400	182400	166400	167400	168400
	WEIGHT PER CENT OXIDES								
0	2.507	2.274	2.617	2.734	1.905	3.171	2.939	2.953	3.449
S102	36.038	35.647	36.757	36.029	36.042	35.090	35.219	35.453	35.697
T102	8.093	7.623	7.829	7.147	8.336	7.028	8.317	7.565	7.363
ZR02	0.0	0.0	0.0	0.0	0.0	0.0	0.0	0.0	0.0
AL2O3	14.219	14.203	14.125	14.201	14.273	13.895	13.679	13.742	13.803
V2O3	0.0	0.0	0.0	0.0	0.0	0.0	0.0	0.0	0.0
CR2O3	0.0	0.0	0.0	0.0	0.0	0.0	0.0	0.0	0.0
FE2O3	0.0	0.0	0.0	0.0	0.0	0.0	0.0	0.0	0.0
FE0	18.403	20.724	15.162	18.999	18.964	22.437	19.663	20.463	18.560
MNO	0.171	0.216	0.119	0.192	0.165	0.335	0.138	0.161	0.120
MGO	11.087	9.750	13.589	11.160	10.676	8.730	10.331	10.111	11.292
CAO	0.086	0.073	0.030	0.036	0.100	0.047	0.029	0.071	0.017
BAO	0.0	0.0	0.0	0.0	0.0	0.0	0.0	0.0	0.0
NA2O	0.573	0.536	0.594	0.578	0.469	0.325	0.540	0.568	0.497
K2O	8.825	8.953	9.177	8.924	9.070	9.032	9.085	8.912	9.001
P2O5	0.0	0.0	0.0	0.0	0.0	0.0	0.0	0.0	0.0
TOTAL	97.493	97.726	97.383	97.266	98.095	96.829	97.061	97.047	100.000

368

FORMULA PROPORTION CATIONS

0	2.588	2.364	2.655	2.823	1.962	3.355	3.067	3.084	3.803
S14+	5.577	5.554	5.590	5.277	5.565	5.564	5.519	5.551	5.577
T14+	0.942	0.893	0.895	0.832	0.968	0.838	0.978	0.890	0.865
ZR4+	0.0	0.0	0.0	0.0	0.0	0.0	0.0	0.0	0.0
AL3+	2.593	2.608	2.532	2.591	2.597	2.580	2.522	2.536	2.541
V3+	0.0	0.0	0.0	0.0	0.0	0.0	0.0	0.0	0.0
CR3+	0.0	0.0	0.0	0.0	0.0	0.0	0.0	0.0	0.0
FE3+	0.0	0.0	0.0	0.0	0.0	0.0	0.0	0.0	0.0
FE2+	2.381	2.699	1.928	2.459	2.448	2.974	2.571	2.678	2.424
MN2+	0.022	0.028	0.015	0.025	0.022	0.045	0.018	0.021	0.016
MG2+	2.557	2.264	3.080	2.575	2.457	2.063	2.469	2.359	2.629
CA2+	0.014	0.012	0.005	0.006	0.017	0.008	0.005	0.012	0.003
BA2+	0.0	0.0	0.0	0.0	0.0	0.0	0.0	0.0	0.0
NA+	0.172	0.162	0.175	0.173	0.140	0.100	0.164	0.172	0.151
K+	1.742	1.760	1.781	1.762	1.787	1.827	1.813	1.780	1.794
P5+	0.0	0.0	0.0	0.0	0.0	0.0	0.0	0.0	0.0
OXYGEN	22.858	22.780	22.773	22.736	22.868	22.729	22.770	22.733	22.740
CM-144	GABBR0-CG,FL		BIOTITE	SEPT-NOV 1970					
CM-174	GABBR0-CG		BIOTITE	SEPT-NOV 1970					
CM-39-6	GABBR0-CG		BIOTITE	SEPT-NOV 1970					
CM-85	GABBR0-CG		BIOTITE	SEPT-NOV 1970					
CM-33-14	GABBR0-CG		BIOTITE	SEPT-NOV 1970					
CM-80	GABBR0-FG DIKE		BIOTITE	SEPT-NOV 1970					
CM-109-5	GABBR0-FG		BIOTITE	SEPT-NOV 1970					
CM-276	GABBR0-FG		BIOTITE	SEPT-NOV 1970					
CM-136	GABBR0-FG		BIOTITE	SEPT-NOV 1970					

Table B-14

MINERALS FROM IGNEOUS ROCKS, CHRISTMAS MOUNTAINS, TEXAS

	1634CC	164400	165400	172402	174402
	2.223	1.486	1.990	2.631	2.935
SI02	36.461	37.984	38.043	35.695	35.736
TIO2	8.066	7.324	6.340	8.882	8.151
ZR02	0.0	0.0	0.0	0.0	0.0
AL2O3	13.749	14.118	13.635	13.962	14.538
V2O3	0.0	0.0	0.0	0.0	0.0
CR2O3	0.0	0.0	0.0	0.0	0.0
FE2O3	0.0	0.0	0.0	0.0	0.0
FE0	16.296	14.500	14.909	18.499	17.187
MNO	0.226	0.184	0.410	0.137	0.125
MGO	13.183	14.427	14.740	10.569	11.666
CAO	0.016	0.034	0.020	0.033	0.047
BAO	0.0	0.0	0.0	0.0	0.0
NA2O	0.607	0.526	0.682	0.543	0.422
K2O	9.173	9.415	9.231	9.048	9.194
P2O5	0.0	0.0	0.0	0.0	0.0
TOTAL	100.000	100.000	98.010	97.369	97.065

369

FORMULA PROPORTION CATIONS

	1634CC	164400	165400	172402	174402
O	2.258	1.483	1.989	2.732	3.028
Si4+	5.551	5.681	5.701	5.556	5.527
Ti4+	0.923	0.824	0.714	1.039	0.948
Zr4+	0.0	0.0	0.0	0.0	0.0
Al3+	2.467	2.488	2.408	2.561	2.650
V3+	0.0	0.0	0.0	0.0	0.0
Cr3+	0.0	0.0	0.0	0.0	0.0
Fe3+	0.0	0.0	0.0	0.0	0.0
Fe2+	2.074	1.813	1.868	2.407	2.222
Mn2+	0.029	0.023	0.052	0.018	0.016
Mg2+	2.991	3.216	3.292	2.452	2.689
Ca2+	0.203	0.005	0.003	0.006	0.008
Ba2+	0.0	0.0	0.0	0.0	0.0
Na+	0.179	0.153	0.198	0.164	0.127
K+	1.782	1.797	1.765	1.797	1.814
P5+	0.0	0.0	0.0	0.0	0.0
OXYGEN	22.728	22.775	22.637	22.896	22.829

1634CC CM-69 PLAG PORPHYRY BIOTITE SEPT-NOV 1970  
 164400 CM-39-1 PLAG PORPHYRY BIOTITE SEPT-NOV 1970  
 165400 CM-39-1 SYENITE DIKE BIOTITE SEPT-NOV 1970  
 172400 CM-33-11 PYROXENITE BIOTITE SEPT-NOV 1970  
 174400 CM-33-13 PYROXENITE BIOTITE SEPT-NOV 1970



Table B-15

MINERALS FROM IGNEOUS ROCKS, CHRISTMAS MOUNTAINS, TEXAS

	1637CC	1647CC	1737CC	1727CC	1747CC	1867CC	1897CC
	WEIGHT PER CENT OXIDES						
SiO2	0.0	0.0	0.0	0.0	0.0	0.0	0.0
TiO2	52.122	50.111	51.331	52.248	52.477	50.807	50.258
ZnO2	0.0	0.0	0.0	0.0	0.0	0.0	0.0
Al2O3	0.076	0.103	0.065	0.088	0.088	0.048	0.088
Cr2O3	0.086	0.086	0.086	0.071	0.072	0.0	0.0
Fe2O3	43.892	44.737	45.736	45.091	44.157	46.741	45.372
MnO	1.588	1.877	1.206	1.447	1.039	2.030	2.065
MgO	2.639	2.579	1.008	1.423	2.150	0.436	2.341
CaO	0.0	0.0	0.0	0.0	0.0	0.0	0.0
Na2O	0.0	0.0	0.0	0.0	0.0	0.0	0.0
K2O	0.0	0.0	0.0	0.0	0.0	0.0	0.0
P2O5	0.0	0.0	0.0	0.0	0.0	0.0	0.0
TOTAL	100.403	99.493	99.432	100.429	99.983	100.122	100.169

371

FORMULA PROPORTION CATIONS

	1637CC	1647CC	1737CC	1727CC	1747CC	1867CC	1897CC
Si4+	0.0	0.0	0.0	0.0	0.0	0.0	0.0
Ti4+	0.964	0.934	0.971	0.975	0.979	0.958	0.932
Zn4+	0.0	0.0	0.0	0.0	0.0	0.0	0.0
Al3+	0.002	0.003	0.002	0.004	0.003	0.001	0.003
Cr3+	0.002	0.002	0.002	0.001	0.001	0.0	0.0
Fe3+	0.0	0.0	0.0	0.0	0.0	0.0	0.0
Fe2+	0.902	0.927	0.962	0.936	0.916	0.987	0.935
Mn2+	0.033	0.039	0.026	0.030	0.022	0.043	0.043
Mg2+	0.097	0.095	0.038	0.053	0.080	0.016	0.086
Ca2+	0.0	0.0	0.0	0.0	0.0	0.0	0.0
Na+	0.0	0.0	0.0	0.0	0.0	0.0	0.0
K+	0.0	0.0	0.0	0.0	0.0	0.0	0.0
P5+	0.0	0.0	0.0	0.0	0.0	0.0	0.0
OXYGEN	2.966	2.936	2.973	2.978	2.981	2.960	2.934

163700 CM-69 PLAG PORPHYRY ILMENITE SEPT-OCT 1970  
 164700 CM-39-1 PLAG PORPHYRY ILMENITE SEPT-OCT 1970  
 173700 CM-33-12 PLAG PORPHYRY ILMENITE SEPT-OCT 1970  
 172700 CM-33-11 PYROXENITE ILMENITE SEPT-OCT 1970  
 174700 CM-33-13 PYROXENITE ILMENITE SEPT-OCT 1970  
 186700 CM-8-9 PLAG PYROXENITE ILMENITE NOVEMBER 1970  
 189700 CM-305 GPX SYENITE ILMENITE NOVEMBER 1970

Table B-16

MINERALS FROM IGNEOUS ROCKS, CHRISTMAS MOUNTAINS, TEXAS

	157900	158900	159900	160900	175900	161900	162900	167900	168900
	WEIGHT PER CENT OXIDES								
SiO2	0.0	0.0	0.0	0.0	0.0	0.0	0.0	0.0	0.0
TiO2	49.212	52.049	52.939	51.740	52.655	50.107	49.896	51.385	51.432
ZrO2	0.0	0.0	0.0	0.0	0.0	0.0	0.0	0.0	0.0
Al2O3	0.454	0.084	0.275	0.078	0.083	0.062	0.069	0.092	0.087
V2O3	0.0	0.0	0.0	0.0	0.0	0.0	0.0	0.0	0.0
Cr2O3	0.106	0.094	0.093	0.096	0.079	0.098	0.094	0.111	0.104
FeO	0.0	0.0	0.0	0.0	0.0	0.0	0.0	0.0	0.0
MnO	48.410	45.870	44.281	45.000	44.255	46.360	45.860	46.802	46.490
HgO	1.488	1.308	1.038	1.380	1.136	2.195	3.102	1.876	1.871
CaO	0.207	1.048	2.865	1.640	2.251	0.148	0.128	0.393	0.322
Na2O	0.0	0.0	0.0	0.0	0.0	0.0	0.0	0.0	0.0
K2O	0.0	0.0	0.0	0.0	0.0	0.0	0.0	0.0	0.0
P2O5	0.0	0.0	0.0	0.0	0.0	0.0	0.0	0.0	0.0
TOTAL	99.877	100.453	101.090	99.934	100.459	98.970	99.147	100.649	100.306

FORMULA PROPORTION CATIONS

J	0.0	0.0	0.0	0.0	0.0	0.0	0.0	0.0	0.0
Si4+	0.0	0.0	0.0	0.0	0.0	0.0	0.0	0.0	0.0
Ti4+	0.929	0.974	0.971	0.969	0.977	0.958	0.952	0.964	0.969
Zr4+	0.0	0.0	0.0	0.0	0.0	0.0	0.0	0.0	0.0
Al3+	0.013	0.012	0.002	0.002	0.002	0.002	0.002	0.003	0.003
V3+	0.0	0.0	0.0	0.0	0.0	0.0	0.0	0.0	0.0
Cr3+	0.002	0.002	0.002	0.002	0.002	0.002	0.002	0.002	0.002
Fe3+	0.0	0.0	0.0	0.0	0.0	0.0	0.0	0.0	0.0
Fe2+	1.516	0.955	0.899	0.937	0.913	0.985	0.973	0.977	0.974
Mn2+	0.232	0.028	0.021	0.029	0.024	0.047	0.067	0.040	0.040
Mg2+	0.008	0.039	0.104	0.061	0.083	0.006	0.005	0.014	0.012
Ca2+	0.0	0.0	0.0	0.0	0.0	0.0	0.0	0.0	0.0
Na+	0.0	0.0	0.0	0.0	0.0	0.0	0.0	0.0	0.0
K+	0.0	0.0	0.0	0.0	0.0	0.0	0.0	0.0	0.0
P5+	0.0	0.0	0.0	0.0	0.0	0.0	0.0	0.0	0.0
OXYGEN	2.937	2.977	2.973	2.971	2.979	2.960	2.954	2.967	2.972

157900	CM-144	GABBR0-CG,FL	ILMENITE	SEPT-OCT	1970
158900	CM-77A	GABBR0-CG	ILMENITE	SEPT-OCT	1970
159900	CM-39-6	GABBR0-CG	ILMENITE	SEPT-OCT	1970
160900	CM-39-6	SYENITE DIKE	ILMENITE	SEPT-OCT	1970
175900	CM-33-14	GABBR0-CG	ILMENITE	SEPT-OCT	1970
161900	CM-80	GABBR0-CG	ILMENITE	SEPT-OCT	1970
162900	CM-80	GABBR0-FG DIKE	ILMENITE	SEPT-OCT	1970
167900	CM-276	GABBR0-FG	ILMENITE	SEPT-OCT	1970
168900	CM-136	GABBR0-FG	ILMENITE	SEPT-OCT	1970

Table B-16

MINERALS FROM IGNEOUS ROCKS, CHRISTMAS MOUNTAINS, TEXAS

	161900	164900	173900	165900	184900	188900	172900	180900
	0.0	0.0	0.0	0.0	0.0	0.0	0.0	0.0
SI02	0.0	0.0	0.0	0.0	0.070	0.034	0.0	0.085
TI02	51.946	51.152	51.692	50.569	50.854	51.304	51.594	50.473
ZR02	0.0	0.0	0.0	0.0	0.0	0.0	0.0	0.0
AL203	0.093	0.148	0.079	0.096	0.121	0.099	0.094	0.098
V203	0.0	0.0	0.0	0.0	0.0	0.0	0.0	0.0
CR203	0.092	0.088	0.084	0.097	0.0	0.0	0.078	0.0
FE203	0.0	0.0	0.0	0.0	0.0	0.0	0.0	0.0
FE0	43.702	43.226	45.208	42.359	47.128	45.365	45.582	47.191
MNO	1.584	1.465	1.550	7.051	1.887	2.421	1.649	2.267
MGO	2.778	3.572	1.374	0.427	0.598	1.037	1.257	1.373
CAO	0.0	0.0	0.0	0.0	0.0	0.0	0.0	0.0
BAO	0.0	0.0	0.0	0.0	0.0	0.0	0.0	0.0
NA2O	0.0	0.0	0.0	0.0	0.0	0.0	0.0	0.0
K2O	0.0	0.0	0.0	0.0	0.0	0.0	0.0	0.0
P2O5	0.0	0.0	0.0	0.0	0.0	0.0	0.0	0.0
TOTAL	100.196	99.651	99.986	100.598	100.657	100.261	100.253	101.488

373

FORMULA PROPORTION CATIONS

	161900	164900	173900	165900	184900	188900	172900	180900
O	0.0	0.0	0.0	0.0	0.0	0.0	0.0	0.0
Si4+	0.0	0.0	0.0	0.0	0.002	0.001	0.0	0.002
Ti4+	0.961	0.945	0.969	0.948	0.952	0.961	0.966	0.930
Zr4+	0.0	0.0	0.0	0.0	0.0	0.0	0.0	0.0
Al3+	0.003	0.004	0.002	0.003	0.004	0.003	0.003	0.003
V3+	0.0	0.0	0.0	0.0	0.0	0.0	0.002	0.0
CR3+	0.002	0.002	0.002	0.002	0.0	0.0	0.002	0.0
FE3+	0.0	0.0	0.0	0.0	0.0	0.0	0.0	0.0
FE2+	0.899	0.888	0.943	0.883	0.981	0.945	0.949	0.967
MN2+	0.033	0.032	0.033	0.149	0.040	0.051	0.035	0.047
Mg2+	0.102	0.131	0.051	0.016	0.022	0.039	0.047	0.050
CA2+	0.0	0.0	0.0	0.0	0.0	0.0	0.0	0.0
BA2+	0.0	0.0	0.0	0.0	0.0	0.0	0.0	0.0
NA+	0.0	0.0	0.0	0.0	0.0	0.0	0.0	0.0
K+	0.0	0.0	0.0	0.0	0.0	0.0	0.0	0.0
P5+	0.0	0.0	0.0	0.0	0.0	0.0	0.0	0.0
OXYGEN	2.964	2.948	2.971	2.950	2.952	2.964	2.968	2.934

- 163900 CM-69 PLAG PORPHYRY ILMENITE SEPT-OCT 1970
- 164900 CM-39-1 PLAG PORPHYRY ILMENITE SEPT-OCT 1970
- 173900 CM-33-12 PLAG PORPHYRY ILMENITE SEPT-OCT 1970
- 165900 CM-39-1 SYENITE DIKE ILMENITE SEPT-OCT 1970
- 184900 CM-41-6 OL-NE-OR GABBRO ILMENITE NOVEMBER 1970
- 188900 CM-320 OL-CPX-AMP-NE SYN ILMENITE NOVEMBER 1970
- 172900 CM-33-11 PYROXENITE ILMENITE SEPT-OCT 1970
- 180900 CM-111B NE-OR-PLAG PYXNT ILMENITE NOVEMBER 1970



Table B-17

MINERALS FROM IGNEOUS ROCKS, CHRISTMAS MOUNTAINS, TEXAS

	164800	173800	169800	170800	160800	165800
WEIGHT PER CENT OXIDES						
O	64.45	2.248	2.951	6.068	6.152	6.052
SiO2	0.0	0.0	0.0	0.0	0.0	0.0
TiO2	19.713	13.413	10.445	13.978	11.395	6.953
ZrO2	0.0	0.0	0.0	0.0	0.0	0.0
Al2O3	1.757	2.798	1.138	1.207	2.616	1.411
V2O5	0.0	0.0	0.0	0.0	0.0	0.0
Cr2O3	0.112	2.226	0.106	5.064	6.112	6.116
Fe2O3	30.346	48.637	52.263	60.792	48.560	68.750
FeO	45.419	35.453	34.776	22.492	36.303	20.930
MnO	1.136	0.499	1.147	1.370	0.505	1.539
MgO	1.479	1.484	0.073	0.112	0.569	0.249
CaO	0.0	0.0	0.0	0.0	0.0	0.0
Na2O	0.0	0.0	0.0	0.0	0.0	0.0
K2O	0.0	0.0	0.0	0.0	0.0	0.0
P2O5	0.0	0.0	0.0	0.0	0.0	0.0
TOTAL	100.000	100.000	99.999	100.000	100.000	100.000

375

FORMULA PROPORTION CATIONS

O	6.011	0.012	0.013	3.017	0.013	6.013
Si4+	0.0	0.0	0.0	0.0	0.0	0.0
Ti4+	0.549	0.378	0.299	0.405	0.322	0.201
Zr4+	0.0	0.0	0.0	0.0	0.0	0.0
Al3+	0.077	0.124	0.051	0.055	0.116	0.064
V 3+	0.0	0.0	0.0	0.0	0.0	0.0
Cr3+	0.003	0.007	0.003	0.002	0.003	0.004
Fe3+	0.846	1.321	1.498	1.762	1.374	1.993
Fe2+	1.407	1.112	1.107	0.725	1.142	0.674
Mn2+	0.036	0.016	0.037	0.045	0.016	0.050
Mg2+	0.082	0.043	0.004	0.006	0.026	0.014
Ca2+	0.0	0.0	0.0	0.0	0.0	0.0
Na2+	0.0	0.0	0.0	0.0	0.0	0.0
K+	0.0	0.0	0.0	0.0	0.0	0.0
P 5+	0.0	0.0	0.0	0.0	0.0	0.0
OXYGEN	4.012	4.045	4.075	4.314	4.069	4.231

163800	CM-69	PLAG	PURPHYRY	MAGNETIT	SEPT-OCT	1970
164800	CM-39-1	PLAG	PURPHYRY	MAGNETIT	SEPT-OCT	1970
173800	CM-33-12	PLAG	PURPHYRY	MAGNETIT	SEPT-OCT	1970
169800	CM-81	SYENITE-CG		MAGNETIT	SEPT-OCT	1970
170800	CM-294A	SYENITE-FG		MAGNETIT	SEPT-OCT	1970
166600	CM-39-6	SYENITE DIKE		MAGNETIT	SEPT-OCT	1970
165800	CM-39-1	SYENITE DIKE		MAGNETIT	SEPT-OCT	1970

Table B-17

MINERALS FROM IGNEOUS ROCKS, CHRISTMAS MOUNTAINS, TEXAS

	188800	189900	184800	172800	176820	176840	180800	186820	186840	187800
	WEIGHT PER CENT OXIDES									
O	0.552	0.551	0.552	0.551	0.547	0.556	0.553	0.550	0.553	0.548
SiO2	0.047	0.043	0.239	0.0	0.0	0.0	0.131	0.053	0.138	0.184
TiO2	9.027	11.023	7.534	9.377	14.287	2.522	7.825	10.604	8.285	13.639
ZrO2	0.0	0.0	0.0	0.0	0.0	0.0	0.0	0.0	0.0	0.0
Al2O3	2.086	1.366	2.507	2.721	2.125	0.557	1.571	1.798	1.792	2.980
V2O5	0.0	0.0	0.0	0.0	0.0	0.0	0.0	0.0	0.0	0.0
Cr2O3	0.0	0.0	0.0	0.0	0.171	0.275	0.0	0.0	0.0	0.0
Fe2O3	54.221	42.902	51.542	55.898	52.675	65.743	39.681	65.853	48.749	36.653
FeO	33.368	42.466	37.274	30.192	28.117	30.525	49.788	20.628	40.207	43.488
MnO	0.705	1.187	0.668	0.409	0.759	0.446	0.508	0.682	0.515	0.824
MgO	0.494	0.963	0.182	0.654	1.826	0.075	0.433	0.330	0.260	2.183
CaO	0.0	0.0	0.0	0.0	0.0	0.0	0.0	0.0	0.0	0.0
Na2O	0.0	0.0	0.0	0.0	0.0	0.0	0.0	0.0	0.0	0.0
K2O	0.0	0.0	0.0	0.0	0.0	0.0	0.0	0.0	0.0	0.0
P2O5	0.0	0.0	0.0	0.0	0.0	0.0	0.0	0.0	0.0	0.0
TOTAL	100.000	100.000	99.999	100.000	99.999	100.000	99.999	100.000	100.001	100.000

376

FORMULA PROPORTION CATIONS

	188800	189900	184800	172800	176820	176840	180800	186820	186840	187800
O	0.013	0.013	0.013	0.013	0.012	0.014	0.013	0.013	0.013	0.012
Si4+	0.002	0.002	0.009	0.0	0.0	0.0	0.005	0.002	0.005	0.007
Ti4+	0.257	0.310	0.213	0.266	0.403	0.073	0.219	0.307	0.235	0.376
Zr4+	0.0	0.0	0.0	0.0	0.0	0.0	0.0	0.0	0.0	0.0
Al3+	0.093	0.060	0.111	0.121	0.094	0.025	0.069	0.081	0.080	0.129
V3+	0.0	0.0	0.0	0.0	0.0	0.0	0.0	0.0	0.0	0.0
Cr3+	0.0	0.0	0.0	0.003	0.005	0.002	0.0	0.0	0.0	0.0
Fe3+	1.543	1.208	1.461	1.538	1.489	1.900	1.114	1.905	1.383	1.011
Fe2+	1.055	1.329	1.174	0.972	0.883	0.980	1.553	0.663	1.267	1.333
Mn2+	0.023	0.038	0.021	0.013	0.024	0.015	0.016	0.022	0.016	0.026
Mg2+	0.028	0.054	0.010	0.037	0.102	0.004	0.024	0.019	0.015	0.119
Ca2+	0.0	0.0	0.0	0.0	0.0	0.0	0.0	0.0	0.0	0.0
Na+	0.0	0.0	0.0	0.0	0.0	0.0	0.0	0.0	0.0	0.0
K+	0.0	0.0	0.0	0.0	0.0	0.0	0.0	0.0	0.0	0.0
P5+	0.0	0.0	0.0	0.0	0.0	0.0	0.0	0.0	0.0	0.0
OXYGEN	4.076	3.946	4.009	4.122	4.197	4.037	3.816	4.302	3.971	3.953

1971 UARE (Univ. of Ariz. Earth Planet. Sci.)

188800 CM-325 OL-CPX-AMP-NE SYN MAGNETIT NOVEMBER 1970  
 189900 CM-365 CPX SYENITE MAGNETIT NOVEMBER 1970  
 184800 CM-41-6 OL-NE-DR GABRO MAGNETIT NOVEMBER 1970  
 172800 CM-33-11 PYROXENITE MAGNETIT SEPT-OCT 1970  
 176820 CM-8-13 PYROXENITE MAGNETIT SEPT-OCT 1970  
 176840 CM-8-19 PYROXENITE MAGNETIT SEPT-OCT 1970  
 180800 CM-1118 NL-UR-PLAG PYXNT MAGNETIT NOVEMBER 1970  
 186820 CM-8-9 PLAG PYROXENITE MAGNETIT NOVEMBER 1970  
 186840 CM-8-9 PLAG PYROXENITE MAGNETIT NOVEMBER 1970  
 187800 CM-41-2 NEPH PYROXENITE MAGNETIT NOVEMBER 1970

APPENDIX C

ELECTRON MICROPROBE ANALYSES OF  
CALC-SILICATE ROCKS AND MINERALS

TABLE C-1

ANALYZED SAMPLES FROM SKARN  
CHRISTMAS MOUNTAINS, TEXAS

Sample	Distance From Pyroxenite (cm)	Mineral Assemblage*	Formation+	Intrusive Rock <sup>o</sup>	Contact Relation**
8-1B	0-1	1	KSp	PG	MC
8-1A	2-4	2	KSp	PG	MC
8-1C	4-6	3	KSp	PG	MC
8-2	13-17	4	KSp	PG	MC
8-3B	33-35	8	KSp	PG	MC
8-3	38-42	8	KSp	PG	MC
8-3C	39-41	8	KSp	PG	MC
8-3D	43-45	9	KSp	PG	MC
8-3E	48-51	9	KSp	PG	MC
8-3F	53-57	9	KSp	PG	MC
8-4	57-61	9	KSp	PG	MC
8-7A	76-79	13,15	KSp	PG	MC
8-17	290	13	KSp	PG	MC
8-19	750	9	KSp	PG	MC
103-6A(1)	0-2	3	KSe	FgG	XL
103-6A(2)	2-4	4	KSe	FgG	XL
103-6B	6-10	5	KSe	FgG	XL
103-5	13-17	5	KSe	FgG	XL
103-4	41-45	5	KSe	FgG	XL
103-2	65-76	9	KSe	FgG	XL
103-3/3	79-86	13	KSe	FgG	XL
108	250	10,14	KSe	FgG	XL
104-2A	2	3	KSe	FgG	XL
104-2B	6	4	KSe	FgG	XL
104-1	40	8	KSe	FgG	XL
319	46	5	KSe	FgG	MC
321	70	9	KSe	FgG	MC
86	200	8	KSe	FgG	XL
91	60	15	KSe	FgG	XL

TABLE 1

AVERAGE MODE AND MINERAL COMPOSITION OF  
COARSE-GRAINED OLIVINE-BIOTITE-TITANAUGITE GABBRO

2%	Olivine	$FO_{57}FA_{43}-FO_{50}FA_{50}$
25%	Titanaugite	$Ca_{0.88}Na_{0.04}Mg_{0.73}Fe_{0.28}Mn_{0.01}Ti_{0.06}Al_{0.16}Si_{1.85}O_6$
2%	Biotite	$K_{1.78}Na_{0.17}Ca_{0.01}(Mg,Fe)_{5.0}Mn_{0.02}Ti_{0.89}Al_{2.54}Si_{5.57}(O,OH)_{24}$
7%	Opaque	Magnetite USP- $USP_{45}$ Exsolved Ilmenite $HEM_2-HEM_3$ Homogeneous Ilmenite $HEM_2-HEM_3$
60%	Plagioclase	$AN_{68}AB_{31}OR_1 - AN_{37}AB_{60}OR_3$
3%	Alkali Feldspar	$AN_3AB_{44}OR_{53}$
1%	Apatite	

TABLE C-2  
ELECTRON MICROPROBE ANALYSES OF MELILITE AND IDOCRASE FROM SKARN  
CHRISTMAS MOUNTAINS, TEXAS

Sample Mineral	8-1A I	8-1C I	8-2B M	8-2B I	8-3B M	8-3B I	8-3 M
SiO <sub>2</sub>	32.41	32.63	30.14	28.76	31.35	29.80	30.00
TiO <sub>2</sub>	0.11	0.01	0.02	0.02	0.01	0.02	0.02
Al <sub>2</sub> O <sub>3</sub>	17.00	17.53	24.23	21.91	23.49	21.94	23.14
FeO	6.39	4.94	5.00	4.56	4.54	4.54	4.68
MnO	0.08	..	0.15	0.10	0.12	0.09	0.09
MgO	1.56	2.40	1.81	1.51	2.80	2.57	2.61
CaO	36.02	35.40	37.59	35.16	38.99	36.91	38.32
Na <sub>2</sub> O	0.01	0.0	0.92	0.02	0.80	0.17	0.80
TOTAL	93.58	92.91	99.85	92.04	102.12	96.04	99.79

FORMULA PROPORTION BASED ON CATION SUM = 5.0

Si 4+	1.64	1.65	1.40	1.46	1.42	1.44	1.39
Al 3+	1.01	1.04	1.32	1.31	1.25	1.25	1.26
Fe 2+	0.27	0.21	0.19	0.19	0.17	0.18	0.18
Mg 2+	0.12	0.18	0.12	0.11	0.19	0.19	0.18
Ca 2+	1.95	1.92	1.87	1.91	1.89	1.92	1.90
Na +	0.0	0.0	0.08	0.0	0.07	0.02	0.07
OXYGEN	7.15	7.17	7.02	7.12	7.01	7.06	6.98
N	4	6	4	6	4	3	8

I = idocrase, M = melilite

TABLE C-2 (CONTINUED)  
 ELECTRON MICROPROBE ANALYSES OF MELILITE AND IDOCRASE FROM SKARN  
 CHRISTMAS MOUNTAINS, TEXAS

Sample Mineral	8-3D M	8-3D I	8-3E M	8-3E I	8-3F M	8-3F I	8-4 M	8-4 I
SiO <sub>2</sub>	30.65	29.17	31.21	20.03	31.14	30.24	30.72	29.33
TiO <sub>2</sub>	0.01	..	0.02	0.01	0.04	0.02	0.02	0.0
Al <sub>2</sub> O <sub>3</sub>	23.30	23.24	22.74	19.84	21.29	19.84	22.04	20.80
Fe <sub>2</sub> O <sub>3</sub>	4.28	4.21	4.46	4.78	4.83	3.92	4.44	3.67
MnO	0.06	0.02	0.09	0.08	0.07	..	0.10	0.08
MgO	2.92	2.32	2.84	2.92	2.83	2.51	3.11	2.84
CaO	38.92	36.01	39.29	36.86	39.14	38.48	37.94	36.14
Na <sub>2</sub> O	0.74	0.08	0.77	0.34	0.76	0.11	0.82	0.13
TOTAL	100.97	95.05	101.50	94.86	100.08	95.12	99.34	92.99

	FORMULA PROPORTION BASED ON CATION SUM = 5.0						
	6	1	6	3	4	2	7
Si 4+	1.40	1.42	1.42	1.47	1.44	1.48	1.46
Al 3+	1.26	1.34	1.22	1.14	1.16	1.14	1.22
Fe 2+	0.16	0.17	0.17	0.20	0.19	0.16	0.15
Mg 2+	0.20	0.17	0.19	0.21	0.20	0.18	0.21
Ca 2+	1.91	1.88	1.92	1.93	1.94	2.02	1.93
Na +	0.07	0.01	0.07	0.03	0.07	0.01	0.01
OXYGEN	6.99	7.09	7.00	7.02	6.99	7.05	7.06
N	6	1	6	3	4	2	7

I = idocrase, M = melilite

TABLE C-2 (CONTINUED)

ELECTRON MICROPROBE ANALYSES OF MELILITE AND IDOCRASE FROM SKARN  
CHRISTMAS MOUNTAINS, TEXAS

Sample Mineral	8-7A M	8-7A I	8-17 M	8-19 M	8-19 I	6-6MB M	6-6MB I	273-5 M
SiO <sub>2</sub>	31.29	30.73	31.48	31.78	30.57	31.25	30.38	30.61
TiO <sub>2</sub>	0.0	0.01	0.01	0.03	0.01	0.01	0.02	0.0
Al <sub>2</sub> O <sub>3</sub>	22.06	19.03	21.17	22.29	21.91	22.45	20.98	23.91
Fe <sub>2</sub> O <sub>3</sub>	2.13	1.97	2.78	4.02	3.69	3.76	3.46	2.76
MnO	..	..	0.01	0.02	0.00	0.05	0.06	0.01
MgO	4.84	5.21	4.80	3.31	3.22	2.83	2.83	2.92
CaO	39.08	37.68	38.39	38.81	37.08	37.88	35.94	38.44
Na <sub>2</sub> O	0.52	0.10	0.65	1.00	0.47	1.32	0.38	1.22
TOTAL	99.92	94.73	99.39	101.35	96.95	99.56	94.05	99.87

FORMULA PROPORTION BASED ON CATION SUM = 5.0

Si 4+	1.43	1.49	1.45	1.44	1.46	1.44	1.50	1.40
Al 3+	1.19	1.09	1.15	1.19	1.23	1.22	1.22	1.29
Fe 2+	0.08	0.08	0.11	0.15	0.15	0.15	0.14	0.11
Mg 2+	0.33	0.38	0.33	0.22	0.23	0.20	0.21	0.20
Ca 2+	1.92	1.96	1.90	1.89	1.89	1.88	1.90	1.89
Na +	0.05	0.01	0.06	0.09	0.04	0.12	0.04	0.11
OXYGEN	7.01	7.03	7.00	7.00	7.05	7.00	7.09	7.00
N	3	3	5	5	3	8	7	1

I = idocrase, M = melillite

TABLE C-2 (CONTINUED)  
 ELECTRON MICROPROBE ANALYSES OF MELILITE AND IDOCRASE FROM SKARN  
 CHRISTMAS MOUNTAINS, TEXAS

Sample Mineral	103-6A I	103-6B M	103-6B I	103-5 M	103-5 I	103-4 M	103-4 I
SiO <sub>2</sub>	32.25	32.13	30.33	30.87	29.08	29.66	28.29
TiO <sub>2</sub>	0.04	0.02	0.05	0.01	0.0	0.02	0.04
Al <sub>2</sub> O <sub>3</sub>	17.91	18.99	18.36	20.40	20.23	22.14	21.15
FeO	4.22	4.26	4.34	4.56	3.86	4.12	3.78
MnO	0.10	0.08	0.08	0.07	0.02	0.05	0.03
MgO	3.52	3.74	3.67	3.54	2.70	3.15	3.09
CaO	36.60	39.16	36.70	39.97	38.08	41.04	37.07
Na <sub>2</sub> O	0.02	0.58	0.01	0.18	0.02	0.24	0.07
TOTAL	94.66	98.98	93.54	99.59	93.99	100.42	93.52

FORMULA PROPORTION BASED ON CATION SUM = 5.0

Si 4+	1.59	1.50	1.51	1.44	1.44	1.37	1.40
Al 3+	1.04	1.05	1.08	1.12	1.18	1.40	1.24
Fe 2+	0.17	0.17	0.18	0.18	0.16	0.16	0.16
Mg 2+	0.26	0.26	0.27	0.25	0.20	0.22	0.23
Ca 2+	1.93	1.96	1.96	2.00	2.02	2.03	1.97
Na +	0.01	0.05	0.00	0.02	0.0	0.02	0.01
OXYGEN	7.11	7.00	7.05	6.99	7.03	6.96	7.02
N	5	5	4	6	2	6	2

I = idocrase, M = melilite

TABLE C-2 (CONTINUED)  
 ELECTRON MICROPROBE ANALYSES OF MELILITE AND IDOCRASE FROM SKARN  
 CHRISTMAS MOUNTAINS, TEXAS

Sample Mineral	103-2 M	103-2 I	103-3A M	103-3A I	108 M	86 M	86 I	91 M
SiO <sub>2</sub>	27.90	26.72	30.07	27.33	32.98	34.47	32.73	29.07
TiO <sub>2</sub>	0.03	0.05	0.03	0.07	0.01	0.0	0.04	0.01
Al <sub>2</sub> O <sub>3</sub>	25.49	21.53	23.22	21.03	19.92	16.26	15.45	23.55
Fe <sub>2</sub> O <sub>3</sub>	3.27	4.09	2.16	2.25	1.78	4.88	3.77	2.09
MnO	0.01	0.04	0.02	0.06	0.01	0.10	0.01	0.02
MgO	2.52	2.00	4.07	4.18	5.48	5.62	5.01	3.94
CaO	41.07	37.37	40.82	36.70	39.69	38.92	36.12	40.69
Na <sub>2</sub> O	0.13	0.03	0.29	0.06	0.65	0.45	0.02	0.22
TOTAL	100.43	91.83	100.69	91.68	100.54	100.76	93.15	99.62

	FORMULA PROPORTION BASED ON CATION SUM = 5.0							
	5	1	6	1	3	4	2	5
Si 4+	1.28	1.35	1.37	1.37	1.50	1.58	1.63	1.34
Al 3+	1.38	1.29	1.25	1.24	1.07	0.88	0.91	1.28
Fe 2+	0.13	0.17	0.08	0.09	0.07	0.19	0.16	0.08
Mg 2+	0.17	0.15	0.28	0.31	0.37	0.38	0.37	0.27
Ca 2+	2.02	2.03	2.00	1.97	1.93	1.92	1.92	2.01
Na +	0.01	0.0	0.02	0.0	0.06	0.04	0.0	0.02
OXYGEN	6.97	7.00	6.98	6.99	7.00	7.00	7.08	6.97

I = idocrase, M = melilite

TABLE C-3

ELECTRON MICROPROBE ANALYSES OF CALC-SILICATE MINERALS CHRISTMAS MOUNTAINS, TEXAS						
Mineral	W	W	R	K	L	S
Sample	33-6	8-1B	8-3	8-3	273-5	8-4
SiO <sub>2</sub>	51.23	50.88	41.65	41.34	34.51	26.08
TiO <sub>2</sub>	0.20	0.12	0.03	0.02	0.01	0.00
Al <sub>2</sub> O <sub>3</sub>	0.06	0.03	0.05	0.03	0.00	0.04
FeO	1.85	0.39	0.23	0.25	0.05	0.12
MnO	0.31	0.22	0.02	0.03	0.00	0.04
MgO	0.30	0.13	0.04	0.06	0.02	0.03
CaO	45.88	47.66	57.72	57.44	63.98	60.16
Na <sub>2</sub> O	0.02	0.01	0.03	0.02	0.55	0.23
TOTAL	99.85	99.44	99.77	99.19	99.12	87.70
Cation Sum	2.0	2.0	5.0	5.0	3.0	7.0
Si 4+	0.995	0.990	2.004	2.001	0.993	2.002
Ti 4+	0.003	0.002	0.001	0.001	0.0	0.0
Al 3+	0.001	0.001	0.003	0.002	0.0	0.004
Fe 2+	0.030	0.006	0.009	0.010	0.001	0.008
Mn 2+	0.005	0.004	0.001	0.001	0.0	0.002
Mg 2+	0.009	0.004	0.003	0.004	0.001	0.004
Ca 2+	0.955	0.993	2.976	2.979	1.973	4.947
Na +	0.001	0.001	0.003	0.002	0.031	0.034
Oxygen	2.999	2.992	7.005	7.002	3.978	8.987

W = wollastonite, R = rankinite, K = kilchoanite, L = larnite and  
S = spurrite

TABLE C-4

ELECTRON MICROPROBE ANALYSES OF ORTHOSILICATES FROM SKARN  
CHRISTMAS MOUNTAINS, TEXAS

Mineral	MO	ME	ME	ME	"T"
Sample	108	108	91	8-7A	273-5
SiO <sub>2</sub>	37.20	37.16	37.47	36.65	34.97
Al <sub>2</sub> O <sub>3</sub>	0.0	0.01	0.04	0.0	0.03
FeO	11.80	1.88	1.81	1.54	2.92
MnO	0.44	0.03	0.07	0.00	0.08
MgO	16.20	11.07	11.33	11.28	4.30
CaO	36.04	50.63	49.86	49.84	56.94
Na <sub>2</sub> O	0.01	0.14	0.10	0.11	0.43
TOTAL	101.69	100.93	100.68	99.42	99.67
Cation Sum	3.0	6.0	6.0	6.0	3.0
Si 4+	1.013	2.031	2.051	2.029	0.991
Al 3+	0.0	0.001	0.002	0.0	0.001
Fe 2+	0.269	0.086	0.083	0.071	0.069
Mn 2+	0.010	0.001	0.003	0.0	0.002
Mg 2+	0.657	0.902	0.924	0.931	0.182
Ca 2+	1.051	2.964	2.924	2.957	1.730
Na +	0.0	0.015	0.011	0.012	0.024
Oxygen	4.013	8.024	8.047	8.024	3.981

MO = monticellite, ME = merwinite and "T" = phase "T"

TABLE C-5  
ELECTRON MICROPROBE ANALYSES OF GARNET FROM SKARN  
CHRISTMAS MOUNTAINS, TEXAS

Sample Assemblage	8-1B 1	8-1B 2	8-1A 1	8-1A 2	8-1C 3	8-2 4	8-3B 8	8-3 8
Si <sub>2</sub> O <sub>2</sub>	36.82	32.17	35.51	25.56	25.40	25.45	23.48	23.01
TiO <sub>2</sub>	0.06	8.35	3.57	13.60	14.37	10.42	10.22	10.36
ZrO <sub>2</sub>	0.0	0.19	0.05	1.67	1.71	5.19	8.23	8.54
Al <sub>2</sub> O <sub>3</sub>	4.85	6.72	8.50	4.03	4.07	3.65	3.40	3.31
Cr <sub>2</sub> O <sub>3</sub>	0.03	..	..	0.12	0.12	0.22	0.40	0.46
Fe <sub>2</sub> O <sub>3</sub>	23.54	19.32	18.22	22.14	22.53	23.37	22.08	22.51
MnO	0.12	0.06	0.09	0.11	0.08	0.05	0.05	0.06
MgO	0.14	0.35	0.21	0.20	0.29	0.20	0.30	0.31
CaO	33.47	33.03	33.85	31.47	31.94	30.85	31.48	30.66
TOTAL	99.02	100.17	100.05	98.91	100.56	99.41	99.64	99.21
			FORMULA PROPORTION BASED ON CATION SUM = 8.0					
Si 4+	3.05	2.65	2.88	2.22	2.17	2.23	2.08	2.06
Ti 4+	0.004	0.52	0.22	0.89	0.92	0.69	0.68	0.70
Zr 4+	0.0	0.01	0.002	0.07	0.07	0.22	0.36	0.37
Al 3+	0.47	0.65	0.81	0.41	0.41	0.38	0.36	0.35
Cr 3+	0.002	..	..	0.01	0.01	0.02	0.03	0.03
Fe 3+	1.47	1.20	1.11	1.45	1.44	1.54	1.47	1.51
Mn 2+	0.01	0.004	0.01	0.01	0.01	0.004	0.004	0.005
Mg 2+	0.02	0.04	0.03	0.03	0.04	0.03	0.04	0.04
Ca 2+	2.97	2.92	2.94	2.93	2.93	2.90	2.99	2.94
OXYGEN	12.03	12.11	12.06	12.10	11.99	12.11	12.04	12.07
ΔSi	..	2.65-2.68	2.59-2.88	2.19-2.35	2.14-2.36	2.08-2.42	1.93-2.21	1.78-2.25
ΔTi	..	0.49-0.52	0.22-0.59	0.79-0.89	0.79-0.95	0.67-0.97	0.68-0.72	0.65-0.81
ΔZr	..	..	..	0.06-0.09	0.04-0.08	0.06-0.33	0.19-0.48	0.20-0.57
N	1	2	2	5	9	13	4	10

TABLE C-5 (CONTINUED)  
ELECTRON MICROPROBE ANALYSES OF GARNET FROM SKARN  
CHRISTMAS MOUNTAINS, TEXAS

Sample Assemblage	8-3D 9	8-3E 9	8-4 9	8-5A 9?	8-7A 13,15 15.49	8-17 13 16.97	8-19 9 26.97
SiO <sub>2</sub>	21.50	22.50	21.51	19.99	8.74	10.46	10.61
TiO <sub>2</sub>	9.89	11.05	10.08	9.97	21.16	17.60	2.45
ZrO <sub>2</sub>	10.96	8.97	10.14	12.60	4.83	4.21	3.17
Al <sub>2</sub> O <sub>3</sub>	2.94	3.19	3.37	3.32	0.26	0.07	0.73
Cr <sub>2</sub> O <sub>3</sub>	0.58	0.35	0.40	0.22	18.68	19.26	22.99
Fe <sub>2</sub> O <sub>3</sub>	21.31	22.31	21.98	22.02	0.0	0.08	0.05
MnO	0.06	0.03	0.10	0.09	0.35	0.35	0.20
MgO	0.20	0.24	0.32	0.31	29.57	29.95	32.45
CaO	30.68	31.65	30.30	30.01	99.12	98.93	99.61
TOTAL	98.14	100.31	98.20	98.57	FORMULA PROPORTION BASED ON CATION SUM = 8.0		
Si 4+	1.97	1.99	1.96	1.84	1.46	1.59	2.32
Ti 4+	0.68	0.74	0.69	0.69	0.62	0.74	0.69
Zr 4+	0.49	0.39	0.45	0.56	0.98	0.80	0.10
Al 3+	0.32	0.33	0.36	0.34	0.54	0.46	0.32
Cr 3+	0.04	0.02	0.03	0.02	0.02	0.01	0.05
Fe 3+	1.47	1.49	1.50	1.52	1.33	1.36	1.49
Mn 2+	0.003	0.002	0.01	0.01	0.0	0.01	0.004
Mg 2+	0.03	0.03	0.04	0.04	0.05	0.05	0.03
Ca 2+	3.01	3.00	2.95	2.96	3.00	3.00	3.00
OXYGEN	12.04	12.04	12.04	12.04	12.00	12.04	12.04
ΔSi	1.68-2.17	1.60-2.22	1.80-2.18	1.63-2.22	1.42-1.55	1.50-1.84	2.11-2.45
ΔTi	0.64-0.76	0.67-0.84	0.63-0.76	0.67-0.85	0.58-0.71	0.65-0.74	0.65-0.73
ΔZr	0.20-0.68	0.08-0.67	0.22-0.62	0.20-0.68	0.86-1.94	0.63-0.92	0.01-0.31
N	7	7	13	9	8	8	5

TABLE C-7 (CONTINUED)

ELECTRON MICROPROBE ANALYSES OF SKARN  
CHRISTMAS MOUNTAINS, TEXAS

Sample	104-2A	104-2B	104-1	319	321	91A	91B
Interval (cm)	2	6	40	46	70	150	150
Assemblage	3	4	8	5	9	15	15
Density (gm/cm <sup>3</sup> )	3.194	3.124	3.098	3.071	3.063	2.767	3.064
SiO <sub>2</sub>	35.69	32.07	29.67	28.52	29.54	10.55	27.63
TiO <sub>2</sub>	1.09	1.59	1.63	1.38	0.81	0.06	0.49
Al <sub>2</sub> O <sub>3</sub>	13.52	16.72	15.08	20.66	12.26	6.74	17.20
FeO	6.17	6.41	4.69	4.53	3.00	1.77	5.04
MgO	2.45	2.96	2.20	2.23	1.38	1.34	3.51
CaO	41.02	40.01	46.46	41.79	52.52	79.38	45.88
Na <sub>2</sub> O	0.06	0.24	0.26	0.88	0.50	0.15	0.25
TOTAL	100.00	100.00	100.00	100.00	100.00	100.00	100.00

TABLE C-7

ELECTRON MICROPROBE ANALYSES OF SKARN  
CHRISTMAS MOUNTAINS, TEXAS

Sample	6-6MA	6-6MB	273-5	6-3BX	29BX
Interval (CM)	100	100	30	0-3	0-3
Assemblage	13	13	6,7	1	1
Density (gm/cm <sup>3</sup> )	2.978	3.045	3.116	3.209	3.174
SiO <sub>2</sub>	27.85	28.94	30.34	36.70	37.32
TiO <sub>2</sub>	0.12	1.13	1.72	1.94	1.36
Al <sub>2</sub> O <sub>3</sub>	0.10	11.91	12.70	19.72	17.48
FeO	2.22	4.53	4.18	6.05	6.12
MgO	0.10	1.46	2.26	1.93	2.83
CaO	69.13	51.08	48.01	32.85	35.38
Na <sub>2</sub> O	0.48	0.94	0.80	0.81	0.51
TOTAL	100.00	100.00	100.00	100.00	100.00

TABLE C-5 (CONTINUED)  
ELECTRON MICROPROBE ANALYSES OF GARNETS FROM SKARN  
CHRISTMAS MOUNTAINS, TEXAS

Sample	103-6A	103-6B	103-5	103-4	103-2	108
Assemblage	3,4	5	5	5	9	
SiO <sub>2</sub>	27.52	29.58	27.68	25.88	17.42	14.90
TiO <sub>2</sub>	12.92	9.88	11.88	12.98	11.67	7.76
ZrO <sub>2</sub>	0.05	0.07	0.33	0.0	14.54	21.66
Al <sub>2</sub> O <sub>3</sub>	4.32	4.07	3.47	3.39	3.87	4.86
Cr <sub>2</sub> O <sub>3</sub>	0.0	0.0	0.0	0.0	0.08	0.06
Fe <sub>2</sub> O <sub>3</sub>	22.19	23.43	24.16	23.78	20.66	18.06
MnO	0.07	0.10	0.05	0.08	0.04	0.02
MgO	0.41	0.37	0.30	0.29	0.23	0.28
CaO	32.49	32.68	32.92	33.43	30.79	29.56
TOTAL	99.96	100.20	100.81	99.87	99.31	97.16
	FORMULA PROPORTION BASED ON CATION SUM = 8.0					
Si 4+	2.33	2.49	2.34	2.21	1.60	1.44
Ti 4+	0.82	0.62	0.75	0.83	0.81	0.56
Zr 4+	0.002	0.003	0.01	0.0	0.65	1.02
Al 3+	0.43	0.40	0.34	0.34	0.42	0.55
Cr 3+	0.0	0.0	0.0	0.0	0.01	0.01
Fe 3+	1.41	1.48	1.53	1.52	1.43	1.31
Mn 2+	0.01	0.01	0.004	0.01	0.003	0.002
Mg 2+	0.05	0.05	0.04	0.04	0.03	0.04
Ca 2+	2.95	2.94	2.98	3.05	3.04	3.06
OXYGEN	12.08	12.06	12.04	11.97	12.00	11.96
Δ Si	2.24-2.52	2.38-2.59	2.28-2.47	2.17-2.32	1.58-1.70	1.40-1.44
Δ Ti	0.61-1.06	0.50-0.71	0.60-0.86	0.72-0.85	0.77-0.87	0.55-0.56
Δ Zr	0.0 -0.03	0.0-0.003	0.0 -0.01	0.0-0.002	0.51-0.71	0.86-1.02
N	14	5	5	6	5	2

3a

CHRISTMAS MOUNTAINS IGNEOUS ROCKS--GABBRO-CG

5.000E-01

FORMULA PROPORTION

4.000E-01

3.000E-01

2.000E-01

1.000E-01

0.0

MPNP= 0 0.0

1.000E-01

2.000E-01

3.000E-01

4.000E-01

5.000E-01

TETRAHEDRAL SILICON DEFICIENCY = 2.0-SI (FORMULA PROPORTION)

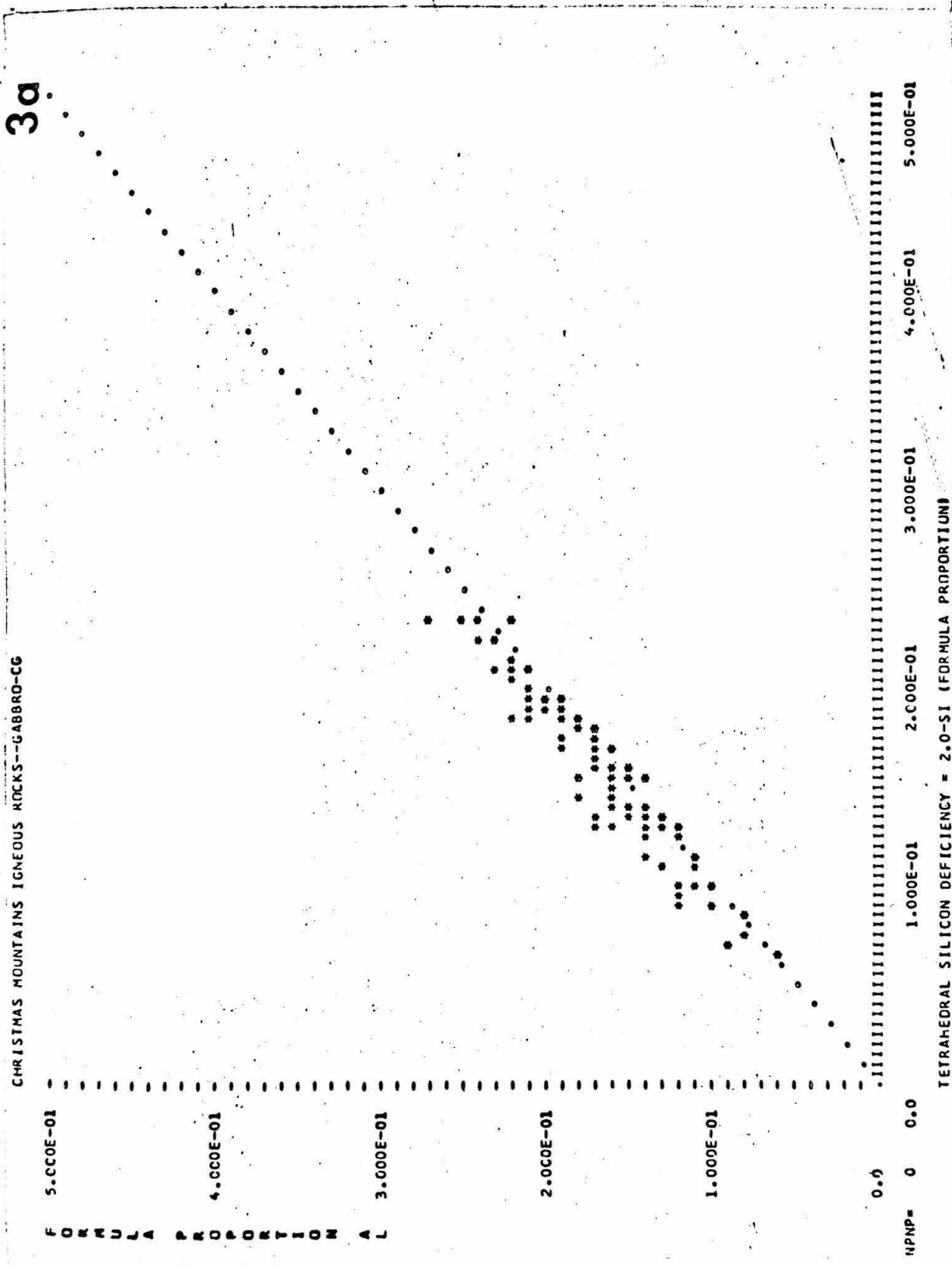


TABLE C-6  
ELECTRON MICROPROBE ANALYSES OF MINERALS FROM SKARN  
CHRISTMAS MOUNTAINS, TEXAS

	P	P	M	M	M	M	M
SiO <sub>2</sub>	8-5A	103-3A	8-1A	8-3	8-4	103-5	103-2
	0.18	0.68	0.16	0.15	0.13	0.52	0.35
TiO <sub>2</sub>	57.14	55.95	2.60	1.08	0.75	0.54	0.82
ZrO <sub>2</sub>	0.07	0.54	..	..	..	0.0	0.0
Al <sub>2</sub> O <sub>3</sub>	0.13	0.22	3.61	2.31	1.95	2.11	2.62
Cr <sub>2</sub> O <sub>3</sub>	..	0.26	..	..	..	..	0.03
Fe <sub>2</sub> O <sub>3</sub>	..	..	71.15	70.75	71.76	71.38	71.12
FeO	0.98	1.23	20.76	23.84	22.53	23.40	22.00
MnO	0.03	0.0	0.78	0.61	0.80	0.64	0.47
MgO	0.00	0.03	0.73	0.92	1.14	1.06	2.13
CaO	41.86	41.34	0.08	0.29	0.87	0.28	0.40
Na <sub>2</sub> O	0.15	0.0	0.07	0.0	0.02	..	..
TOTAL	100.54	100.25	99.95	99.95	99.95	99.95	99.95
CATION SUM	2.0	2.0	4.0	4.0	4.0	4.0	4.0
Si 4+	0.004	0.015	0.006	0.006	0.005	0.020	0.013
Ti 4+	0.962	0.947	0.074	0.031	0.021	0.015	0.023
Zr 4+	0.001	0.006	..	..	..	0.0	0.0
Al 3+	0.004	0.006	0.161	0.103	0.087	0.094	0.116
Cr 3+	..	0.005	..	..	..	..	0.001
Fe 3+	..	..	2.027	2.021	2.046	2.037	2.007
Fe 2+	0.018	0.023	0.657	0.756	0.714	0.742	0.690
Mn 2+	0.001	0.0	0.025	0.020	0.026	0.021	0.015
Mg 2+	0.0	0.001	0.041	0.052	0.064	0.060	0.119
Ca 2+	1.004	0.997	0.003	0.012	0.035	0.011	0.016
Na +	0.007	0.0	0.005	0.0	0.001	..	..
OXYGEN	2.965	2.973	4.171	4.098	4.092	4.101	4.098

P = perovskite, M = magnetite

TABLE C-7  
ELECTRON MICROPROBE ANALYSES OF SKARN  
CHRISTMAS MOUNTAINS, TEXAS

Sample	8-1A	8-1C	8-2B	8-3B	8-3	8-3C
Interval (cm)	2-4	4-6	13-17	33-35	38-42	39-41
Assemblage	2	3	4	8	8	8
Density (gm/cm <sup>3</sup> )	3.039	3.052	3.129	3.066	3.056	3.047
SiO <sub>2</sub>	40.42	44.54	37.65	33.66	32.69	33.33
TiO <sub>2</sub>	1.66	0.58	0.41	0.75	0.68	0.46
Al <sub>2</sub> O <sub>3</sub>	7.41	7.02	13.65	15.88	16.46	14.08
FeO	7.16	3.69	4.24	4.87	4.77	4.43
MgO	1.05	0.66	0.92	1.84	1.77	1.62
CaO	42.24	43.45	43.05	42.45	43.18	45.62
Na <sub>2</sub> O	0.06	0.06	0.08	0.55	0.51	0.46
TOTAL	100.00	100.00	100.00	100.00	100.00	100.00

Sample	8-3D	8-3E	8-3F	8-4	8-7A
Interval (cm)	43-45	48-51	53-57	57-61	76-79
Assemblage	9	9	9	9	13,15
Density	3.041	3.057	3.120	3.099	2.913
SiO <sub>2</sub>	30.23	30.17	30.26	30.67	22.94
TiO <sub>2</sub>	0.42	0.52	0.75	0.54	0.34
Al <sub>2</sub> O <sub>3</sub>	12.56	11.29	12.98	11.92	6.50
FeO	3.21	3.57	5.08	3.59	1.96
MgO	1.57	1.69	1.77	1.61	1.83
CaO	51.56	52.21	48.94	51.41	66.15
Na <sub>2</sub> O	0.44	0.54	0.22	0.26	0.29
TOTAL	100.00	100.00	100.00	100.00	100.00

TABLE C-7 (CONTINUED)

ELECTRON MICROPROBE ANALYSES OF SKARN  
CHRISTMAS MOUNTAINS, TEXAS

Sample Interval (cm)	103-6A (1) 0-2	103-6A (2) 2-4	103-6B 6-10	103-5 13-17	103-4 41-45	103-2 65-76	103-3 79-86	108 250
Assemblage	3	4	5	5	5	9	13	10,14
Density (gm/cm <sup>3</sup> )	3.176	3.182	3.111	3.078	3.106	3.087	3.105	2.787
SiO <sub>2</sub>	35.39	34.84	32.94	31.69	30.54	28.88	29.58	18.08
TiO <sub>2</sub>	1.24	0.99	0.62	0.59	1.56	1.39	0.33	0.43
Al <sub>2</sub> O <sub>3</sub>	13.59	14.69	17.22	17.96	18.38	9.81	5.19	2.21
FeO	5.67	5.68	6.05	5.27	5.18	3.80	2.31	2.46
MgO	2.37	2.57	3.04	2.87	2.84	1.54	1.19	4.05
CaO	41.56	41.15	39.82	41.42	41.17	54.32	61.13	72.64
Na <sub>2</sub> O	0.19	0.08	0.30	0.19	0.18	0.26	0.26	0.14
TOTAL	100.00	100.00	100.00	100.00	100.00	100.00	100.00	100.00

TABLE C-8

SPECTROGRAPHIC DETERMINATION OF ZIRCONIUM IN  
LIMESTONE, SKARN, PYROXENITE, GABBRO AND SYENITE  
CHRISTMAS MOUNTAINS, TEXAS

- E.Bingham, Analyst -

SAMPLE	ROCK TYPE	PPM ZR
39-6	Cg Gabbro	100
136	Fg Gabbro	140
39-1	Porph. Gabbro	260
294A	Syenite	370
29B	Pyroxenite	280
8-1A	Pyroxenite	450
29-70	Neph Syenite	460
141-4	Wo-Neph Syenite	450
8-1A	Wo-Skarn	260
8-1C	Wo-Skarn	280
8-2	Wo-Skarn	130
8-3B	Ra-Sp Skarn	270
8-3D	Sp Skarn	110
8-4	Sp Skarn	130
8-7A	Sp-Ca Marble	55
8-19	Sp Skarn	79
336-1L	Sue Peaks Ls.	85
336-1D	Sue Peaks Ls.	71
103-6A(1)	Wo-Skarn	240
103-6B	Wo-Ra Skarn	69
103-5	Wo-Ra Skarn	70
103-4	Wo-Ra Skarn	93
103-2	Sp Skarn	190
103-3B	Sp-Ca Skarn	33
29BX	Wo-Skarn	95
335-2	Santa Elena Ls.	< 20
332	Del Carmen Mbl.	< 20

TABLE C-9

ELECTRON MICROPROBE ANALYSES OF SUE PEAKS LIMESTONE  
CHRISTMAS MOUNTAINS, TEXAS

Sample	336-1D	336-1L	336-2	8-17	8-19
SiO <sub>2</sub>	23.49	31.48	31.39	26.30	30.88
TiO <sub>2</sub>	0.33	0.38	0.36	0.38	0.31
Al <sub>2</sub> O <sub>3</sub>	9.00	11.03	12.93	7.28	10.95
FeO	2.00	2.63	3.02	2.84	2.31
MgO	1.98	3.32	4.74	1.74	1.61
CaO	62.78	50.74	47.36	61.15	53.56
Na <sub>2</sub> O	0.42	0.42	0.19	0.30	0.37
TOTAL	100.00	100.00	100.00	100.00	100.00

SEMIQUANTITATIVE SPECTROGRAPHIC ANALYSES OF LIMESTONE  
CHRISTMAS MOUNTAINS, TEXAS

E. Bingham, Analyst

	Del Carmen 332	Santa Elena 335-2
SiO <sub>2</sub>	2.6	7.1
TiO <sub>2</sub>	< 0.006	< 0.006
Al <sub>2</sub> O <sub>3</sub>	0.4	1.4
FeO	0.1	0.1
MgO	4.7	2.5
CaO	92.2	89.0
Na <sub>2</sub> O	< 1	< 1
TOTAL	100.0	100.0